INFORMATION TO USERS

This manuscript has been reproduced from the microfilm master. UMI films the text directly from the original or copy submitted. Thus, some thesis and dissertation copies are in typewriter face, while others may be from any type of computer printer.

The quality of this reproduction is dependent upon the quality of the copy submitted. Broken or indistinct print, colored or poor quality illustrations and photographs, print bleedthrough, substandard margins, and improper alignment can adversely affect reproduction.

In the unlikely event that the author did not send UMI a complete manuscript and there are missing pages, these will be noted. Also, if unauthorized copyright material had to be removed, a note will indicate the deletion.

Oversize materials (e.g., maps, drawings, charts) are reproduced by sectioning the original, beginning at the upper left-hand corner and continuing from left to right in equal sections with small overlaps.

Photographs included in the original manuscript have been reproduced xerographically in this copy. Higher quality 6" x 9" black and white photographic prints are available for any photographs or illustrations appearing in this copy for an additional charge. Contact UMI directly to order.

Bell & Howell Information and Learning
300 North Zeeb Road, Ann Arbor, MI 48106-1346 USA
800-521-0600

Impact of added insulation on the hygrothermal performance of leaky exterior wall assemblies

Submitted by:
Guylaine Desmarais

Thesis at the
Department of Building, Civil, and Environmental Engineering

Presented in Partial Fulfillment of the Requirements for
The Degree of Master of Applied Science
At
Concordia University
Montreal, Quebec, Canada

March 2000

Abstract

Increasing the thermal insulation of the envelope reduces energy consumption. The effect on energy consumption of increased thermal resistance can be calculated with simple measures. However, other impacts of adding insulation, such as the potential for condensation due to moisture and air movement through the exterior wall assembly, are often not taken into account.

To avoid problems, the post-retrofit hygrothermal performance of exterior wall assemblies, which can be leaky, should be evaluated prior to the addition of insulation with computer simulations. However, no previous test assessed the hygrothermal performance of leaky assemblies and the impact of adding insulation. This project proposes an experimental procedure to evaluate the effect of adding insulation to leaky exterior wall assemblies and to monitor air leakage paths within them.

The procedure involves the construction of a full-scale test hut exposed consecutively to climatic conditions representing winter and late spring, inside the environmental chamber. Two re-insulation strategies are studied, with three different air leakage patterns, and compared to an insulated base-case. The construction of the hut is typical of low-rise wood frame residences in Quebec, insulated with glass fiber batt insulation between the studs.

The objectives of the experimental work are:

- To study the effect of different insulating strategies for exterior wall assemblies having different air leakage characteristics on the moisture content and temperature distribution patterns in walls when exposed consecutively to wetting and drying conditions;
- To develop and implement a method of characterizing air leakage paths so that more is known about the movement of air through exterior wall assemblies;
- To produce patterns that could be used to validate existing models.

It was seen that adding insulation on the cold side of a leaky existing assembly increases the risk for condensation, while adding insulation on its warm side reduces it. The best strategy remains improving airtightness, as the airtight section with the base-case composition had the least moisture accumulation.

The results of the two air leakage characterization methods, 2-D grid moisture content and 3-D temperature monitoring, are presented graphically, using moisture content and temperature maps. From these maps, it can be concluded that a correlation exists between the moisture content accumulation pattern and the air leakage path and between the temperature profiles and the air leakage path.

Acknowledgements

I undertook this Master thesis project not fully aware of its scope and how consuming it would be. Despite obstacles, I kept on going and carried it out to its completion. However, this would have been totally impossible without the help of many people who deserve to be thanked for their part in this achievement.

- To **Dr. Paul Fazio** and **Dr. Dominique Derome**, my supervisors, thank you for your precious guidance and constant support. Thank you also for always expecting the best from me and for providing me with extraordinary learning experiences. I will forever be grateful for everything.
- To **Dr. Jiwu Rao** and **Luc Demers**, thank you for the technical support you provided and for the huge amount of work that you put into this experiment. And thank you for being able to solve so many problems!
- To **Jacques Payer**, **Sylvain Bélanger**, **Joe Hribb** and **Dorina Banu**, thank you for providing me with what I needed to complete my experiment. You really spoiled me!
- To Dr. Andreas Athienitis, thank you for the support you provided during the heat transfer modelling.
- To **Jean-Claude Desjardins** and **Guy Fournier**, **Sandrine Bertrand** and **Philippe Brosseau**, thank you for your help in building the test hut and carrying out the test procedure.
- To **Dr. Mark Bomberg**, **Dr. Michael Lacasse** and **Madeleine Rousseau**, thank you for your extremely valuable input in the final version of this thesis, in spite of your busy schedule.
- To **Sandra Marshall**, thank you for your useful comments.

The following provided funding:

- **FCAR**, under Dr. Paul Fazio's team research grant;
- **NSERC** research grant (from Dr. Paul Fazio grant);
- **ABB** grant for research on the building envelope;
- and the **Canadian Mortgage and Housing Corporation (CMHC)**, under the External Research Program of Dr. Dominique Derome.

Finally, but not least,

- **Mom** and **Dad**, thanks for your encouragements and for raising me to believe that I could achieve anything I want.
- **Jean-François**, thanks for sharing my life and thank you for your love, support, understanding and... patience.

This brick is for all of you! Thank you again,

Guylaine Desmarais

Table of Contents

List of Figures

List of Tables

1. INTRODUCTION

1.1 Context and objectives of the research project

Increasing the amount of thermal insulation in the envelope of residential buildings is done to reduce energy consumption. The domestic sector uses 30 to 50% of the total energy used by the building sector and represents a good target for implementing energy conservation measures. Research has shown that adding thermal insulation is one of the most effective measures to decrease energy use for heating and cooling (Hens, 1996). The benefits of additional insulation on energy consumption are easy to evaluate because many simple calculations methods exist (Jones, 1995). However, other consequences of adding insulation, such as the potential for condensation due to moisture and air movement through the exterior wall assembly, are often not taken into account. Increasing the thermal resistance of exterior wall assemblies modifies their temperature gradient, and the risk for moisture condensation may increase, especially if there are paths to allow warm, moist indoor air to flow through them. Moisture may then accumulate in the hygroscopic materials (wood, fiberboard sheathing) and the insulation of the assembly, inducing the reduction of the thermal performance of the insulation and, eventually, the deterioration of the building envelope. For a long time, it has been acknowledged that moisture was a principal agent of deterioration for exterior wall assemblies (Latta and Beach, 1964). It is further said that moisture poses the biggest threat to the integrity and durability of the envelope by accounting for up to 80% of damage in building envelopes (Bomberg and Brown, 1993).

Moisture from indoors can move through the wall either by diffusion or exfiltration. Of the two, exfiltration is the main moisture transfer vehicle into the building envelope

(Kumaran, 1996). Exfiltration is one of the leading causes of moisture related problems in exterior wall assemblies. Besides bringing into the wall moisture that can condense, exfiltration has been linked to efflorescence, spalling of masonry, high energy costs, and poor control over the indoor humidity conditions (Quirouette, 1985). Most air exfiltrates through paths created by cracks, joints between materials, or junctions between components. The latter are often the weak points of the assembly and are critical because of their potential for becoming concentrated areas of deterioration. Forest (1989) indicated that walls with point defects on the warm side of the assembly showed moisture accumulation directly opposite the defect on the cold side when tested. Yet, the airtightness of residential buildings is currently evaluated only in a macroscopic manner, with methods such as the fan-pressurization test. Although useful for energy consumption evaluation, a total air leakage rate for a building provides little information on the location of the potential moisture accumulation areas inside the building envelope. Moisture transfer by exfiltration is likely to occur since the exterior walls of most existing residential buildings are not airtight, as demonstrated in a survey by Hamlin and Gusdorf (1997). This suggests that the initial air leakage characteristics of the assembly should be considered when adding insulation to leaky exterior wall assemblies. The questions are how can insulation be added, yet moisture accumulation be avoided? Also, what effect do the initial air leakage characteristics have on moisture accumulation? Where in the assembly should the insulation be added to minimize the likelihood of moisture related problems? Finally, where does air flow in the assembly and would knowing this help in identifying potential problem areas?

Moisture related problems could be avoided by evaluating the potential effects of specific re-insulation strategies on the hygrothermal performance of exterior wall assemblies prior to carrying out the changes. This could be done with computer simulations of combined heat, moisture, and air transfer to study the effect of adding insulation on moisture contents and temperatures within these walls. Among the shortcomings of current computer codes is the unavailability of information on the trajectory of air through the envelope assembly, as well as temperature and moisture content data for further validation. It has been said that once airflows have been determined, the associated amount of moisture transport could be easily determined (TenWolde, 1989).

In this project, an experimental procedure is proposed to evaluate the hygrothermal performance of leaky exterior wall assemblies with added insulation and to monitor the impact of air leakage paths within these walls. The procedure involves the construction of a full-scale test hut inside an environmental chamber where conditions representing Montreal winter followed by late spring weather are reproduced. Two re-insulation strategies having three different air leakage patterns are studied, and compared to an insulated base-case. The construction of the test hut is typical of Quebec low-rise wood frame residences, insulated with glass fiber batt insulation between the wood studs.

The objectives of the experimental work are:

- To study the effect of different re-insulating strategies on the hygrothermal performance of exterior wall assemblies having different air leakage characteristics when exposed consecutively to wetting and drying conditions;

- To develop and implement a method of mapping air leakage paths to document the movement of air through exterior wall assemblies;
- To develop and use a graphic mode of presenting air leakage patterns within wall assemblies.

The methods implemented to characterize air leakage patterns are two-dimensional grid moisture content monitoring (using gravimetry and moisture content sensors) and three-dimensional grid temperature monitoring (using thermocouples). The results from these two methods are presented graphically.

The 2-dimensional grid moisture content monitoring of the fiberboard exterior sheathing (using gravimetry) allows for the development of *isohygrons*, or contour lines of equal moisture contents. Assuming that moisture in the indoor air acts as a marker for exfiltrating air, then the moisture content maps should reflect air leakage patterns, and hence make identification of areas potentially having moisture problems possible. Through the 3-dimensional grid temperature monitoring, temperatures along planes located at two different depths within the assemblies are measured, i.e. at the cold side and at the warm side of the glass fiber batt insulation. The measured temperatures are compared to temperatures calculated using a 3-dimensional conduction heat transfer model, without the impact of exfiltration. The measured and calculated temperatures are presented using isotherms for each plane. Following the hypothesis that exfiltrating air will warm the materials it comes in contact with, it is suggested that a relationship can be established between the temperature profiles and that an air leakage pattern may be derived from these temperature maps.

1.2 Thesis organization

The context and objectives set for the present research project have been stated in the previous section of Chapter 1.

A literature review follows in Chapter 2. This chapter presents a review of previous experimental as well as modeling work pertinent to the stated objectives of the project. The review will be useful in guiding the definition of research needs and the elaboration of the experimental protocol.

The experimental protocol is described in full detail in Chapter 3. The experimental facility, test specimens, monitoring protocol and climatic conditions are presented. The history of the experiment, i.e. what happened during the testing period in terms of climatic conditions and data acquisition is also described.

Results are presented and discussed in Chapter 4 and Chapter 5. In Chapter 4, the results are analysed in terms of the effect of added insulation and air leakage path on the hygrothermal performance of the assemblies. Chapter 5 presents the results using moisture content and temperature maps and discusses the relationship between those maps and the path of air within the assemblies.

Conclusions, including contributions and recommendations for future work, end the thesis, in Chapter 6.

2. LITERATURE REVIEW

All buildings have an exterior shell that is referred to as the building envelope. This envelope is by definition exposed to the elements, which may lead to its deterioration and prevent it from fulfilling it functions prematurely. Research work has been carried out to understand how building envelopes can be made durable. This research has yielded a significant body of knowledge. This literature review first presents background knowledge regarding the composition and hygrothermal behaviour of exterior wall assemblies and identifies specific problems. Then, previous research work is reviewed in order to guide the elaboration of the experimental protocol to be conducted for the present project.

2.1 Basic principles of the building envelope

First, the basic principles of the building envelope related to its purpose and the function of its components are presented. As stated by Hutcheon (1963), the main function of the building envelope "*is to provide a barrier between the indoor and outdoor environments, so that indoor conditions can be adjusted and maintained within acceptable limits*". The principal requirements of an exterior wall are to control heat flow, air flow, water vapour flow, rain penetration, light, solar and other radiation, noise, fire, provide strength and rigidity, be durable, aesthetically pleasing, and economical.

In order to meet these performance requirements, different components having specific function(s) are integrated in the building envelope assembly. They are frequently: an air barrier to control air flow, a vapour barrier to control vapour flow, thermal insulation to control heat flow, and a rain screen to prevent rain water entry. All these components, which are described below, work together to form a complex system,

and cannot be considered independently one from the other, as heat, air, and moisture transfer mechanisms are interrelated and affect one another. This means that, although a specific function may be assigned to a particular element, this element may also perform other functions. For example, the vapour barrier may also act as an air barrier and the thermal insulation may help reduce condensation by increasing temperatures in the cavity. Materials are assigned functions and separated in the way described below mainly for the simplification of the design process (Bomberg and Brown, 1993).

The thermal barrier. Heat transfer through the building envelope must be minimized to keep indoor conditions comfortable for the occupants and to minimize energy consumption. Materials with a low thermal conductivity are selected for the purpose of reducing the conductive heat transfer. Some commonly used insulating materials include glass or mineral fiber batt insulation, extruded or expanded polystyrene, blown mineral, glass or cellulose fiber, and polyisocyanurate. This barrier must be as continuous as possible to avoid thermal bridging, which may cause cold spots on the interior finish, leading to staining or condensation.

The vapour barrier. As moisture within exterior walls can potentially cause significant damage, it is important to include a material in the assembly that will retard diffusion of water vapour, from the interior environment, into the wall (Latta and Beach, 1964). The material acting as vapour barrier in an assembly must have a low water vapour permeability. Usually, the vapour barrier consists of a membrane such as a polyethylene or aluminium sheet having a high resistance to the passage of moisture. Some paint products, insulation adhesives (mastics), metal, glass, and even concrete of sufficient thickness may also be suitable vapour barriers (Quirouette, 1985).

To prevent moisture migration by diffusion only, the vapour barrier does not need to be perfectly continuous, even though it is desirable to avoid imperfections such as perforations, unsealed laps and minor cuts (Quirouette, 1985). However, the position of the vapour barrier within the exterior wall assembly is important. The vapour barrier should prevent indoor moisture from migrating into the wall, but not trap it inside. To do this, the vapour barrier should be placed on or near the warm side of the insulation, which is normally the high vapour pressure side in cold climates (Quirouette, 1985). The Canadian Building Code 1995 specifies minimum ratios of thermal resistance on either side of *low permeability materials* (LPMs), based on the number of heating degree-days (this is explained in "*Systèmes d'étanchéité à l'air pour murs de bâtiments de faible hauteur: Performance et évaluation*" (NRCC - IRC, 1997) and specifics are found in Table A-9.25.1.2.A of the *National Building Code* 1995). For example, the city of Montreal has less than 5000 heating degree-days, corresponding to a ratio of 0.2. Therefore, according to this rule, the total thermal resistance of materials on the exterior side of the LPM over the total thermal resistance of the materials on the indoor side of the low water vapour permeability should be at least 0.2.

The air barrier system. The role of the air barrier is to "*stop outside air from entering the building through the walls, windows or roof, and inside air from exfiltrating through the building envelope to the outside*" (Quirouette, 1985). Air leakage through the wall should be controlled so that: (1) condensation within hygroscopic materials in the assembly occurs rarely or that accumulated amounts are below levels required for mold and fungi growth and (2) drying is fast enough to avoid deterioration of materials or growth of mold or fungi (NRCC - IRC, 1997).

The air barrier is actually a system composed of different materials that are connected together. To be used in an air barrier system, a material must meet the following criteria: (1) have a low air permeability (0.02 l/(s • m^2) at 75 Pa air pressure difference or lower according to Part 5 of the 1995 National Building Code of Canada), (2) have structural rigidity to resist air pressure differentials and transfer those to the building structure, (3) be continuous around the whole building, (4) be durable or maintainable, and (5) be buildable (NRCC - IRC, 1997). Continuity is critical, as even a small hole in the air barrier through which warm, moist indoor can exfiltrate may cause significant damage. Maximum air leakage rates through the air barrier system are recommended in part 5 of the National Building Code of Canada (1995), in relation to the relative humidity maintained indoors: 0.15 l/(s • m^2) for 27% RH or less, 0.10 l/(s • m^2) for 27% to 55% RH, and 0.05 l/(s • m^2) for 55% RH or more (Table A-5.4.1.2 of the National Building Code 1995). Section 9.25.3 provides some requirements for the air barrier system for houses and small buildings (3 storeys or less), which are covered by Part 9 of the National Building Code of Canada (1995). Though this section contains no quantitative requirements, it mentions that all walls, ceilings, and floors with thermal insulation must incorporate a continuous air barrier system to prevent infiltration and exfiltration, and defines details and joints where continuity must be maintained.

The water vapour permeability of the air barrier materials will dictate where they can be located within the assembly. If it has low water vapour permeability, it must be located according to the rules previously described for vapour barriers.

Different strategies may be used to create the air barrier system. Interior and exterior approaches have been proposed (CMHC 1999). For example, one interior air

barrier approach is the *sealed polyethylene approach.* In this case, the polyethylene membrane commonly used in residential construction is installed such that the functions of vapour barrier and air barrier are combined. Another example of interior approach is the *Airtight Drywall Approach* (ADA). In this case, the gypsum board interior finish is used as an air barrier material and joints with the floor, the ceiling, and other walls are sealed. The level of performance and longevity of this approach is dependent on the occupants and the extent to which they maintain the integrity of the interior walls and hence prevent any breach of the air barrier system (e.g. make holes for pictures, new electrical outlets). Moreover, cracks may develop and if not sealed, the efficiency of the air barrier system may be reduced.

Exterior air barrier approaches include the *exterior membrane approach* and the *exterior sheathing approach.* In the exterior membrane approach, the weather barrier is sealed to be part of the air barrier system. Because the air barrier system has to be rigid, the weather barrier has to be supported in order to perform as an air barrier material. When using the exterior sheathing approach, it is the exterior sheathing that is sealed to the other materials of the air barrier system.

The weather barrier. In most residential buildings, a weather barrier is installed over the backwall, on the exterior sheathing or rigid insulation, before the exterior veneer. Building paper products, spun bonded polyolefin, or cross-woven polyolefin or polyethylene membranes are commonly used. This layer helps limit air leakage and protects the backwall against the effects of wind washing. Air leakage and wind washing increase heat loss and contribute to reduced temperatures within the wall (which increase

the risk of condensation). It also protects the backwall against rainwater that might penetrate behind the exterior cladding, while permitting moisture to breathe through.

The thermal, vapour, air, and weather barriers, together with the framing and the interior finish form the core of the wall, commonly known as the *backwall*. It is this backwall that will be the focus of this research project. The veneer, usually applied with an air gap between it and the backwall, acts mainly to protect the backwall against rainwater penetration. The veneer is not subjected to the temperature, water vapour, and air pressure differentials found across the backwall and will not be considered here.

2.2 Transfer mechanisms in the building envelope

The main components of the backwall have been described above. Depending on the climate to which the backwall is exposed to, it will be subjected to various levels of air, heat and moisture transfer. The present section focuses on providing a brief overview of those transfer mechanisms in the building envelope.

2.2.1 Heat transfer through materials and the building envelope

The transport of heat can occur in three different ways: radiation, conduction or convection. These modes of heat transfer can happen either simultaneously or individually, and they all necessitate a temperature difference in order to take place.

2.2.1.1 Radiation

Heat transfer by radiation is a direct transfer of energy between two bodies, without the help of a medium like air or water. Presently, the phenomenon of radiant energy is explained by two different approaches, where energy is considered to be transferred through waves of electromagnetic radiation or via very small particles called *photons*. Each of these models can accurately describe some conditions. The quantity of radiation

exchanged between bodies is a function of the temperature difference, distance between the bodies, properties of the materials involved (absorptivity, emissivity, transmittance) as well as the surface areas and angle of exposure to one another. In a building enclosure, heat transfer by radiation occurs at the interior and exterior surfaces and inside the cavities of the wall. Exchanges by radiation are not typically considered a significant heat transfer mechanism in the building envelope.

2.2.1.2 Conduction

Conduction is a phenomenon by which heat travels through a solid. At a molecular level a multitude of collisions between molecules that make up the material propagate the energy from a warmer to cooler region. This transfer is proportional to the thermal conductivity (a physical property of the material) and the temperature difference between each surface of the material or assembly, but inversely proportional to the distance over which the transfer occurs (or the thickness of the material).

In envelope assemblies composed of a series of homogeneous layers, i.e. where the properties, such as conductivity, are constant through each layer, the energy is propagated consecutively from one layer to the next. For assemblies consisting of a series of non-homogeneous layers (where the properties are not the same for the layers), the energy circulates from the warmest to the coolest region while passing simultaneously through regions more or less *resistant* to its passage. Again, the comparison can be made with the conduction of electricity in circuits in *series* (flow through a sequence of non-homogeneous materials) and in *parallel* (flow through assemblies with layers counting two or more non-homogeneous materials).

2.2.1.3 Convection

In convection, the exchange of energy occurs by contact between a fluid in motion and a solid, immobile surface. The rate of transfer per unit area will depend on the physical characteristics of the fluid, the temperature difference between the fluid and the surface, and the velocity of the fluid in contact with the surface. Within the context of building systems, two types of convection are identified: (1) forced convection, induced by the mechanical systems in a building, and (2) natural convection, which occurs when a temperature difference exists between a surface and a fluid. In the case of natural convection, gravity must also be considered.

Even though it is not considered the most important mode of heat transfer inside the building enclosure, convection can have a great impact on the thermal performance of an exterior wall. Air circulating inside a cavity of the assembly or flowing through an air leakage path may significantly increase the rate of heat transfer. However, these phenomena are very difficult to quantify because it is difficult to evaluate the convection heat transfer coefficient.

2.2.1.4 Mathematical solutions to heat transfer problems

Mathematically, all modes of heat transfer in steady-state can be described by *Fourier's law*, given by:

$$q = -k\,A\,dT/dx \qquad \text{Equation 2.1}$$

where:

q = rate of heat transfer [W] during the time period θ [s]

k = thermal coefficient of heat transfer or conductivity[1] [W/m • K]

A = surface area perpendicular to the direction of the flow [m^2]

dT/dx = temperature gradient over the thickness considered [K /m]

For uni-directional steady-state heat conduction, the following equation derived from Fourier's law is used:

$$q = A\ k/l\ (T_1 - T_2) \qquad \text{Equation 2.2}$$

where:

q = rate of heat transfer [W]

A = surface area perpendicular to the direction of the flow [m^2]

k = coefficient of conductivity of the material[2], [W/m • K]

l = distance covered [m]

$T_1 - T_2$ = temperature difference [K]

The ASHRAE Handbook of Fundamentals (1993) provides three methods to calculate the overall thermal resistance of exterior wall assemblies that are based on Fourier's law: (1) isothermal plane method, (2) parallel path method, and (3) finite-difference method. For all methods, a representative section of the assembly, with adiabatic conditions at the boundaries, is first defined.

When using the isothermal plane method, the defined section is divided into planes perpendicular to the path of heat transfer as shown in Figure 2.1. Temperatures at the

[1] Since the parameters influencing the rate of heat transfer are different for each mode, this coefficient will be defined differently for each, taking into account those parameters. The "nomenclature" will also be different. For example : k for conduction, h_c for convection, h_r for radiation and U for the total transmission coefficient for the assembly including all forms of heat transfer and all layers present are commonly used.

[2] The "k" values for different materials are measured by experimentation. Tables listing those values are available in many books, for example in the "***ASHRAE Handbook of Fundamentals, 1993***".

interface of these planes are assumed to be constant. A weighted average of the thermal resistance of each layer is calculated. Take the example of an assembly composed only of these two layers: (1) insulation and studs and (2) fiberboard sheathing, which is shown in Figure 2.1.

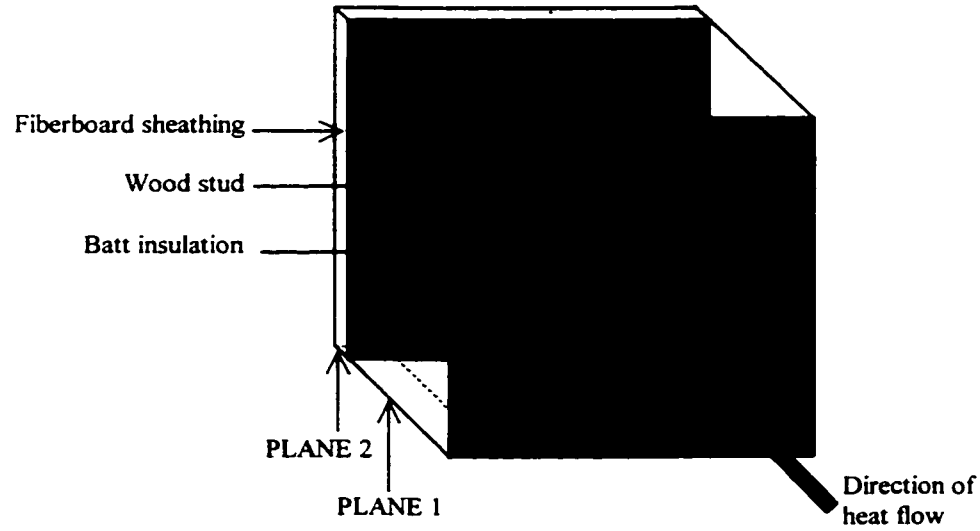

Figure 2.1 Illustration of the isothermal plane method.

The resulting equation is then:

$$R_{total} = \frac{1}{\frac{ratio\ i}{R_i} + \frac{ratio\ ws}{R_{ws}}} + R_f \qquad \text{Equation 2.3}$$

where:

R_{total} = total thermal resistance [$m^2 \cdot °K/W$]

R_i = thermal resistance of the insulation [$m^2 \cdot °K/W$]

R_{ws} = thermal resistance of the wood studs [$m^2 \cdot °K/W$]

R_f = thermal resistance of the fiberboard sheathing [$m^2 \cdot °K/W$]

ratio i = surface area of insulation over total surface area of the section

ratio ws = surface area of wood studs over total surface area of the section

When the parallel path method is used, the same section is divided into paths parallel to the direction of heat flow, as shown in Figure 2.2. For the same assembly as before, there would be two paths:

1. wood stud, fiberboard sheathing
2. insulation, fiberboard sheathing

For each path, the total conductance is calculated by adding the conductance of each of the materials in this path.

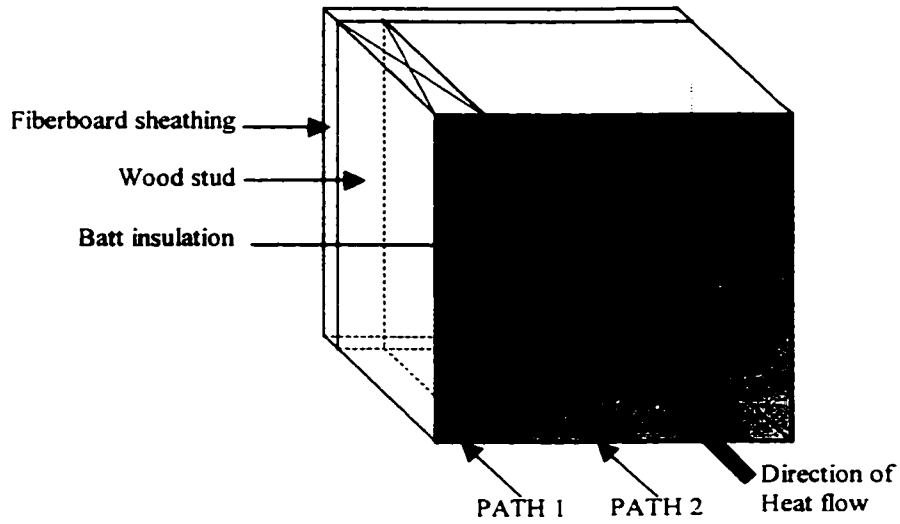

Figure 2.2. Illustration of the parallel path method.

Then, the overall conductance is calculated using equation 2-4.

$$U_{total} = (ratio_1 \bullet U_1) + (ratio_2 \bullet U_2) \qquad \text{Equation 2.4}$$

where:

U_{total} = overall conductance of the section [W/m^2 • K]

U_1 = conductance of path 1 [W/m^2 • K]

U_2 = conductance of path 2 [W/m^2 • K]

$ratio_1$ = surface area of path 1 over total surface area of the section

$ratio_2$ = surface area of path 2 over total surface area of the section

then:

$$1 / U_{total} = R_{total} \qquad \text{Equation 2.5}$$

where R_{total} is the total resistance of the section.

It is generally accepted that the isothermal plane method underestimates the thermal resistance of the assembly because it gives too much importance to lateral heat transfer and that the parallel path method overestimates the thermal resistance by not taking lateral heat transfer into account. According to the ASHRAE Handbook of Fundamentals (1993), the average of both results for the same assembly is thought to give a good estimate of the overall thermal resistance.

The finite-difference method is the approach used in the conductive heat transfer model selected to calculate the thermal resistance and the temperatures of the assemblies. It is described in section 5.2.2.

As opposed to conduction heat transfer problems for which enough measurements of material conductance are available, convection heat transfer problems cannot be solved using only analytical methods. Experiments have to be performed for each situation encountered (natural convection, forced convection, shape of solid, temperature difference, nature of fluid, etc.) and correlation established with the results. Some tables listing surface or air space convective heat transfer coefficient (h_c) for different cases are available, for example in the "*ASHRAE Handbook of Fundamentals*" (1993).

2.2.2 Moisture transfer in materials and the building envelope

Moisture transfer through the building envelope is a complex multi-dimensional process involving vapour diffusion, air movement, capillary flow, and moisture storage (Fazio et al., 1997). The two main transfer modes for moisture from indoor through the envelope under normal operating conditions are diffusion and exfiltration.

Diffusion is the process by which water vapour migrates through a material. Moisture migrates through virtually all materials, but at different rates. This property of the material is known as the *permeance*. This property is usually expressed in terms of the weight of moisture that will diffuse through a given area and thickness of material, over a specified period of time at a unit water vapour pressure difference: ng/m • s • Pa (Quirouette, 1985). The potential for diffusion is the water vapour pressure differential across the material. The vapour flow through a material is equal to the vapour pressure difference multiplied by the permeability of the material. This relationship is similar to that of heat transfer with one important difference, which is the ability of moisture to condense. When condensation occurs, the continuity of flow is broken because not all the vapour that migrates into the wall will necessarily migrate out if the dew point is reached along the way. Another difference is that it is often impossible to describe the water vapour permeability of a material in terms of a single coefficient applicable over a wide range of conditions, as in heat transfer (k, or conductivity to heat), because the permeability varies with temperature, moisture content, and relative humidity.

One method that can be used to calculate the vapour diffusion is the dew-point method (ASHRAE, 1993). This method assumes one-dimensional moisture transfer across the assembly, and that vapour diffusion is the only moisture transfer mechanism.

Conductive heat transfer is considered according to Fourier's law (see Equation 2-1), but convective heat transfer due to airflow is not included.

The dew-point method is based on the following form of Fick's law of diffusion (ASHRAE, 1993):

$$w = -\mu (dp/dx) \qquad \text{Equation 2.6}$$

where:

w = mass of vapour flow diffusing through unit area in unit time [ng/m • s]

p = vapour pressure [Pa]

x = distance along flow path [m]

Hence:

dp/dx = vapour pressure gradient [Pa/m]

μ = permeability [ng/m • s • Pa]

The temperature at each interface between materials is calculated using the thermal conductivity of the materials and the known temperature boundary conditions. Once the temperatures are known, the corresponding water vapour pressures can be calculated using the wet cup/dry cup permeability and the known water vapour boundary conditions. The calculated water vapour pressures are compared with the saturation vapour pressure for steady-state conditions. There is a possibility for condensation when the calculated vapour pressure is higher than the saturation vapour pressure.

The other mode through which moisture from indoor can be transported into an assembly is convection, or more precisely in this case exfiltration. Air exfiltrating through cracks can carry large amounts of moisture in vapour form into the wall. Air at a higher temperature can contain more water vapour than colder air. When an air-vapour

mixture is cooled, it will reach a temperature at which it will be saturated, also called the *dew point*. If cooling is continued below this point, water will condense (Latta and Beach, 1964). Condensation will not necessarily occur exactly at the dew point in the assembly, which is often in the insulating material, but will rather collect on the first solid surface that is below the dew point temperature, usually the wall or roof sheathing (Hansen, 1984). The extent of condensation will depend on indoor humidity, outdoor temperature and on the rate and duration of airflow (Wilson, 1961).

Of these two moisture transfer modes, diffusion and exfiltration, exfiltration can carry much more moisture into the wall. For example, assume a single stud space wall that exposes to the room 1 m^2 of a vapour barrier having a permeance of 5 ng/Pa s m^2. The conditions inside the room are 21°C and 30% RH, while the sheathing is at -20°C. Were these conditions to prevail for one month, approximately 6 g of moisture would diffuse into the cavity, creating only a thin layer of frost on the inside surface of the exterior sheathing. If the same wall had an opening with an area of 625 mm^2, this opening would allow 2600 m^3 of air through it under an air pressure differential of 10 Pa over one month. With the indoor air again at 21°C and 30% RH, this would amount to approximately 3000 kg of air and 14 kg of water. If even only 10% of this moisture condenses, this still amounts to 233 times more water in the wall due to air leakage than to diffusion. The amount of moisture transported by diffusion is so small compared to air leakage that if the air barrier is not continuous and allows warm humid air to exfiltrate, the vapour barrier will be completely useless, even if it is of zero permeance (Latta, 1976).

2.2.3 Air leakage in building envelopes

The air leakage referred to here is the "*uncontrolled flow of air through unintentional openings driven by wind, temperature difference and/or appliance-induced pressures across the building envelope*" (ASHRAE, 1993). The amount of air leakage depends on the design and condition of the building envelope, the quality of the materials and workmanship as well as the air pressure differentials acting across the cracks and openings (Wilson, 1961). As air carries with it heat, moisture and pollutants, it is desirable to control and minimize air leakage in the building envelope so that it does not become a liability in energy consumption, thermal comfort, indoor air quality, or airflow. Air leakage may also disable a rain screen system by creating air pressure differences that can become driving forces for water (Quirouette, 1985).

The most common paths for air leakage in exterior walls are holes for electrical boxes, oversized holes for electrical wiring and plumbing, and the intersections between the exterior wall and the floor and between the exterior wall and the ceiling. Door and window perimeters represent other important potential areas of air leakage. Air may also go through porous materials. Paths for air leakage may exist right from the beginning due to poor detailing or workmanship or may develop over time, when the framing dries and shrinks (Hansen, 1984).

Air pressure differentials, which induce air movement, may be caused by the wind, the stack effect, or the ventilation system. The wind causes variations in pressure around a building, depending on its speed and direction, the height and shape of the building, and the surrounding terrain. The pressures are positive on the windward side and negative on the leeward side, wind pressures on the remaining sides are dependent on the angle of the

wind (Wilson, 1961). The stack effect occurs when air masses, on either sides of the building enclosure, are at different temperatures, i.e. during the heating season. It is proportional to the temperature difference between outside and inside air and the height of the building. The temperature difference causes a difference in density, the warmer air being lighter than the colder air. The warmer indoor air will tend to rise and flow out at the top and be replaced at the bottom by cold outdoor air. Therefore, the pressure will tend to be negative in the lower portion of the building, while the upper part will be pressurized causing exfiltration. The *neutral pressure plane* is the level at which the interior and exterior pressure are equal. The height of the neutral pressure plane at zero wind speed depends on the vertical distribution of cracks and openings in the building envelope (ASHRAE, 1993). If the upper part of the building is very leaky, then the neutral pressure plane will be higher. Figure 2.3 illustrates pressure differentials in buildings due to the stack effect. An example of the calculation of the air pressure differential due to the stack effect in the second storey of a typical low-rise residential building is shown in Appendix A.

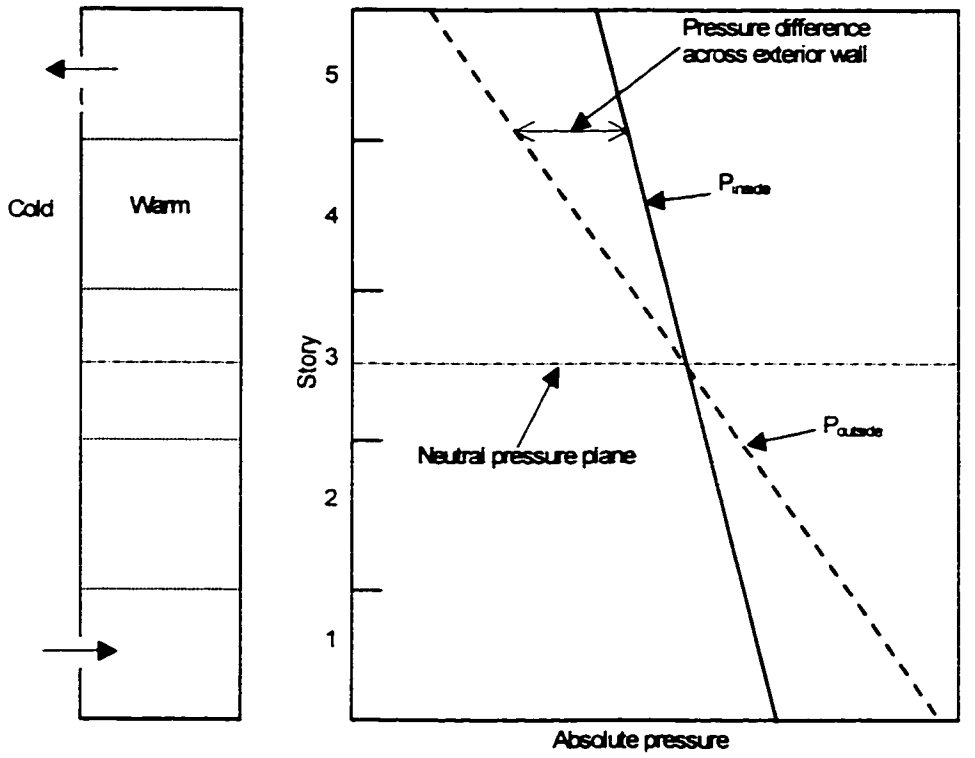

Figure 2.3. Illustration of stack effect. (as per Hutcheon and Handegord, 1989)

There are different methods used to locate and assess the air leakage in a building. First, signs such as dust stains on the interior finish at the perimeter of a window or door, *efflorescence* on the brick below windows or at the parapet of a building, and mortar joints spalling may be evidence that air leakage has been occurring at this location (Garden, 1965). Smoke pencils and infrared thermography can be used to locate the leaks, and blower doors and tracer gas to quantify the amount of air leaking.

2.2.3.1 Blower-Door testing

The most common utilization of the Blower-Door technique consists in mounting a variable-speed fan in a door, hence the generic term *blower door*. Blower-Doors can be used for component or multizone leakage measurements, but most measurements have been made for single-zone situations, such as single-family homes. The test can be

performed before completion of construction, to help find defects, or for retrofit purposes to improve an existing building. Blower-Doors are used to help locate leaks in the envelope, but the values generated are mostly used to estimate infiltration for both indoor air quality and energy consumption estimates (Sherman, 1995). When used to locate air leaks, the Blower-Door is normally used in conjunction with other methods, such as smoke pencil or thermography. The test itself consists in pressurizing or depressurizing the building, using the fan inserted in the door opening, and recording the airflow rate required to maintain the pressure. This is based on the requirement that the mass flow of air into the building equals the mass flow out. The leakier the building, the more airflow is necessary to induce a specific indoor-outdoor air pressure difference. The data collected therefore consists in pairs of pressures and airflow rates. Intentional openings, such as fireplaces and vents, are normally sealed during testing. It is recommended to perform the blower door test when wind and temperature differentials are sufficiently mild because the pressure differences they induce may interfere with the test pressures and cause measurement errors (ASHRAE, 1993). Because they vary with the weather under field conditions, blower door test results are not constant. This complicates the analysis of the data, and Sherman (1995) warns that the equivalent constant air leakage rate calculated from blower test data is "*not simply related to the average of the instantaneous values*". The readings are taken at a series of specified air pressure differentials. Usually ranging from 10 Pa to 75 Pa, those differentials are higher than those typically found under normal operating conditions. The standards also specify whether to pressurize, depressurize, or both, limiting weather conditions, pressure tap location, expression of results and stated accuracy. Standards that use blower testing to

evaluate air leakage in buildings and building envelope components in the field include the Canadian Standard CAN/CGSB 149.10 "Determination of the airtightness of building envelopes by the fan pressurization method", ASTM E 779-99 "Standard Test method for Determining Air Leakage Rate by Fan Pressurization", E 1827-96 "Standard Test Methods for Determining Airtightness of Buildings Using an Orifice Blower Door", and ASTM E 783-91 "Standard Test Method for Field Measurement of Air Leakage Through Installed Exterior Windows and Doors" (Sherman, 1995). The results from pressurization and depressurization are usually not the same, because the inward and outward flow paths through the envelope are not symmetrical.

The blower door test method can also be used to measure the leakage of a single component of a building. One way is to seal the component with a chamber on the interior side, and then pressurizing or depressurizing this chamber. Balancing the pressures in the chamber and in the room where the chamber is can improve the accuracy of this test by ensuring the leakage flow being measured occurs through the component, not around or through the chamber (Colliver et al., 1994). Another way is the *Selective Progressive Sealing*. This is an indirect method for determining air leakage through a component that has been sealed with an impermeable cover, which is assumed to stop airflow completely through the component. The test is first performed on the whole building and is then repeated with the component sealed. The difference between both results quantifies the air leakage through the component. There are potential problems with this procedure. Errors in accuracy that may occur when reading the total air leakage might make the errors in the differential readings quite large when compared with the actual values of the readings for the components, which are usually much smaller.

Another point is that there appear to be a hysteresis effect in the sealing order, where the reduction in building leakage does not match the increase in building leakage if the components are unsealed in a different order. This might indicate that the results are not independent of other sealed components and that it is common that some communication of air between the components being sealed exists (ASHRAE, 1993).

The relationship between the airflow through one opening in the building envelope and the pressure difference across it is called the *leakage function* of the opening. The form of the leakage function depends of the geometry of the opening. The most commonly used expression for the airflow rate through an opening is (ASHRAE, 1993):

$$Q = C_D A (2 \Delta P / \rho)^{1/2} \qquad \textit{Equation 2.7}$$

where:

Q = airflow rate [m^3/s]

C_D = discharge coefficient for openings, dimensionless

A = cross-sectional area of opening [m^2]

ΔP = pressure difference across opening [Pa]

ρ = air density [kg/m^3]

For the whole building, the relationship between the pressure difference across the building envelope and the airflow rate through the building envelope can be approximated by the *power law* equation (Colliver, 1994):

$$Q_f = c (\Delta P)^n \qquad \text{Equation 2.8}$$

where:

Q_f = airflow [m^3/s]

c = flow coefficient [$m^3/(s \cdot Pa^n)$]

ΔP = pressure differential [Pa]

n = flow exponent, dimensionless

The most common way of determining the values for C and n is to do a logarithmic transformation on the data in Equation 2.7 (ASHRAE, 1993):

$$lnQ = lnC + n\, ln(\Delta P) \qquad \text{Equation 2.9}$$

The value for n should be expected to lie between 0.5, approximating orifice or turbulent flow, and 1.0, approximating fully developed laminar flow (Colliver et al., 1994). The value for n often lies around 0.6.

The discharge coefficient C_D is a dimensionless number that depends on the opening geometry and the Reynolds number of the flow (ASHRAE, 1993). Low Reynolds numbers are characteristic of laminar flows, and high Reynolds numbers are characteristic of turbulent flows.

The airflow rate at a reference pressure can be converted to a leakage area by using the following equation (Sherman, 1995):

$$L = Q_r\ (\rho / 2\Delta P_r)^{0.5} / C_D \qquad \text{Equation 2.10}$$

where :

L = equivalent or effective leakage area [m^2]

ΔP_r = reference pressure difference [Pa]

Q_r = air flow rate at ΔP_r [m^3/s]

C_D = discharge coefficient, dimensionless

This method combines all the openings in the building envelope into an overall opening area and discharge coefficient for the whole building. "*The leakage area of a building is, therefore, the area of an orifice (with an assumed discharge coefficient) that*

would produce the same amount of air leakage as the building envelope at the reference pressure" (ASHRAE, 1993). The assumed discharge coefficient can be set at 0.6, which is that of a sharp-edged orifice. It can also be set at 1, meaning the shape of the opening offers negligible resistance to air flow.

Leakage areas at one reference pressure can be converted to leakage areas at another reference pressure by using the following equation (ASHRAE, 1993):

$$L_{r,2} = L_{r,1} (C_{D,1}/C_{D,2})(\Delta P_{r,2}/\Delta P_{r,1})^{n-0.5} \qquad \text{Equation 2.11}$$

where:

$L_{r,1}$ = leakage area at reference pressure $\Delta P_{r,1}$, [m^2]

$L_{r,2}$ = leakage area at reference pressure $\Delta P_{r,2}$, [m^2]

$C_{D,1}$ = discharge coefficient used to calculate $L_{r,1}$

$C_{D,2}$ = discharge coefficient used to calculate $L_{r,2}$

n = flow exponent

The flow exponent to be used is normally the one that is reported with the results. If it is not available, a value has to be assumed. According to the ASHRAE Handbook of Fundamentals (1993), using a value between 0.6 and 0.7 for the flow exponent is said to be reasonable.

Colliver et al. (1994) distinguish between effective and equivalent leakage areas. The Effective Leakage Area (ELA_4 or EfLA) uses a discharge coefficient of 1.0 and uses a pressure differential of 4 Pa. In the Equivalent Leakage Area (ELA_{10} or EqLA), the discharge coefficient is assumed to be 0.611, which is a value found to be representative of the types of openings found in building envelopes. It is calculated for a reference pressure differential of 10 Pa.

Whether an airflow rate at a specific pressure or an effective leakage area is used to rate the airtightness of a building, it is usually normalized to account for factors such as floor area, exterior envelope area, and building volume. Colliver et al. (1994) describe the Specific Leakage Area and the Normalized Leakage Area. The Specific Leakage Area (SLA_4 or SLA_{10}) is either the ELA4 or the ELA10 divided by the total floor area of the building. It enables to establish a basis for comparison of the leakage between different buildings. It has the advantage to be easy to obtain. However, one must determine if the basement is included, and whether the net area (area not including exterior walls) or gross area (outside dimensions) is used for the calculations. Depending on what is used, the number may vary widely. The leaks are in the envelope, which is generally not the same area as the floor area. The term Normalized Leakage Area (NLA_4 or NLA_{10}) takes into consideration the area of the building envelope that is exposed to the pressure differentials that drive airflow. This term includes all exposed surfaces above the grade line, ceilings, and floor above grade (but not the floor on a slab in contact with the soil). The Normalized Leakage Area is considered the most comprehensive and representative number of leakage for comparison purposes (Colliver et al., 1994).

Finally, Sherman (1995) has found that blower door data can also be used to approximate an air exchange rate at usual pressure differential by relating the seasonal amount of natural air exchange to the airflow necessary to pressurize the building to 50 Pascals with the following rule of thumbs:

$$ACH \approx ACH_{50} / 20$$ Equation 2.12

where:

ACH = number of air changes per hour at around 4 Pa.

ACH_{50} = number of air changes per hour measured at 50 Pa.

2.2.3.2 Tracer gas testing

The tracer gas test procedure is used to determine the air exchange rate of a building. A gas is injected to mark the indoor air and its concentration is monitored and related to the building's air exchange rate. Preferably, the tracer gas selected should be detectable, nonreactive, non-toxic, and have a low concentration in the ambient air (ASHRAE, 1993). One of three methods may be used: (1) the decay method, (2) the constant concentration method, and (3) the constant injection method. All these techniques are based on a mass transfer of the tracer gas within the building. It is assumed that the outdoor concentration of the gas is zero, and the mass balance equation takes the following form (ASHRAE, 1993):

$$V(dc/d\theta) = F(\theta) - Q(\theta)\, c(\theta)$$ Equation 2.13

where :

V = volume of the space being tested [m^3]

$c(\theta)$ = tracer gas concentration at time θ [ppm]

$dc/d\theta$ = time rate of change of concentration [ppm/s]

$F(\theta)$ = tracer gas injection rate at time θ [m^3/s]

$Q(\theta)$ = airflow rate out of building at time q [m^3/s]

θ = time [s]

To use this equation, it is assumed that no unknown tracer gas sources exist, that the tracer gas does not react chemically within the space, that it is not absorbed by surfaces, and that it is uniformly mixed in the space.

The decay method is the simplest. A small amount of tracer gas is injected into the space and is allowed to mix with the interior air. After the injection, $F = 0$ and the solution to Equation 2-13 is:

$$C(\theta) = c_0 e^{-I\theta} \qquad \text{Equation 2.14}$$

where I is the air exchange rate.

Equation 2-14 is solved for I by measuring the tracer gas concentration periodically during the decay and fitting the data to the log form of Equation 2-14:

$$\ln C(\theta) = \ln c_0 - I\theta \qquad \text{Equation 2.15}$$

This equation has the advantage of providing an exact solution to the mass balance equation (Equation 2-13). The most common problem when using the decay technique is the imperfect mixing of the tracer gas with the indoor air.

As the name implies, in the constant concentration technique, the injection rate is adjusted so that a constant concentration is maintained within the building. The initial mass balance equation then becomes:

$$Q(\theta) = F(\theta)/c \qquad \text{Equation 2.16}$$

No initial mixing period is needed for the constant concentration method. It should be taken into consideration however that imperfect mixing causes a delay in the response of the concentration of the gas to changes in injection rates. This would make it impossible to keep the tracer gas concentration constant. The absolute tracer concentration and injection rates are required to use this method. Equation 2-16 should

not be considered as an exact solution, but rather as an approximation. This method is not widely used.

The third tracer gas measurement method is the constant injection method, where the tracer gas is injected at a constant rate. The solution to the initial mass balance equation (Equation 2-13) becomes:

$$c(\theta) = (F/Q)\ (1-e^{-I\theta}) \qquad \text{Equation 2.17}$$

The transient term eventually reduces to zero and the concentration reaches equilibrium. Equation 2-17 reduces to:

$$Q = F/c \qquad \text{Equation 2.18}$$

This method is only valid for systems at or near equilibrium, i.e. when the air exchange rate is constant. Absolute concentration and injection rate measurements are required.

2.3 Review of some previous experimental work

In the previous sections of this chapter, the basic building envelope components and the transfer mechanisms they are subjected to, i.e. heat, moisture and air transfer, have been described. Experimental work has been performed to study the hygrothermal performance of various building envelope specimens when subjected to these three transfer mechanisms. In this section, experiments conducted in laboratory settings are reviewed. Table 2.1 provides an overview of some of this previous work. The experiments are listed in reverse chronological order. From these, information is provided on testing procedures, such as specimen configuration, monitoring protocol and climatic conditions, that permits and assessment of the significance of each study.

The specimens studied in the experiments included in Table 2.1 were residential wood frame exterior wall assemblies. In most cases full-scale wall specimens, including two or three stud spaces and one storey high, were used. Full-scale specimens are more realistic because available materials and field construction techniques can be used. They also eliminate the need to make assumptions regarding scaling effects of heat, air, and moisture transfer.

Fazio et al. (1998) studied roof assemblies, but their work is included because the objectives and experimental protocol are relevant to the present research project. They studied two types of single-cavity flat roof assemblies normally un-insulated in the field, which were packed with cellulose fiber. Air leakage paths commonly occurring in the field were studied, i.e. the intersection with the interior partition and the exterior wall. For each type of roof assembly, three sections had moisture transfer by exfiltration and diffusion, one section had transfer by diffusion, and one section was left without insulation to serve as a reference.

Ojanen and Simonson (1995) studied a wall/wall junction and a wall/roof junction. Those assemblies were investigated with different re-insulation strategies and exterior sheathing and vapour barrier materials. The impact of air barriers was studied in Ojanen and Kohonen (1995), Trechsel (1986), and Trechsel (1985). In some of the experiments, moisture was introduced directly into the assemblies (Ojanen and Kohonen, 1995) to study their mode of drying. In others, interior air was allowed to flow through the wall assemblies. For example, Trechsel (1986) made holes in the interior finish (two at the top and two at the bottom) at the beginning of the test, where as in another experiment, Simpson (1994) added holes mid-way through the experiment. In both cases, the

openings did not represent any specific air leakage path. In his experiment, Trechsel (1986) also provided holes that could be hermetically sealed to allow the introduction of tracer gas.

The duration of the exposure to wetting climatic conditions varies from a series of 5-day tests (Trechsel et al. 1985 and 1986) to 242 days for two consecutive periods (Simpson and O'Connor, 1994). The shorter 5-day period allowed Trechsel et al. (1986) to compare moisture accumulation in the different specimens. However, due to the longer time constant required by moisture transfer to attain equilibrium, this short test period does not give an idea of the moisture levels that would be reached under real operating conditions and therefore prevents from establishing if conditions favouring growth of mold and rot would be attained. Ojanen and Kohonen (1995), Ojanen and Simonson (1995), Simpson and O'Connor (1994), Verschoor (1986), and Trechsel et al. (1985 and 1986) conducted their tests under steady-state temperature conditions where as Fazio et al. (1998) and Zarr et al. (1995) included sine wave temperature changes to monitor time-dependent transfer of heat and moisture. As for the exterior temperatures, they varied from 7.2°C for mild winter conditions (Zarr et al., 1995) to -18°C for extreme Swedish winter conditions (Ojanen and Simonson, 1995). In most cases, the selection of the exterior temperature conditions were linked to a particular climate, although Simpson and O'Connor (1994) used theoretical predictions to determine conditions under which interstitial condensation would occur and applied these as exterior boundary conditions. Fazio et al. (1998) and Ojanen and Kohonen (1995) applied positive air pressure differentials to the specimens. The others applied only temperature and water vapour pressure differentials across the specimens. In Fazio et al. (1998) and Zarr et al. (1995),

the specimens were also subjected to drying conditions - exterior temperatures were increased to simulate spring to summer weather - after moisture had accumulated. The drying was performed in order to provide a more complete picture of the hygrothermal behaviour of the assemblies studied.

All experiments used methods to keep track of moisture distribution in the materials of the assemblies. In some cases, moisture content sensors consisting of two metal pins inserted in the material at a specified distance were used. The resistance to electric current between the two pins, which is inversely proportional to the moisture content of the material, is measured. The relationship between the resistance and the moisture content is specific to each material. Therefore, the sensors need to be calibrated for each material they are inserted into. One such calibration procedure is described in Zarr et al. (1995). Gravimetry is another method used to monitor moisture contents of the materials. This procedure consists in weighing samples from the specimen (or the whole specimen, as in Verschoor (1996)) and then drying them to determine the moisture content per dry weight. The samples may be collected and weighed once at the end of the testing period, as in Ojanen and Simonson (1995), providing only the moisture content per dry weight at this time. They can also be collected throughout the test using reusable samples, as in Fazio et al. (1998). This allows to follow variations in moisture content over time, and provides information on the rate of moisture accumulation. It is especially useful when the testing periods are long. In one case (Ojanen and Kohonen, 1995), condensation water was collected at the bottom of the specimen. In that test, moisture distribution (the mass of moisture in each layer) was also recorded.

Temperatures were monitored using Type "T" thermocouples, consisting of one copper and one constantan wire. In some cases, they were installed at different depths within the materials of the specimens (as in Zarr et al., 1995) to get the temperature gradient across the material. In other cases, they were installed on the surfaces of the material layers. For example, Ojanen and Simonson (1995) monitored temperatures at the interface between the new and the old construction to get an indication of the airflow pattern at this plane. The results, showing temperatures 7°C to 15°C higher at the top than at the bottom of the assemblies they tested, led them to conclude that warm air entered at the top of the wall and cooled while flowing down the structure, along the air leakage route.

Trechsel et al. (1985 and 1986) used tracer gas (SF_6) to get a sense of the airflow. A specific quantity of gas was injected in the assembly through holes in the interior finish of the specimens, and samples were taken at regular intervals to measure the concentration of remaining gas. Air leakage measurements were also performed on the two test huts by Derome et al. (2000). This approach, a variation of the selective sealing approach for blower-door testing described in section 2.2.3.1, is suitable when the roof (or walls) of a test hut is divided into sample sections.

Table 2.1 Summary of some previous moisture transfer laboratory experiments.

Authors	test duration/ conditions	test setup
Fazio, P. Derome, D. Gerbasi, D. Athienitis, A. Depani, S. (1998, 1999) Derome, D. Fazio, P. (2000)	Complete wetting/drying weather cycle for the city of Montreal: (daily sinusoidal temperature curve for all exterior temperature conditions) - Period 1 (Nov. 8 to Dec. 31) Ext.: -7°C to 0°C, Int.: 23°C, 50% RH - Period 2 (Jan. 1 to Feb. 8) Ext.: -11°C to -3°C, Int.: 22°C, 40% RH - Period 3 (Feb. 9 to April 8) Ext.: -8°C to 6°C, Int.: 23°C, 55% RH - Period 4 (April 9 to April 29) Ext.: 1°C to 20°C, Int.: 21°C, 45% RH - Period 5 (April 30 to May 29) Ext.: 9°C to 27°C, Int.: 21°C, 45% RH - Period 6 (May 30 to June 28) Ext.: 13°C to 35°C, Int.: 23°C, 50% RH - Period 7 (June 29 to July 14) Ext.: 16°C to 38.5°C, Int.: 23°C, 50% RH	SPECIMENS: - 2 test huts built on top of each other inside an environmental chamber. Each represents a type of single-cavity flat roof assembly, packed with cellulose fiber. - Roofs are divided in 5 cavities, 4.8 m X 0.8 m: 3 with moisture transfer by exfiltration and diffusion, 1 only by diffusion, 1 without insulation to serve as a reference - Main leakage paths (as field) located at the intersection with the interior partition and with exterior walls. MONITORING (262 sensors in total): - Temperatures: Type "T" thermocouples installed at both surfaces of the wood planking, in the insulation and at the warm side of the wood joist. - Moisture content sensors: pins inserted at specific distance in the joists and the planking - Gravimetry: 40 samples taken from planking and joists, 80 from cellulose throughout the whole experiment. - Relative humidity: capacitance sensors installed in the cellulose insulation.
Zarr, R.R Burch, D.M. Fanney, A.H. (1995)	Interior conditions: 21°C, 50% RH 104 days in total: - 42 days at 21°C , 50% RH (pre-conditioning) - 1 day at 7.2°C steady-state (preparation for the 1st cycle) - 6 days of daily sine waves, 1.1°C to 15.6°C (transfer in dry walls) - 34 days at 7.2°C steady-state (moisture accumulation period) - 7 days of daily sine waves, same as first series (transfer in moist walls) - 14 days at 32°C (drying)	SPECIMENS: - 12 small wall samples (1.0 m X 1.1 m) were studied simultaneously in a calibrated hot box. - A circular "carrot" was cut in the middle of each to ensure one-dimensional heat and moisture transfer. - Specimens consisted of 3 or 4 layers, typical of residential wood-frame construction: gypsum board, glass fiber or loose-fill cellulose fiber, fiberboard or plywood sheathing, foil-faced polyisocyanurate in some, pine or vinyl siding. - Holes were made in 2 of the specimens to allow air leakage, 11.5 mm and 7.9 mm in diameter respectively. MONITORING: - Temperatures: Type "T" thermocouples, at different depths in the center of the specimen. - Moisture content sensors: electrical resistance method (moisture pins), applied to interior and exterior surfaces of sugar pine, interior surfaces of plywood and fiberboard.

Ojanen, T. Kohonen, R. (1995)	- Interior conditions: 20°C - Different air pressure differentials were used for each sample: 3 Pa/m for #1, 65 Pa for #2, and 35 Pa for #3. Climatic conditions: - 20 days at -10°C, 70% RH - 15 days at 3°C, 60% RH - Moisture was fed into the structure by a continuous wetting of a capillary saturated cellulose fiber layer between insulation and vapour barrier (for 1rst 20-day period)	SPECIMENS: - Large scale tests on 3 samples 2.2 m X 0.33 m typical of Swedish residential timber-frame construction with glass fiber batt insulation. - Inside surface of structure was assumed to be totally airtight: no infiltration or exfiltration. MONITORING: - Condensation water collected at the bottom of the specimen. - Results presented in terms of mass of water per layer of material.
Ojanen, T. Simonson, C. (1995)	Interior conditions: 22°C, 40% RH - 50 days at -18°C, except for 5 thawing cycles. (no mention of air pressure differential.)	SPECIMENS: - 50 mm mineral wool or expanded polystyrene added on inside surface of walls typical of Swedish residential construction. - In some, a gap was left between the existing structure and the new layer of insulation, in others, the two layers were in contact. The existing wall was assumed to be airtight - A new vapour barrier was added to all specimens, in some cases existing vapour barriers were kept. MONITORING: - Temperature fields were measured at the interface between the old and the new construction. - Moisture contents: small wooden samples were placed at the interface between the internal sheathing of the old wall and the additional insulation, in the center of the wall at the stud and distributed along the height of the wall. The wood samples were weighed and dried at the end of the 50-day test period.
Simpson O'Connor (1994)	- 66 days, "wet" cycle: Interior conditions: 20°C, 60% RH Exterior conditions: 0°C, 80% RH, samples intact - 176 days, "dry" cycle: Interior conditions: 20°C, 25% RH Exterior conditions: 0°C, 55% RH	SPECIMENS: - 2 specimens 2.9 m high by 0.62 m wide. - for the first cycle, the walls were intact, in second half of the test, one is perforated with 1 hole 20 mm in diameter, the other with 2 holes. MONITORING: - Temperature measured with thermocouples on each surface, and at various points. - Moisture contents were monitored using electrical resistance probes distributed over the surface of the specimen. - Temperatures and moisture contents were logged every day.

Verschoor, J.D. (1986)	- exterior conditions: -7°C, almost saturated air - interior conditions: 21 °C, 50% RH - pressure differentials of 0, 25 (equivalent to winds of 24 km/h) and of -25 Pa were induced. - exposure to conditions until rate of moisture change appeared uniform, 1 to 4 weeks	SPECIMENS: - specimens: 38mm X 89mm studs; 7 layers of mineral wool, 13mm each (easier observation and installation of thermocouples in the insulation), fiberboard, aluminium siding; MONITORING: - Temperatures were measured daily between the insulation layers, in the central portion of the specimen. (allowing to follow the temp. grad.) - The moisture content of the whole assembly was measured by gravimetry. The whole assembly was rotated and weighed daily.
Trechsel, H.R. Achenbach, P. Knight, H.J. Lou, G.W. (1986)	- Series of 5 day tests: Interior conditions: 21°C, 30% RH. Exterior conditions: -1°C, 70% RH. - Pressure differentials of 0, 25, and 75 Pa were applied, depending on the test.	SPECIMENS: - The test specimen in the chamber included 3 panels of 1.2m X 2.7m, with 3 stud spaces each. - The central stud space had 13 mm diameter openings, 2 at top and 2 at bottom. MONITORING: - Individual surface temperatures at each location measured on both sides of the sheathing and interior plywood. Mid-insulation temperatures also measured. They were recorded every 15 minutes, averaged for every 6-hour period and again for the last 3 days of the 5-day period. - Moisture accumulation in the sheathing measured by weighing samples from the top and bottom sample ports at the start and end of each test, and by 3 electric gauges at the top, middle, and bottom, 2 to 3 times daily. - Moisture accumulation in the insulation was only measured by weighing samples for the top and bottom sample ports. - Air movement was determined by injection of tracer gas (SF_6) at the center of each of the 3 stud spaces. The tracer gas was injected through holes that could be sealed.

Trechsel, H.R. Achenbach, P. Ebbets, J.R. (1985)	- series of 5-day tests, or until moisture has ceased to increased. - The conditions represent moderate and cold climates over extended periods of time: Interior conditions: 70°F, 30% RH for all. Exterior conditions: 1. 30°F, 70% RH 2. 10°F, 40% RH 3. 30°F, 70% RH 4. 30°F, 70% RH	SPECIMENS: - The specimen consisted of three 1.2 m X 2.7 m panels with 3 stud spaces each, insulated with glass fiber batt insulation, interior finished with plywood painted with aluminium paint as a vapour barrier. - the sheathing and siding had different air leakiness by providing holes. - 13 mm diameter holes were connected to provide closed air loops at the top and bottom in which air was pumped. MONITORING: - Temperatures were measured in the center of the insulation at the top, mid-high, and bottom of the center stud space. Surface temperatures were measured on the exterior of the siding, on the exterior and interior side of the sheathing and the plywood panel. - Moisture contents in the sheathing were monitored by 12 moisture probes, to observe trends in moisture levels. - Sheathing and insulation samples were weighed and dried. - The air exchange rate was measured with tracer gas injected in the assembly.

2.4 Review of some heat, air, and moisture transfer computer models

Experiments conducted on exterior wall assemblies, such as those described in the previous section, provide useful information on their hygrothermal behaviour. However, they are time consuming and expensive. Computer models, on the other hand, can be used to evaluate the hygrothermal behaviour of exterior wall assemblies in a relatively short amount of time. The experimental and modeling approaches are complementary and should both be used. As stated in the Final Report of Annex 24 of the International Energy Agency (Hens, 1996), "models help in understanding experiments and experiments help in verifying, validating and upgrading models". Ideally, the experimental data generated from the test to be performed in the present research project should be used to validate or verify existing computer models. A brief review of some existing models was performed within the frame of Annex 24 of the International Energy Agency (Hens, 1996).

Assemblies are exposed to simultaneous heat, air and moisture transfer under real operating conditions. In modelling, these transfer mechanisms should therefore be considered 2- or 3-dimensionally. However, the Annex 24 review demonstrates that no matter how advanced they are, models are still limited by the geometry of the assembly, the boundary conditions and the numerical mathematics (Hens, 1996). Furthermore, material properties are not constant over a range of conditions. For example, vapour permeability is a function of temperature, moisture content and vapour flow direction, and thermal conductivity is a function of temperature, moisture content, time and heat flow direction (Hens, 1996).

Of all the models reviewed by Annex 24, very few were considered to (nearly) fully take all the phenomena into account. In addition, the reliability of those models simulating convection could be improved with specific information about the trajectory of air in the assemblies.

2.5 Conclusions

It has been seen that moisture from indoor getting into exterior wall assemblies can deteriorate their materials. Although moisture transfer by diffusion cannot be neglected, air exfiltration is the principal transfer mode for moisture from indoors into the assembly. According to a survey on the airtightness of residential single family buildings in Canada (Hamlin and Gusdorf, 1997), houses built in the 1970's and 1980's - which generally would benefit from additional insulation - are leakier than more recent construction in Quebec and subject to improvement by their owners. Done in the context of energy efficiency retrofit measures, could adding insulation to existing leaky exterior walls increase the potential for moisture-related problems?

As previous experiments showed that moisture accumulation tends to occur in the wall assembly opposite the air entry point, more knowledge about the path of air leakage in walls with added insulation is necessary to estimate where moisture may accumulate and to develop guidelines for retrofit work.

Few experimental works have dealt with the addition of insulation in existing assemblies. In Fazio et al. (1998), blown cellulose fiber was added to existing non-insulated roofs. An experiment on walls with added insulation (Ojanen and Simonson, 1995) considered insulation added on the warm side of airtight assemblies. Previous experiments have attempted to quantify the air leakage rate or to estimate the direction of airflow, but none provided detailed information on the path of air leakage inside the wall assembly, nor on the temperature and moisture content variation along that path.

No previous experimental work considered existing leaky walls with added insulation. Furthermore, there is a lack of information on the path of exfiltrating indoor air inside the wall. The following work looks at the impact of adding insulation to envelopes that have different air leakage paths.

3. EXPERIMENTAL PROTOCOL

This project investigates air leakage through the envelope, first by looking at its role on re-insulated assembly hygrothermal performance, and second, by proposing a method for the mapping of air leakage through extensive moisture content and temperature monitoring and the production maps of different air leakage paths within the assemblies using the moisture content and temperature data.

3.1 Development of the protocol

To document the hygrothermal performance of re-insulated assemblies, the specimens should be full scale and built using materials and techniques commonly found in the field. The specimens are therefore included in a full-scale test hut, 4.2 m long by 2.5 m wide by 3 m high, built inside the environmental chamber. The test hut models the second storey of a two-storey single-family house in Quebec, built in the 1970's or 1980's, which typically could benefit from added insulation. The base-case exterior wall assembly is a platform frame system with 38 mm x 89 mm wood and with glass fiber batt insulation between the studs. Adding insulation between the studs is therefore not considered. Two re-insulation strategies are studied. The first strategy is to add insulation on the cold side of the wood studs, over the existing exterior sheathing. As removal of the exterior veneer is necessary for re-insulating a house by the exterior, this method would be used in the case when the exterior veneer needs to be replaced. Airtightness can then be improved from the outside, by sealing the sheathing or the insulation panels. The second strategy is to add insulation on the inside of the assembly, on the warm side of the wood studs and glass fiber batt insulation. This method would be used if interior renovations are being performed and removal of the existing interior

finish is necessary. The airtightness of the assembly can be improved from the interior. If both the interior and exterior finishes appear to be in good condition, either of these two re-insulation strategies could be used to increase the thermal resistance of the exterior wall assembly. The insulation material selected for both re-insulation strategies is a 38 mm rigid board of extruded polystyrene. This insulating material is often selected by homeowners due to its high thermal resistance per unit of thickness and because it has the advantage of not being sensitive to water that might penetrate behind the cladding. The weather barrier can also be mechanically attached to it. Whether it is added on the cold or warm side, the installation of this insulation material does not require additional wood framing.

To study the impact of air leakage, the three exterior wall compositions described above are studied with three different air leakage paths through intentional openings simulating typical conditions. The first path provided is a *long* air leakage path. The air enters through a narrow crack at the bottom of the wall, flows up inside the wall and exits at the top of the exterior sheathing panel. This is the case when the gap between the interior finish and the floor, and between sheathing panels are not sealed properly. The second is a *concentrated* air leakage path. The air enters through a circular opening, concentrated in one area of the interior finish, and flows out through the whole surface of the exterior sheathing. This might occur, for example, when air exits through an electrical outlet but there is not necessarily a corresponding hole on the cold side of the assembly. The third path, a *distributed* air leakage path, consists of a series of small holes uniformly distributed across the surface of the interior finish. Though this type of air leakage is not likely to occur in buildings, it is included to get experimental results for

a uniform airflow across the surface of the assembly. The openings for the long and concentrated leakage paths have the same area, only their distribution across the specimen is different. This allows to evaluate the impact of the air leakage path on the hygrothermal performance of the assemblies, not the impact of the leakage area or air leakage rate.

The test hut is exposed consecutively to simulated winter, and then spring, outdoor weather conditions. Only outdoor temperatures are considered, not sun radiation or wind. It is assumed that all facades are facing north. Weather data collected for Montreal over the last 12 years are used to determine the conditions in the climatic chamber. The conditions inside the test hut are based on the conditions proposed by the Standard ANSI/ASHRAE 55-1992 "Thermal Environmental Conditions for Human Occupancy". It is assumed that the two storeys are connected and that openings are uniformly distributed between the two floors. The neutral pressure plane is then at mid-height of the house and the second storey is subjected to a positive air pressure differential during the winter months, due to the stack effect. Exfiltration is induced because it represents a worse case scenario than infiltration, which is not desirable for comfort and energy efficiency considerations but is not as likely to cause moisture related damages.

To monitor the performance of the envelope assemblies, temperature and moisture contents are measured across the assemblies throughout the test. By increasing the amount of sensors and placing them according to a pre-defined grid pattern, the results can be used to develop temperature and moisture content maps.

Hence, *moisture content marking* is used to track the path of air. It is based on the hypothesis that as air exfiltrates, the moisture it contains is adsorbed by hygroscopic

materials of the assembly. Moisture content maps establish a relationship with air leakage patterns. This requires 2-dimensional moisture content monitoring in the hygroscopic layer found in most residential assemblies, the exterior sheathing.

Temperature marking is also used to track the path of air. Following the hypothesis that exfiltrating air would warm the materials it comes in contact with, it may be possible to establish a relationship between the measured temperatures within the assembly and the air leakage pattern. To visualise the effect of air leakage on temperature profiles within the assembly, temperature maps are generated. A 2-dimensional grid temperature monitoring is implemented in order to provide data for the production of those temperature maps. To provide more complete information, this temperature monitoring is performed at two different planes within the wall assemblies, thus becoming 3-dimensional temperature monitoring.

3.2 Experimental Facility

The Environmental Chamber is a research facility where the overall hygrothermal performance of exterior walls, with or without doors and windows and/or roofs, can be evaluated. Figure 3.1 illustrates the main components of the Environmental Chamber Facility that was used. For the present test, the facility is used in the environmental chamber mode, shown in Figure 3.2. The cold and hot boxes are joined, forming a 7.5 m high by 4.4 m wide by 10.5 m deep climatic chamber.

- The **cold box** is a 7.5 m high by 4.4 m wide by 3.6 m deep chamber, in which temperatures ranging from -40°C to 50°C can be maintained. The conditions are produced using a 5 ton screw compressor, a 12,000 cfm re-circulation fan and a 25 kW re-heating heater. This box is fixed on the ground. Its walls are

made of 150 mm foamed polyurethane boards, laminated between 1 mm aluminium sheets outside and 1 mm stainless steel sheets inside.

- The **hot box** is a 7.5 m high by 4.4 m wide by 6.1 m deep chamber, heated with a 20 kW heater and cooled with a 1.5 ton cooling unit. Temperatures ranging from 5°C to 50°C can be obtained. This hot box is equipped with a 600 cfm air re-circulation system, a fresh air supply/return damper and a humidification system. 4 compressed air pads afford movement to and from the cold box. The composition of the walls is the same as for the cold box.
- The **data acquisition system**. It has 400 input channels and 10 output channels. Readings are taken every 10 minutes for each measurement point.

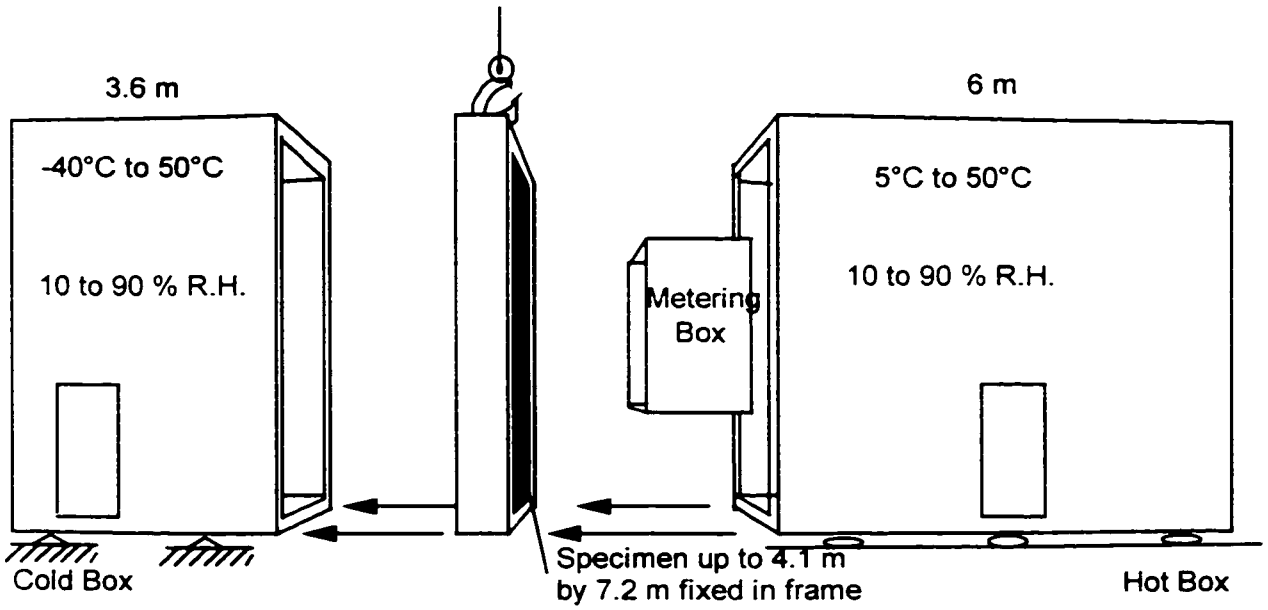

Figure 3.1. Environmental Chamber Facility (Fazio et al., 1998).

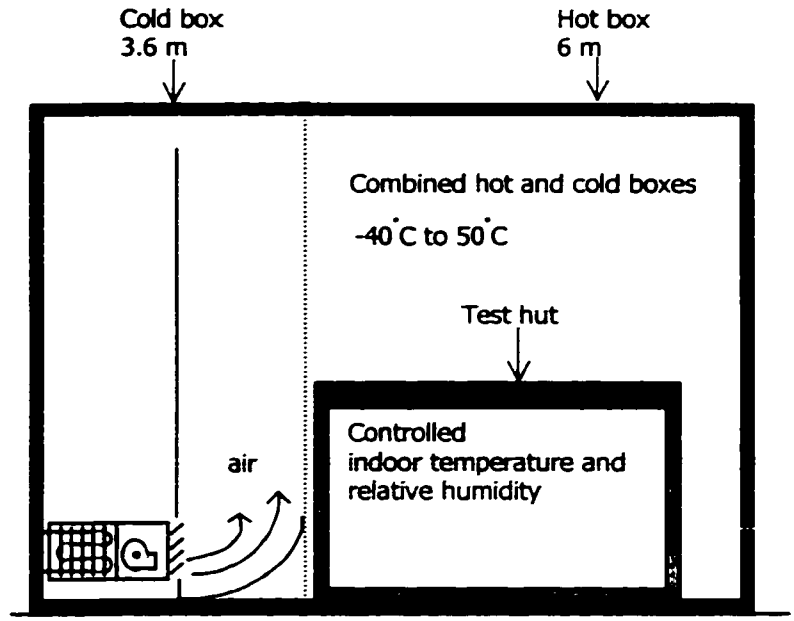

Figure 3.2. Environmental chamber in climatic chamber mode (Derome et al., 1997).

3.3 Description of the test setup

The three wall compositions and three air leakage paths described in section 3.1 are combined to investigate the impact of the air leakage characteristics on the temperature and moisture content in the basic assembly and those with added insulation. Ideally, each composition would have been tested with all three air leakage paths, and with an airtight configuration to serve as a reference, for a total of 12 specimens. However, the space limitations within the environmental chamber allowed only 9 specimens. The base-case assembly (with no insulation added) and the base-case assembly with rigid insulation added on the cold side, are tested with all three air leakage paths. The base-case assembly with insulation added on the warm side is tested only with the long and the concentrated air leakage paths. The distributed air leakage path is omitted when insulation is added on the warm side because the insulation is assumed to be airtight, and therefore holes in the interior finish would not really affect the results. The base-case

assembly serves as the reference to evaluate the impact of added insulation and of the different air leakage paths on the temperatures and moisture contents. It is therefore the only one that will be tested in an airtight configuration. This reduces the total of specimens to nine. Figure 3.3 is a schematic plan view of the test hut that shows the location of the different sample sections. The shorter end walls were part of another project and will not be discussed in the present thesis.

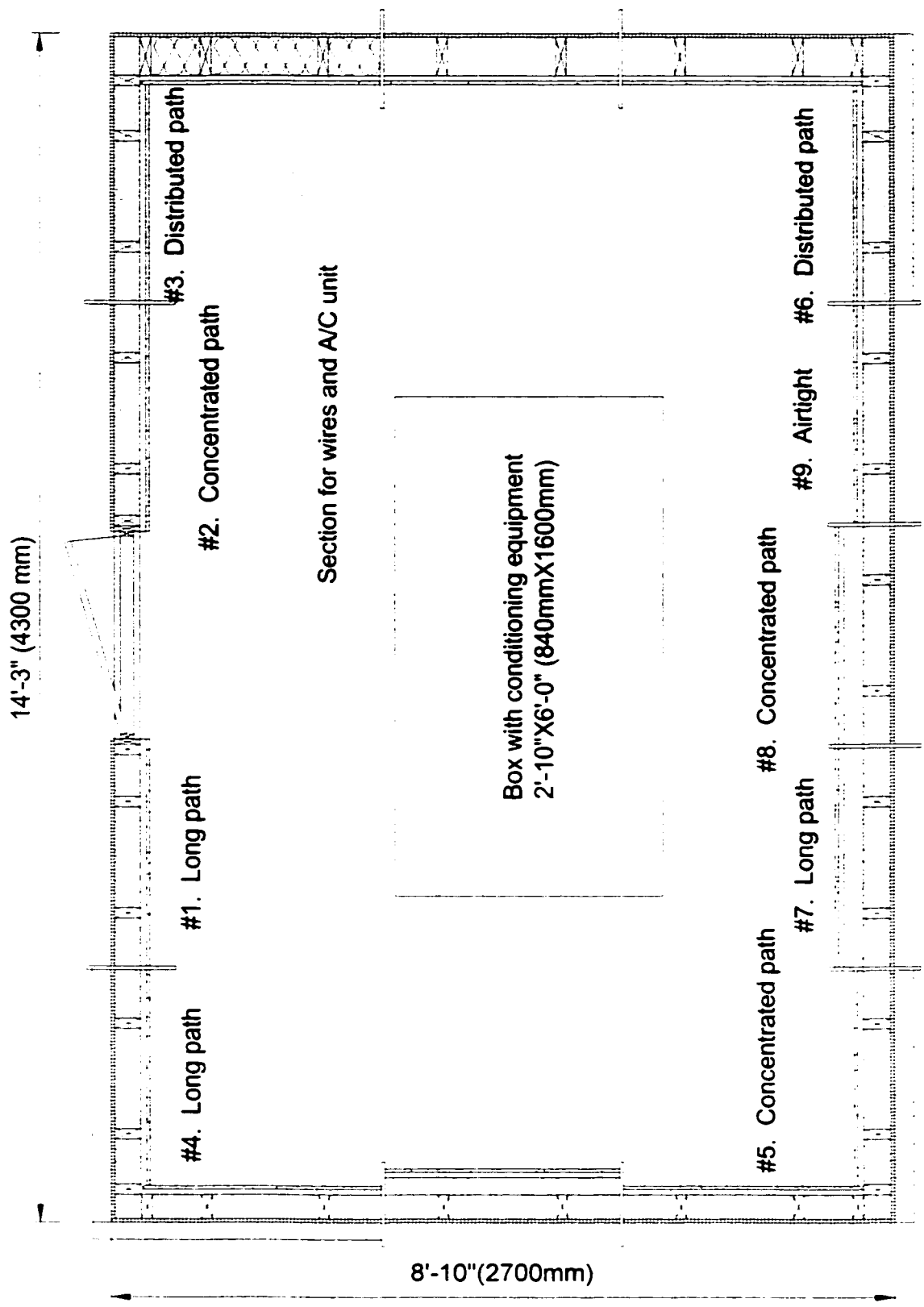

Figure 3.3. Plan view of the test hut.

The nine sample sections being studied are 800 mm wide by 2.4 m high. A sample section is defined as one complete 360 mm cavity, flanked on each side by a 38 mm X 89 mm stud and a 180 mm cavity. This width of the central portion reflects the usual spacing between wood studs, which is 400 mm on center. The width of the two portions on each side is half of this space. Each sample section is completely insulated according to the insulation strategy being investigated. Monitoring is performed only in the 400 mm central portion. The two half-cavities act as insulated *buffers* between the sample section and the adjacent ones. The sample sections are separated by Oriented Strand Board panels (OSB), 16 mm thick by 300 mm wide to prevent moisture and air transfer between the sample sections (see Figure 3.4). The OSB panels are painted with two coats of vapour barrier paint and are wider than the assemblies to facilitate caulking of the interior finish against them. The panels are sealed to the bottom and top plates. At the roof level, OSB panels spanning the width of the test hut are sealed to the top plate and to the OSB panels separating the wall sample sections.

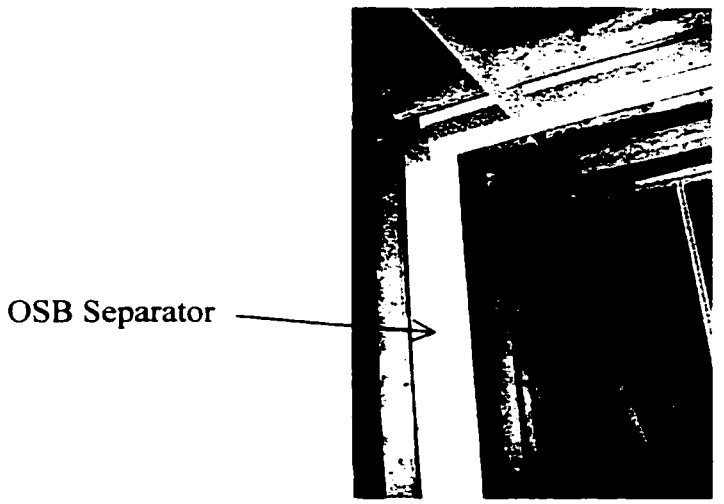

Figure 3.4. Test hut wood structure and OSB separators.

3.3.1 Composition of the assemblies

Statistics from the "l'Association provinciale des constructeurs d'habitations du Québec" (APCHQ) were used to select the construction materials of the assemblies.

The junction between the exterior walls and the roof is built using commonly used techniques and materials. The set up simulates a typical ventilated roof. Although it is not directly monitored, the junction of the roof is included in the overall hygrothermal behaviour of the specimens.

The composition of the roof, from outside to inside, is:

- waterproofing membrane;
- 13 mm plywood;
- 38 mm x 140 mm wood joists @ 400 mm o.c.;
- 250 mm air space (ventilated to outside);
- 38 mm x 140 mm wood joists @ 400 mm o.c.;
- 250 mm of glass fiber batt insulation;
- 6 mil polyethylene sheet;
- 19 mm x 64 mm @ 400 mm o.c. wood strapping;
- 13 mm gypsum board;
- latex paint (two coats).

The base-case wall composition, simulating typical existing conditions without modifications, is:

- Spun bonded polyolefin membrane;
- 10 mm asphalt impregnated fiberboard;
- 38 mm x 89 mm @ 400 mm o.c. wood studs;
- 89 mm glass fiber batt insulation between the studs;
- 6 mil polyethylene sheet;
- 19 mm x 64 mm @ 400 mm o.c. horizontal wood strapping;
- 13 mm gypsum board;
- latex paint (two coats).

In these compositions, the spun bonded polyolefin sheet serves as a wind/weather barrier and the asphalt-impregnated fiberboard is the sheathing. The wood studs give the structural strength to the wall. The insulation minimizes conductive heat losses. The

wood strapping is used, among other reasons, to: minimize the staining of the interior finish that frequently occurs in front of the cold wood studs, protect the air/vapour barrier from being perforated by nails used to hang pictures, provide a straighter base to install the interior finish on, and allow running of electrical and telephone wires. The polyethylene sheet acts as an air/vapour barrier. The gypsum board is the interior finish, which is then painted with two coats of latex paint.

For the sections with insulation added on the cold side, the rigid extruded polystyrene (38 mm) is added directly outside the existing fiberboard sheathing. In the case of the sections with insulation added on the warm side, the rigid extruded polystyrene (38 mm) is added on the warm side of the wood studs and glass fiber batt insulation. Installation of the air/vapour barrier membrane, wood strapping, and interior finish then follows.

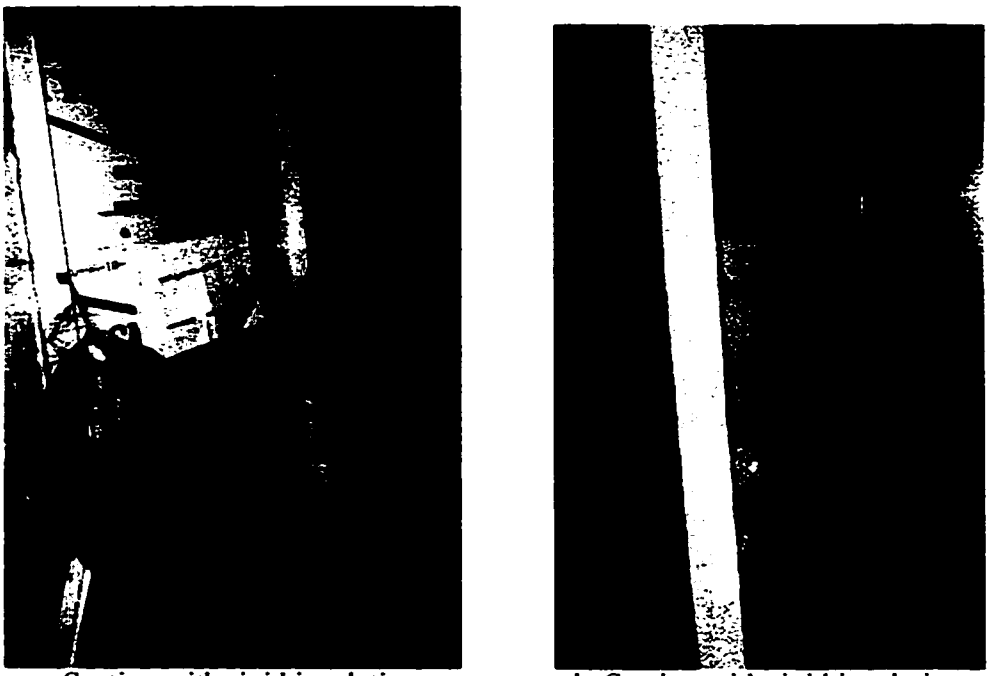

a. Section with rigid insulation added on the warm side.

b. Section with rigid insulation added on the cold side.

Figure 3.5. Sections with added extruded polystyrene insulation.

Figure 3.5 above shows one sample section with rigid insulation added on the warm side of the glass fiber batt insulation (before the installation of the air/vapour barrier, the wood strapping, and the interior finish) and one with rigid insulation added on the cold side of the glass fiber batt insulation (before the installation of the spun- bonded polyolefin membrane). The composition of the assemblies is illustrated in Figure 3.6.

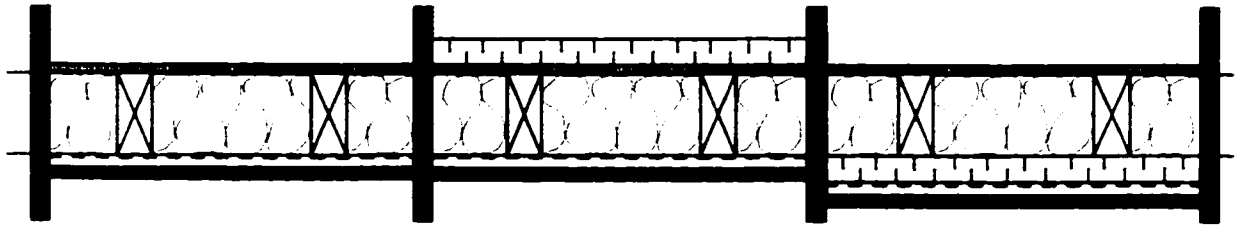

Figure 3.6. Composition of the specimens.

3.3.2 Air leakage characteristics

The wall compositions described above are studied with the following air leakage characteristics, as illustrated in

Figure *3.7.*

- Long air exfiltration path: Air enters the wall through a 2 mm by 360 mm horizontal opening (between the wood studs) at the bottom of the interior finish and out through a 5 mm high horizontal opening at the top of the exterior sheathing, just below the top plate. The polyethylene membrane is not sealed at the bottom of the section.

- Concentrated air exfiltration path: Air flows into the wall through a 30 mm diameter opening in the interior finish (centred between the studs, 300 mm above the floor) and out through the whole surface of the fiberboard sheathing on the exterior side of the assembly.
- Distributed exfiltration path: Air flows into the wall uniformly through 42 holes, 4 mm in diameter (spaced 50 mm o.c. horizontally and 300 mm o.c vertically), drilled in the interior finish. There are no holes through the fiberboard sheathing.

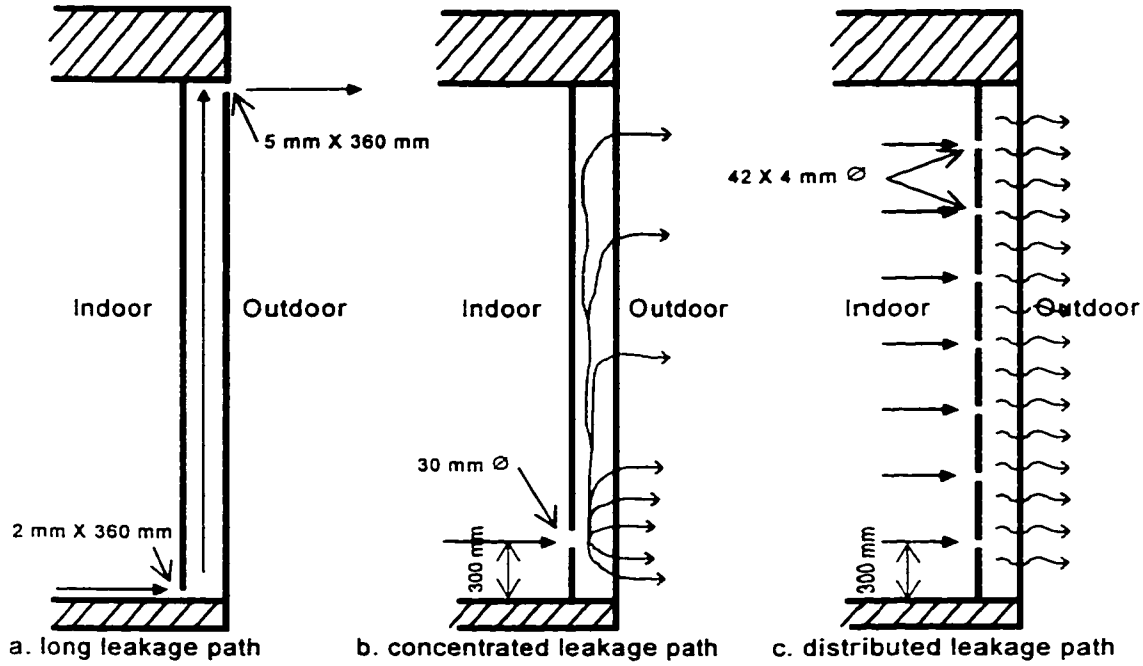

Figure 3.7. Air leakage paths.

From a survey conducted on the airtightness of house across Canada (Hamlin and Gusdorf, 1997), it was found that the average normalized leakage area at a reference pressure of 50 Pa was 5.20 cm^2 per 1 m^2 of building envelope for houses built in Quebec between 1971 and 1980. Using equation 2.11, the leakage area at 50 Pa may be

converted to a leakage area at 4 Pa, which is the air pressure differential in the test hut during the wetting conditions. For the calculations, it is assumed that the discharge coefficient C_D is the same in both cases and that the flow exponent n is 0.65, between turbulent and laminar flow. This gives a leakage area of 3.56 cm^2 per m^2 of envelope. Since each section is 2 m^2, this means 7.12 cm^2 per section. The areas of the openings for the long and the concentrated leakage paths are based on this, being 7.2 cm^2 for the long leakage path and 7.1 cm^2 for the concentrated leakage path. Their total area is the same; it is their distribution in the surface of the sample section that is different. The total area of openings for the distributed leakage path is 5.3 cm^2. The number of holes that could be made was limited because of the presence of the wood strapping and of the thermocouples on the warm side of the batt insulation. The intention was also to keep them as small as possible, and not to have them too close together. This explains the smaller area of openings for the distributed leakage path.

3.3.3 Summary of sample sections

Table 3.1 presents a summary of the nine insulation strategy/air leakage path combinations studied.

Table 3.1. Sample sections parameters

Section number		89 mm glass fiber only	38 mm polystyrene added on the exterior side	38 mm polystyrene added on the interior side
1	Long leakage path	■		
2	Concentrated leakage path	■		
3	Distributed leakage path	■		
4	Long leakage path		■	
5	Concentrated leakage path		■	
6	Distributed leakage path		■	
7	Long leakage path			■
8	Concentrated leakage path			■
9	Airtight	■		

3.4 Climatic conditions

The baseboard heater and dehumidifier used to condition the test hut are located in a 1.6 m long by 0.84 m wide by 0.65 m high plywood box in its center. The air is mixed inside this box before circulating in the hut, ensuring uniform conditions for all sample sections. The installation of the wall-mounted air conditioning unit and the passage of the electrical and sensor wires are concentrated in one section between two studs, where no monitoring is performed (refer to Figure 3.3).

3.4.1 Criteria for selecting the climatic conditions

The climatic conditions were established with the following criteria:

- To obtain a representative hygrothermal behaviour of the specimens, the conditions provided in the environmental chamber are based on real outdoor weather conditions for a specific location and those provided inside the test hut are typical of conditions maintained by occupants.
- The exterior wall assemblies are subjected to weather conditions favourable to moisture accumulation, to study their potential for moisture related problems.
- After moisture has accumulated, the exterior wall assemblies are subjected to weather conditions causing moisture to evacuate, to study their mode and potential for drying.
- For the length of each climatic period, the temperature, water vapour pressure, and air pressure are maintained constant. This could allow an eventual comparison of the experimental results with analytical results from a steady-state, 3-dimensional conductive heat transfer model.

3.4.2 Weather data

Actual daily average temperatures collected in Montreal (Quebec) from January 1986 to November 1997 by Environment Canada at the Dorval weather station are used to calculate monthly averages for each month of the 12-year period. Those averages are then compiled to obtain an overall average temperature for each month of the year. Results are shown in Table 3.2. The daily average temperature is used because it is more realistic than exposing the specimens to daily maximum or minimum temperatures.

Table 3.2. Average monthly temperatures.

	1986	1987	1988	1989	1990	1991	1992	1993	1994	1995	1996	1997	**Overall monthly averages**
January	-9	-8	-8	-7	-4	-10	-11	-9	-16	-6	-11	-10	**-9**
February	-10	-11	-8	-8	-6	-5	-9	-13	-11	-10	-8	-8	**-9**
March	-1	0	-3	-5	-1	-1	-5	-3	-3	0	-2	-4	**-2**
April	9	9	6	5	7	8	5	6	5	4	5	5	**6**
May	14	13	15	15	12	15	13	13	12	13	12	11	**13**
June	17	19	18	19	18	19	18	18	19	20	19	20	**19**
July	20	22	23	22	21	21	19	22	22	22	20	21	**21**
August	19	19	21	20	21	21	19	21	18	20	20	19	**20**
September	14	15	15	16	15	14	15	14	15	13	16	15	**15**
October	8	8	7	9	9	10	7	7	10	11	8	8	**9**
November	1	1	3	0	3	3	2	2	4	-1	0	1	**2**
December	-4	-3	-7	-16	-4	-7	-4	-5	-3	-9	-1	n/a	**-6**

3.4.3 Proposed conditions

To study moisture accumulation and evacuation, the experiment is divided into two distinct climatic periods: a wetting period and a drying period. Moisture from indoor accumulates in the building envelope materials when temperature, air and vapour pressure gradients are important from the inside out, corresponding to winter conditions. The assemblies dry when the temperature increases and the air and vapour pressure gradients are reduced. This happens in late spring for Montreal.

3.4.3.1 Wetting period

The assemblies are subjected to wetting conditions in order to identify the assemblies with the greatest and the least potential for moisture accumulation problems. In addition, by allowing moisture to accumulate, areas of moisture accumulation in each assembly can be identified.

- Exterior conditions: **-8.5°C**

  In Montreal, the coldest weather occurs from mid-December to the end of February, lasting 75 days. The average temperature of the last 15 days of December and the average temperature for January and February are averaged to obtain an overall outdoor temperature for the wetting period of -8.5°C.

- Interior conditions: **22°C, 50% RH, +4Pa**

  According to Standard ANSI/ASHRAE 55-1992 (Thermal Environmental Conditions for Human Occupancy), the winter comfort zone lies between 20°C and 24°C for indoor temperature and between 25% and 60% for relative humidity. The temperature in the middle of this range, 22°C, is selected as indoor conditions. The relative humidity of 50%, closer to the higher end of the spectrum, is selected because it represents a worst-case scenario and will accentuate the moisture related problems.

  A positive air pressure differential of 4 Pa is created inside the test hut to create a typical stack effect pressure for a Montreal winter climate (see calculations in Appendix A).

- Duration: **66 days**

  The initial protocol consisted of 75 days of wetting conditions or less, if constant moisture accumulation conditions were achieved. Since the rate of moisture accumulation appeared constant and the wetting trends could be identified within this time, the testing period for wetting conditions were limited to 66 days.

3.4.3.2 Drying period

The specimens are subjected to conditions favouring moisture egress in order to study whether a particular insulation strategy or air leakage path impedes or facilitates drying and to identify the potential problem areas in the exterior wall assemblies.

- Exterior conditions: **17°C**

  Late spring conditions are selected for the drying period because, having a smaller drying potential, they represent a worst-case scenario in comparison to summer conditions. With a slower drying process, moisture evacuation problems related to the insulation strategies or to the air leakage characteristics can be identified.

  Typically, the second half of the month of May represents the onset of the drying period, when exterior temperatures significantly increase in Montreal. Before this time, drying may not occur every day, and when it does occur, it may be reversed at night when temperatures drops. Exterior conditions are based on the average temperature over the last 15 days of May and the month of June, representing an overall outdoor average temperature of 17°C over 45 days.

- Interior conditions: **23°C, 45% RH, +1 Pa**

  According to Standard ANSI/ASHRAE 55-1992, the indoor temperature comfort zone for summer is in a higher range than for winter, between 22°C and approximately 27°C. Since the outdoor conditions for this drying period represent spring and not summer, the indoor temperature is chosen where winter and summer conditions overlap, i.e. between 22°C and 24°C.

The same amount of moisture in the air is maintained, because it is assumed that the occupants would maintain the same rate of moisture generation. From the psychrometric chart, at 23°C this translates into a relative humidity of 45%.

The positive air pressure differential due to the stack effect is proportional to the temperature differential. Since it is significantly lower, the pressure differential is reduced to 1 Pa (see calculations in Appendix A).

- Duration: **47 days**.

  As previously mentioned, the spring period considered, the last 15 days of May and the month of June, lasts 45 days. The drying conditions were to be maintained until the moisture contents in the assemblies were stable, point at which their drying trends could be established. This did not require the materials to be totally dry. Stable moisture contents occurred at the end of 45 days of exposure to late-spring weather conditions. Due to the gravimetry weighing schedule, the conditions were actually maintained 47 days.

3.5 Monitoring protocol

Monitoring of temperatures and moisture contents is performed in the 400 mm central portion between the wood studs, which is assumed to be vertically symmetrical on each side of its central axis. The temperatures are therefore measured only on one side of the central axis. Moisture contents are measured automatically with moisture content sensors on one side, and manually on the other, using gravimetry. Temperatures and moisture contents are monitored according to a grid related to the air leakage path of the sample section. The grid is tighter (150 mm) around indoor air entry points and looser (600 mm) for the rest of the expected path. Temperatures are monitored for the whole height of the sections with the long and distributed leakage path, as the expected air paths are from bottom to top and uniformly distributed respectively. For the sections with the concentrated leakage path, temperatures and moisture contents are monitored only in the lower portion, as it is expected that the most significant impact of air leakage will occur around the air entry point, 300 mm above the floor. Figure 3.8 shows the monitoring grid for each of the three air exfiltration paths studied.

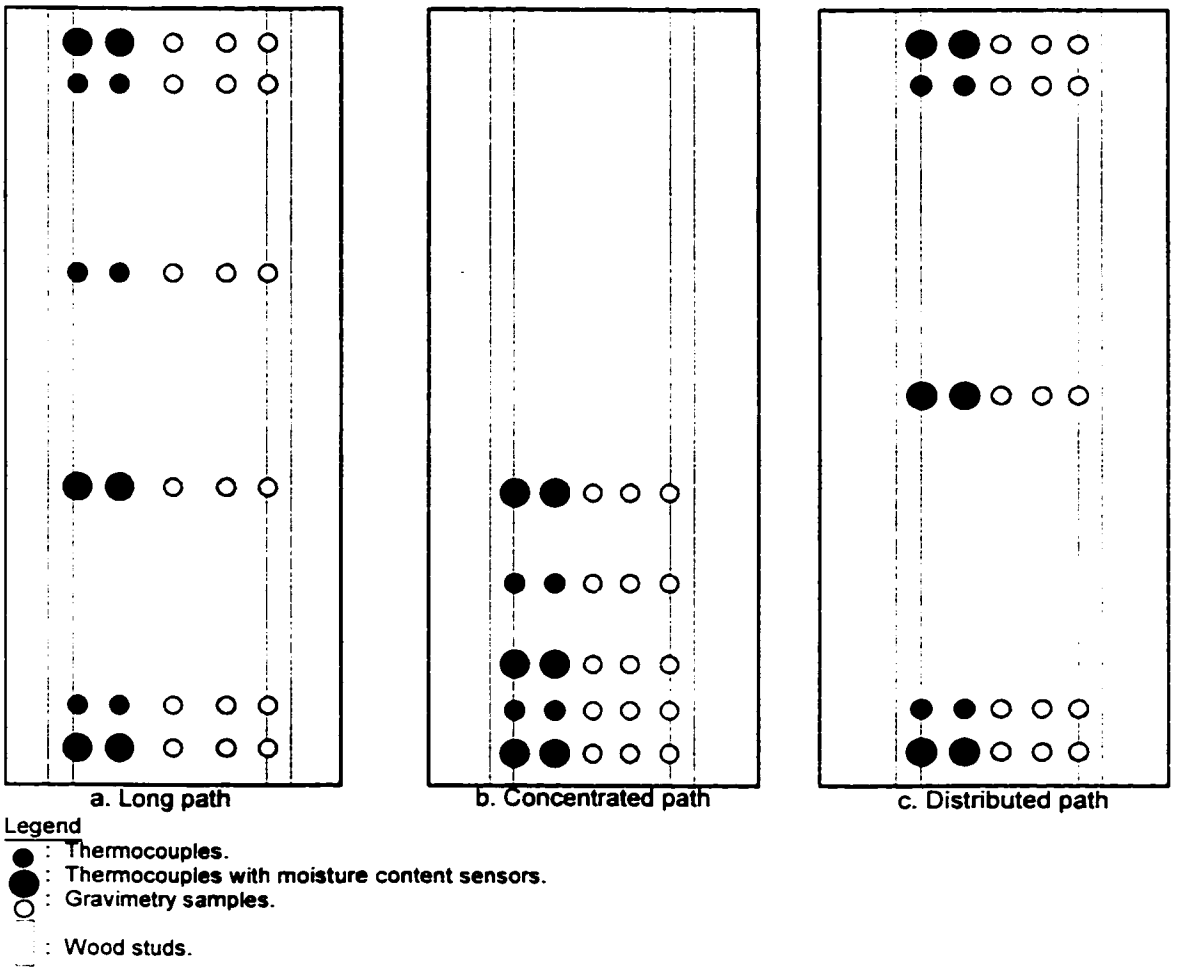

Figure 3.8. Monitoring grid on elevation view of the specimens.

3.5.1 2-D grid moisture content monitoring

Moisture content monitoring is used to assess where potential moisture related problems are likely to occur in the exterior wall assemblies being studied. By monitoring moisture contents over a plane at locations corresponding to a two-dimensional grid, the results can be presented in a graphic form by drawing curves of equal moisture contents, called *isohygrons*.

Moisture could then be used as a marker for air movement through the assembly. As indoor air exfiltrates, the moisture it contains is deposited in the hygroscopic materials of the assembly. The moisture maps produced would show the impact of air exfiltration, and an air leakage pattern may emerge from the isohygrons.

Moisture contents are monitored extensively, using moisture content sensors and gravimetry samples, along the grids shown in Figure 3.8. Both methods are used because they measure different characteristics. When sensors are installed, the moisture content at a specific location in the material is measured. Gravimetry gives an average moisture content for a larger area of the material being monitored.

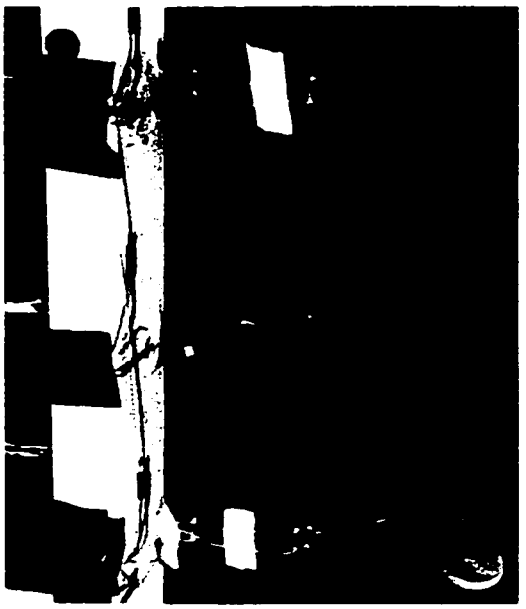

8a. Thermocouples and moisture content sensors on the cold side of the glass fiber batt insulation.

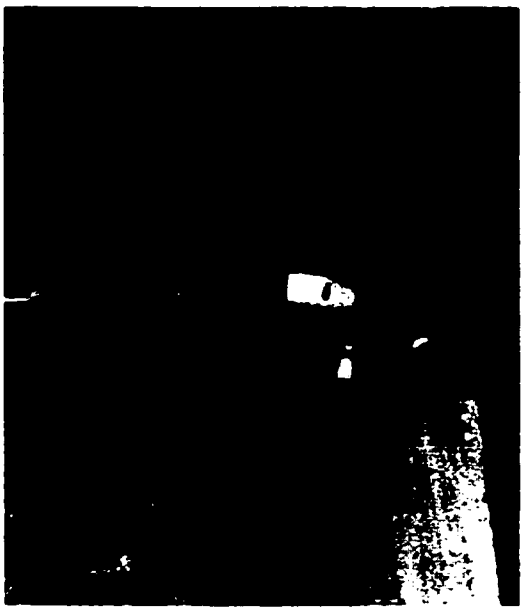

8b. Thermocouples on the warm side of the glass fiber batt insulation.

Figure 3.9. Thermocouples and moisture content sensors.

3.5.1.1 Gravimetry monitoring

A total of 144 gravimetry samples are taken on the cold side of the wood studs and in the fiberboard sheathing. The wood stud samples are 12.5 mm deep by 12.5 mm high by 38 mm wide. The fiberboard samples are disks 38 mm in diameter, except for those in front of the studs, which are 50 mm in diameter to provide access to the stud samples. The perimeter of the fiberboard samples is sealed with tape to avoid moisture transfer through this surface. All of the gravimetry samples are accessible from the outside of the test hut. For the sample sections with 38 mm rigid insulation added on the exterior, a removable piece of the insulation is cut out in front of the gravimetry samples to give access to them. Air leakage around the gravimetry samples has to be avoided in order to minimize the effect of the samples on the hygrothermal behaviour of the assembly. However, the perimeter of the gravimetry sample holes cannot be sealed directly because tape or caulking would damage the fiberboard. The fiberboard samples must fit tightly enough so that as little air as possible can flow around them, but not so tight that they cannot not be removed without being damaged. A spun bonded polyolefin membrane, which has a low air permeability and a high vapour permeability, is used to address this issue of airtightness. A rectangular window is cut out of the polyolefin membrane in front of each row of gravimetry samples, and the perimeter of this opening is sealed with highly adhesive tape to the fiberboard sheathing. This window is covered between and during weighing with a rectangular piece of the same polyolefin membrane, sealed with the same type of tape. A photo of the gravimetry setup, without the fiberboard samples and the spun bonded polyolefin, is shown in Figure 3.10.

During the experiment, all samples are weighed once a week for the first 30 days, and then every 2 weeks for the remainder of the climatic period. The gravimetry samples are put in sealed plastics bags for handling, weighed inside the test hut using a scale precise to the microgram, and then put back in their respective positions. The sample holes are blocked while the samples are being weighed to avoid airflow through them. The procedure is completed as fast as possible so that the moisture content of the samples does not have time to vary significantly. At the end of the experiment the wood samples are oven-dried at 103°C, according to ASTM D 4442-92 "Standard Test Methods for Direct Moisture Content Measurement of Wood and Wood-Base Materials", and the fiberboard samples at 57°C to avoid evaporation of chemical agents.

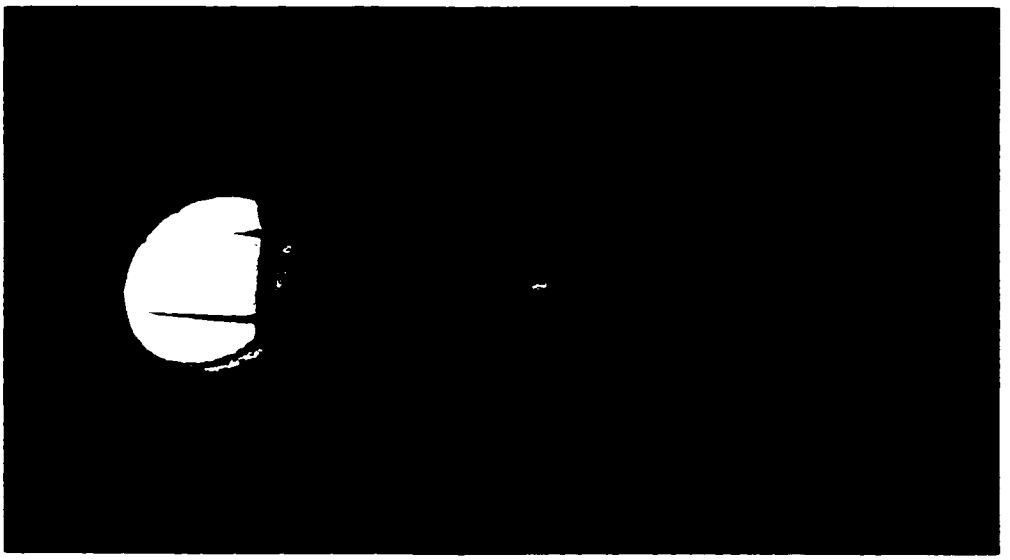

Figure 3.10. Holes for fiberboard and for wood stud gravimetry samples.

Before beginning the experiment, an air leakage test was conducted to evaluate the impact of the fiberboard gravimetry samples. For this test, a 60 mm x 60 mm fiberboard sample, with spun bonded polyolefin, is placed on a 5-sided airtight box. Positive air pressures of two, five, six, and 10 Pa are applied inside the box, and the airflow required to maintain these pressures is measured. This procedure is performed five times, with the following five different configurations:

1) setup covered with an airtight polyethylene membrane, to measure the exfiltration rate of the setup itself;
2) setup without polyethylene (the polyethylene membrane is cut out without being removed, so as not to disturb the setup), to measure the exfiltration rate of the fiberboard/spun bonded polyolefin assembly without gravimetry samples;
3) setup with a hole cut out of the spun bonded polyolefin membrane, to measure the exfiltration rate of the fiberboard sheathing;
4) setup with two holes[3] drilled for gravimetry (identical to those in the test hut sample sections), and with the spun bonded polyolefin taped as on the test hut sample sections;
5) setup with holes[4] drilled for gravimetry, but without the spun bonded polyolefin membrane, to measure the exfiltration rate of the fiberboard sheathing with gravimetry samples.

[3] With a sample inserted in the holes.
[4] With samples inserted in the holes.

For configurations 1, 2, and 4, the air leakage of the whole setup was so low that at the low air flow rate of 0.01 litre per minute, the air pressure continued to build up, indicating that the air leakage, if any, was extremely low. These configurations are therefore considered airtight. For configurations 3 and 5, the results are presented in Table 3.3.

Table 3.3. Air leakage measurements for gravimetry sample holes.

	2 Pa	5 Pa	6 Pa	10 Pa
Fiberboard, continuous, no SB polyolefin (#3.)	0.37 l/min.	0.96 l/min.	1.53 l/min.	1.89 l/min.
Fiberboard, with holes filled, no SB polyolefin (#5.)	0.38 l/min.	0.98 l/min.	1.56 l/min.	1.93 l/min.

As can be seen, at 5 Pa (the pressure closest to that maintained inside the test hut) the difference between the fiberboard with and without holes and gravimetry samples is 0.02 l/min. Transposed to one sample section having 10 or 12 of these holes, the air leakage would be 0.1 l/min. However, all of these holes are covered with a Tyvek membrane, as tested in configuration 4, which is shown to be relatively airtight according to these results.

3.5.1.2 Moisture content sensor monitoring

A total of 54 moisture content sensors were used to measure automatically moisture contents in the 12.5 mm thick fiberboard sheathing. The sensors consisted of two metal pins, 1 mm in diameter by 6 mm in length, plated with gold to avoid oxidation. The resistance of the material to electric current, which is inversely proportional to the moisture content, is measured across the two pins inserted in the material. Readings are taken by applying a voltage to the pins, which ionizes the pin materials. The ionization is proportional to the number and duration of exposures to the voltage and it causes corresponding errors in the readings. This appears to be incompatible with the

continuous moisture monitoring required for the 113 days of the experiment. A monitoring system was developed so that short readings are taken automatically from each sensor every 10 minutes and that each time the polarity of the pins is reversed. This minimizes the error due to the ionization. The moisture content sensors were installed, from inside the test hut, in the fiberboard sheathing to measure the average moisture content of its interior surface layer. Figure 3.9 shows installed moisture content sensors.

The relationship between the electric resistance and moisture content depends on the material and on the average temperature the material is subjected to. The data to establish this relationship was not available for the asphalt impregnated fiberboard sheathing used in the assemblies, so a calibration curve was developed. The calibration procedure is based on a similar one described in Zarr et al. (1995). For the calibration procedure, moisture content sensors are installed on five 40 mm x 40 mm fiberboard samples. These samples are placed in a small conditioning chamber, where the temperature and relative humidity can be controlled. For the first phase, the temperature is held constant at 17°C, while the relative humidity is increased until moisture content equilibrium in the fiberboard is attained. Tests were conducted at relative humidities of: 50%, 75%, 85%, 90%, 95%, and 97%. To obtain the temperature correction, this procedure was repeated at 4°C for relative humidities of 50%, 75%, 85%, and 92%. Voltage readings were taken from the moisture content sensors daily, and the samples were weighed immediately after each reading. At the end of the procedure, the samples were oven-dried at 57°C and weighed.

The maximum fiberboard moisture content obtained in the conditioning chamber (17°C, 97% R.H.) was below those reached during the experiment. To achieve readings at higher moisture contents, water is sprayed on the fiberboard calibration samples to simulate the occurrence of condensation. The wet samples were then placed in sealed plastic bags until the water was uniformly distributed. Voltage readings were then taken and the samples are weighed. Different amounts of water were used, to increase the number of points on the curve. Figure 3.11 shows the conditioning chamber and the fiberboard calibration samples.

Figure 3.11. Calibration samples in the conditioning chamber.

The actual moisture contents, determined by gravimetry, are then plotted against the voltage readings, to determine the calibration curve, from which voltage readings taken during the test can be translated into moisture contents. Figure 3.12 and Figure 3.13 show the actual data points at 4°C and 17°C, and Figure 3.14 shows the curve from which the equation is generated.

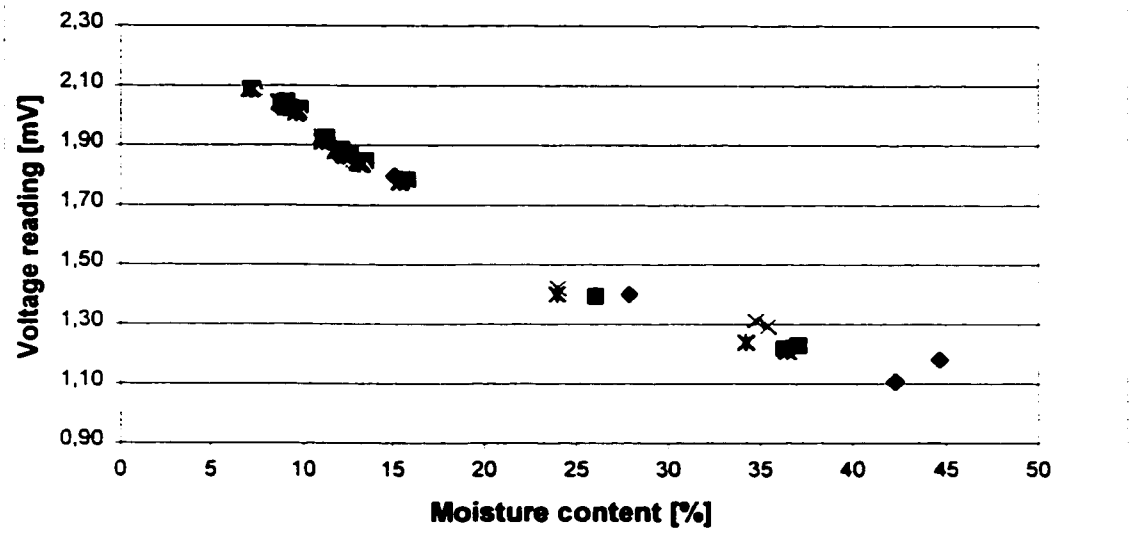

Figure 3.12. Calibration data points at 4 °C.

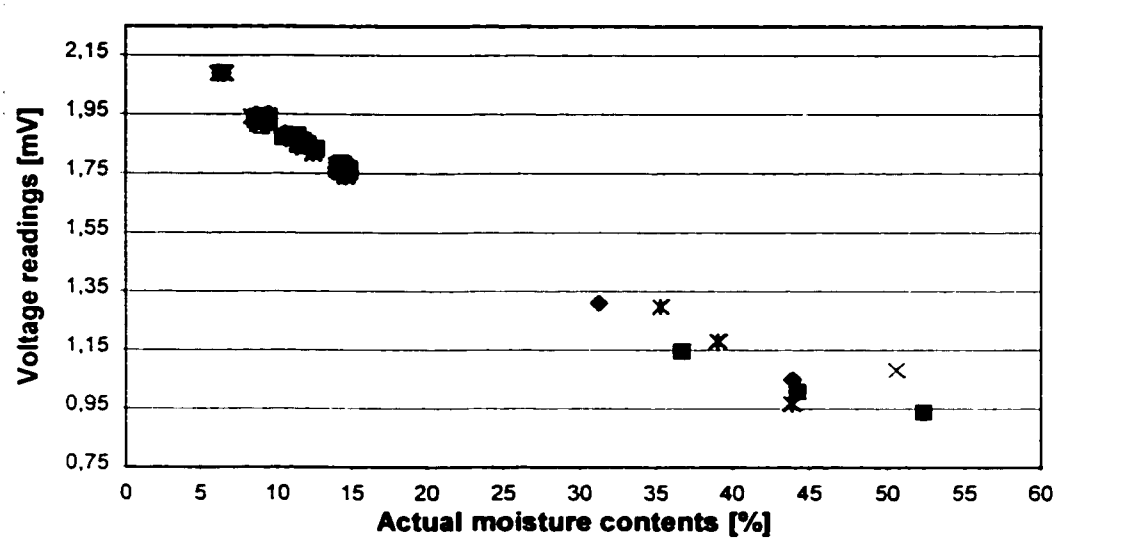

Figure 3.13. Calibration data points at 17°C.

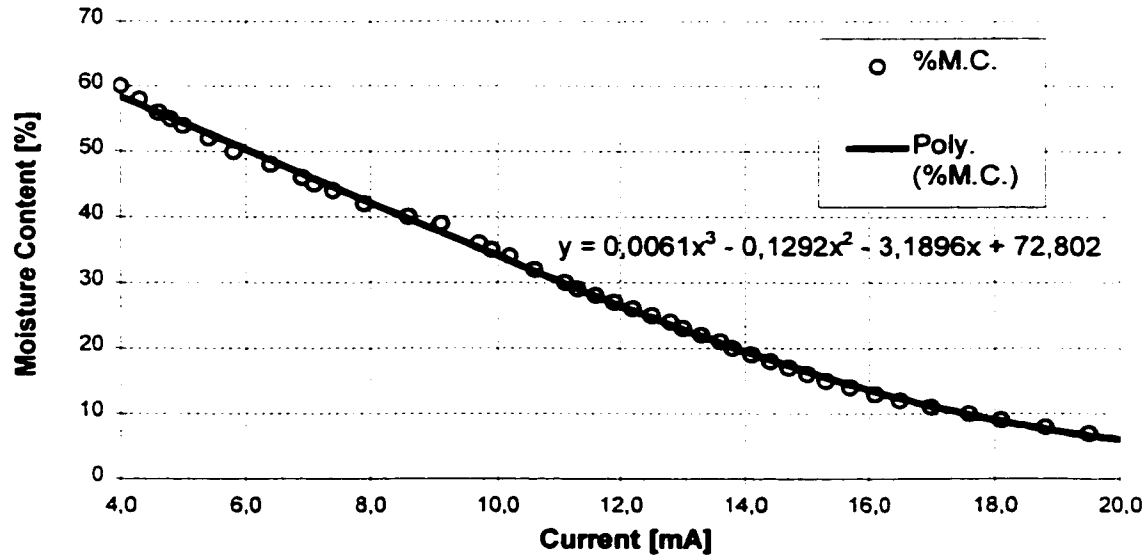

Figure 3.14. Moisture content sensor calibration curve at 17 °C.

The calibration equation, not including the temperature correction, is:

$y = 0.006x^3 - 0,129x^2 - 3,19x + 72,8$ Equation 3.1

where:

y = moisture content per dry weight [%]

x = current [mA]

3.5.2 3-D grid temperature monitoring

Temperature within an exterior wall assembly can give indications on the movement of air exfiltrating through it. Exfiltrating air warms the materials it comes in contact with, thus mapping its own trajectory. This mapping should be identifiable as long as a sufficient temperature differential exists between outdoor air and indoor air, i.e. during the winter climatic conditions inside the environmental chamber. As mentioned in section 2.3, Ojanen and Simonson (1995) used an approach similar to this when they used temperature monitoring to determine the direction of airflow in wall assemblies with insulation added on the indoor side.

Temperatures within the exterior wall assemblies were measured with 192 type "T" thermocouples (copper and constantan) having an accuracy of 0.5°C and verified with a temperature controlled (to 0.1%) reference bath. Readings were taken automatically by the data acquisition system every 10 minutes throughout the test period.

The thermocouples were installed according to a two-dimensional grid, at two planes within the assemblies: on the cold side and on the warm side of the glass fiber batt insulation. The thermocouple grid on the cold plane was installed on the interior surface of the fiberboard sheathing, and the thermocouple grid on the warm plane was installed on the interior surface of the glass fiber batt insulation. The same grid, shown in Figure 3.8, was repeated for both thermocouple layers, providing three-dimensional temperature monitoring. Figure 3.9 shows thermocouples installed on the cold and on the warm side of the glass fiber batt insulation respectively.

By measuring temperatures in such a way, two-dimensional temperature maps, at two different planes within the building envelope, were produced and from which air exfiltration patterns may be extrapolated. Those experimental results are compared to analytical results from a 3-dimensional heat conduction computer model that calculates temperatures in the assembly for conditions excluding exfiltration and moisture transfer.

3.5.3 Air leakage measurements

The airtightness of each sample section is measured using the standard test procedure ASTM E 283-91 ("Standard Test Method for Determining the Rate of Air Leakage Through Exterior Windows, Curtain Walls, and Doors Under Specified Pressure Differences Across the Specimen") just before the beginning and right after the end of the experiment. Positive air pressure differentials ranging from 10 Pa to 60 Pa are created on

the indoor side of the specimens. The airflow necessary to maintain them, which is equal to the amount of air exfiltrating through the specimen, is measured.

Before the procedure, all intentional openings provided in the sample sections (crack at the bottom for long path, hole for concentrated path, and grid of hole for distributed path) are sealed with tape. Then, each wall sample section is sealed with a polyethylene membrane to isolate it from the other sections.

The procedure used is a variation of the progressive sealing approach described in the literature review. First, air is blown into the test hut to measure its air leakage rate at the various specified air pressure differentials. Then, the polyethylene covering the sample section to be evaluated is cut and the procedure is repeated. These measurements are subtracted from the test hut measurements to give the air leakage of the samples section without the openings in the interior finish. The tape covering the openings is removed and the procedure is repeated again. Those measurements subtracted from the test hut measurements give the air leakage of the sample section with the openings. After these measurements are taken, the polyethylene is re-sealed over the sample section. This sequence is carried out for each of the 9 sample sections. The difference between measurements with and without the openings gives the air leakage of the openings. Figure 3.15 shows some samples sections covered with the polyethylene membrane. The procedure was performed before the test in April 1998, and repeated after the test in September 1998.

Figure 3.15. Test hut prepared for air exfiltration rate measurements.

3.6 Experiment history

3.6.1 Climatic Conditions

The experiment was conducted from May 19th to September 8th, 1998 using consecutively two distinct sets of climatic conditions: a wetting period, from May 19th to July 23rd, and a drying period from July 23rd to September 8th.

The test hut and chamber temperature readings are plotted over time in Figure 3.16. Overall, the chamber and the test hut temperatures conditions were maintained constant during both periods. The repetitive peaks that can be seen for the chamber temperatures are caused by the daily defrost operations of the cooling coil during the wetting period. They were of a short duration (15 to 20 minutes) with no significant impact on temperature and moisture content within the test specimens. Two events temporarily

disrupted the running of the wetting portion of the test. A power failure on June 16th caused the computers controlling the climatic conditions and the data acquisition system to shut down. The temperature in the test hut went up to a peak of 35°C. On June 24th, a problem with the compressor caused the temperature in the chamber to rise, also to a peak of 35°C. In both cases, the overall temperature rise lasted a few hours. Only the June 24th event had some impact on the fiberboard moisture contents, which is discussed later in Chapter 4. There was a third event on July 16th in which the baseboard heater inside the test hut stopped functioning due to an electrical problem. This caused the temperature in the test hut to go down to 16°C for a very short period.

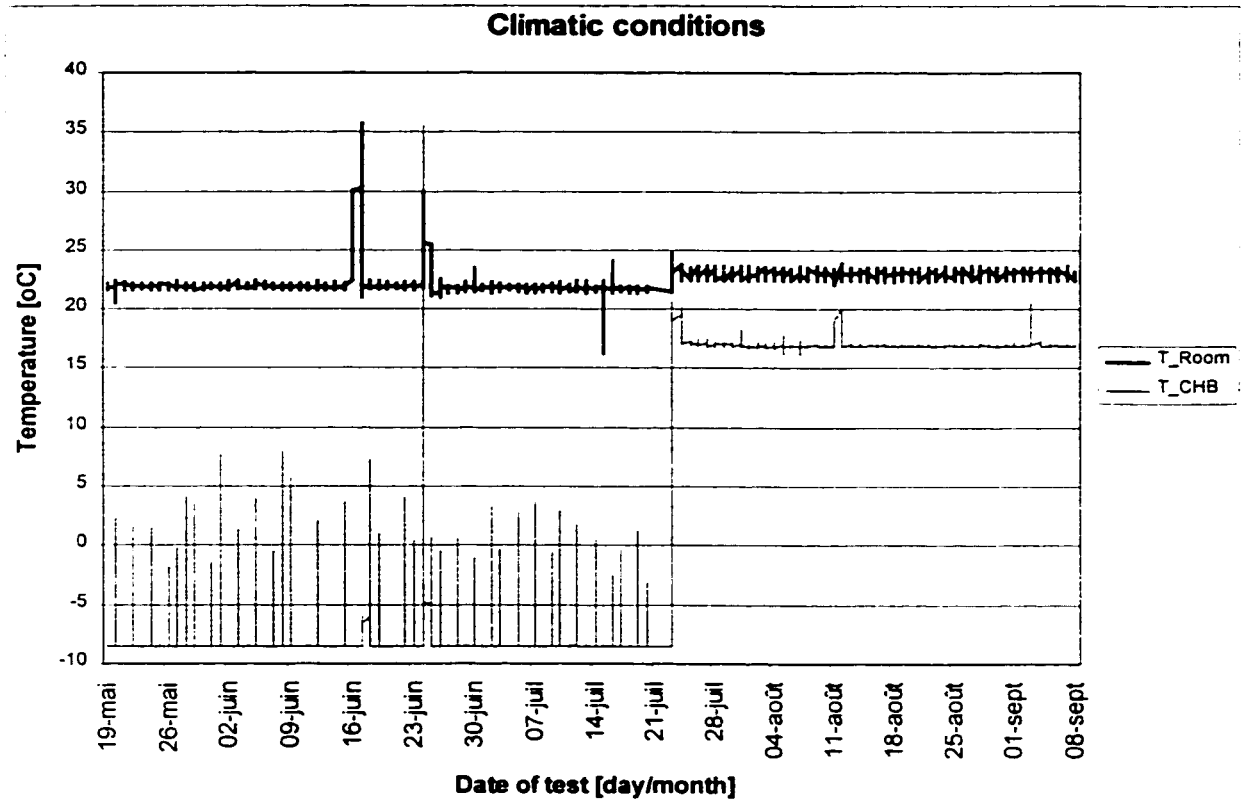

Figure 3.16. Climatic conditions inside the test hut and the chamber.

3.6.2 Data Acquisition

3.6.2.1 Temperatures

Over the course of the experiment, the data acquisition system warned that some thermocouples temporarily gave error readings. This data was removed before analysis. Approximately 95% of the temperature data was used for the analysis.

3.6.2.2 Gravimetry

The gravimetry samples were weighed 8 times during the wetting period, and 7 times during the drying period. Table 3.4 show the actual gravimetry weighing schedule.

Table 3.4. Gravimetry schedule for sample sections with glass fiber batt insulation.

Wetting period [day/month]							
19/05	27/05	3/06	12/06	18/06	26/06	10/07	23/07

Drying period [day/month]						
24/07	31/07	7/08	17/08	24/08	2/09	8/09

3.6.2.3 Moisture content sensors

The first part of the wetting period allowed to correct the soldering of wires that had failed for three moisture content sensors: MC01-2, MC04-2 and MC07-3. These sensors were located in the sections with the long air leakage path. For the base-case assembly and the section with insulation added on the cold side, the defective moisture content sensors (MC01-2 and MC04-2) were located at the top, 100 mm from the stud. For the section with insulation added on the warm side, the defective moisture content sensor was located close to the stud, 900 mm from the floor. Those sensors gave completely flat readings until June 22nd, when the faulty connection was corrected. It is difficult to identify defective moisture content sensors because they simply give the equivalent of a very low moisture content.

3.6.2.4 Air leakage measurements

Air leakage measurements were performed before and after the test. However, on both occasions and regardless of the care demonstrated during the installation of the set-up, the data resulting from the pressurization is not conclusive. The complicated geometry of each assembly rendered the sealing of the polyurethane membrane difficult to attain.

The results from the air leakage measurements do not allow for a conclusive analysis, nor to quantify the air leakage rate through the assemblies or the intentional openings provided in the interior finish, even though precautions were taken to avoid the potential problems associated with the selective method used, as were mentioned in the literature review conducted above.

A highly adhesive tape was used and great care was taken when sealing the polyethylene sheets to the OSB separators, in order to minimize as much as possible air leakage between the sections. However, it was noted during the first series of tests that the air leakage rates kept increasing, caused by the failure of the adhesion of the tape. One explanation for this failure is that static electricity caused dust to stick to the polyethylene membrane, which prevented a proper bond. To try to correct this problem, the adhesion was verified between the measurements performed for each section and the base leakage rate of the test hut was measured before the leakage of each section. For the second series of measurements, an additional effort was made to keep the polyethylene as dust free as possible. Unfortunately, the same phenomenon occurred. The fact that the base air leakage rate for the test hut was changing as measurements were made reduces the confidence in the accuracy in the results.

The low range of air leakage rates measured and the related accuracy problems could not be avoided. The test hut was full-scale, but it had a smaller envelope area than the typical house, and therefore a smaller air leakage rate. It was also noted that the person performing the test had an impact on the results. For the second series of air leakage tests, three persons took readings for the same section. Each obtained slightly different results, although the same apparatus and same method were used. Because the leakage rates were small, these differences became significant relative to the measured leakage rate. This had not been apparent for the first series of tests, where only one person was taking measurements.

For these reasons the results from both series of air leakage measurements are not presented nor discussed in this thesis.

3.6.3 Dismantling of the test setup

The dismantling of the test setup was conducted in two stages, with a visual inspection performed for each:

1. Removal of the interior finish. The state of the insulation between the studs was evaluated. A gap in the glass fiber batt insulation was found at the top of the base-case assembly with distributed air leakage, shown in Figure 3.17.
2. Removal of the insulation materials and sheathing. The spun bonded polyolefin membrane and the fiberboard sheathing were removed to expose the wood structure. A visual inspection was conducted to detect fungus staining. A few areas with staining fungi were found indicating that high moisture contents were reached. Figure 3.18 illustrates an example of the staining that was found.

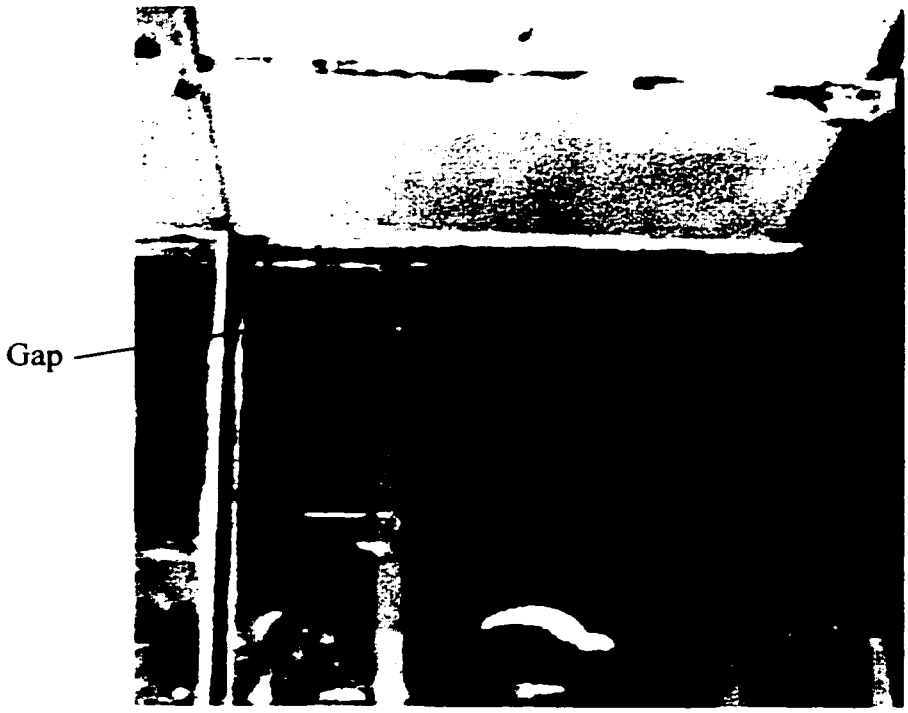

Figure 3.17. Gap in the glass fiber batt insulation.

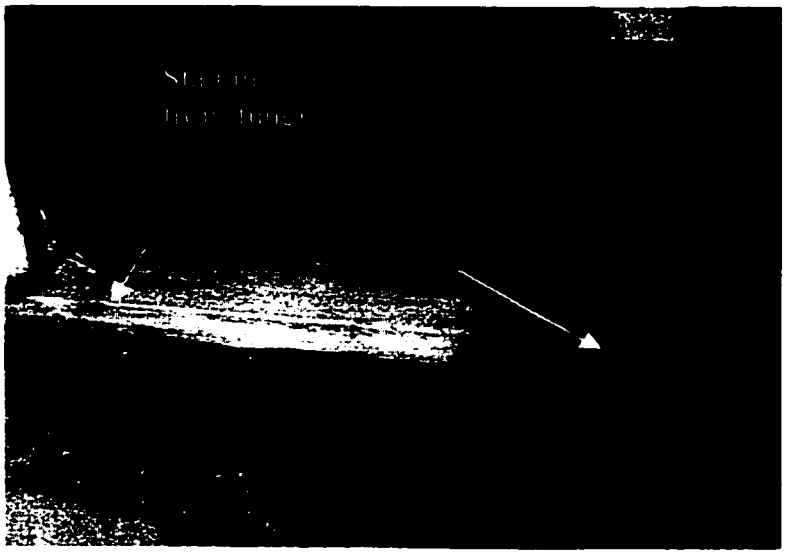

Figure 3.18. Example of fungi staining, in the section with rigid insulation added on the cold side, and long air leakage path.

3.7 Conclusions

No previous experimental work had looked at the evaluation of the hygrothermal performance of leaky building envelopes with added insulation. In the proposed experimental protocol, nine full-scale assemblies, representative of field construction, were exposed simultaneously to climatic conditions simulating real weather conditions. This experimental protocol provides a methodology on the design of the specimens, the conditions and the monitoring to document the hygrothermal performance of re-insulated leaky building envelopes, which may be used to elaborate guidelines for performing retrofit work.

In addition, the monitoring plan developed to monitor moisture contents and temperatures within the assemblies innovates from prior work as its deployment on the interior planes of the walls is based on the expected air leakage path. The data yielded by this monitoring is able to provide detailed information about the moisture content and temperature profiles of the tested assemblies. This data can be used to produce moisture content and temperature maps, to provide a visual representation of the hygrothermal performance of the walls. This type of data has not been produced so far with the more usual types of monitoring.

4. HYGROTHERMAL PERFORMANCE OF ASSEMBLIES TESTED

The moisture content and temperature results are presented and analyzed in this section. The hygrothermal behaviour of the assemblies tested depends on the side chosen to add insulation and on the air leakage path provided. The gravimetry results are first presented, followed by the moisture content sensor results and then temperature results.

4.1 Moisture content monitoring

4.1.1 Gravimetry results

The gravimetry moisture contents in the fiberboard sheathing and in the cold side of the wood studs plotted over time are presented in Figure 4.1 to Figure 4.9. Three scales of moisture contents, on the vertical axis, are used. In most cases, a range of 0% to 40% moisture content per dry weight was used. For two charts, Figure 4.5a and Figure 4.6a, a range of 0% to 75% was used, and in one case, Figure 4.4b, a scale of up to 110% was necessary. The moisture content axis is located at the July 23rd mark, corresponding to the last day of the simulated winter conditions. For every section, in the graphic "a. Moisture content - fiberboard", the darker lines follow the fiberboard moisture contents for the gravimetry samples in the center of the sample section, and the lighter curves follow the moisture contents for the gravimetry samples between the center and the wood stud. They are numbered from top to bottom. In the graphics "b. Moisture content - fiberboard (in front of studs) and wood studs", the dark lines follow the moisture content for the fiberboard samples in front of the studs, and the dark lines the moisture content of the wood stud samples.

The section with the least moisture accumulation over the wetting period of the test is the airtight base-case assembly (Figure 4.1). This section also had the least variation

between moisture contents at different locations. On June 18th, during the wetting period, the gravimetry samples from the top of the airtight section were accidentally interchanged with those from the top of the section with distributed air leakage and rigid insulation added on the cold side. The peaks seen in Figure 4.1 are due to this misplacement of the samples. They show that moisture contents varied rapidly in the fiberboard (Figure 4.1a), and more slowly in the wood (Figure 4.1b). The two consecutive weighing procedures performed on July 23rd and July 24th, just before and after the climatic conditions were changed, further confirm this. In most sections, a significant change in moisture content can be observed between these two measurements. In some cases, it was a decrease (as in the airtight section, Figure 4.1) while in others was an increase (as in the base-case assembly with the distributed leakage path, Figure 4.4). The moisture content in the wood studs and in the fiberboard in front of the wood studs of the airtight section (Figure 4.1b) also increased slightly more than those in the fiberboard between the studs (Figure 4.1a). After the drying period was completed, the moisture contents of all samples, fiberboard and wood, were close to the original value, 2% higher on average.

The other three base-case assembly sections, with the long (Figure 4.2), concentrated (Figure 4.3), and distributed air leakage paths (Figure 4.4), also remained fairly dry. Moisture contents did not rise above 25%, except for the bottom wood stud samples for the section with the distributed air leakage (Figure 4.4b). In the case of the base-case assembly with the distributed air leakage path, the moisture contents at the top of the wood studs reached 105% (Figure 4.4b). This important moisture accumulation is caused by the gap in the insulation at the top of the section, shown in Figure 3.17. Warm, moist indoor air was entering directly into this gap through the holes provided in the

interior finish for the distributed air leakage path, and condensing on this part of the wood stud. Otherwise, after the initial accumulation the moisture content was relatively stable in the base-case samples. When the temperature was increased for the drying period, the moisture content of these samples dropped rapidly to just above the initial level. However, for the section with the long air leakage path, moisture content of the samples in the wood stud and in the fiberboard in front of the studs (Figure 4.2b) dropped more slowly than those in the center of the cavity, and some did not return to their initial moisture content.

A similar trend is observed for the section with rigid insulation added on the cold side and long air leakage path (Figure 4.5b). The moisture content of the samples was also much higher, up to 70% compared to just about 25% in the base-case assembly with the long air leakage path (Figure 4.2b). The section with rigid insulation added on the cold side and concentrated air leakage path (Figure 4.6) reached high moisture contents as well, up to a maximum of 55%. For these two sections with rigid insulation added on the cold side (Figure 4.5 and Figure 4.6), the moisture contents did not seem to reach a plateau, as in the other cases. Moisture contents kept increasing until the drying period was started. These high moisture contents and the steady increase can be explained by the fact that the temperature at the interface between the fiberboard sheathing and the rigid insulation was above freezing, but below the dew point of the indoor air, at 11°C. When moisture, transported by exfiltrating air, reached this point it condensed on the indoor surface of the rigid insulation and was absorbed by the fiberboard and the wood. When the piece of rigid insulation was removed to access the gravimetry samples, water was observed on its indoor surface. For the section with the distributed air leakage, the

moisture contents went up to 35% (Figure 4.7). For all sections with rigid insulation added on the cold side, the moisture contents at the drying period remained approximately 5% to 7% higher than before testing, suggesting that their drying potential is slightly lower. This applies especially to the fiberboard in front of the studs and to the wood studs (Figure 4.5b, Figure 4.6b, and Figure 4.7b).

The moisture content in the two sections with rigid insulation added on the warm side (Figure 4.8 and Figure 4.9) did not rise above 25%, with the exception of three locations in the wood stud of the section with the concentrated air exfiltration path, right after the conditions were changed from wetting to drying. During the experiment, frost was observed on the exterior surface of the fiberboard sheathing. At the change of temperature, this frost melted and momentarily increased the moisture content in the wood stud and the sheathing in front of the stud. By the next weighing, moisture content had significantly lowered. This effect, although less pronounced, can also be observed in the base-case with distributed air leakage path (Figure 4.4b).

The June 16th power failure does not appear to have had any significant impact on the moisture accumulation in the specimens as measured by gravimetry, but the June 24th compressor failure had a noticeable impact. Before this date, after an initial sharper increase, moisture content was generally rising slowly, almost reaching a plateau. After this date, the measurements returned to the slower rate of moisture accumulation. The only exceptions were the sections with insulation added on the cold side, which kept accumulating moisture at a greater rate until the climatic conditions were changed.

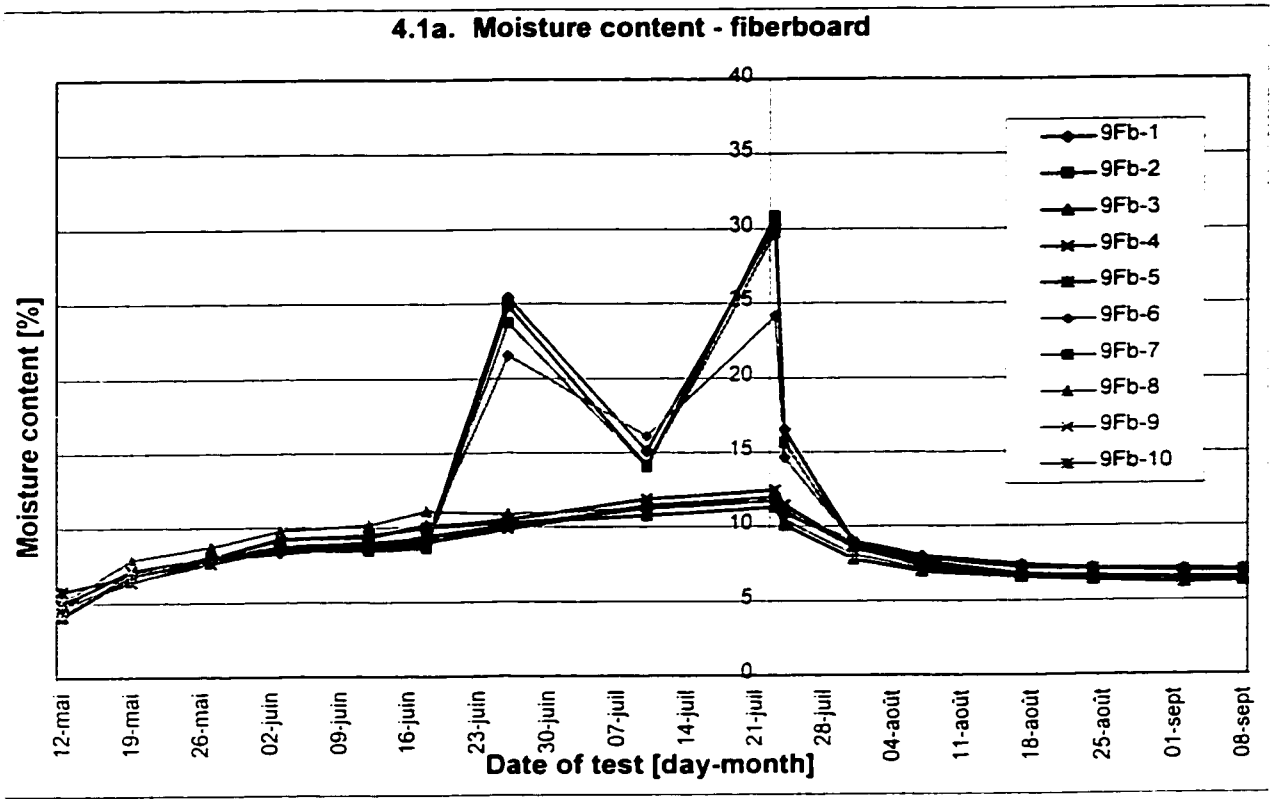

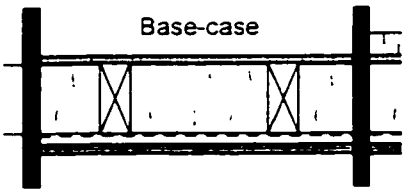

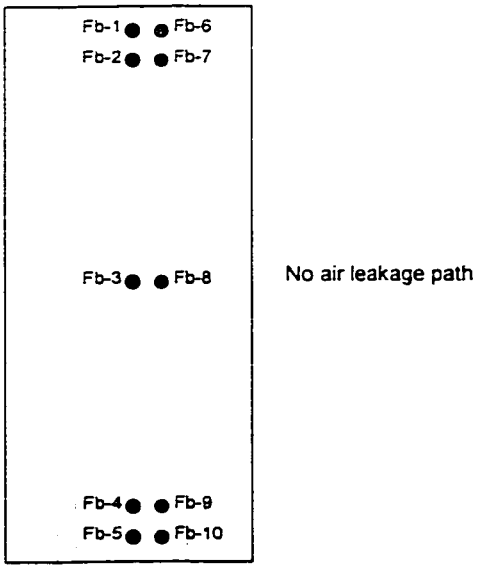

Figure 4.1. Gravimetry results, base-case assemblies, airtight.

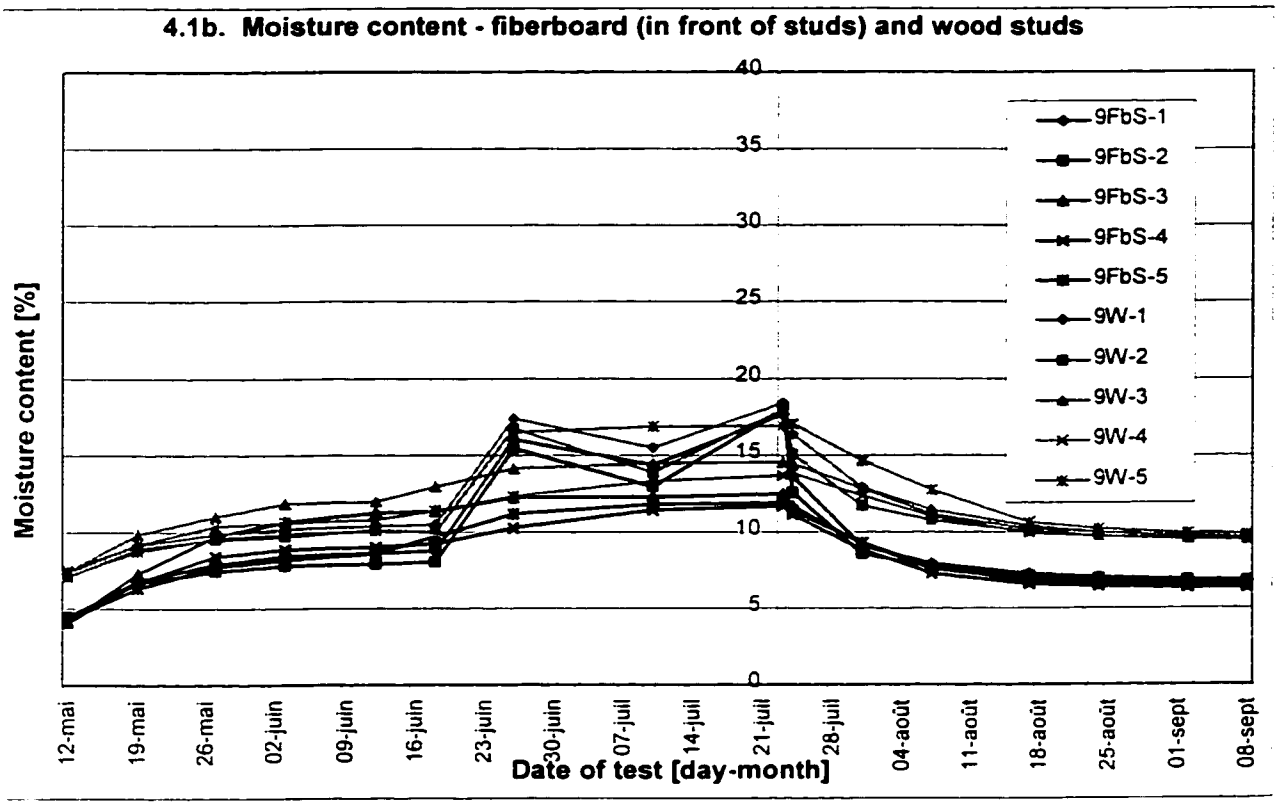

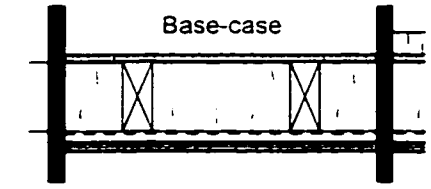

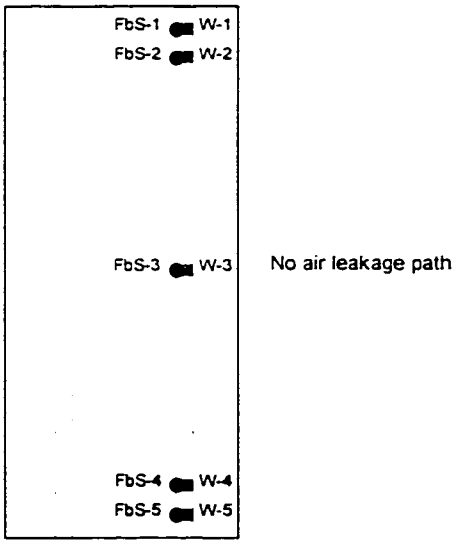

Figure 4.1. Gravimetry results, base-case assembly, airtight.

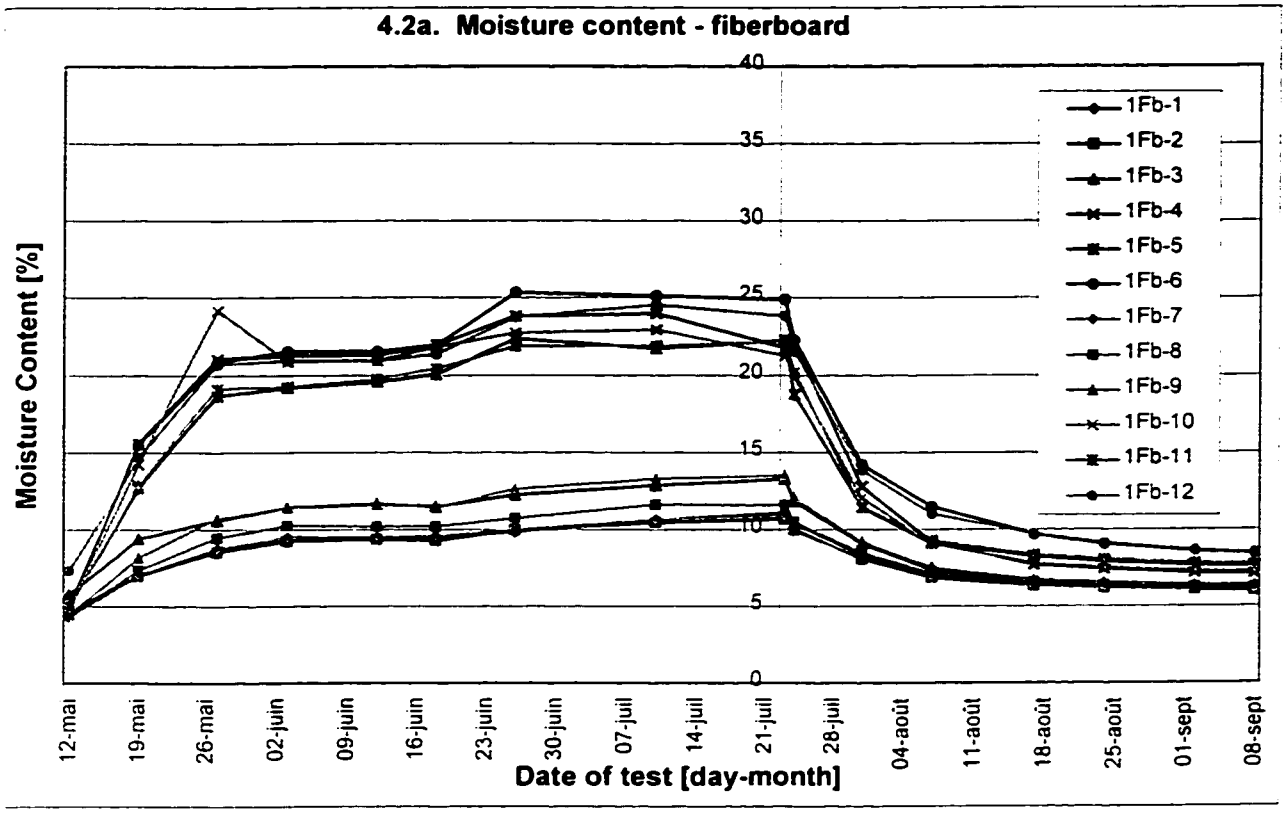

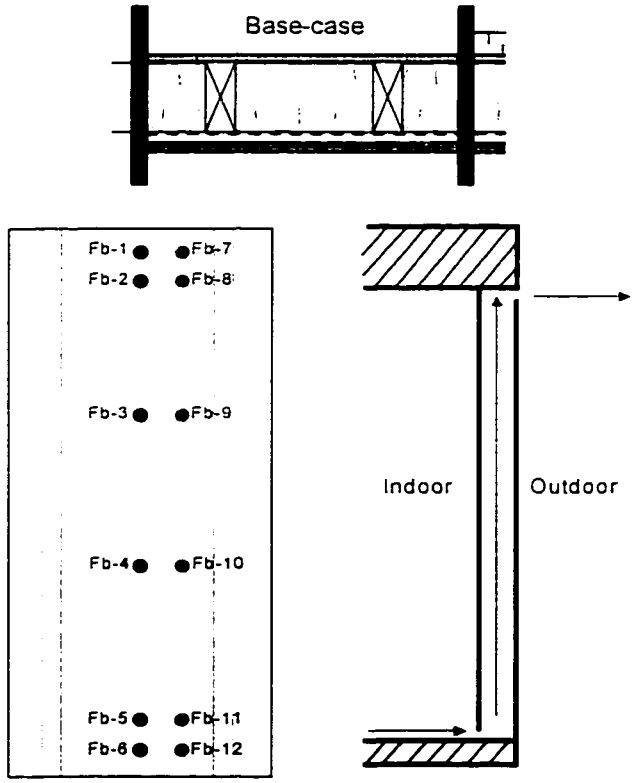

Figure 4.2. Gravimetry results, base-case assembly, long path.

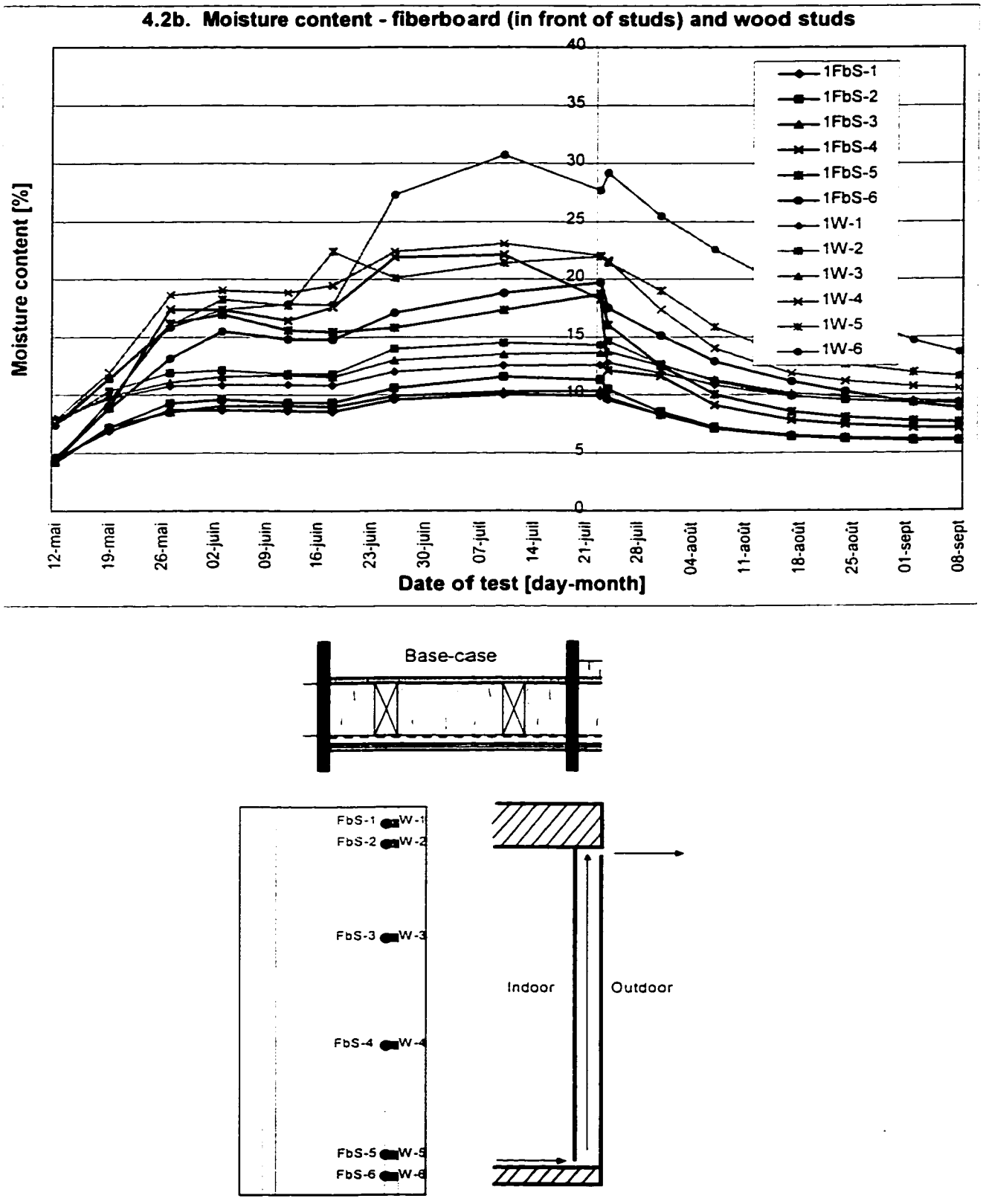

Figure 4.2. Gravimetry results, base-case assembly, long path.

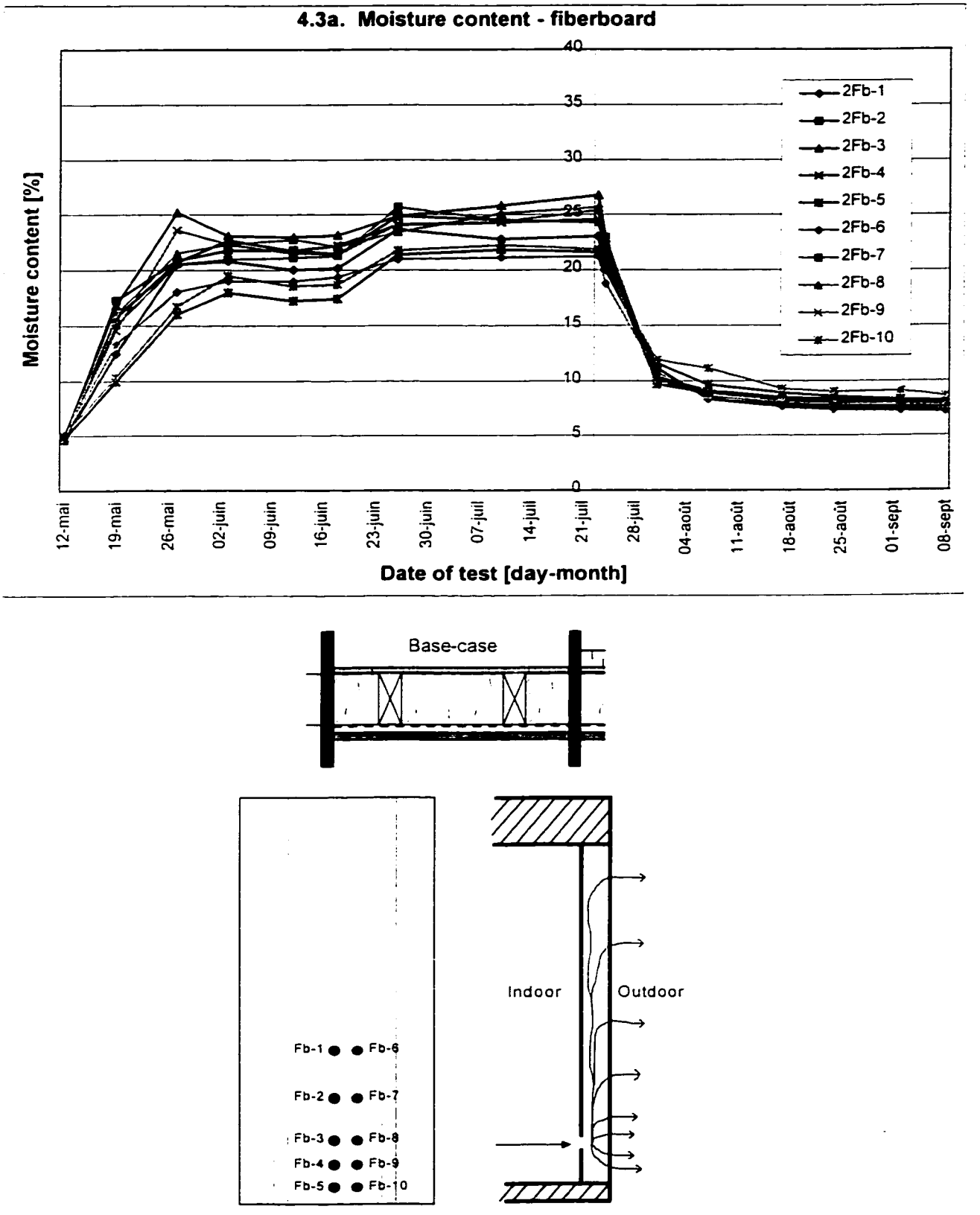

Figure 4.3. Gravimetry results, base-case assembly, concentrated path.

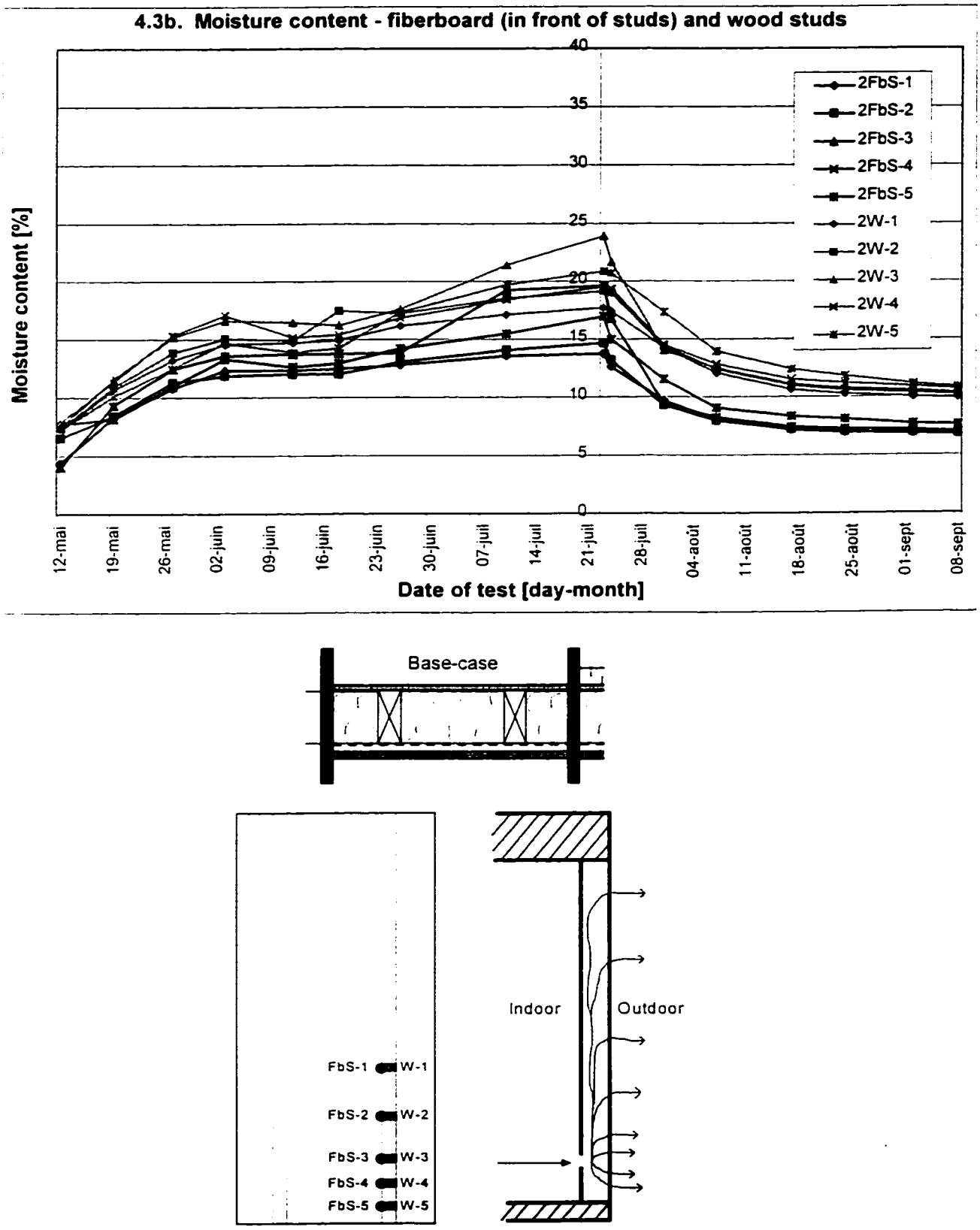

Figure 4.3. Gravimetry results, base-case assembly, concentrated path.

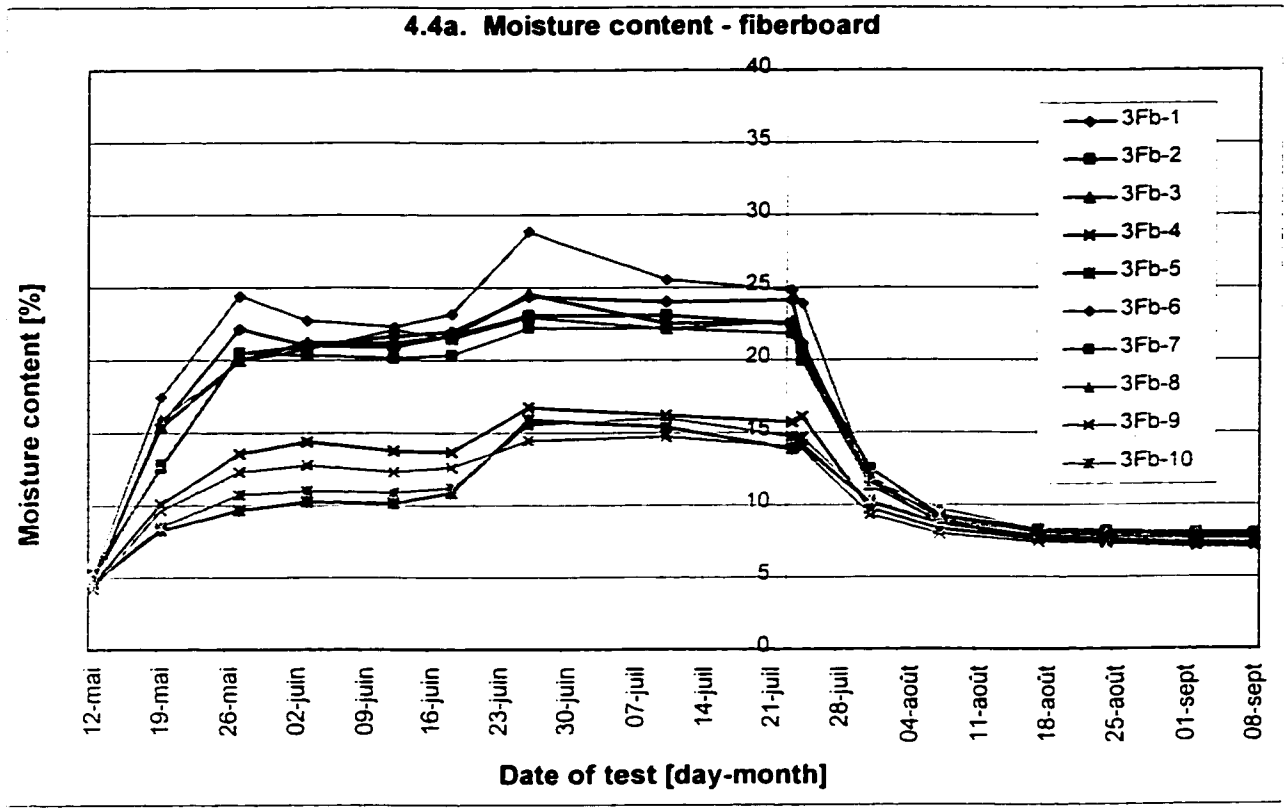

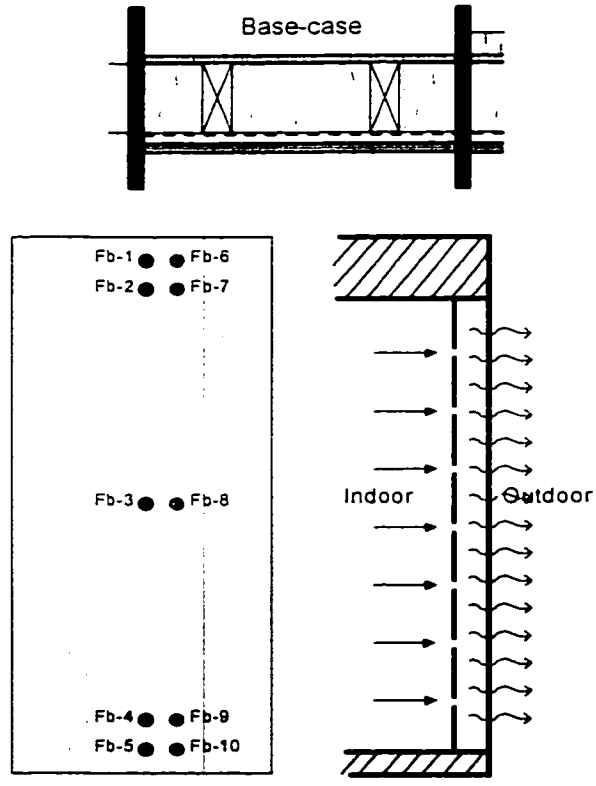

Figure 4.4. Gravimetry results, base-case assembly, distributed path.

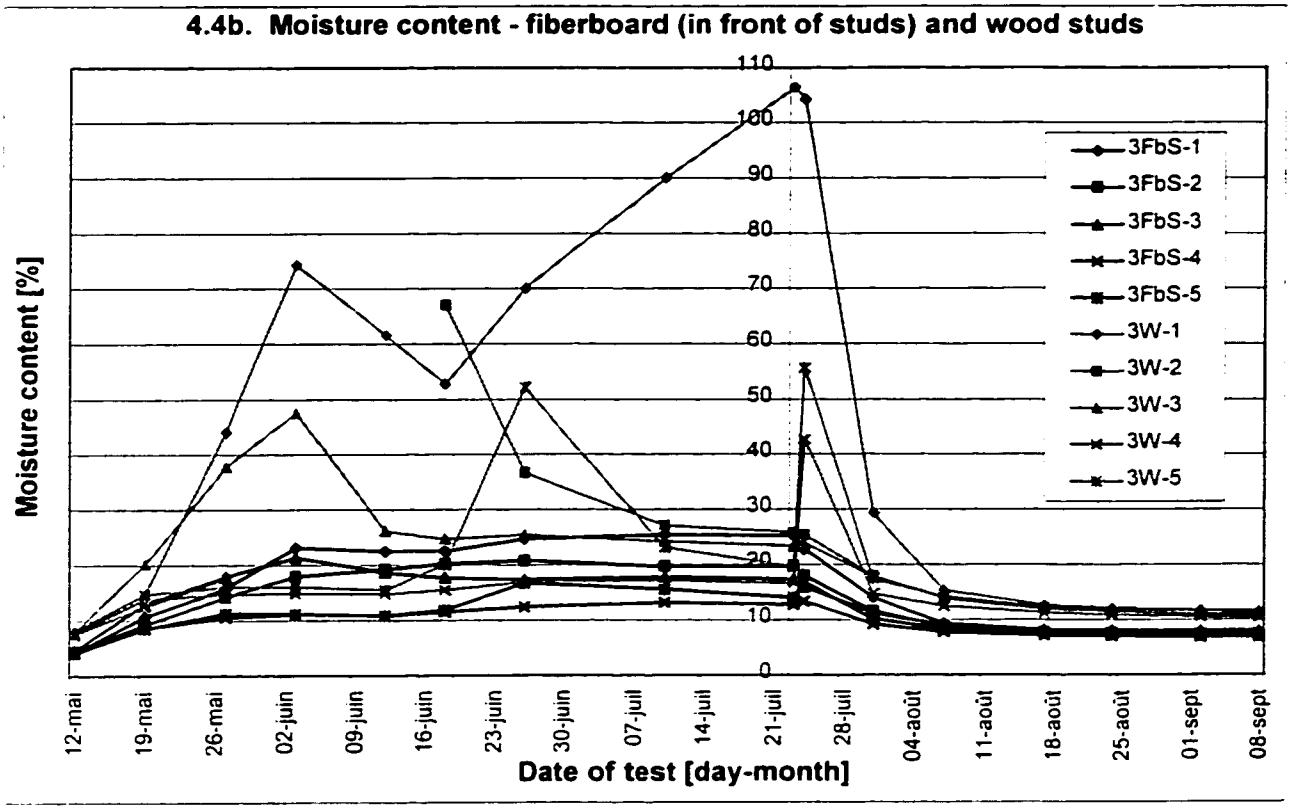

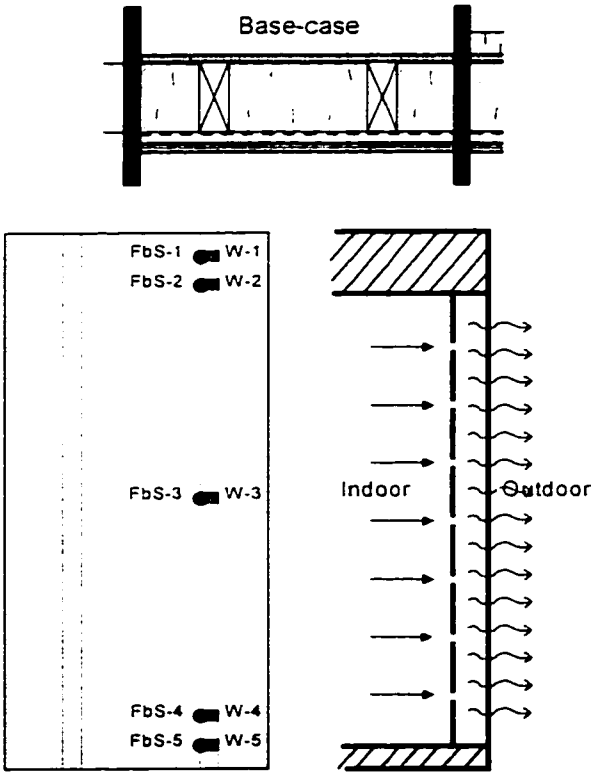

Figure 4.4. Gravimetry results, base-case assembly, distributed path.

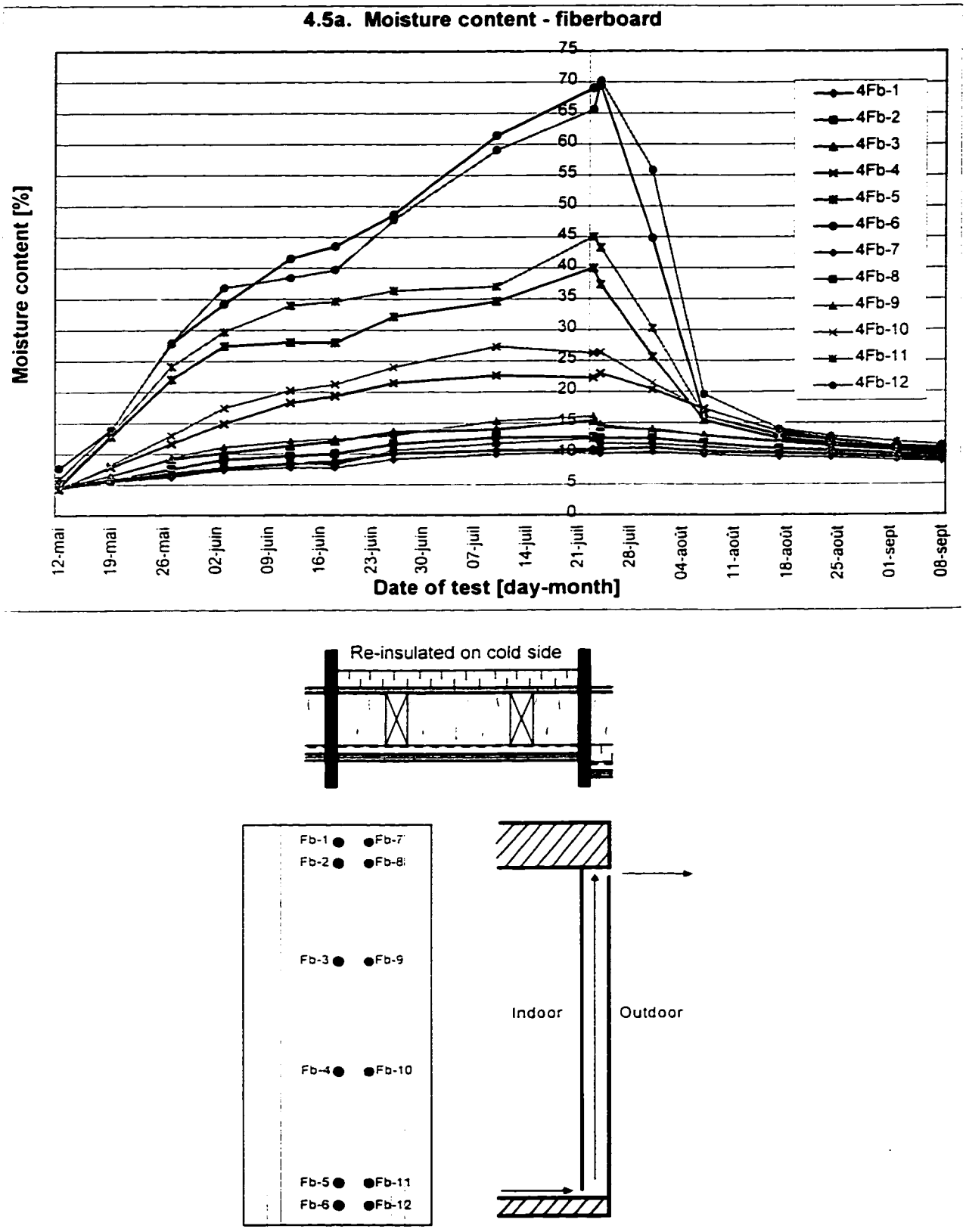

Figure 4.5. Gravimetry results, insulation added on cold side, long path.

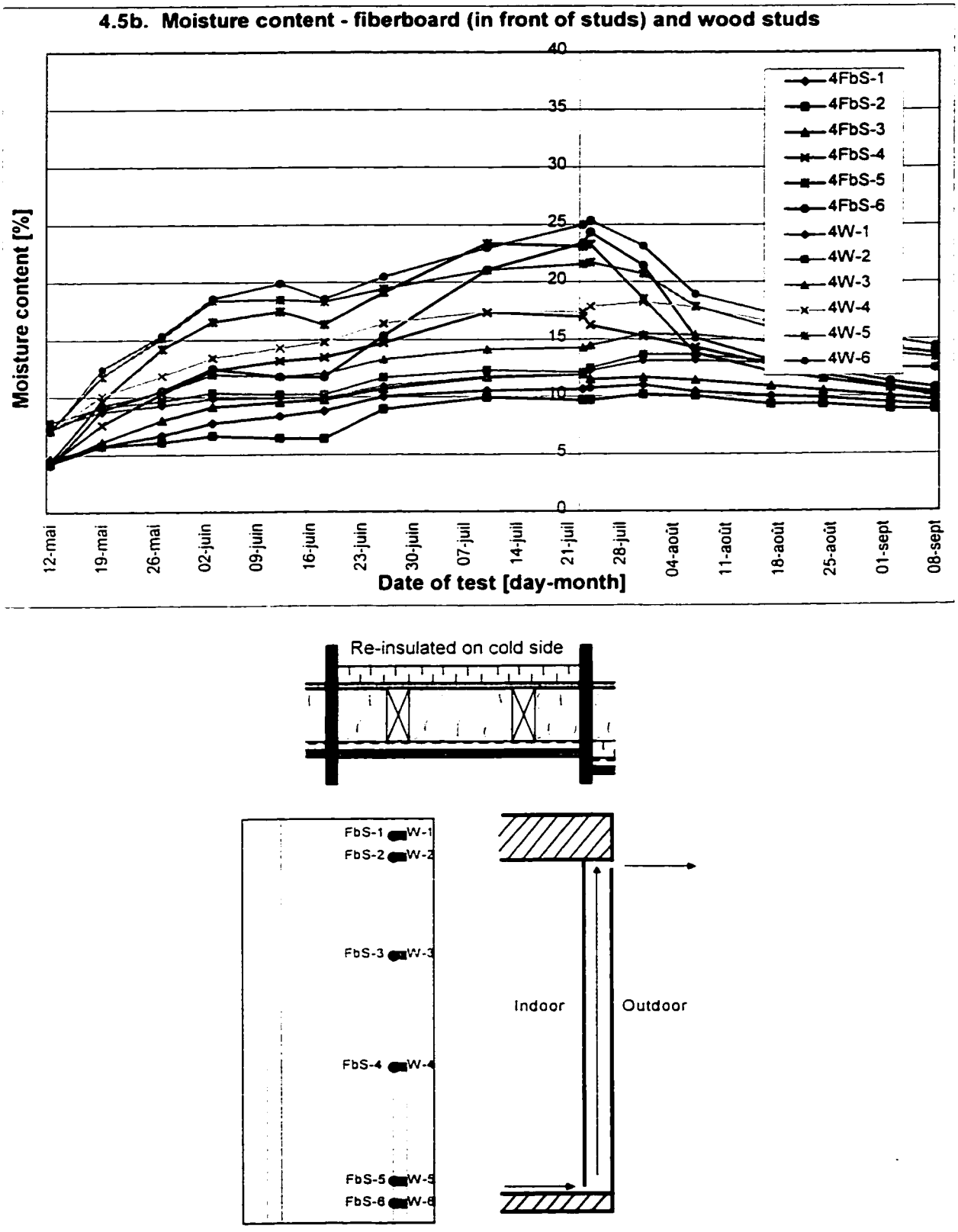

Figure 4.5. Gravimetry results, insulation added on cold side, long path.

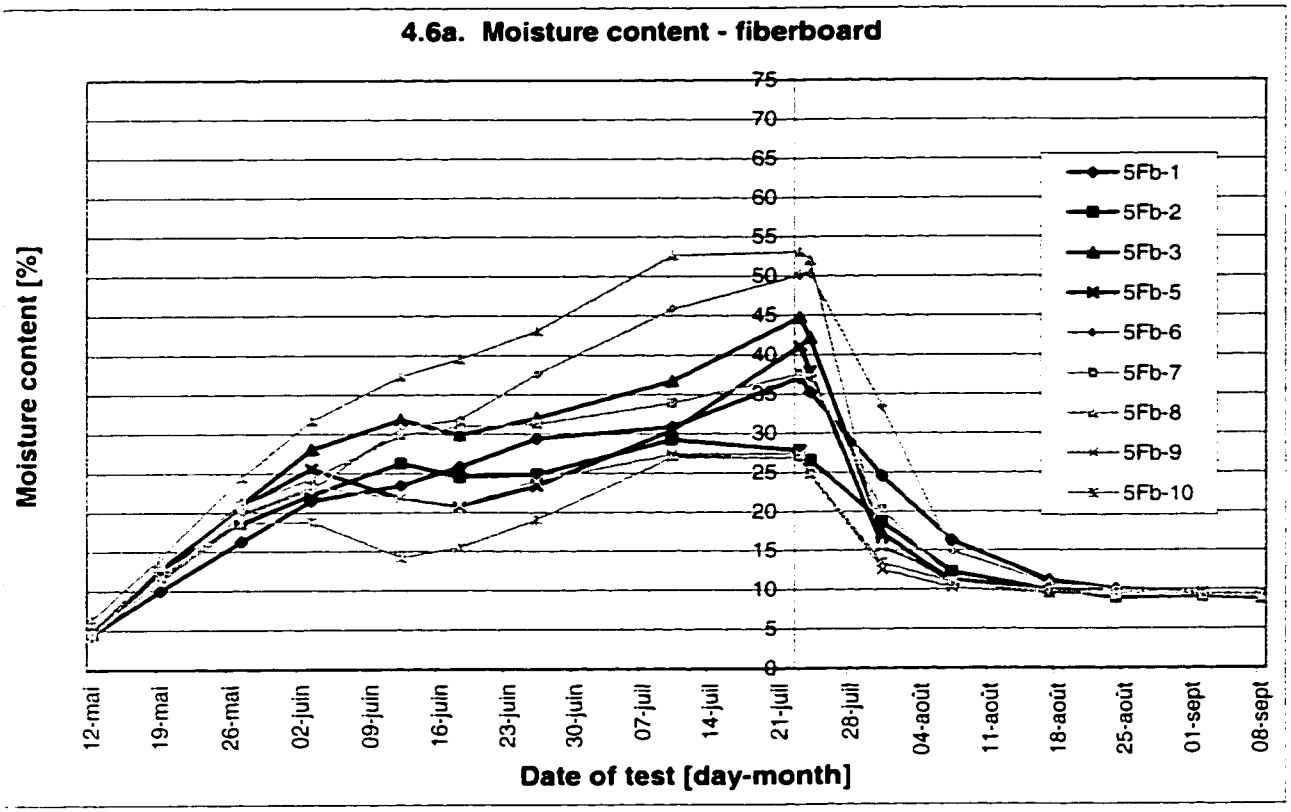

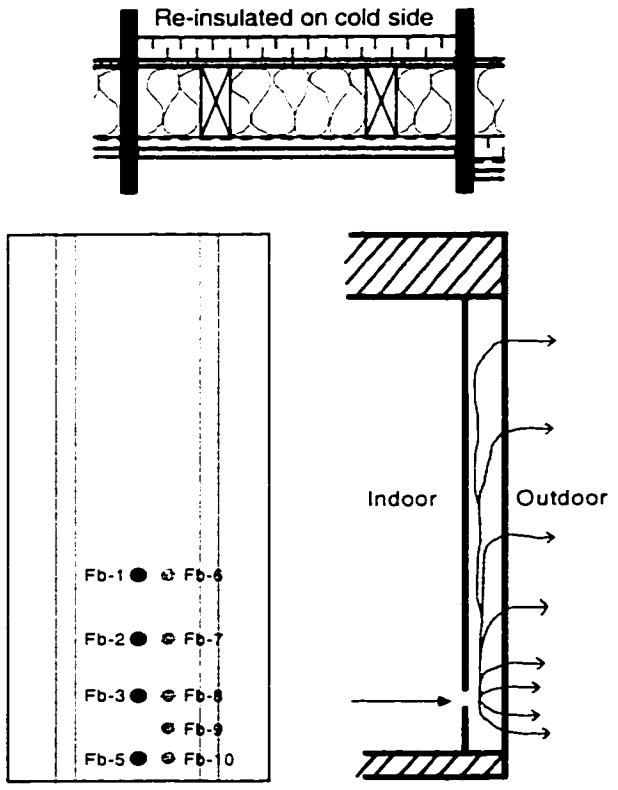

Figure 4.6. Gravimetry results, insulation added on cold side, concentrated path.

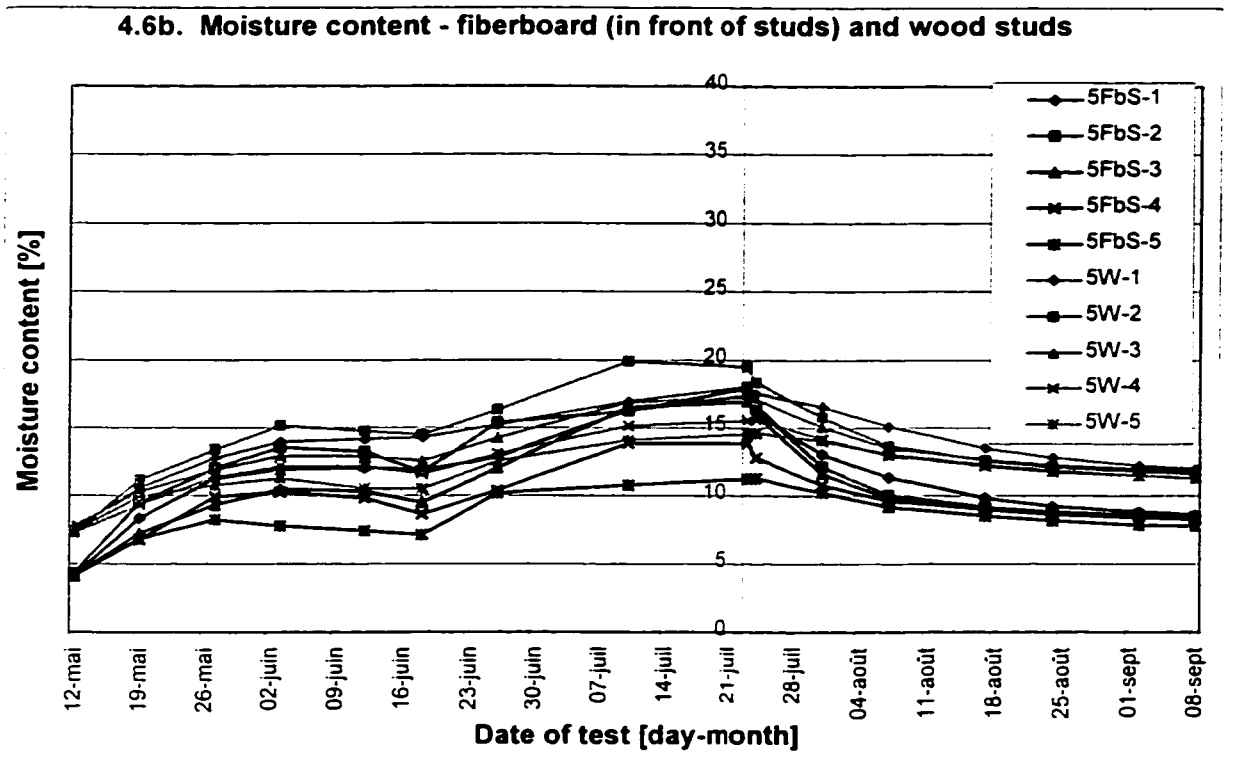

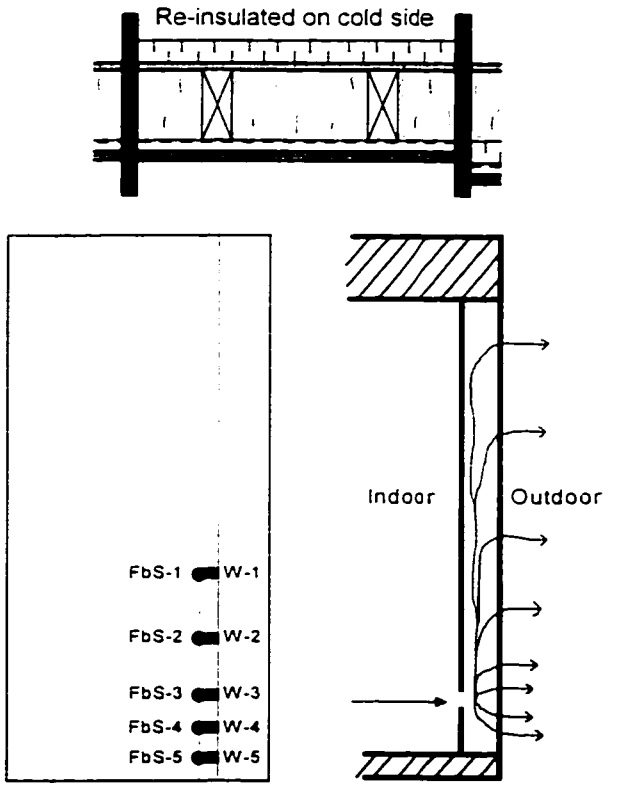

Figure 4.6. Gravimetry results, insulation added on cold side, concentrated path.

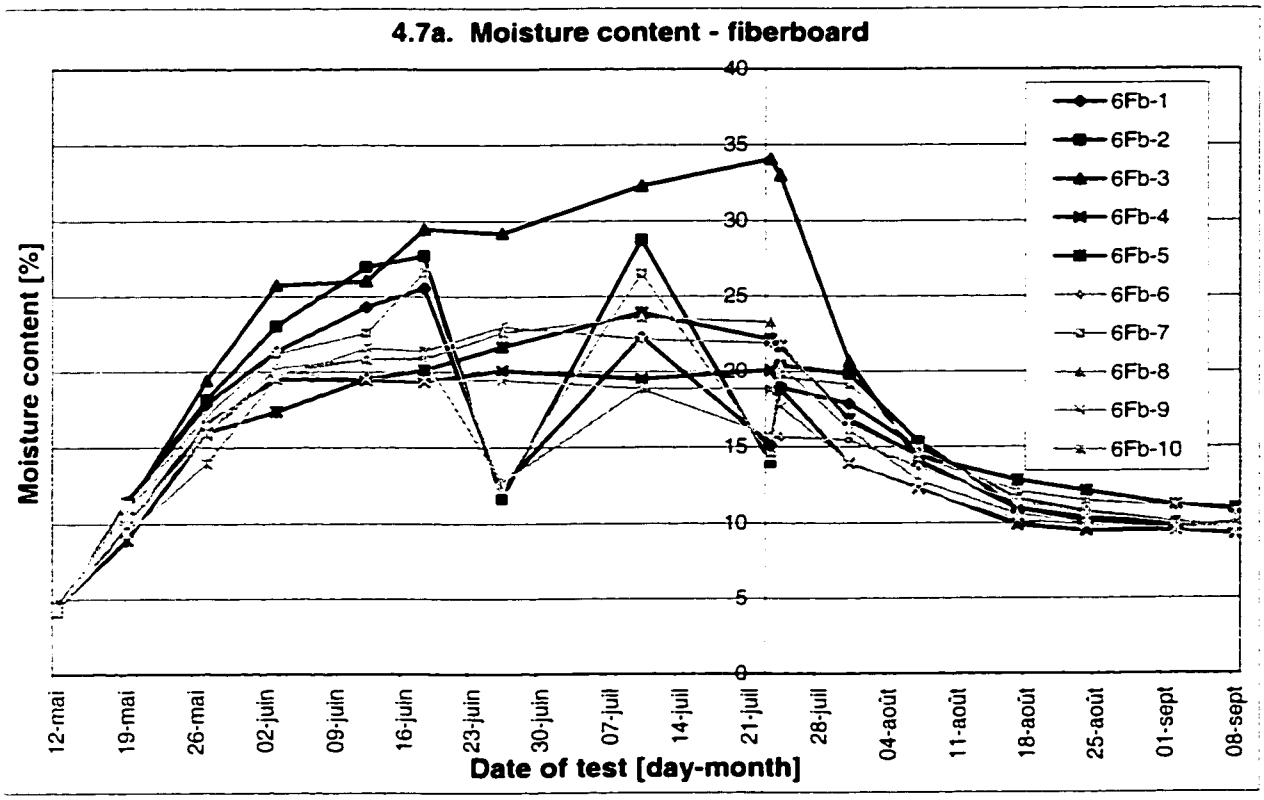

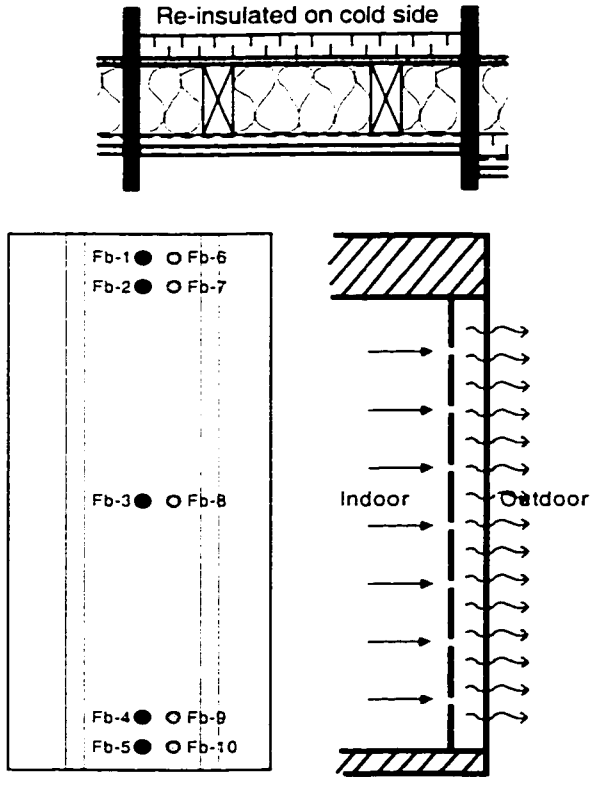

Figure 4.7. Gravimetry results, insulation added on cold side, distributed path.

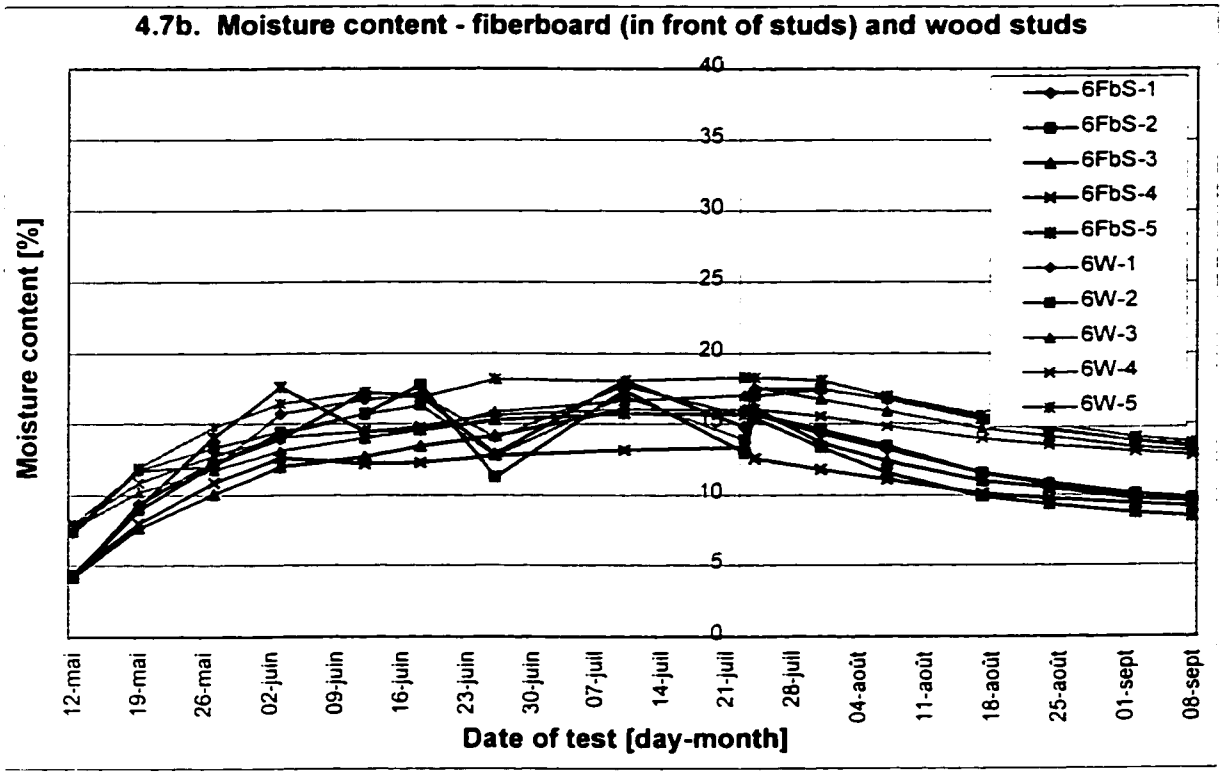

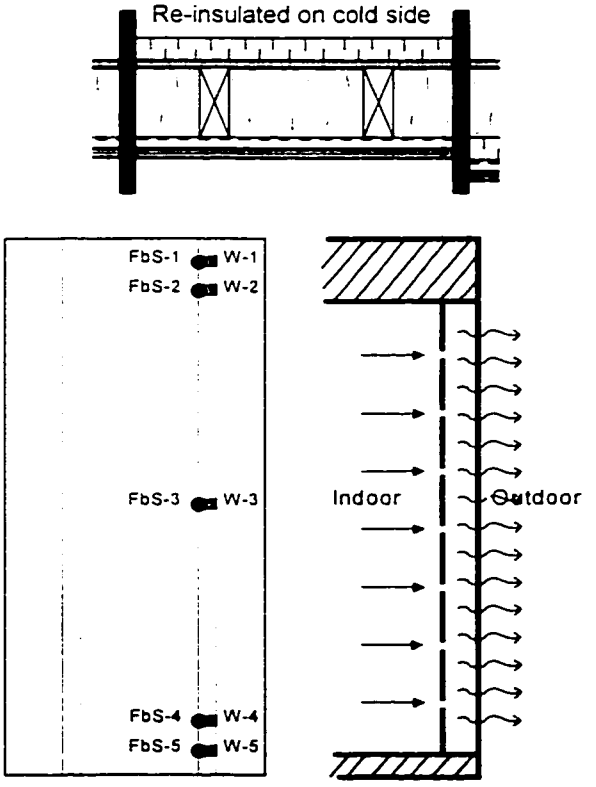

Figure 4.7. Gravimetry results, insulation added on cold side, distributed path.

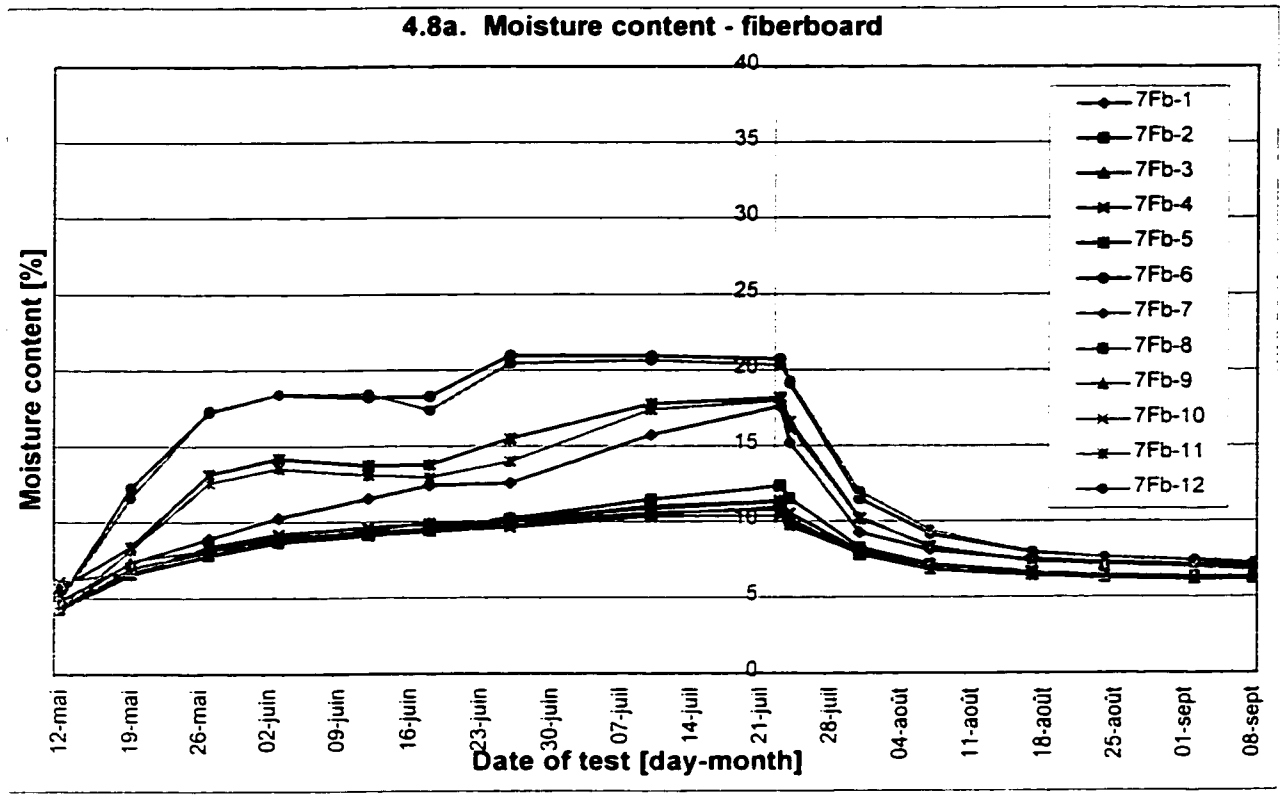

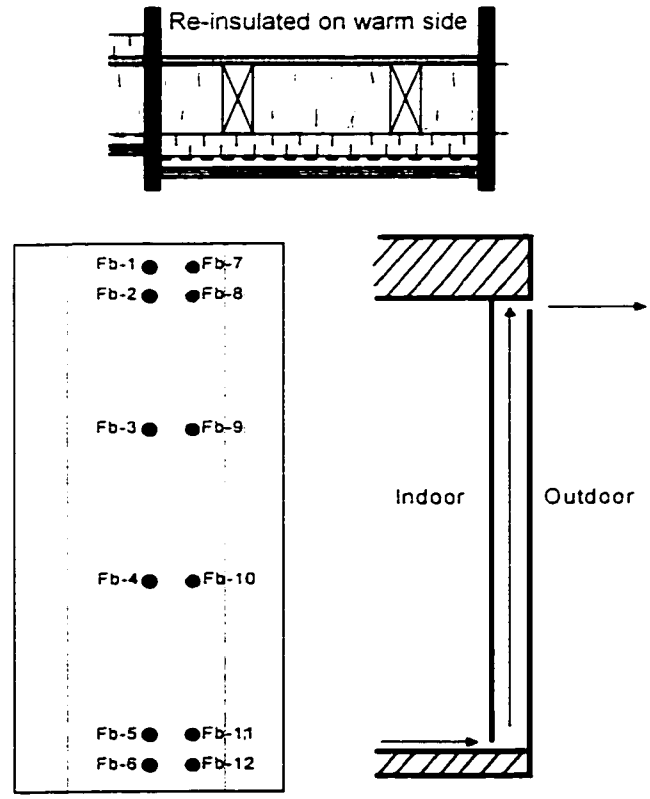

Figure 4.8. Gravimetry results, insulation added on warm side, long path.

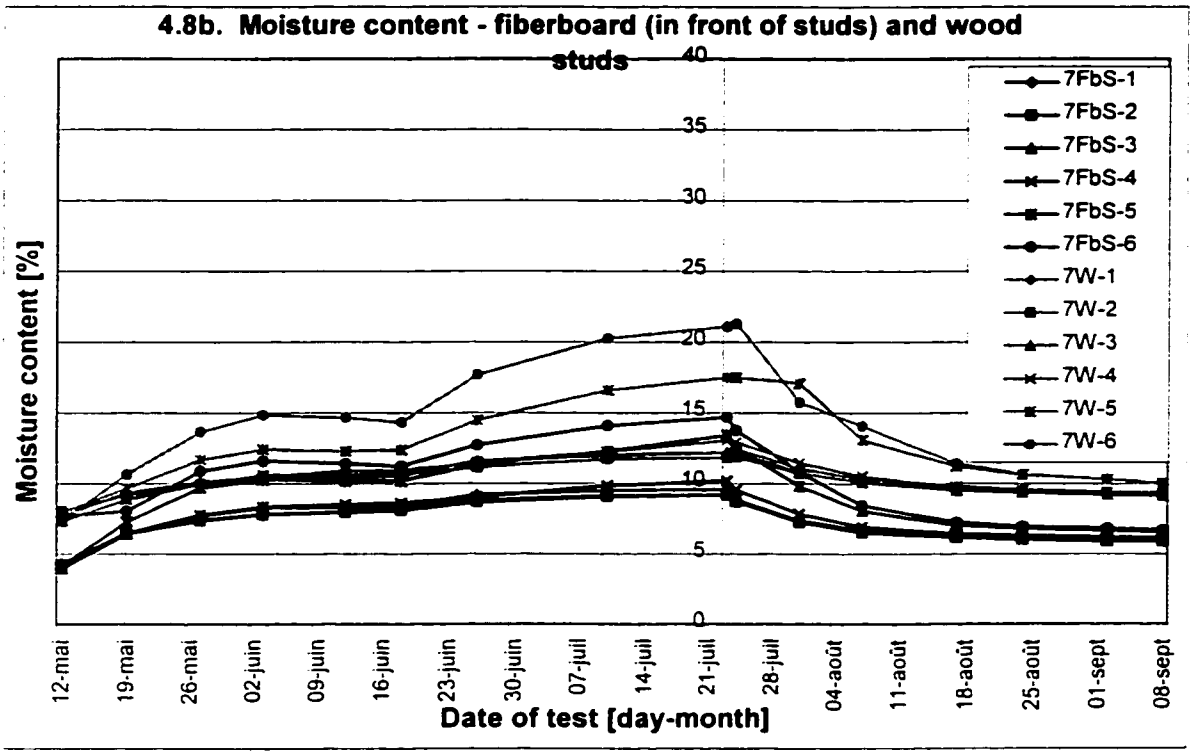

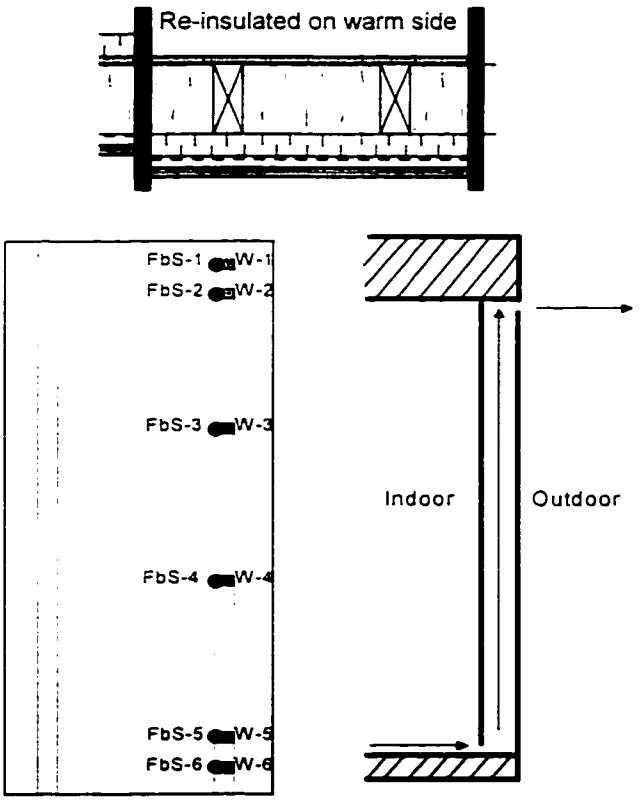

Figure 4.8. Gravimetry results, insulation added on warm side, long path.

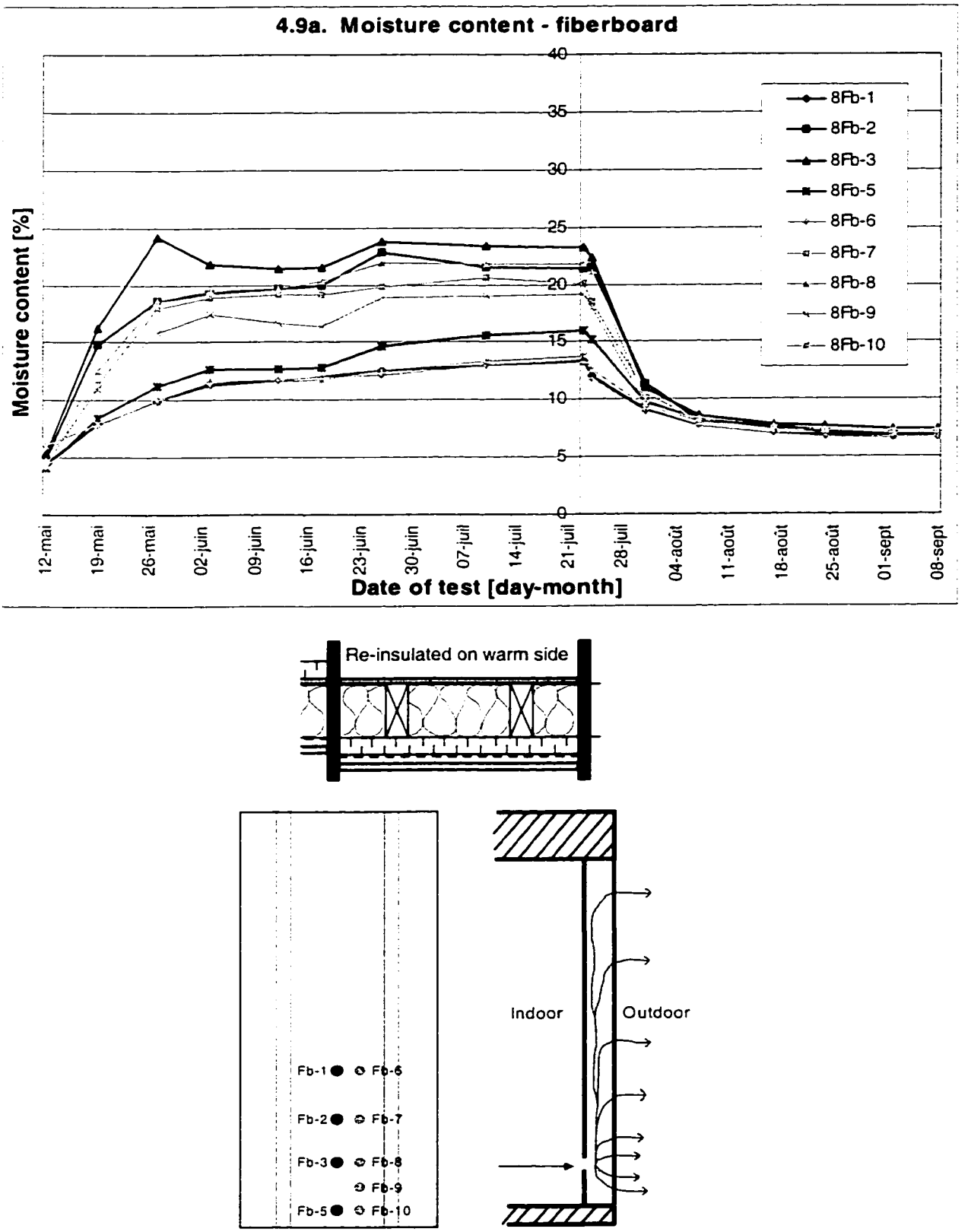

Figure 4.9. Gravimetry results, insulation added on warm side, concentrated path.

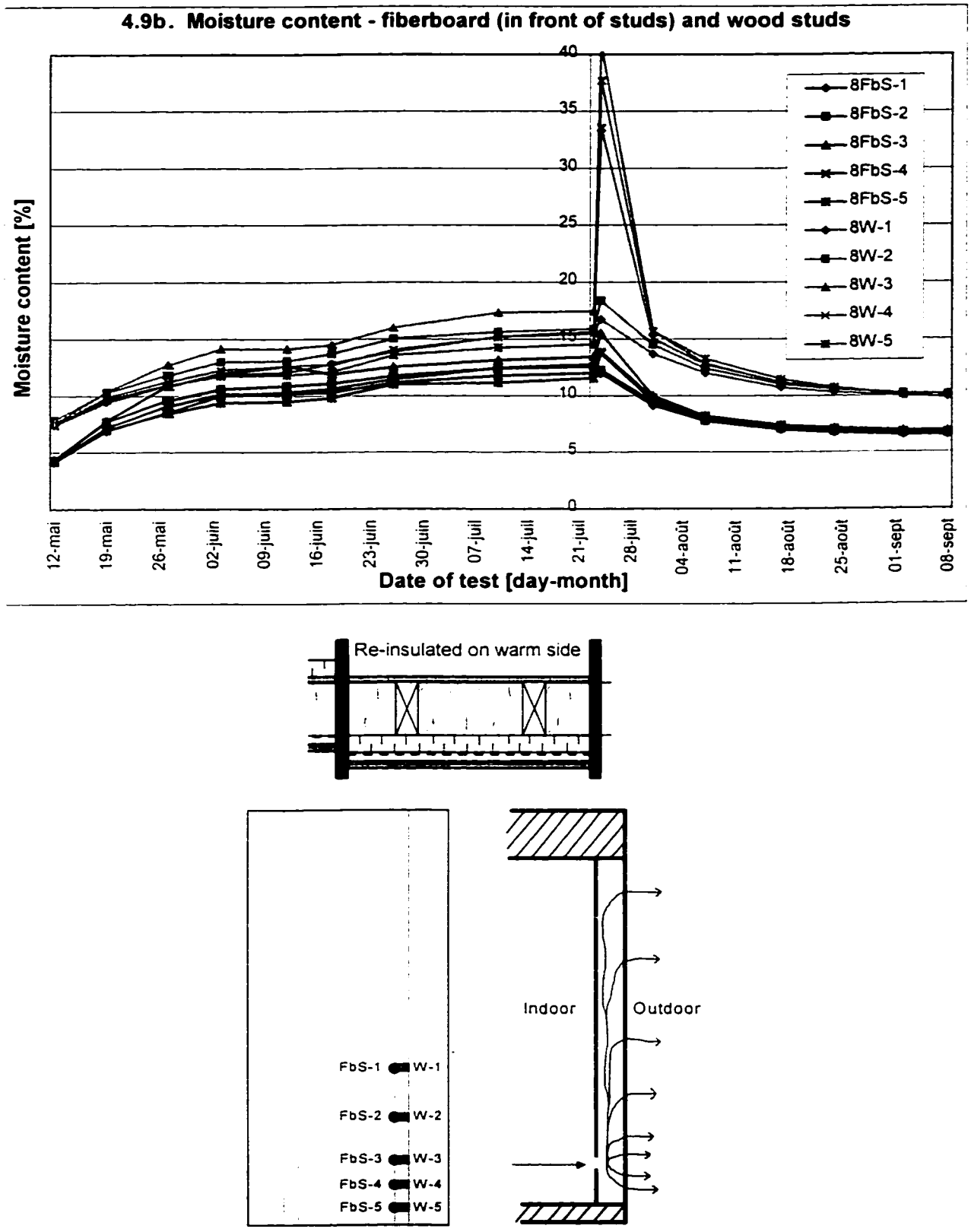

Figure 4.9. Gravimetry results, insulation added on warm side, concentrated path.

Analysis of the average fiberboard moisture content for entire sections provides further insight into the results. In Table 4.1, July 10th gravimetric fiberboard moisture content measurements are averaged for each sample section. This table shows that the sections with rigid insulation added on the cold side of the glass fiber batt insulation have the highest average moisture contents at 23%, and that the sections with the concentrated and distributed air leakage paths have higher average moisture contents than those with the long air leakage path or the airtight section. Those with rigid insulation added on the warm side of the glass fiber insulation show average moisture contents lower than the base-case assemblies. The sections with the lowest average moisture contents are the airtight section and the section with the long air leakage path and insulation added on the warm side of the glass fiber batt insulation, both at 13%. Adding rigid insulation on the warm side of the assemblies may have helped decrease the flow of air, and therefore the amount of indoor moisture getting inside the wall, while adding rigid insulation on the cold side apparently prevented moisture from indoor that had accumulated from drying toward the outdoor side.

Table 4.1. Average of gravimetric moisture content values in the fiberboard, July 10th.[5,6]

	Long path	Concentrated path	Distributed path	Airtight	**Average**
Base-case	17%	20%	19%	13%*	**17%**
Cold side	22%	27%	20%*		**23%**
Warm side	13%	15%			**14%**
Average	**17%**	**21%**	**20%**	**13%**	

[5] Switching samples from the top of these sections did not affect the overall moisture content average by more than 1% for the July 10th measurements. Assuming switched samples would have followed the trends of the others, the average moisture content would be around 12% for the airtight section and 21% for the section with the distributed air leakage path and rigid insulation added on the cold side.

[6] The area of openings in the interior finish for the distributed air leakage path is smaller than the area of openings for the long and concentrated air leakage paths (5.3 cm^2 compared to 7.1 cm^2).

The maximum moisture content values measured in the fiberboard for each section on July 10th are presented in Table 4.2. When comparing the two tables, Table 4.1 shows lower numbers and a variation of 14% between the lowest and the highest moisture content averages, while Table 4.2 shows higher numbers and a variation of 45% between the lowest and the highest maximum moisture content values. The fiberboard in the three sections with rigid insulation added on the cold side of the glass fiber batt insulation reached the highest moisture content, particularly those with the long and concentrated air leakage paths (61% and 53% maximum moisture content respectively). Fungus can grow (but not germinate) in wood from a moisture content of 19%, and both grow and germinate at moisture content above 28%, which is the fiber saturation point of the wood (CMHC, 1999). The high maximum moisture content values presented in Table 4.2 therefore constitute a warning that although the average moisture content did not rise above 27% for any of the sample sections studied, potential local problem areas may still exist. These problem areas are generally linked to the indoor air entry point into the assembly.

Table 4.2. Maximum gravimetric moisture content values in the fiberboard, July 10th.[7,8]

	Long path	Concentrated path	Distributed path	Airtight	**Average of maximum**
Base-case	25%	26%	26%	16%*	**23%**
Cold side	61%	53%	32%*		**49%**
Warm side	21%	23%			**22%**
Average of maximum	**36%**	**34%**	**29%**	**16%**	

[7] Switching samples from the top of these sections did affect the maximum moisture content in the airtight section on July 10th. Assuming the switched samples would have followed the trends of the others, the maximum moisture content would be around 12% for the airtight section.

[8] The area of openings in the interior finish for the distributed air leakage path is smaller than the area of openings for the long and concentrated air leakage paths (5.3 cm^2 compared to 7.1 cm^2).

4.1.2 Moisture content sensors results

Moisture content measurements from moisture content sensors are plotted over time and presented in Figure 4.10 to Figure 4.18. As for the gravimetry results graphs, the moisture content axis is located at the July 23rd mark, corresponding to the last day of simulated winter weather conditions. The darker curves show fiberboard moisture contents measured close to the wood stud, and the lighter curves show fiberboard moisture contents measured between the wood stud and the center of the section.

Looking at the graphs from the moisture content sensors, presented for all sample sections, a number of observations can be made. The June 16th power failure described in section 3.6.1 does not appear to have had a significant impact on the moisture contents measured by the sensors. However, as noted from the gravimetry results, the June 24th compressor failure had some impact on the moisture contents. An increase in moisture content can be seen for all monitored points from this date on, varying from 2% in the airtight section (Figure 4.10) to 8% for one location in the section with rigid insulation added on the cold side, concentrated air leakage path (Figure 4.15). Before that date, they seemed to have reached a plateau, and after, they reached another plateau, at higher moisture contents than before the June 24th event. A high rate of moisture content increase can be observed for all monitored points from July 21rst to July 24th, the first day of the late-spring simulated weather conditions. By August 4th, all measured moisture content values were back to their initial levels or below. After this date, most moisture content curves are flat, indicating that moisture content for these monitoring points was at or below 7% since moisture content sensors cannot read levels below this.

As for the gravimetry results, moisture content sensor results were the lowest for the airtight section, generally below 10% throughout the test, except for one location (bottom, between stud and center of the section) where the moisture content went up to 17% (Figure 4.10). Moisture content values reached the highest levels for the base-case assemblies with the concentrated and distributed air leakage paths, rising up to 47% and 53% respectively (Figure 4.12 and Figure 4.13). This is not coherent with the gravimetry measurements for the same sections. However, these high levels were not sustained for a long period in either case, as they were reached just before the change of climatic conditions. Moisture content values for these sections did otherwise remain below the 28% level during the winter conditions, which is consistent with the gravimetry results obtained for these sections.

A significant difference in moisture content from both measurement methods can be observed for the sections with rigid insulation added on the cold side. The moisture content sensor measurements (Figure 4.14 to Figure 4.16) are much lower that the gravimetry measurements (Figure 4.5 to Figure 4.7) for these sections. According to moisture content sensor measurements, moisture contents did not rise above 30% for any of the section, compared to levels of up to 70% according to gravimetry measurements. Moisture content sensor readings do not seem to be accurate for moisture content values above 30%. For the sections with rigid insulation added on the warm side, moisture contents measured by both methods are consistent.

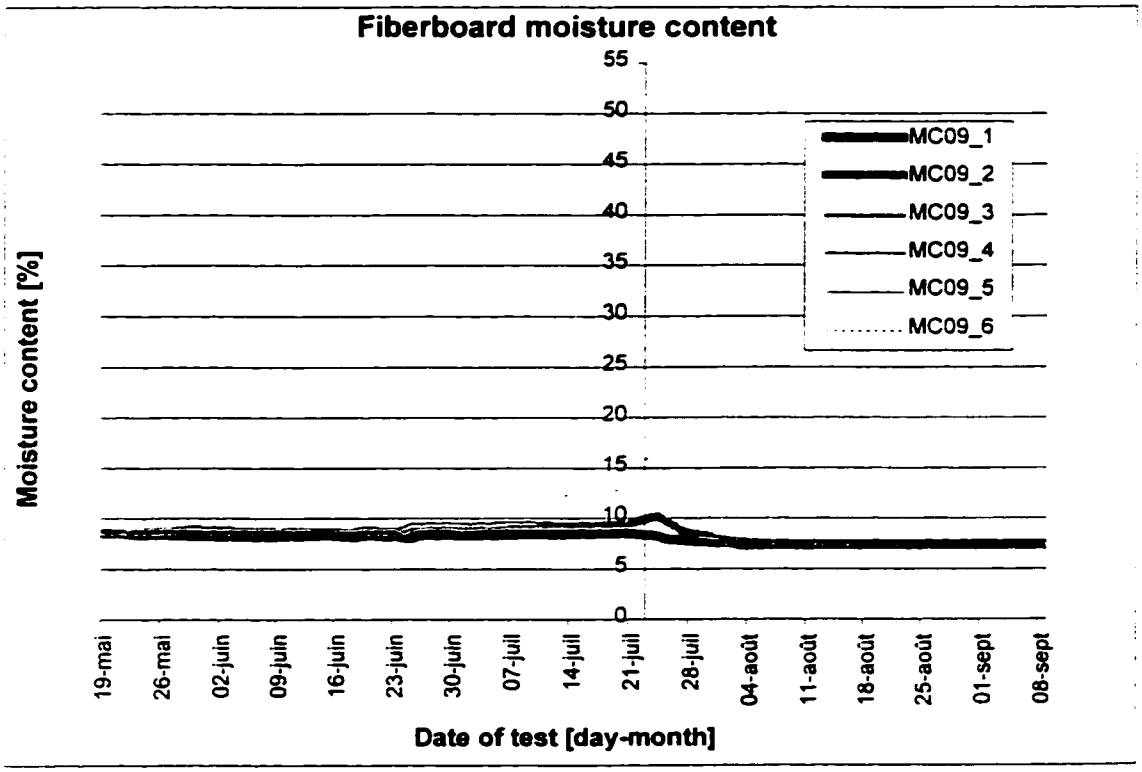

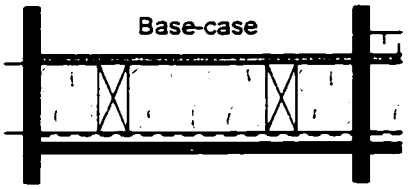

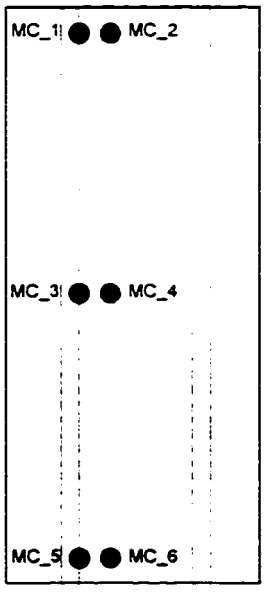

No air leakage path

Figure 4.10. MC sensor results, base-case assembly, airtight.

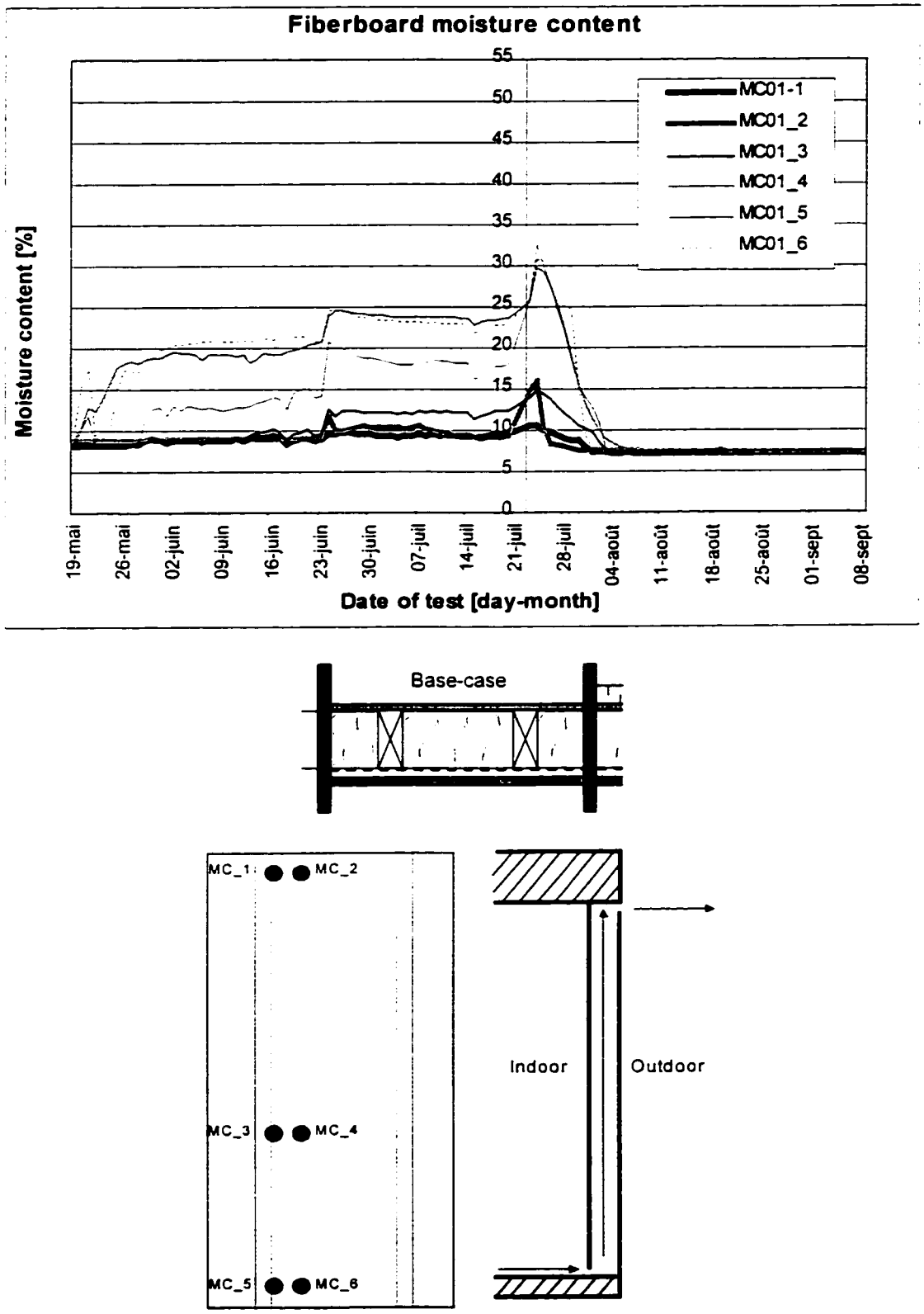

Figure 4.11. MC sensor results, base-case assembly, long path.

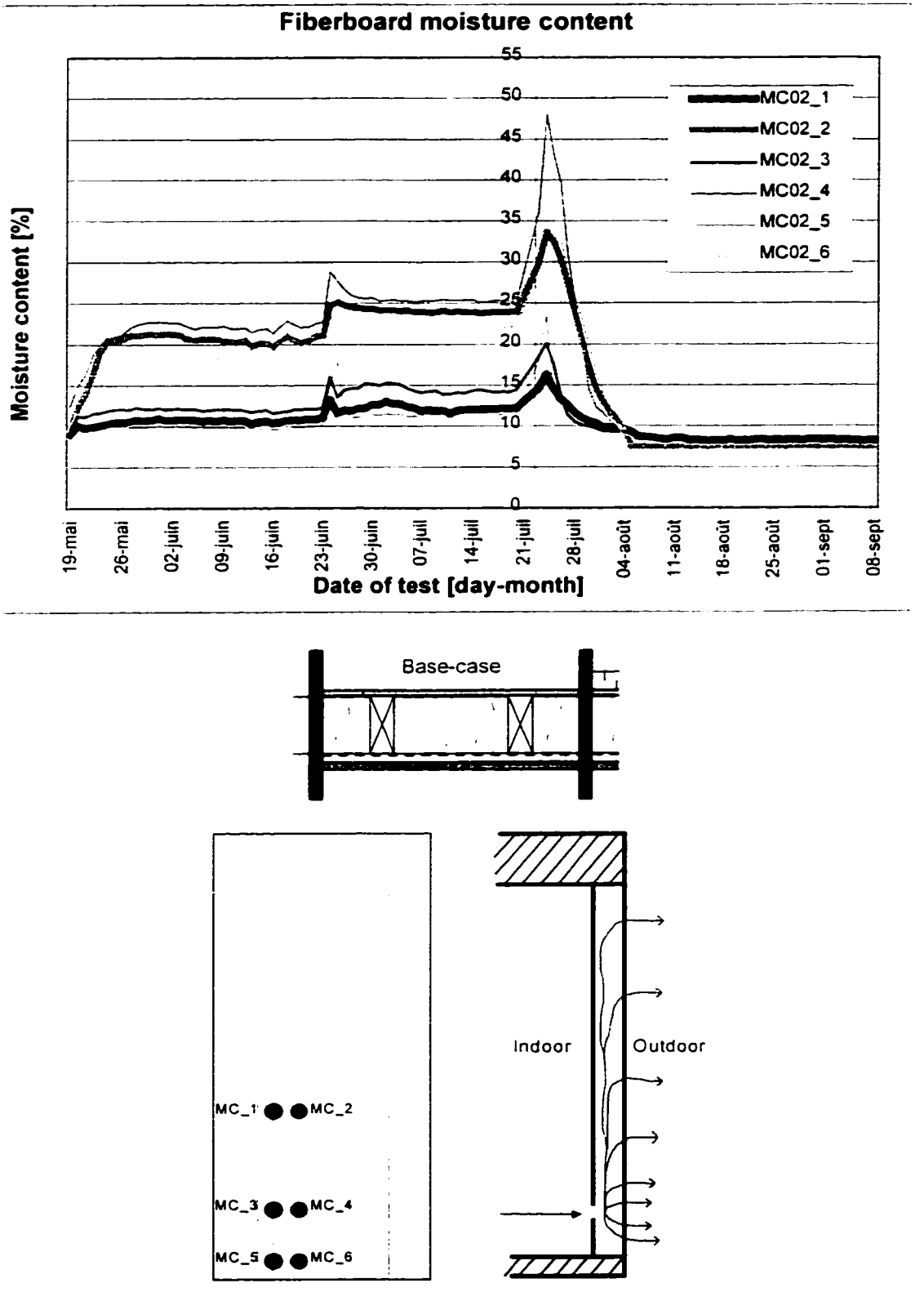

Figure 4.12. MC sensor results, base-case assembly, concentrated path.

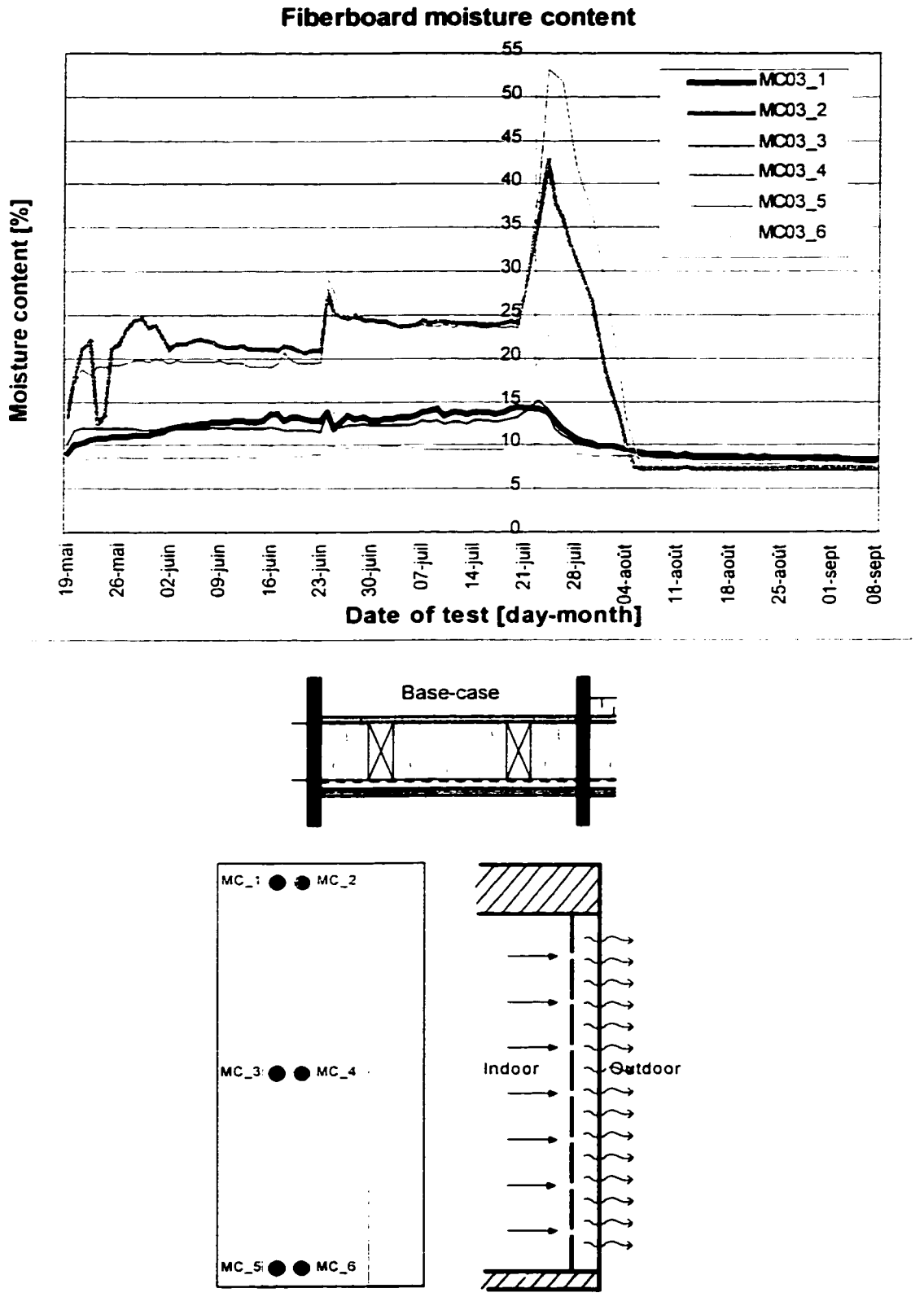

Figure 4.13. MC sensor results, base-case assembly, distributed path.

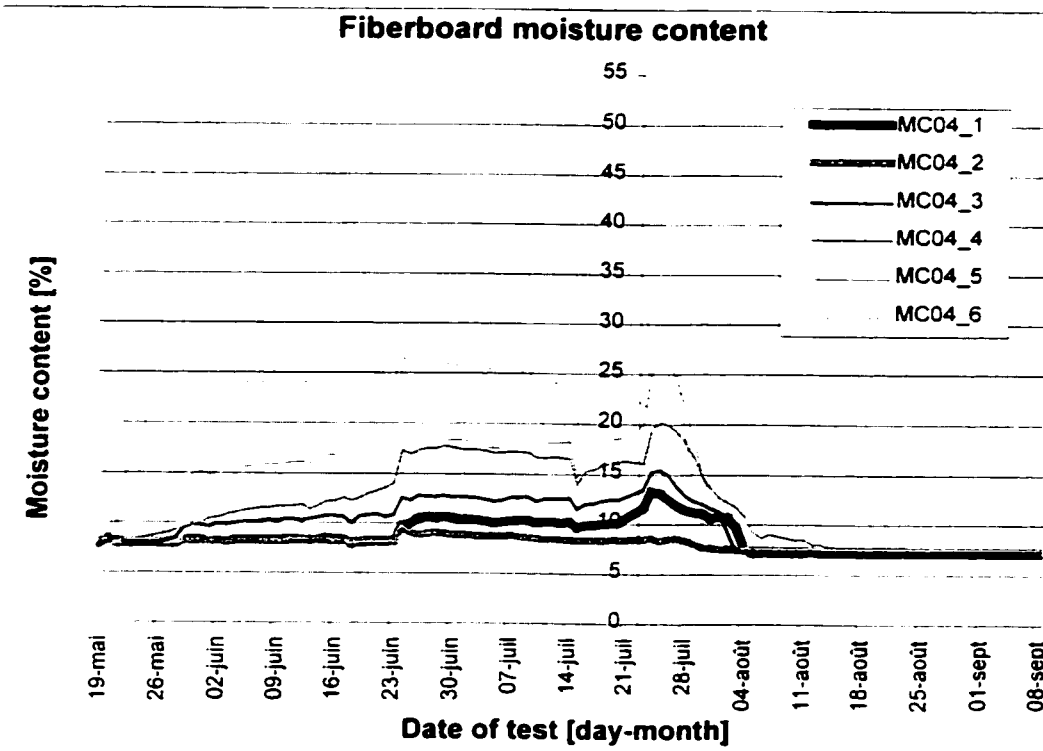

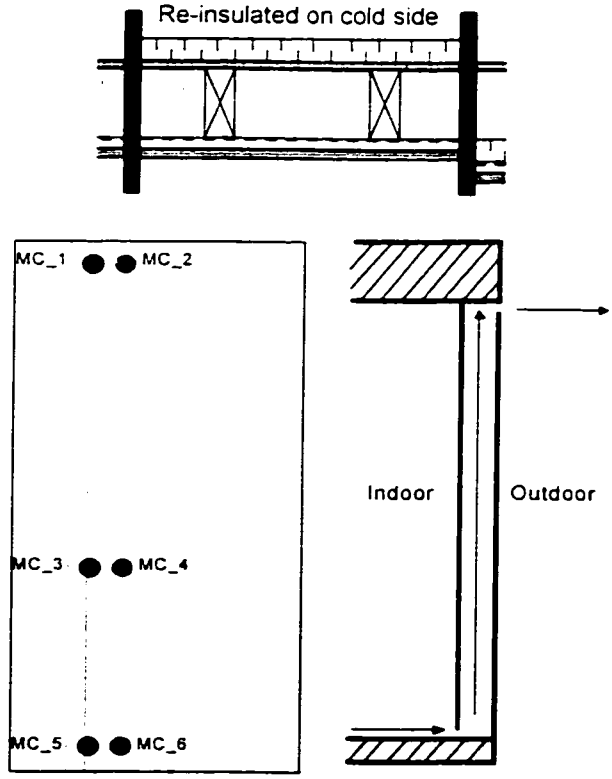

Figure 4.14. MC sensor results, insulation added on cold side, long path.

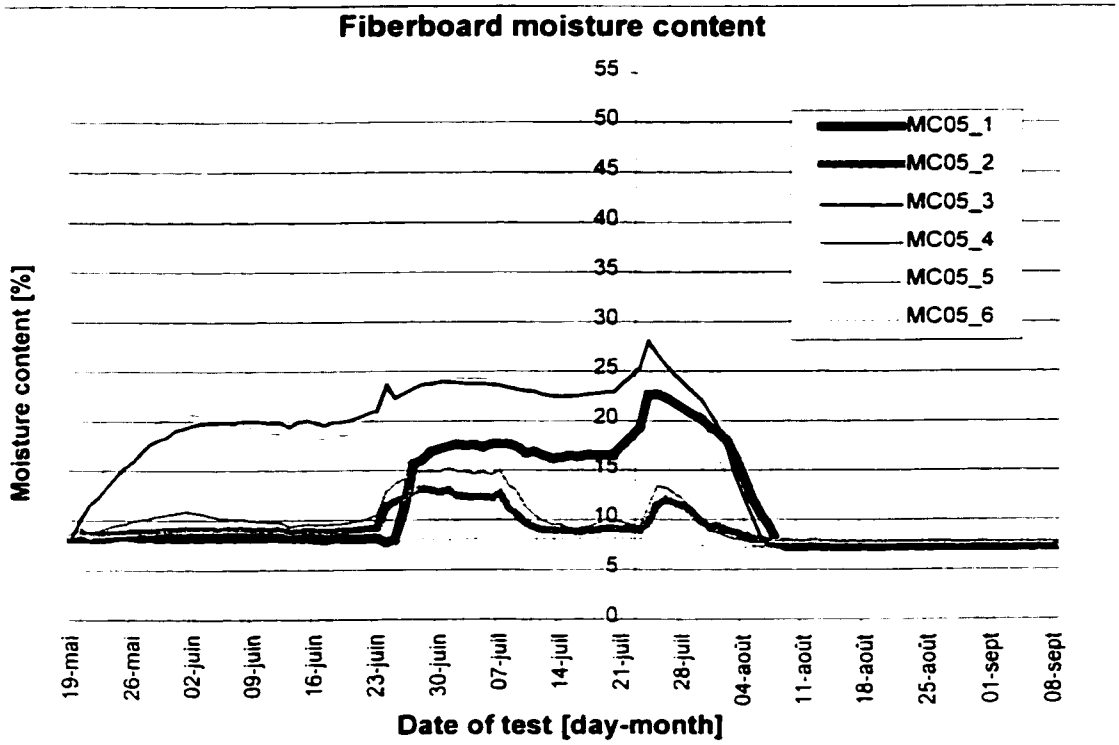

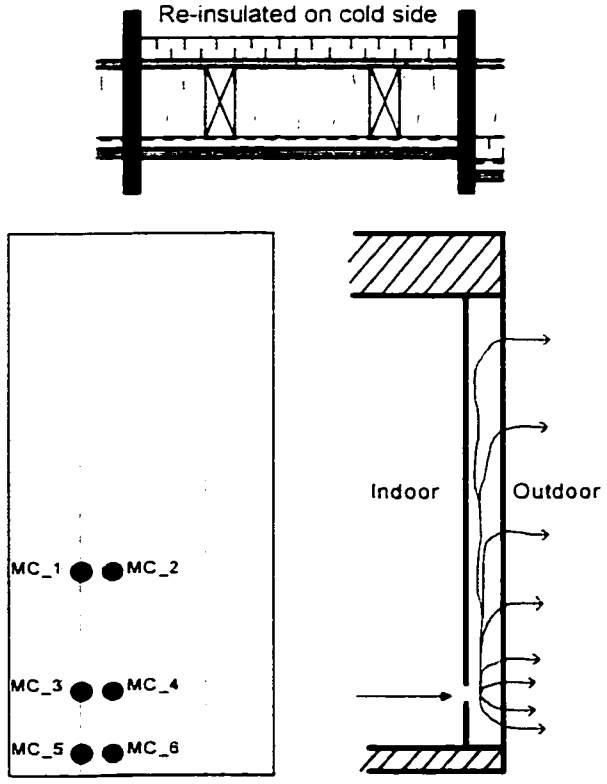

Figure 4.15. MC sensor results, insulation added on cold side, concentrated path.

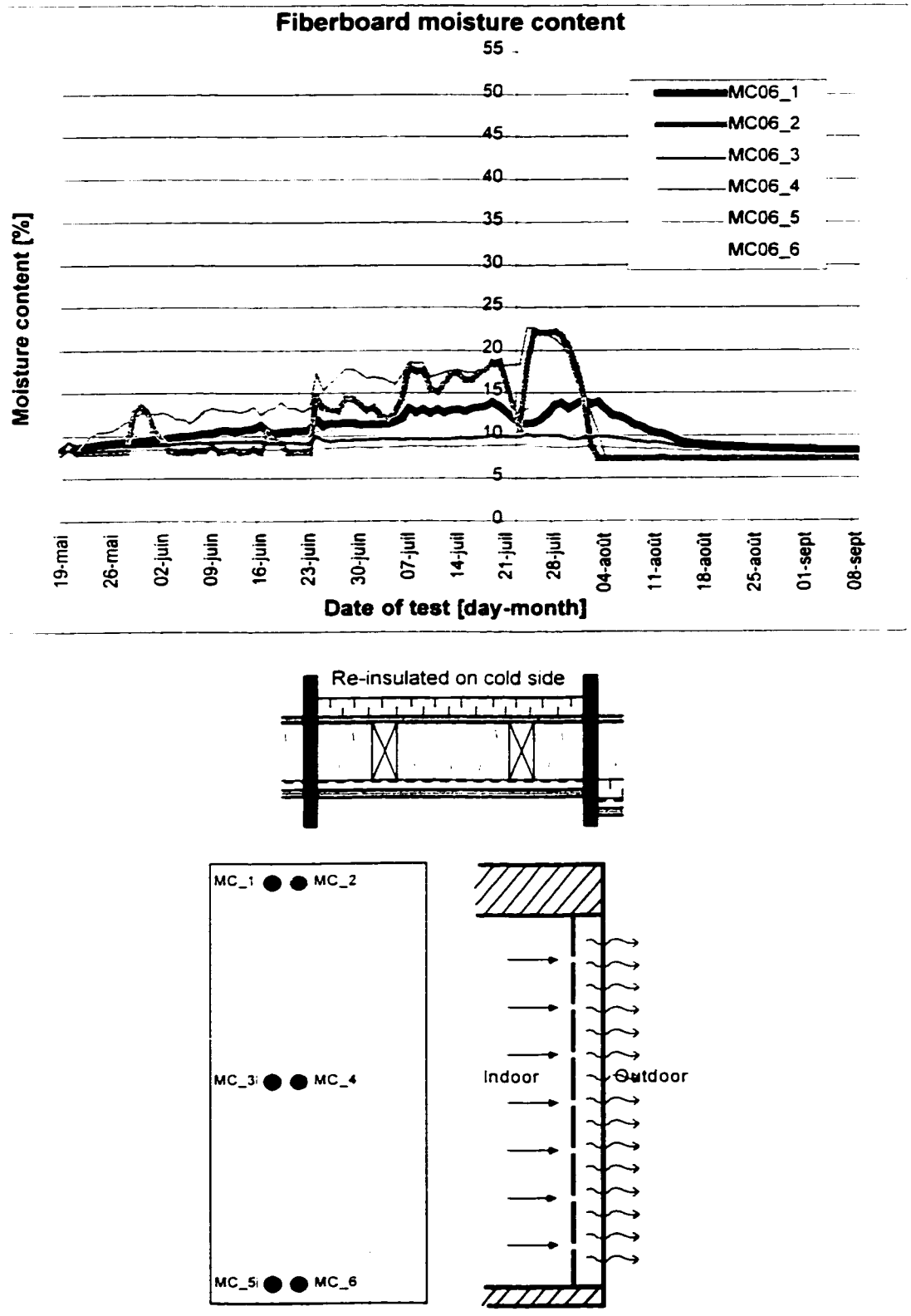

Figure 4.16. MC sensor results, insulation added on cold side, distributed path.

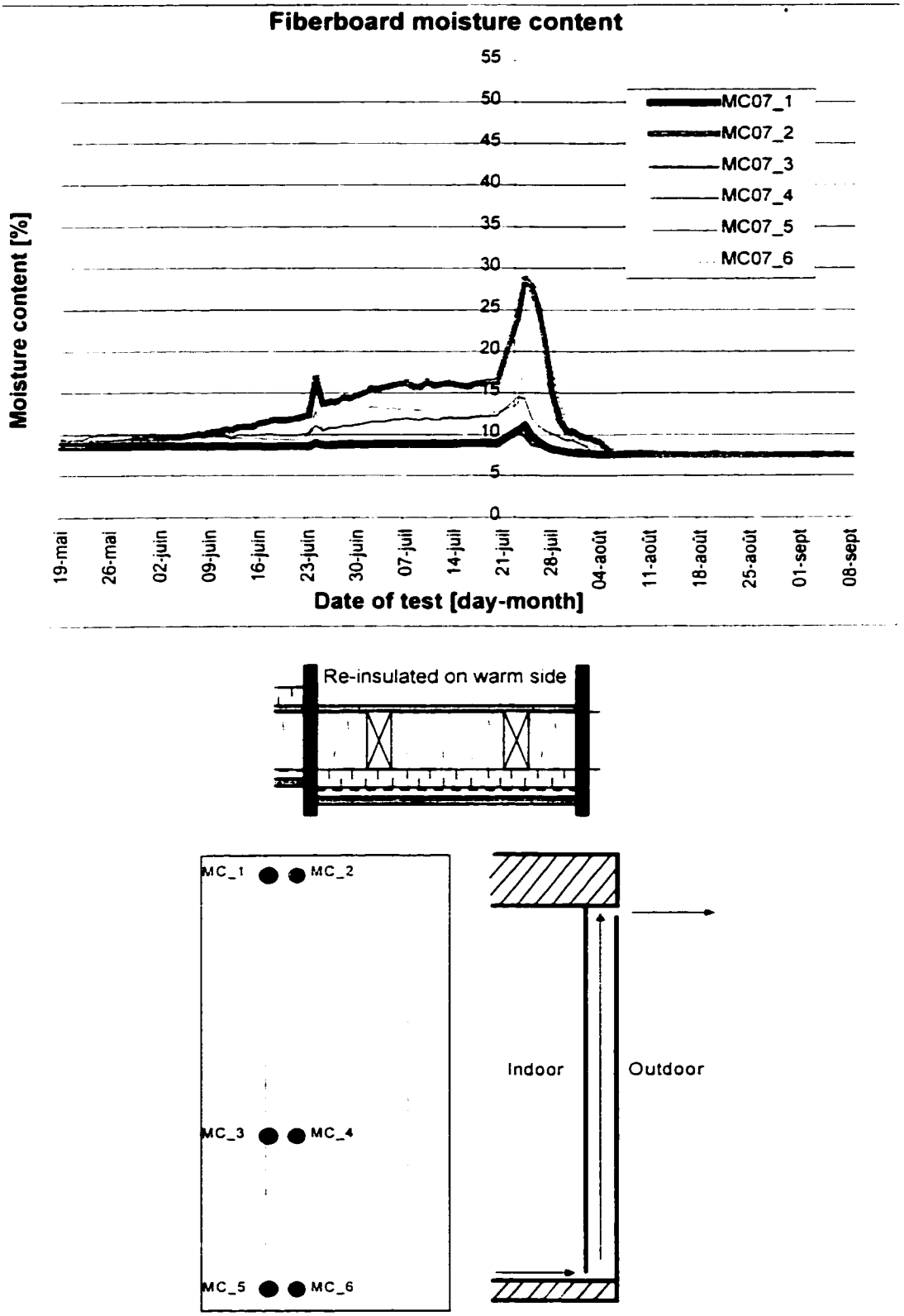

Figure 4.17. MC sensor results, insulation added on warm side, long path.

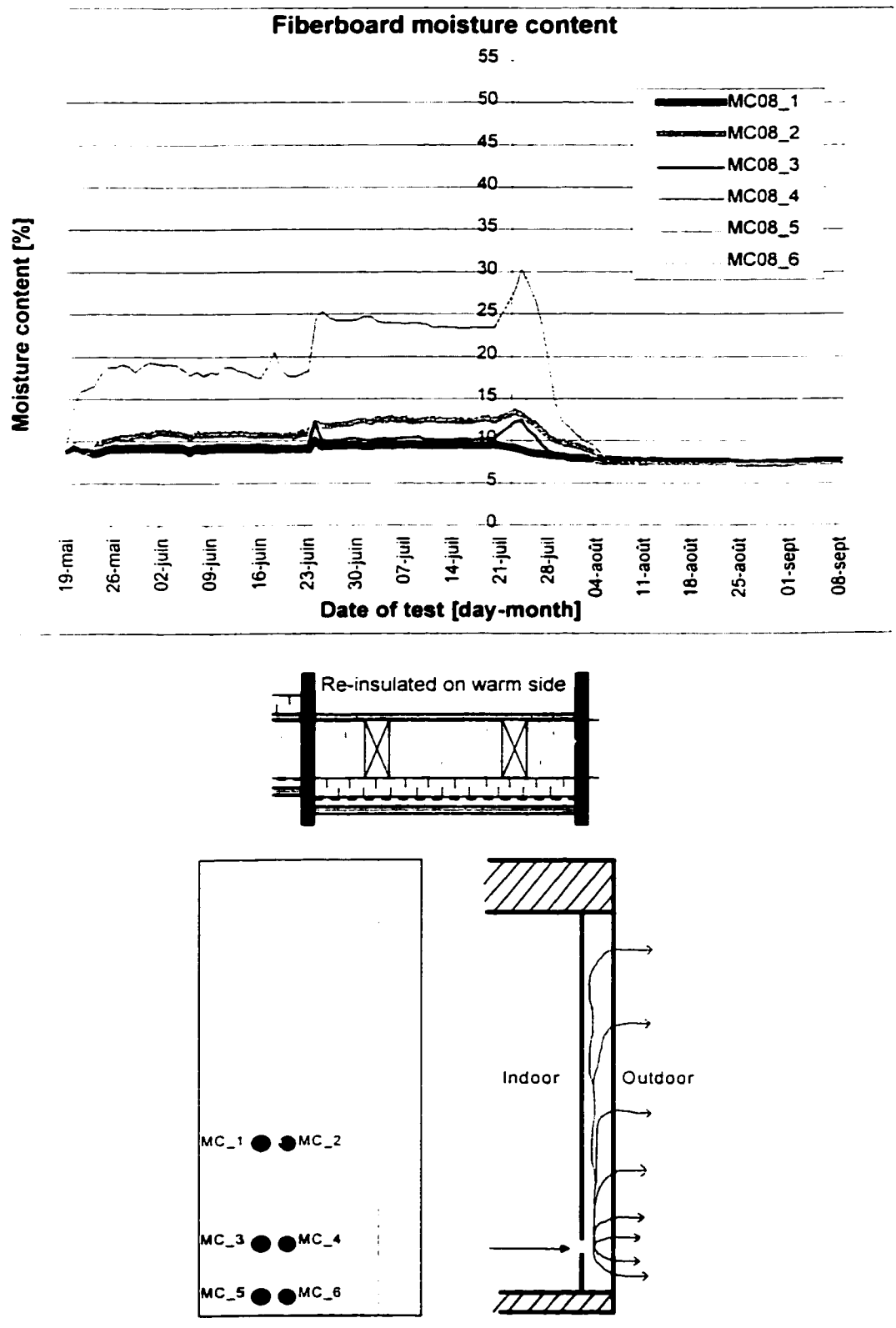

Figure 4.18. MC sensor results, insulation added on warm side, concentrated path.

4.2 Temperature monitoring

Adding rigid insulation to the base-case assembly had a strong impact on measured warm plane and cold plane temperatures. Throughout the wetting period, the assemblies with rigid insulation added on their cold side had higher measured temperatures, and those with rigid insulation added on their warm side had lower measured temperatures than the base-case assemblies.

Temperatures plotted over time are presented in Appendix B for each of the 192 points monitored. One typical temperature graph is included for discussion in Figure 4.19. This graph shows the temperatures on the warm side of the wood stud for the base-case assembly with the long air leakage path. In this graph, the two testing periods are identifiable by the two distinct temperature levels. Two temperature peaks are seen around June 16th and 25th for all monitored points. These peaks are caused by the two events described in section 3.6.1, i.e. a power failure on June 16th and a compressor failure on June 24th. Although most monitored points remained at a fairly constant temperature for the duration of each climatic period, the temperature of some of the points was varying. For example, the bold curve in Figure 4.19 shows temperatures at the bottom of the wood stud did not remain stable. This might indicate a more complex behaviour due, for example, to the presence of convection loops within the assemblies. These findings have not been further investigated.

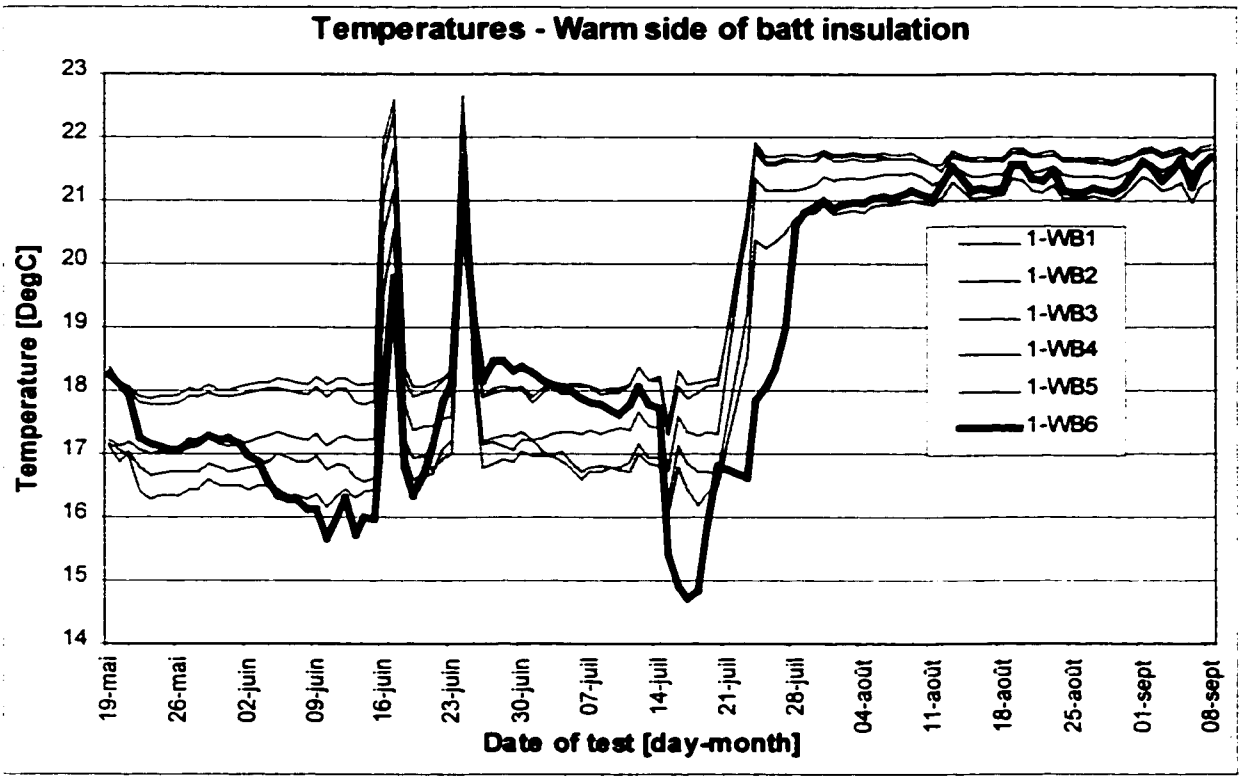

Figure 4.19. Temperatures for the base-case assembly, long leakage path.

The subsequent analysis examines data after steady-state for the first climatic period was established. The temperatures measured at the indoor surface of the glass fiber batt insulation will be referred to as *warm plane* temperatures, and those at its outdoor surface as *cold plane* temperatures.

Temperature averages for each monitoring point between May 26th and 30th, when no significant moisture build up had occurred but temperature equilibrium had been reached, were used for the analysis.

In Figure 4.20 to Figure 4.22, the averaged measured temperature gradients across the edge of the wood studs and across the glass fiber batt insulation for the May 26th to 30th period are shown at three different heights, 300 mm, 900 mm, and 2100 mm, for each wall composition. The temperature gradients calculated using the three-dimensional

conductive heat transfer model are also plotted on these figures. The points used for the calculations were the same as those for monitoring. This representation allows to compare the monitored temperature gradients across the edge of the studs and across the batt insulation at different heights for different air leakage patterns, and monitored versus calculated temperature gradients.

Figure 4.20 to Figure 4.22 shows the effect of the thermal bridges caused by the wood studs, temperature gradients being greater across the batt insulation than across the edge of the wood studs.

The measured and calculated temperature gradients for the base-case assemblies are shown in Figure 4.20. At the 900 mm and 2100 mm levels, the temperatures are higher in both planes for the long leakage path than for the concentrated leakage path and the airtight section, as if the air is warming the materials as it flows up. At the 300 mm level, which is the height of the concentrated leakage opening and warm air entry point, higher temperatures are found in the concentrated path wall. The difference in temperature gradients between the different air leakage paths is more pronounced across the studs than across the insulation. This is likely due to the thermal bridge effect of the studs. Before the installation of the interior finish, the construction was checked to ensure that there was no gap between the studs and the glass fiber batt insulation, so that no air could flow along the studs. The calculated temperature gradients are slightly greater than the measured temperature gradients across the insulation and across the edge of the studs. One explanation would be the presence of convection between the batt insulation and the studs for the measured results.

Figure 4.21 shows measured and calculated temperature gradients for the sections with insulation added on the cold side. It can be seen that measured and calculated temperatures are higher for these sections than for the airtight base-case assembly. The calculated temperature gradient across the edge of the wood studs and across the batt insulation is similar to the measured temperature gradients. The measured temperatures across the edge of the wood studs tend to be slightly lower than calculated temperatures, especially at the cold plane.

Figure 4.22 shows measured and calculated temperature gradients for the sections with insulation added on the warm side. For these sections, the measured and calculated temperatures are lower than those measured for the airtight, base-case assembly. Temperatures measured for the section with the long path are higher than those calculated at the 300 mm and 2100 mm levels. This is more pronounced across the edge of the wood stud than across the batt insulation. For the section with the concentrated path, at the 300 mm level, the measured temperature gradient at the edge of the stud is greater than the calculated temperature gradient. At the 900 mm level, the measured temperature gradient is smaller than that calculated, both across the edge of the studs and the batt insulation.

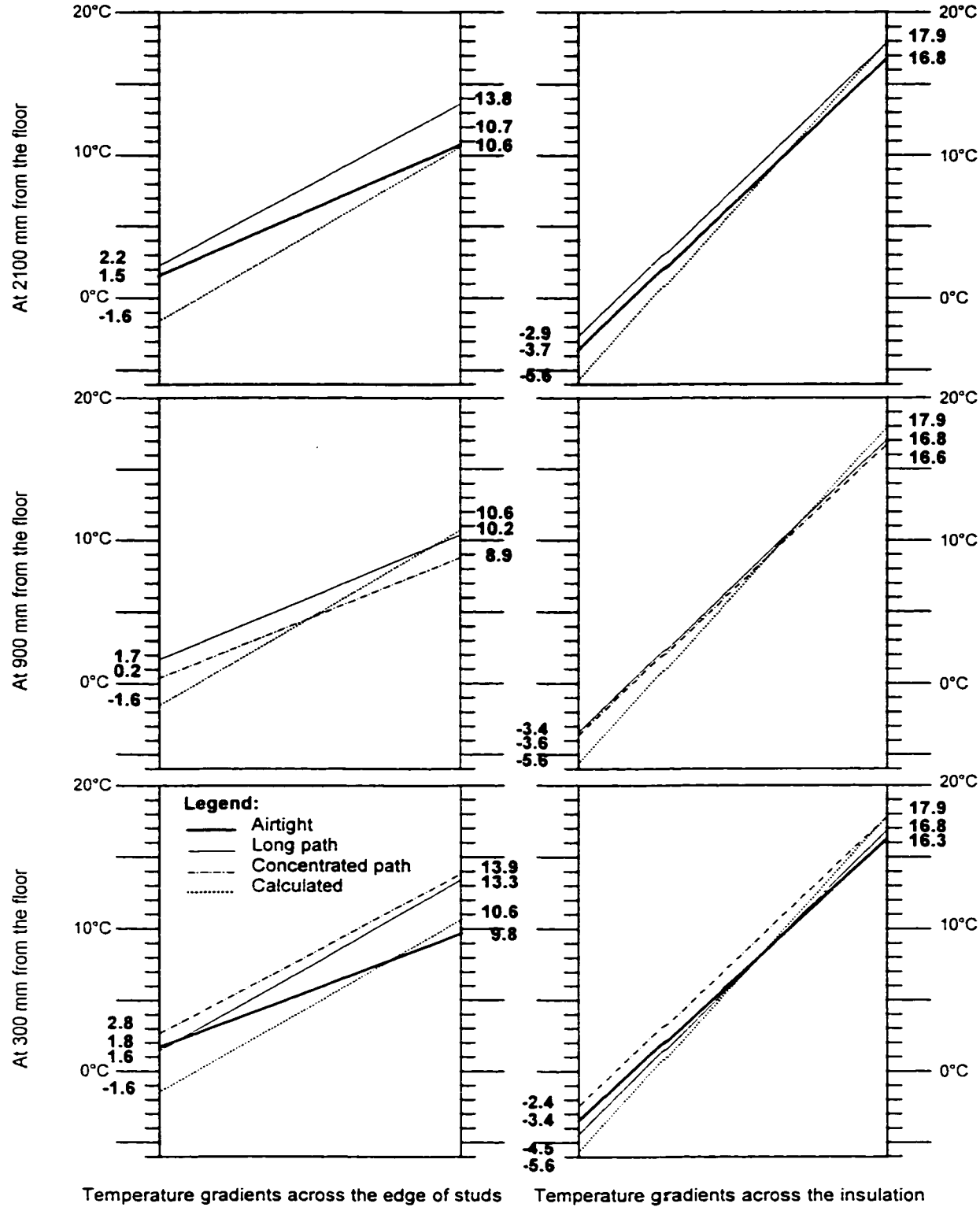

Figure 4.20. Measured and calculated temperature gradients across side of wood stud and batt insulation - base-case assemblies.

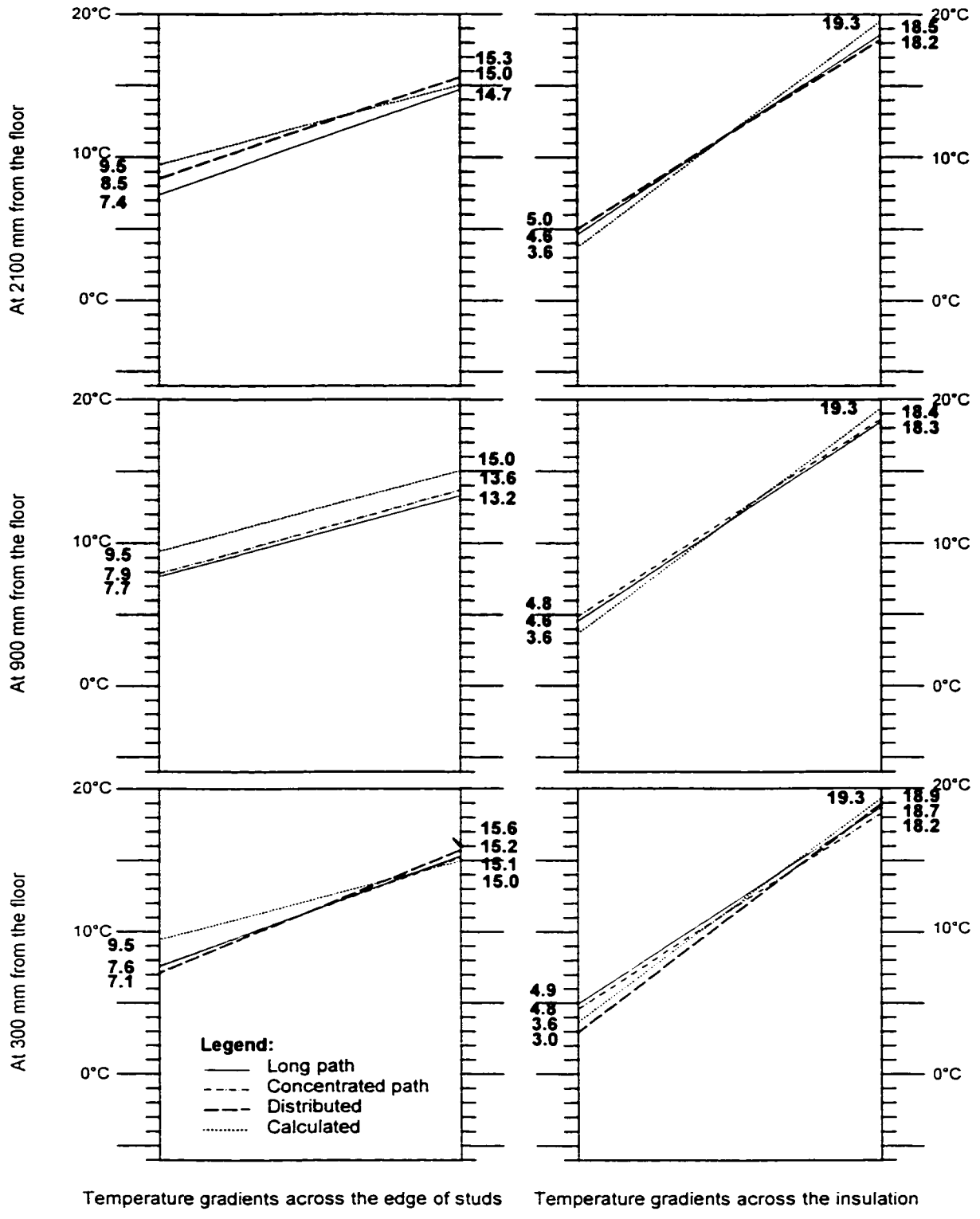

Figure 4.21. Measured and calculated temperature gradients across side of wood stud and batt insulation - insulation added on the cold side.

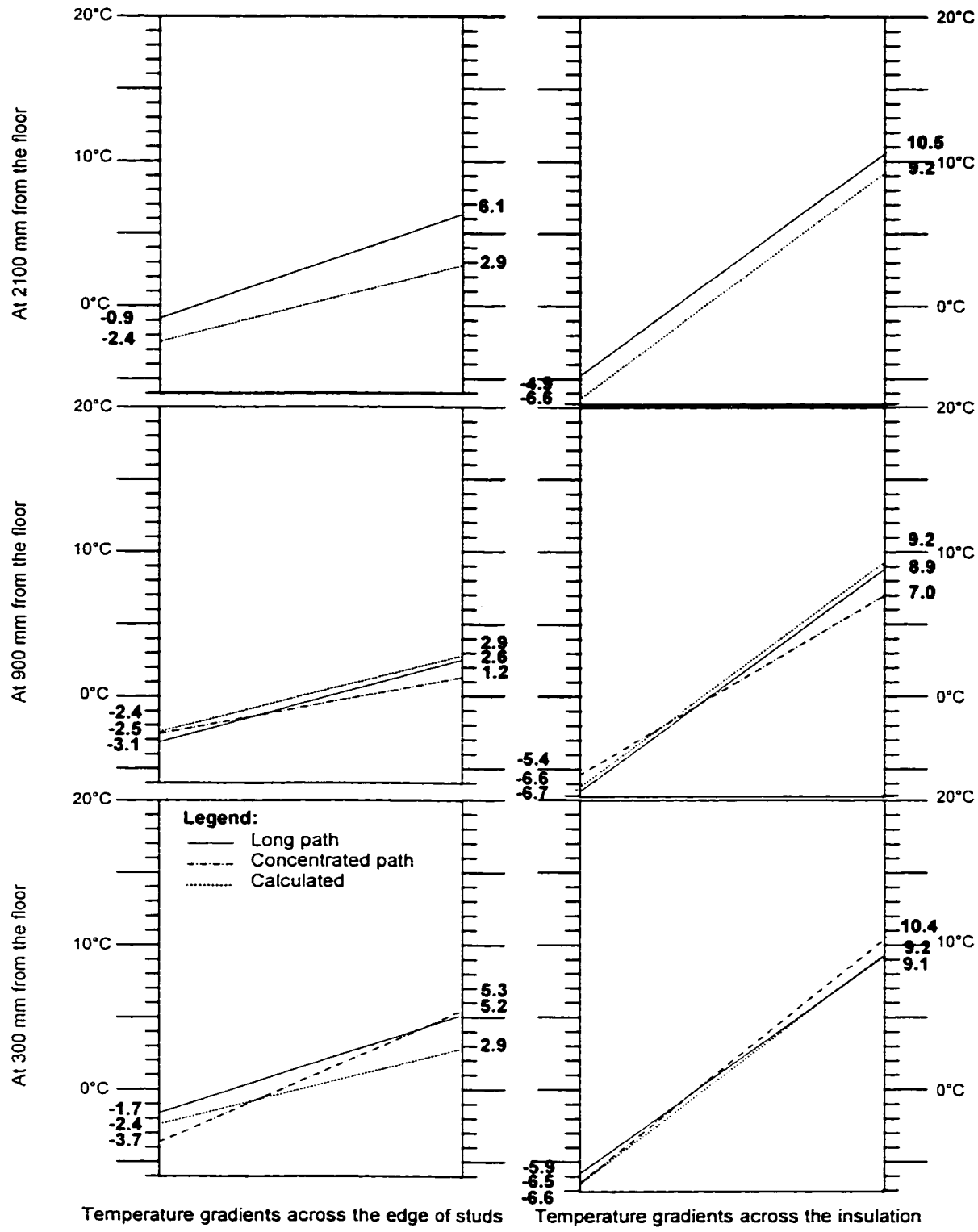

Figure 4.22. Measured and calculated temperature gradients across side of wood studs and batt insulation - insulation added on the warm side.

The average temperatures measured between May 26th and May 30th are presented in Table 4.3 and Table 4.4. The sections with the distributed path have the highest temperature average, while the sections with the concentrated path have the lowest temperature average. The airtight section has the highest temperature gradient, 16°C compared to 12°C (long path), 11.7°C (concentrated path) and 12.9°C (distributed path). From the temperature averages for each insulation strategy, it can be seen that the effect of adding insulation on the cold side is most accentuated on the cold plane: the average temperature is 2°C warmer than for the base-case on the warm plane and 7.5°C warmer than the base-case on the cold plane. When adding insulation on the warm side, the effect is most visible on the warm plane temperatures: the average temperature is 7.2°C colder than the base-case for the warm plane and 2.4°C colder than the base-case for the cold plane.

Table 4.3. Average warm plane temperatures [DegC] for the May 26th to May 30th period in the test.[9]

	Long path	Concentrated path	Distributed path	Airtight	**Average**
Base-case	15.3	13.8	13.7	14.8	**14.4**
Cold side	16.4	16.3	16.5		**16.4**
Warm side	7.9	6.6			**7.2**
Average	**13.2**	**12.2**	**15.1**	**14.8**	

Table 4.4. Average cold plane temperatures [DegC] for the May 26th to May 30th period in the test.

	Long path	Concentrated path	Distributed path	Airtight	**Average**
Base-case	-0.4	-0.9	-2.0	-1.2	**-1.1**
Cold side	6.5	6.3	6.5		**6.4**
Warm side	-3.2	-3.8			**-3.5**
Average	**1.0**	**0.5**	**2.2**	**-1.2**	

[9] The area of openings in the interior finish for the distributed air leakage path is smaller than the area of openings for the long and concentrated air leakage paths (5.3 cm^2 compared to 7.1 cm^2).

4.3 Overall performance of the wall assemblies tested

The results have shown that the assemblies with insulation added on their cold side were exposed to higher moisture content conditions and those with insulation added on the warm side to lower moisture content conditions that the base-case assemblies. Moisture content levels in the sections with insulation added on the cold side also dropped more slowly and remained higher at the end of the drying period than for the other sections. The base-case airtight section remained the driest. The temperature results show that the addition of the insulation of the cold side of the assembly raised the average temperature of the sheathing from -1.1°C to 6.4°C. The fact that the temperature is above the freezing point but below the dew point of the indoor air of 11°C means that the temperature conditions at the interface between the rigid insulation and the fiberboard sheathing are favourable to condensation. Addition of insulation on the warm side lowered the average temperature of the fiberboard from -1.1°C to -3.5°C.

These results highlight how adding insulation affects the hygrothermal behaviour of assemblies, depending on the side chosen to add insulation and the air leakage provided.

5. MOISTURE CONTENT AND TEMPERATURE MAPPING

The assemblies tested were exposed to three different air leakage paths. Moisture content and temperature were monitored with a specific monitoring grid that included gravimetric samples, moisture content sensors and thermocouples. These grids were devised with the intent of producing maps from the data. The present section presents the moisture content contour lines produced for the fibreboard, on the cold side of the studs and the temperature contour lines for two planes, on each side of the studs. The curves were produced using the monitored points and in between points, which values were extrapolated in order a sufficient number of points.

5.1 Moisture content mapping

5.1.1 Mapping using gravimetry data

The gravimetry data collected for the fiberboard sheathing on July 10th (corresponding to the 7^{th} weighing, on the 53^{rd} day into the test) was chosen to produce contour lines of equal moisture content, called isohygrons. As is seen in the graphs where moisture content values are plotted over time (Figure 4.1 to Figure 4.9), this data corresponds to high or near peak moisture content for the fiberboard gravimetry samples. The isohygrons are presented in Figure 5.1 to Figure 5.4. The numbers on the curves correspond to the fiberboard moisture content in percentage per dry weight.

By comparison with neighbouring gravimetry samples, the data used to generate the isohygrons for the base-case airtight section were corrected to eliminate the effect of the misplacements of the samples. The resulting isohygrons are presented in Figure 5.1. The moisture contents are very low, and there is no significant vertical moisture content gradient.

Isohygrons for the sections with the long air leakage path are shown in Figure 5.2. For these three sections, the fiberboard moisture content is higher toward the bottom, at the air entry point. The vertical gradient is most accentuated for the section with rigid insulation added on the cold side of the batt insulation (Figure 5.2b), a difference of approximately 55% between the bottom and the top, while the range for the other two insulation strategies is around 15% for the base-case assembly and 10% for the section with insulation added on the warm side. The sample section with insulation added on the cold side also reached the highest moisture content value: 60% compared to 25% for the base-case assembly and 21% for the section with insulation added on the warm side. It might be concluded that the higher moisture content at the bottom is due to a gravity effect. However, if this were the case, then the same phenomenon would be observed for the sections with the concentrated and distributed air leakage paths. As is explained below, the moisture content maps show different accumulation patterns for these sections.

In the sections with the concentrated air leakage path (Figure 5.3), moisture is concentrated at the height of 450 mm, just above the circular air entry point in the gypsum board. The section with insulation added on the cold side reaches the highest moisture content (Figure 5.3b). The concentric pattern of moisture accumulation, following the shape of the hole in the interior finish, is clear for the base-case assembly (Figure 5.3a) and the section with rigid insulation added on the warm side (Figure 5.3c), but less obvious for the section with rigid insulation added on the cold side (Figure 5.3b), where fiberboard moisture content values remain higher even above this height. This would indicate that warm air is flowing up, its moisture condensing at the indoor surface

of the rigid insulation and then being absorbed by the fiberboard sheathing over a bigger area of fiberboard. This condensation was actually observed during the test for all samples with the rigid insulation added on the cold side. When the piece of rigid insulation was removed to allow collection of the gravimetry samples, its interior surface was covered with drops of water.

Figure 5.4 shows isohygrons for the sections with the distributed air leakage path. For the base-case assembly (Figure 5.4a), moisture contents range from 15% to 25%, being higher at the top of the section. This vertical moisture content gradient is caused by a gap in the batt insulation at the top of the section (see Figure 3.17). When the holes to allow air leakage were drilled, the drill caught the insulation, which twisted and got displaced, leaving this gap. It was suspected from the beginning because of the cold temperature readings for this location, but it was decided not to open the section to make the correction. The section with rigid insulation added on the cold side (Figure 5.4b) has slightly higher moisture content values than for the base-case assembly (Figure 5.4a, ranging from around 18% to 28%. The moisture content values are higher toward the center of the cavity, and slightly higher toward the top of the section.

As can be seen, a correlation exists between moisture distribution patterns in the fiberboard sheathing and the air leakage configuration for the long and concentrated air leakage paths. Moreover, by representing moisture contents with this graphic method, local problem areas can be easily identified. The isohygrons also demonstrate that these problem areas are generally linked to the entry point(s) of warm indoor air into the cavity.

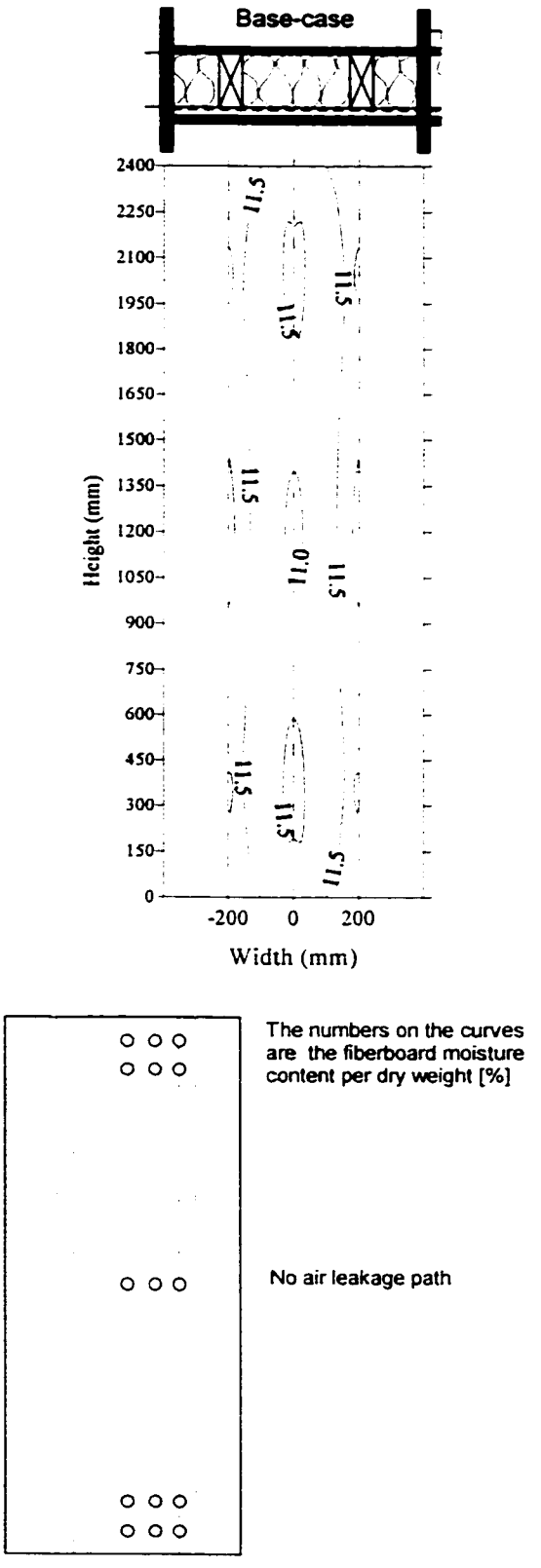

Figure 5.1. Isohygrons - airtight section (gravimetry data).

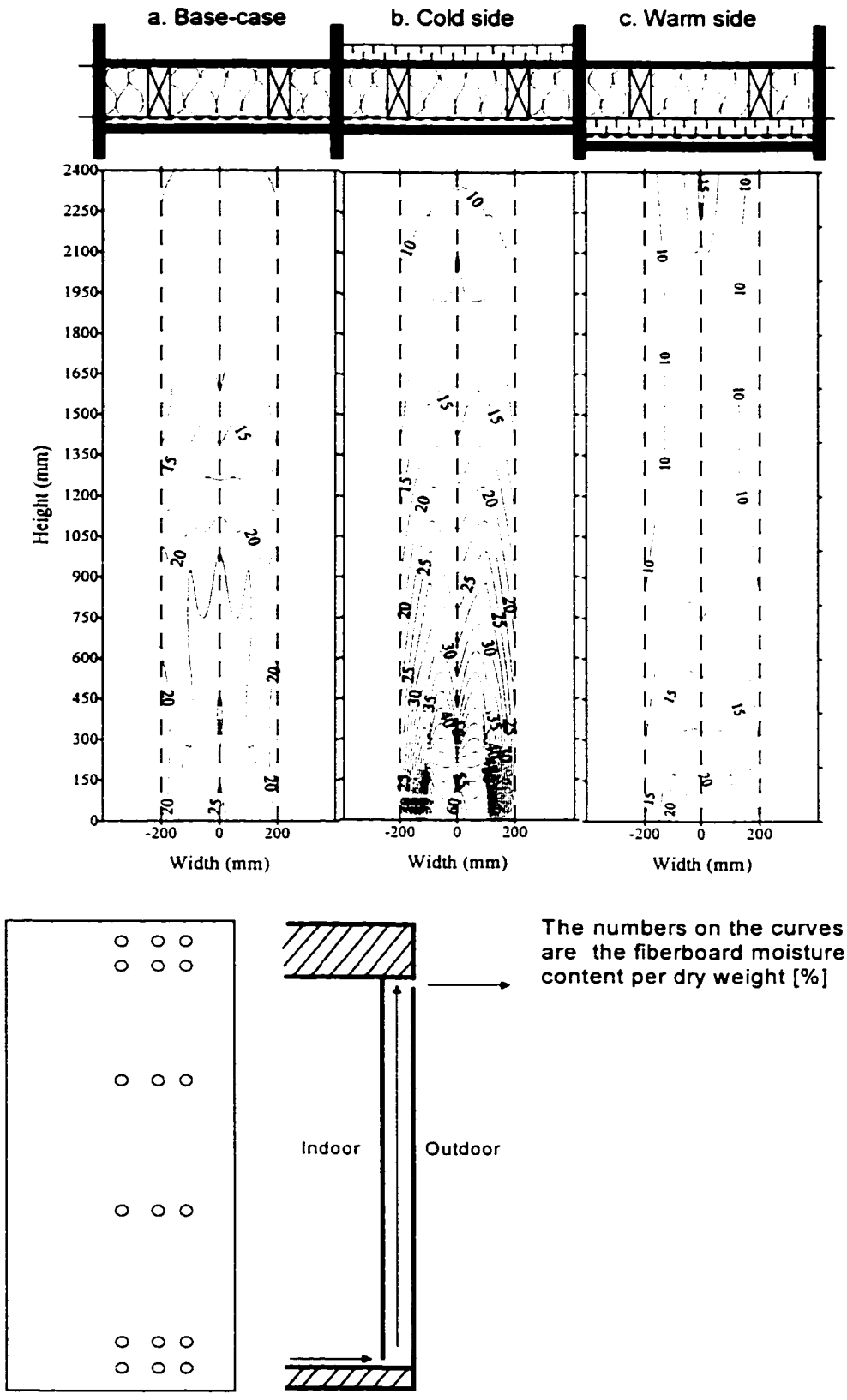

Figure 5.2. Isohygrons - long leakage path (gravimetry data).

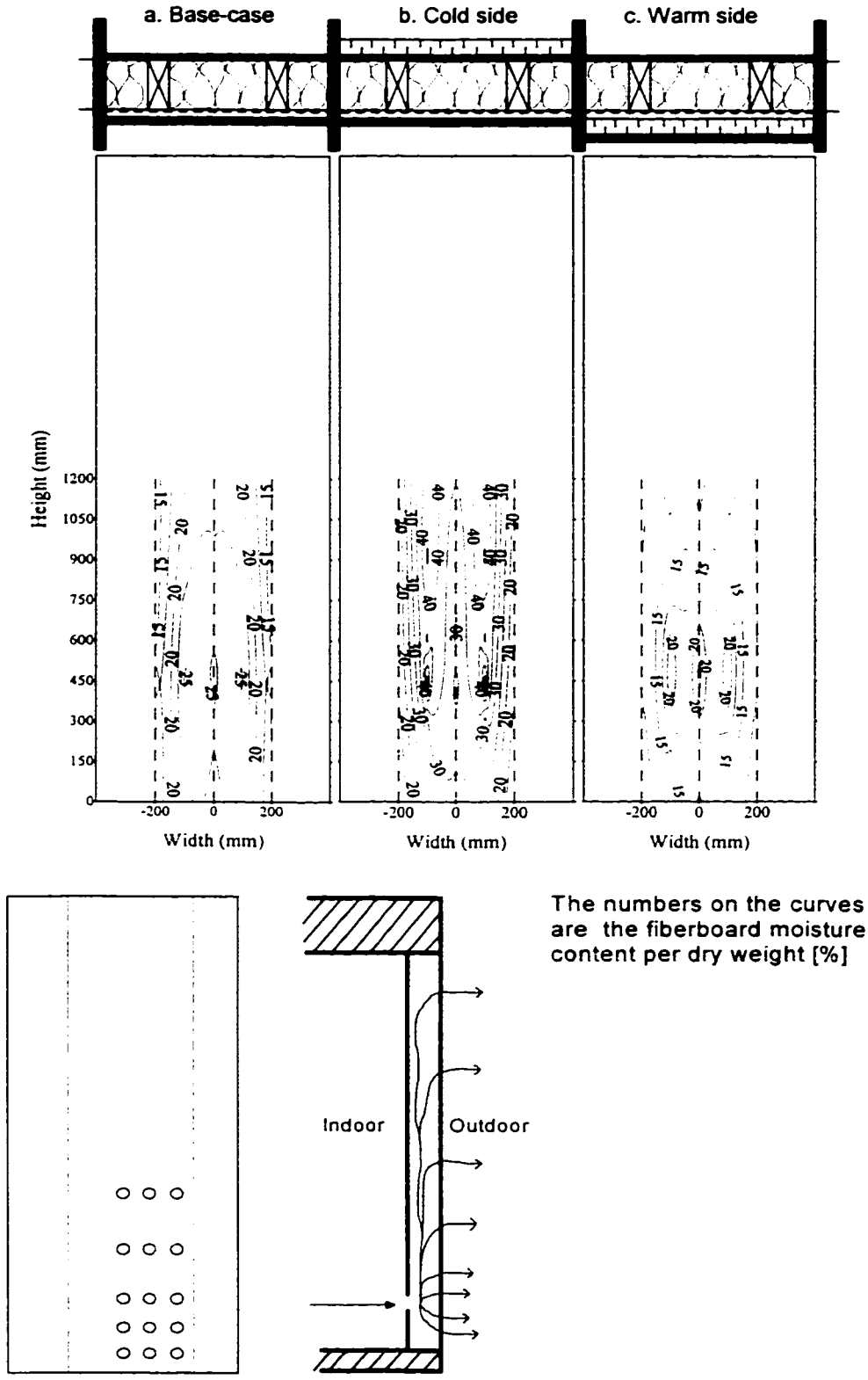

Figure 5.3. Isohygrons - concentrated leakage path (gravimetry data).

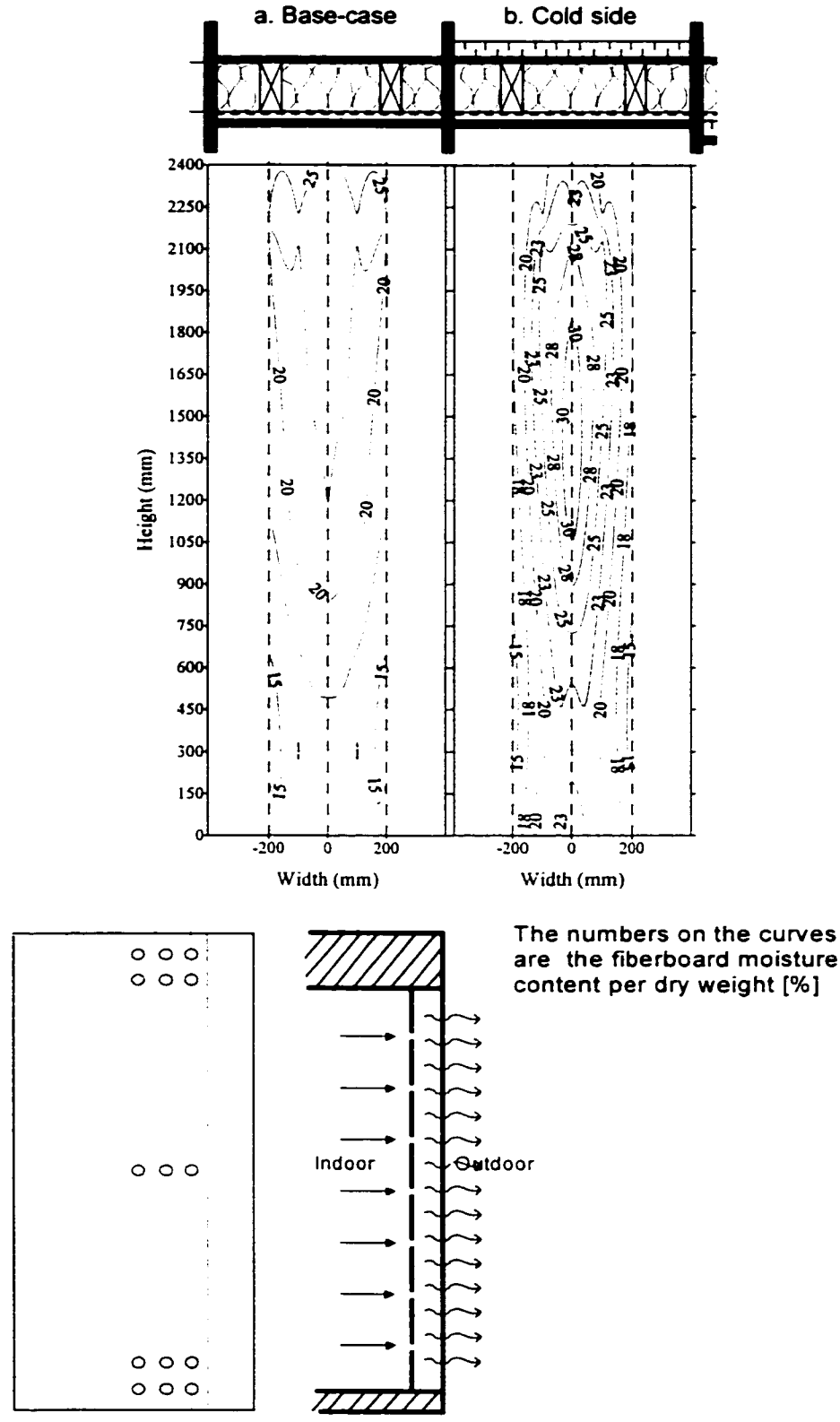

Figure 5.4. Isohygrons - distributed leakage path (gravimetry data).

Figure 5.5 shows the July 10th isohygrons for all sections. The same scale is used for all nine assemblies, from 10% to 64% moisture content per dry weight in the fiberboard sheathing, allowing comparison of the moisture contents and of their distribution patterns among the sections. Between adjacent curves, there is a 3% moisture content difference.

The airtight section (top right corner) shows no curves because moisture content values are very low and do not vary by more than 3% across the whole section. The sections with added insulation on the cold side have areas with lower moisture content, but other areas reach the top of the scale. These sections also have the highest number of curves, corresponding to the largest variation in moisture content across the area of the sample sections. The base-case assemblies and the sections with insulation added on the warm side all have moisture content toward the low end of the scale, and fewer lines of moisture content change.

From these maps, it can be concluded that the insulation strategy had more impact on moisture content levels reached than the type of air leakage. But the absence of air leakage has an even bigger impact, as the airtight section reached moisture content values too low to be registered on the scale that was used.

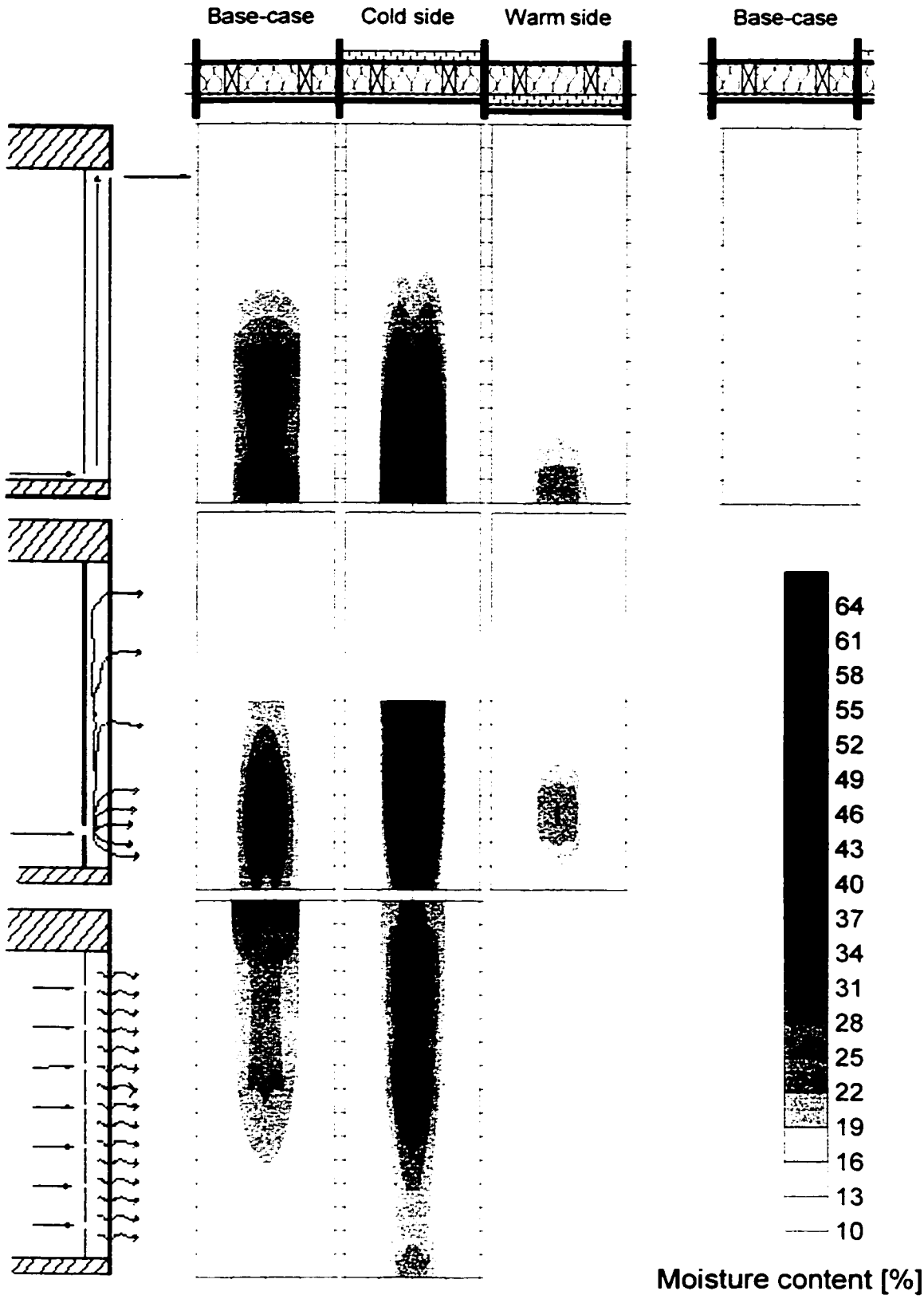

Figure 5.5. Isohygrons for July 10th (gravimetry data).

5.1.2 Mapping using moisture content sensor data

The July 10th average data from the six moisture content sensors on each section was used to produce moisture content maps. They are presented from Figure 5.6 to Figure 5.9. It has to be noted that less monitored values were used to generate these curves than for the moisture content measurements using gravimetry: 6 measurement points compared to 18 measurement points respectively. The moisture content sensor locations correspond to gravimetry sample locations (refer to Figure 3.8)

The moisture content map for the airtight section (Figure 5.6) shows a vertical moisture content gradient of 3% between the top and the bottom. Moisture contents are below 12% for the section. These moisture content values are in the range of those measured with gravimetry.

A vertical moisture content gradient can also be noted on the moisture content maps generated for the sections with the long air leakage path (Figure 5.7). This pattern seen for the moisture content sensor results is coherent with the one observed for the same sections using the gravimetry data (Figure 5.2), where moisture contents were higher at the bottom, the location of the air entry point. Moisture contents are in a similar range as well, except for those measured in the section with insulation added on the cold side. In this section, moisture content by gravimetry goes up to 60%, but moisture content sensor readings only reach about 24% (Figure 5.2b and Figure 5.7b). For the base-case assembly, the moisture content from both measurement methods range from around 25% toward the bottom to 10% toward the top (Figure 5.2a and Figure 5.7a) and for the section with insulation added on the warm side they go from about 20% toward the bottom to 16% toward the top (Figure 5.2c and Figure 5.7c).

The same trends can be observed for the sections with the concentrated air leakage path (Figure 5.8) The patterns demonstrated by the isohygrons are similar for both moisture content measurement methods (Figure 5.3 and Figure 5.8). Moisture content sensor results are in the same range as those measured by gravimetry for the base-case assembly (from approximately 15% to 25%) and for the section with insulation added on the warm side (from approximately 13% to 20%). However, moisture contents sensor results are much lower than those measured by gravimetry for the section with insulation added on the cold side, around 22% compared to 40% (Figure 5.8b and Figure 5.3b).

Once again, for the sections with the distributed air leakage path (Figure 5.9), the pattern is similar for both moisture content measurement methods. For the base-case assembly, moisture content readings are higher toward the top and for the section with insulation added on the cold side, they are higher toward the center close to the top of the section. For the base-case assembly, moisture content values are in the 15% to 25% range for both measurement methods (Figure 5.4a and Figure 5.9a), but for the section with the insulation added on the cold side, moisture content sensor results, which go up to about 17%, are lower than those measured by gravimetry, reaching almost 30% (Figure 5.9b and Figure 5.4b).

Moisture content maps generated from data measured by gravimetry and moisture content sensors seem to generally agree for the patterns and moisture content levels, with the exception of those for the sections with rigid insulation added on the cold side. Although the number of monitoring points is less, six compared to 15 or 18 for gravimetry, the patterns are similar.

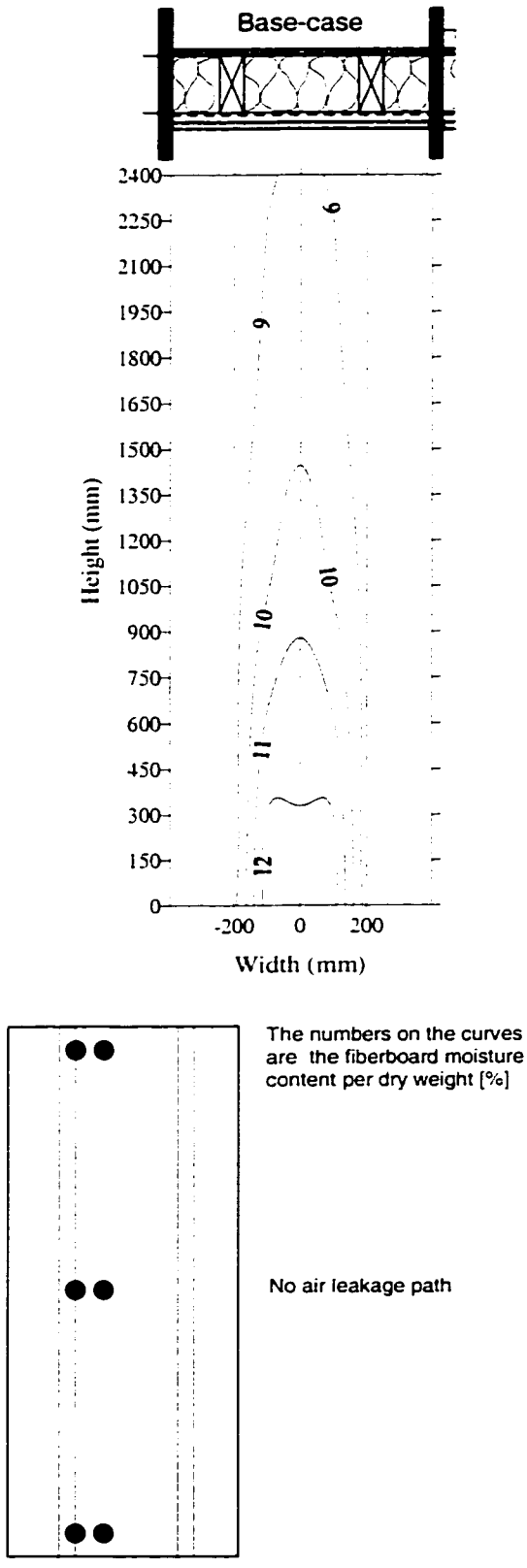

Figure 5.6. Isohygrons for the airtight section (moisture content sensor data).

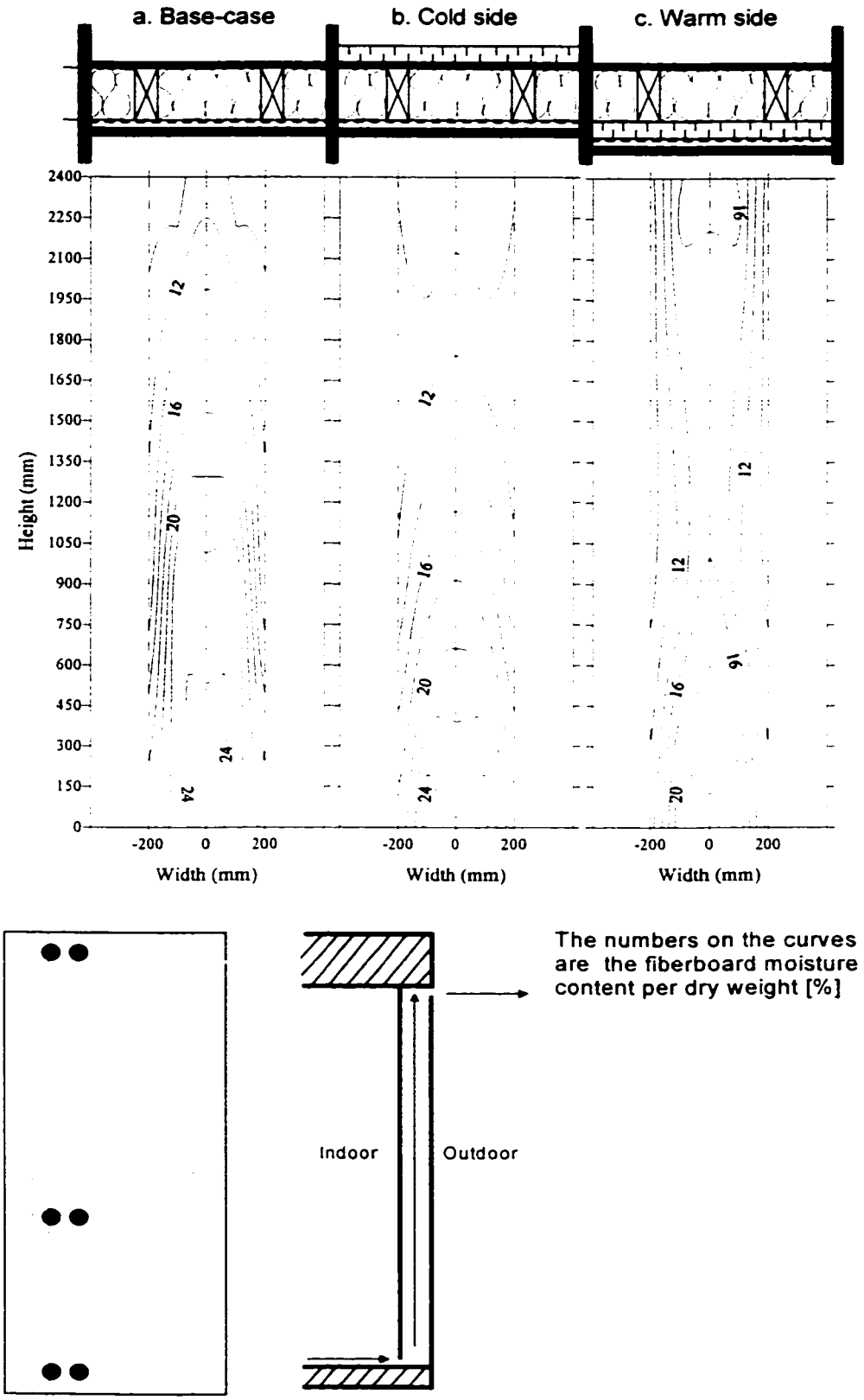

Figure 5.7. Isohygrons - long leakage path (moisture content sensor data).

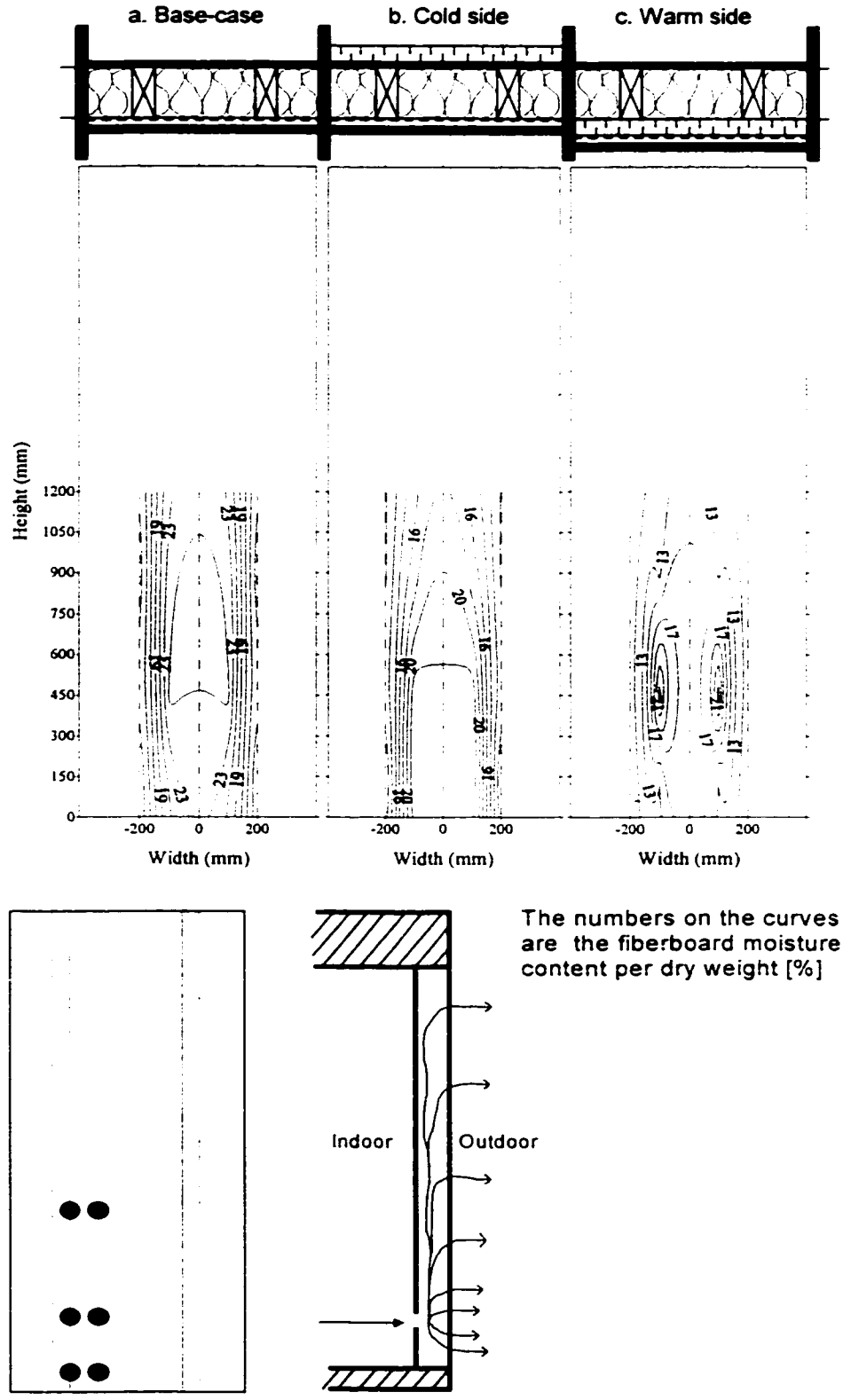

Figure 5.8. Isohygrons - concentrated leakage path (moisture content sensor data).

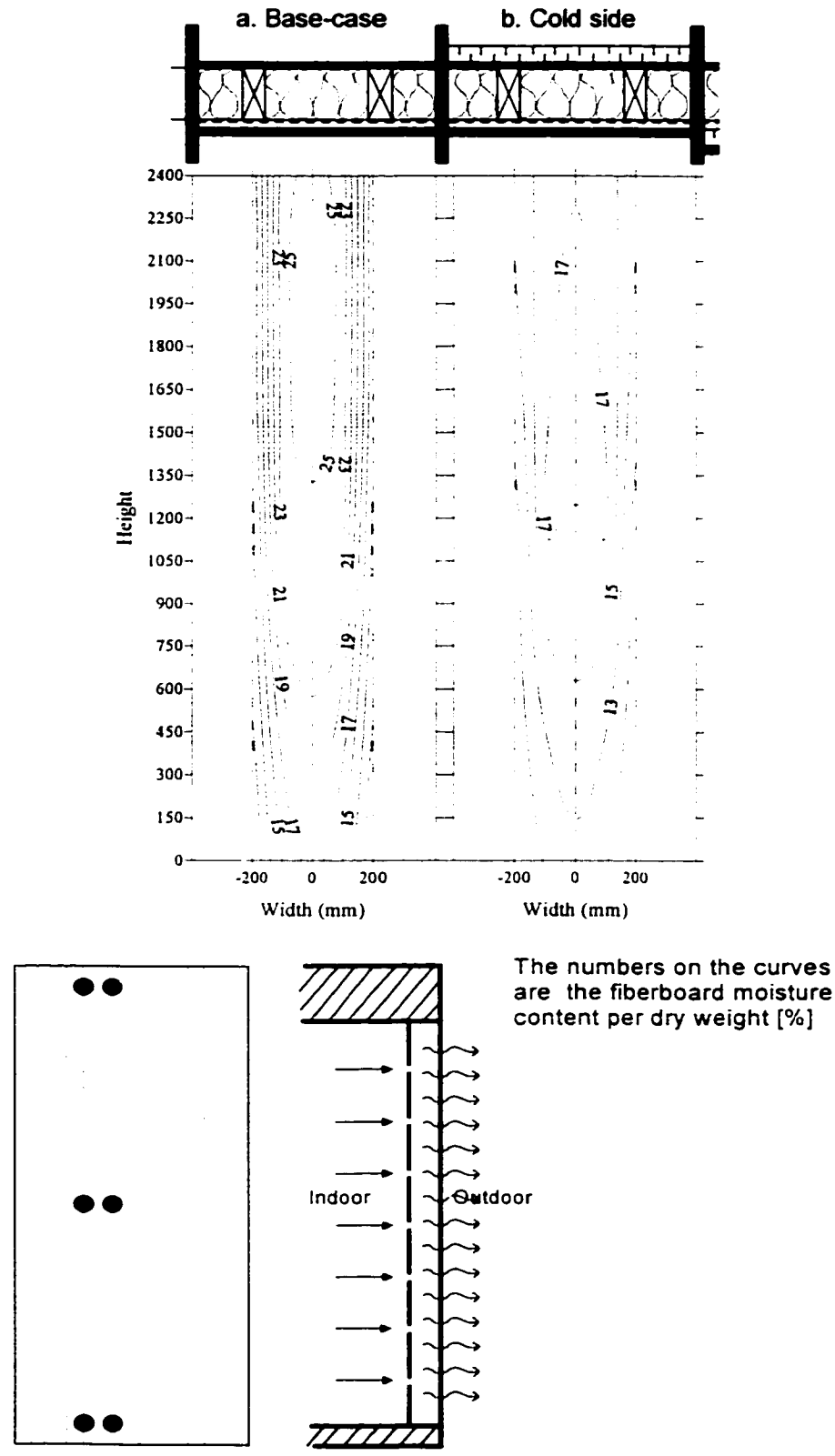

Figure 5.9. Isohygrons - distributed leakage path (moisture content sensor data).

Figure 5.10 shows all moisture content maps generated using the averaged data from moisture content sensors for July 10th. The same scale as for gravimetry results is used, i.e. from 10% to 64% moisture content per dry weight, allowing comparison of the moisture content values and of their distribution patterns among the sections and between the two moisture content measurement methods, the other results being on Figure 5.5. Between adjacent curves, there is a 3% moisture content difference. The darker areas represent higher moisture content, lighter areas lower moisture content.

According to these maps, the base-case assemblies had the highest moisture content, and the airtight section the lowest. This does not concur with the gravimetry data analysis, where the sections with insulation added on the cold side had reached the highest moisture contents. As mentioned above, the moisture content measured by the sensors was lower than those measured by gravimetry for the sections with insulation added on the cold side.

However, as for the gravimetry results, these moisture content maps show that the insulation strategy had more impact on moisture content levels reached than the type of air leakage of the sample section, and that reducing air leakage has an even bigger impact than the insulation strategy, as the average July 10th moisture content in the airtight sections is too low (below 10%) to register with the scale used.

5.1.3 Observations on moisture content mapping

The isohygrons presented in Figure 5.5 to Figure 5.10 are the first measured account of the impact of air leakage on the moisture content distribution within an assembly. The patterns produced concord with expected path of air, given the inlet and outlet holes provided. The gravimetry results are more convincing than the moisture

content sensor results. Moisture content cannot be measured accurately by moisture content pins below 6% and above 30%. Below 6% the material is dry and the resistance is too high. Above 30% (approximately the fiber saturation point), the electrical resistance is too low. However, although a calibration curve was required for the material being used, moisture content pins require little labour during testing and are useful when moisture content values are in the 6%-30% range. The gravimetry method required a high level of manual labour during testing but provided reliable data. When using removable gravimetry samples, care has to be taken to avoid influencing the behaviour of the specimen.

The next section analyses the mapping results obtained with the thermocouple measurements at two planes within the assemblies: on the warm side and on the cold side of the fibreglass batt insulation. This method that was labour intensive at the time of fabrication and installation, but not during the experiment.

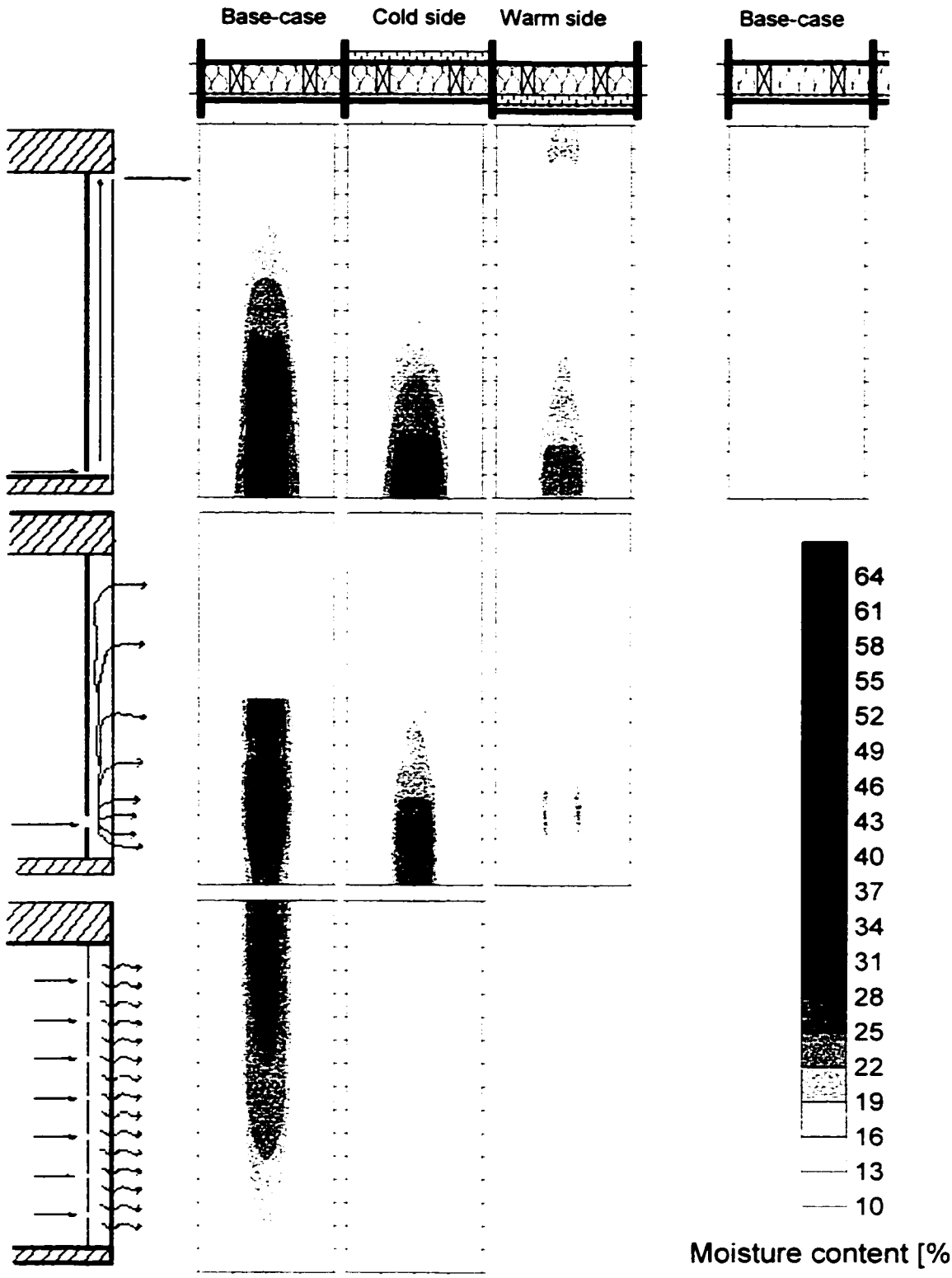

Figure 5.10. Isohygrons for July 10th (moisture content sensor data).

5.2 Temperature mapping

5.2.1 Measured temperatures

The following isotherms are generated using the average monitored temperatures for the May 26th to 30th period. For the sections with the long air exfiltration path, data from 12 points for each plane, mirrored according to a vertical axis of symmetry, are used to produce the isotherm curves. For the other sections (concentrated and distributed air leakage paths, airtight section), data from 10 points for each plane are used. The isotherms are plotted over an elevation view of the sample sections. To find out the impact of moisture accumulation on warm and cold plane temperatures, maps were also produced for the July 10th, when moisture accumulation was high.

Figure 5.11 shows the warm and cold plane isotherms for the airtight section, with no rigid insulation added. Isotherms on the warm plane are generally parallel (Figure 5.11a), indicating that the vertical temperature gradient is small. This pattern is analogous to that of conductive heat transfer, without the influence of convective heat transfer. Temperatures at the cold plane are slightly warmer in the top half of the section (Figure 5.11b).

Isotherms for the sample sections with the long air exfiltration path are presented in Figure 5.12. Temperatures at the warm plane of the sections with the base-case composition and with insulation added on the cold side are warmer toward the top (Figure 5.12a and Figure 5.12b). In the case of the section with rigid insulation added on the warm side, the temperatures are warmer at the bottom (Figure 5.12c). At the cold plane, the temperatures are colder at the top for the section with rigid insulation added on

the cold side (Figure 5.12e), but slightly warmer at the top for the base-case section and for the one with rigid insulation added on the warm side (Figure 5.12d and Figure 5.12f).

Figure 5.13 shows isotherms for the sections with the concentrated air exfiltration path. For the base-case assembly, the warm plane temperatures are warmer around the indoor air entry point (Figure 5.13a). For the section with rigid insulation added on the cold side, the warm plane temperatures are warmer just above the opening (Figure 5.13b), where as they are warmer just below and on each side of the opening for the section with rigid insulation added on the cold side (Figure 5.13c). At the cold plane (Figure 5.13d to Figure 5.13f), temperatures are slightly colder opposite the air entry point, although the patterns are not as clearly defined as those for the warm plane temperatures.

The isotherms for the sections with the distributed air exfiltration path are shown in Figure 5.14. A vertical temperature gradient of 5°C is observed for the base-case assembly, temperatures being warmer toward the top of the section. This gradient is due to the gap in the batt insulation at the top of the section (Figure 3.17). For the section with insulation added on the cold side, the vertical temperature gradient is of only 1°C. The main temperature gradient is horizontal and reflects the wood stud thermal bridges.

These maps confirm that temperatures for both planes are warmer for the sample sections with insulation added on the cold side and colder for the sections with insulation added on the warm side than those of the base-case assembly. Also, the temperature distribution patterns within the assemblies are related to the air leakage path, indicating that some correlation exists between the temperature distribution and the air leakage path. This suggests that temperature monitoring according to a 3-dimensional grid could be used to characterize the path of exfiltrating air.

In Figure 5.15 to Figure 5.18, isotherms from monitored temperatures at the beginning of the wetting period (from May 26th to May 30th) when the wall sample sections were dry can be compared with isotherms from monitored temperatures toward the end of the wetting period (July 10th) when moisture had accumulated. No significant change in temperature profiles can be detected for either the warm plane or cold plane temperatures.

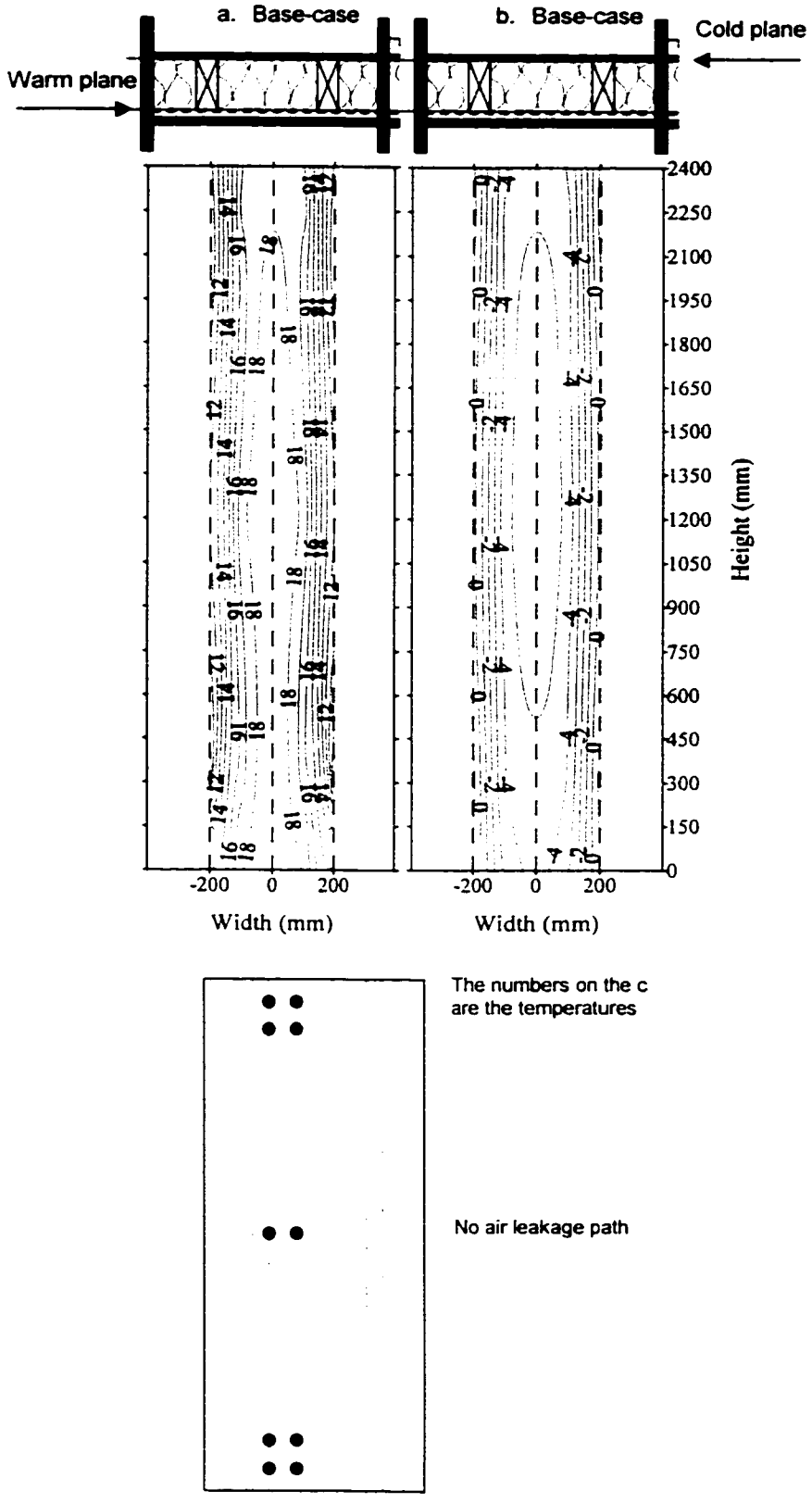

Figure 5.11. Isotherms for the airtight section.

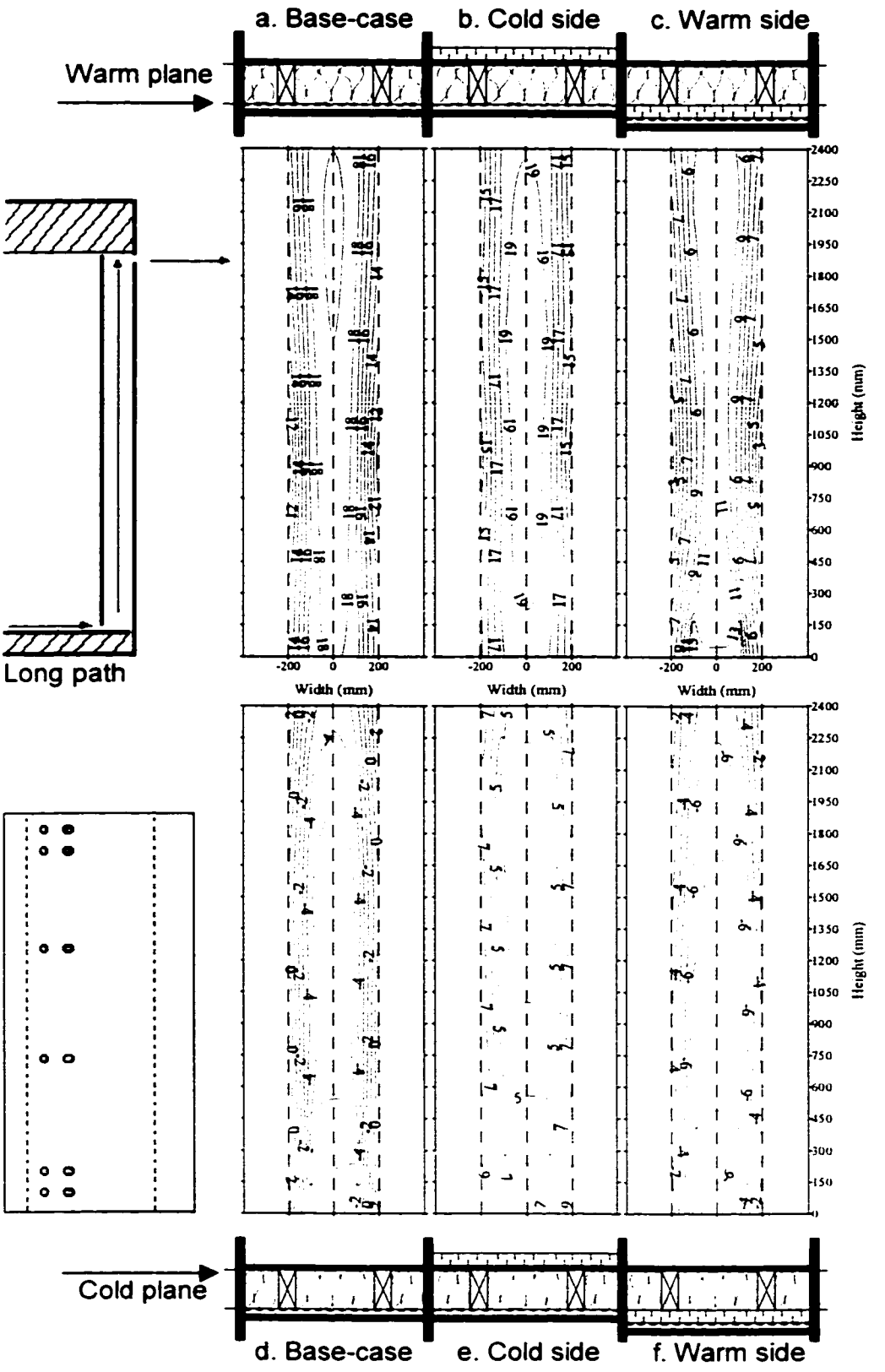

Figure 5.12. Isotherms - long leakage path.

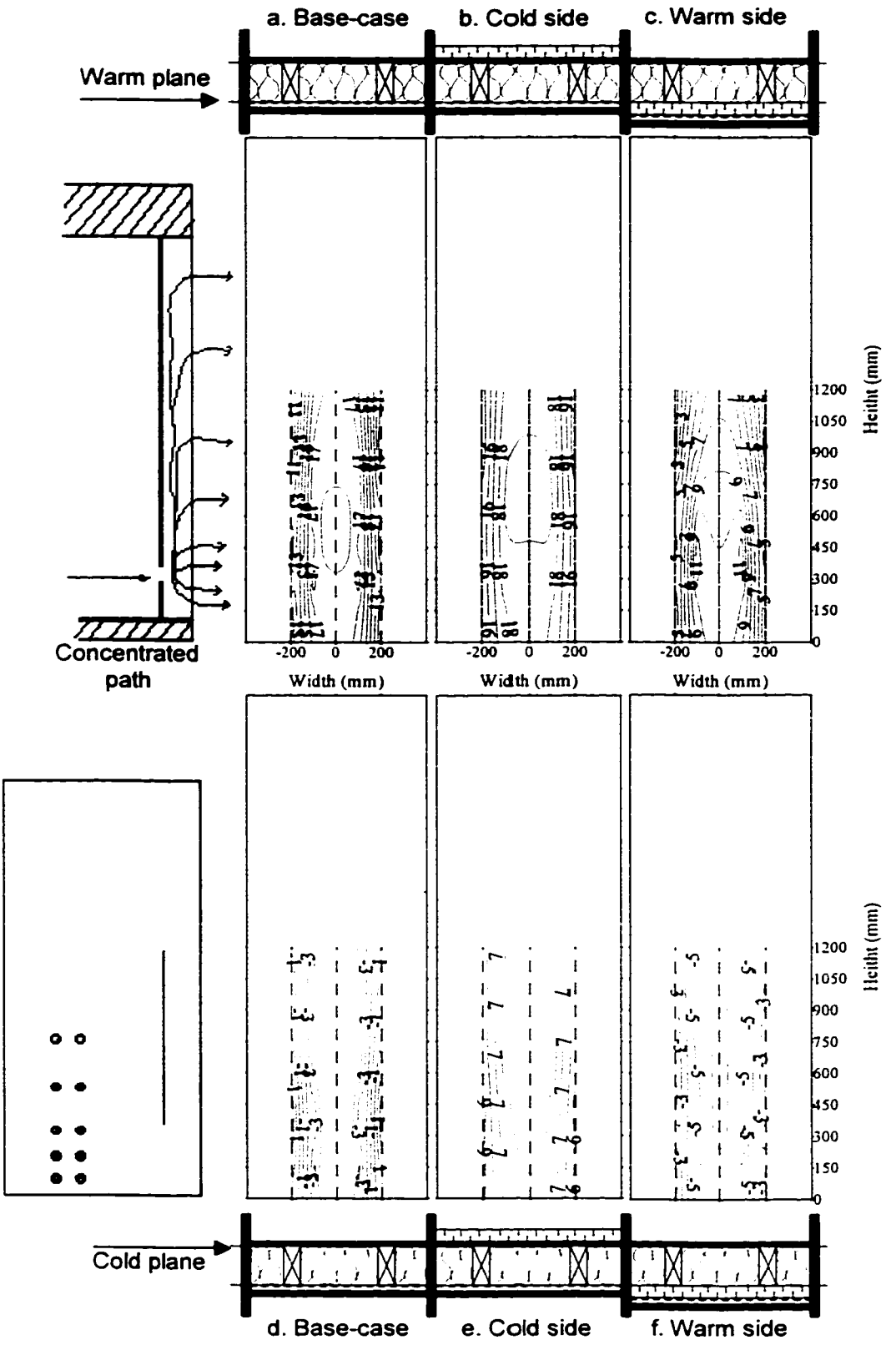

Figure 5.13. Isotherms - concentrated leakage path.

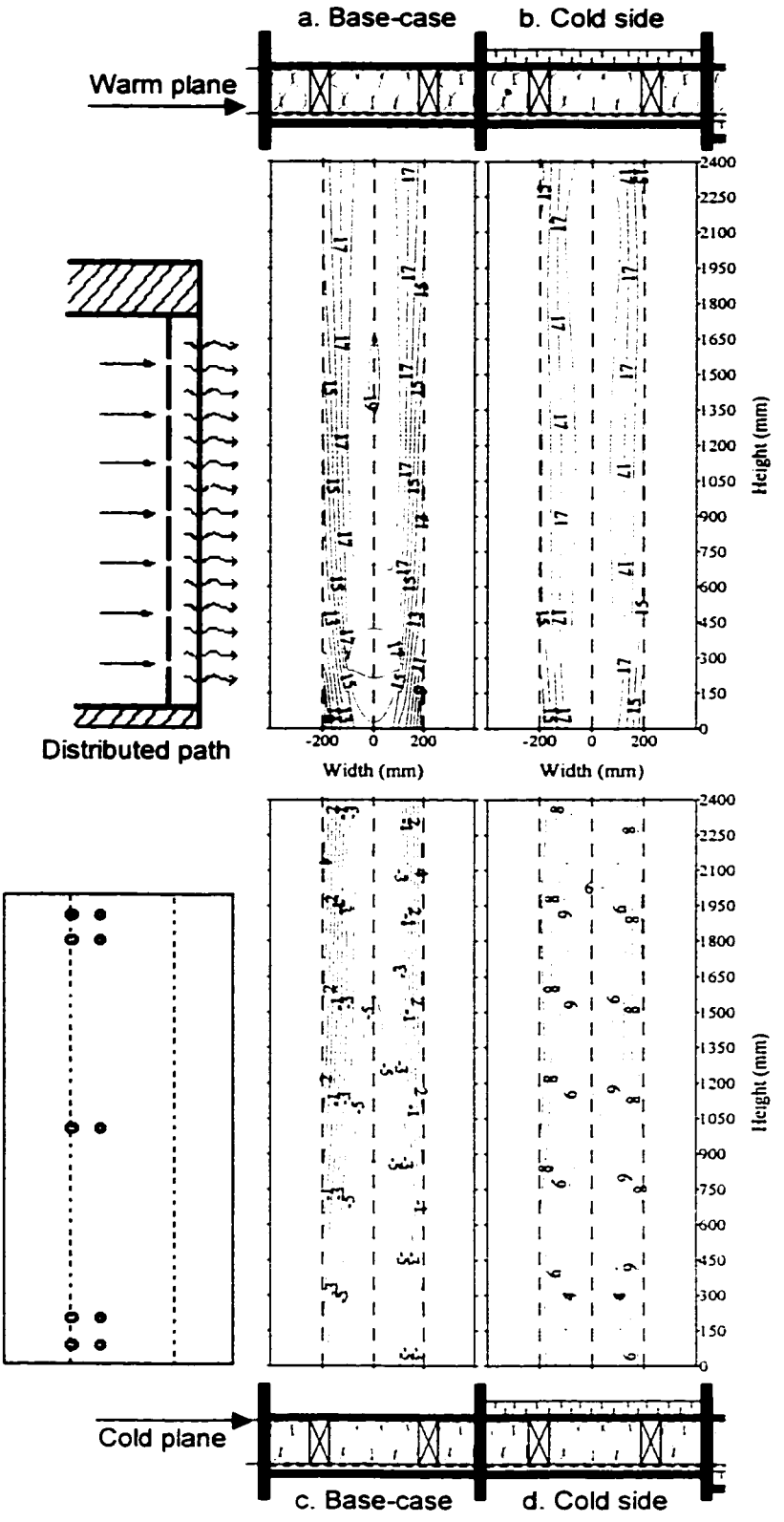

Figure 5.14. Isotherms - distributed leakage path.

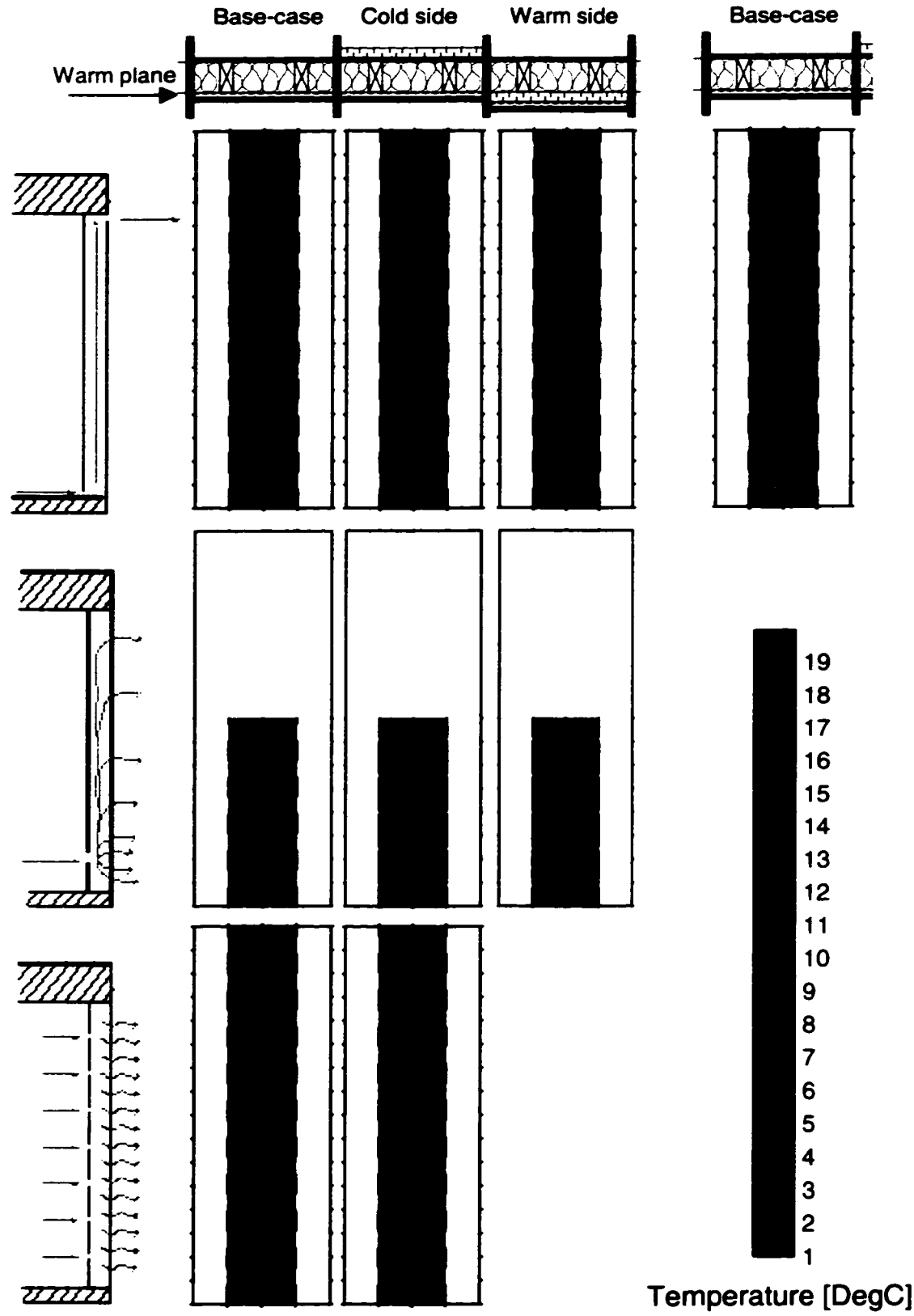

Figure 5.15. Warm plane isotherms - May 26th to May 30th period.

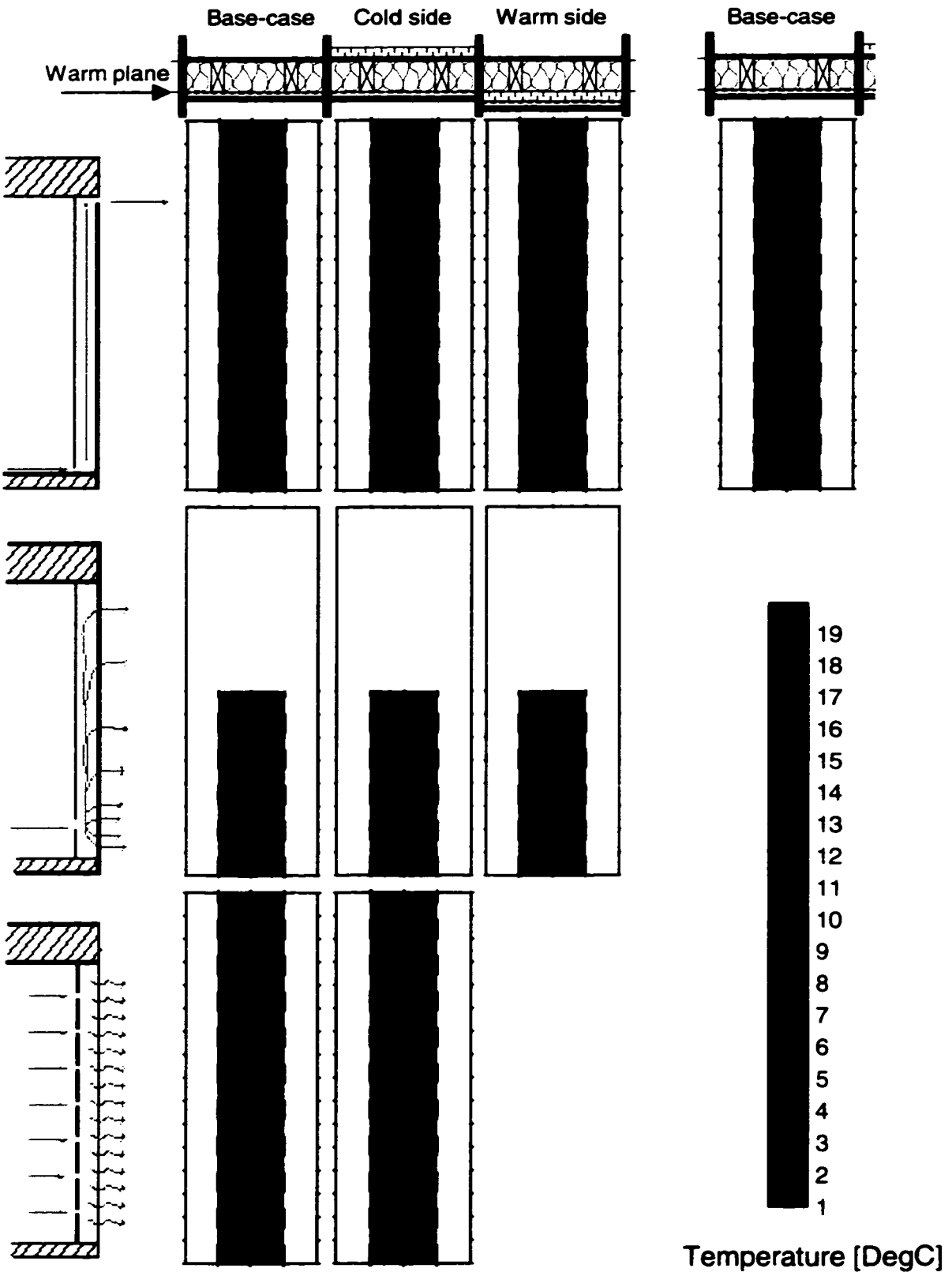

Figure 5.16. Warm plane isotherms - July 10th.

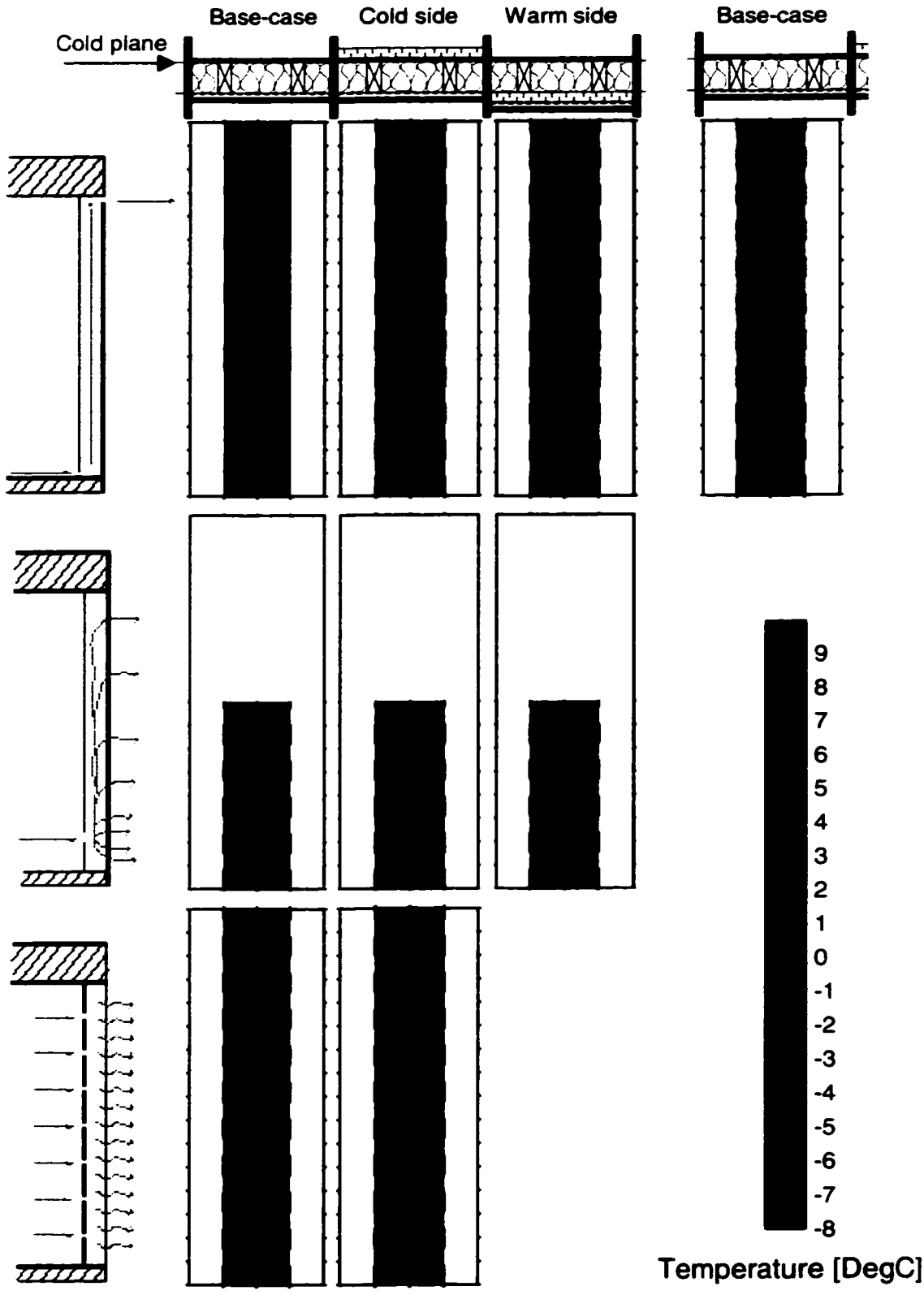

Figure 5.17. Cold plane isotherms - May 26th to May 30th period.

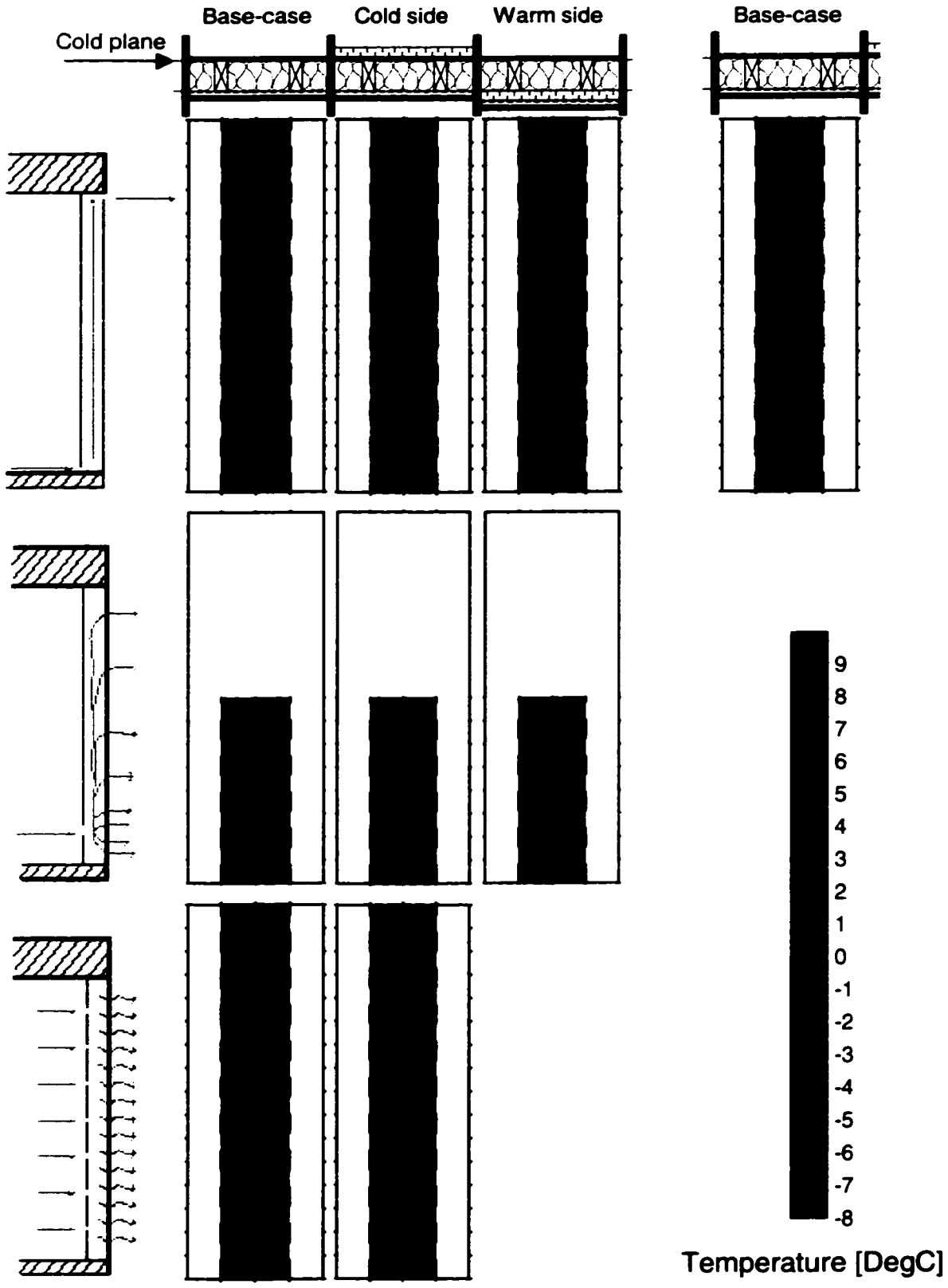

Figure 5.18. Cold plane isotherms - July 10th.

5.2.2 Calculated temperatures

The curves obtained with the temperature measurements provide indications about the effect of air leakage within assemblies. To investigate the appropriateness of the grid method further, the temperature measurements are compared with temperature calculated for airtight assemblies in the following discussion.

A steady-state modeling approach using 3-dimensional finite-difference element is used to simulate the conductive heat transfer through the assemblies in order to calculate temperatures inside the assemblies tested and their thermal resistance. The calculations are based on the steady-state 2-dimensional conductive heat transfer model described in Athienitis (1994). To fit the cases considered, this model was expanded to include up to 96 control volumes in 3 dimensions. Sketches of the control volumes for the three compositions studied are presented in Figure 5.19 to Figure 5.21. The temperature and R-value calculations are performed for an area 200 mm by 200 mm. It is assumed that adiabatic conditions exist at the side boundaries of the whole volume. The defined area spans vertically from the center of the sample section, between the studs, to the center of the stud, and horizontally, from the center of the space between the wood strapping, to the center of the wood strapping. The compositions are divided in different layers, corresponding to the different materials they are made of. The glass fiber batt insulation is split in two layers to improve accuracy. The material conductivities used in the calculations were taken from the manufacturers for the two insulation materials and the fiberboard. For the gypsum board and the wood (studs and strapping), the values were taken from the "*ASHRAE Handbook of Fundamentals*" (1993). Temperatures are calculated at points corresponding to the experimental temperature monitoring grid.

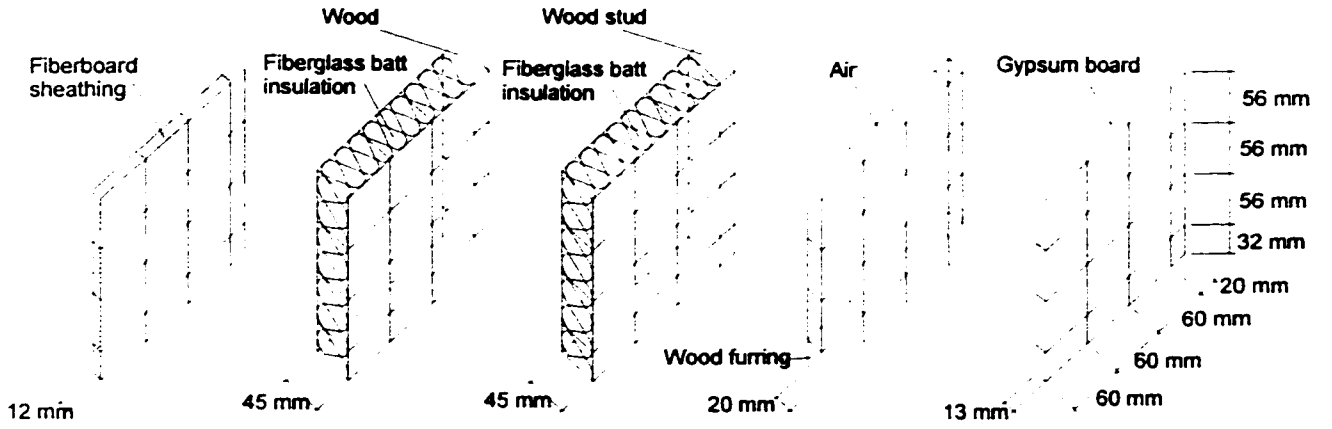

Figure 5.19. Control volumes - base-case assembly.

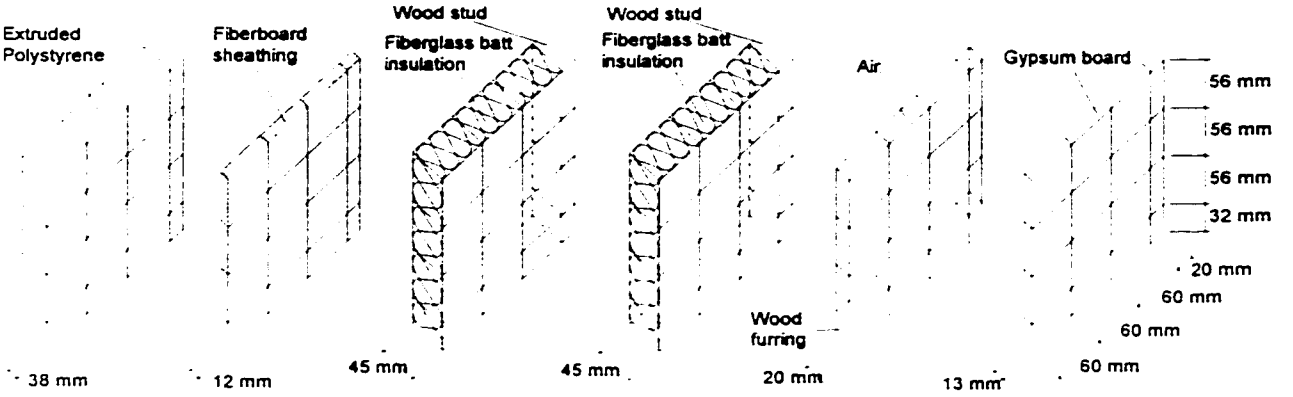

Figure 5.20. Control volumes - insulation added on the cold side.

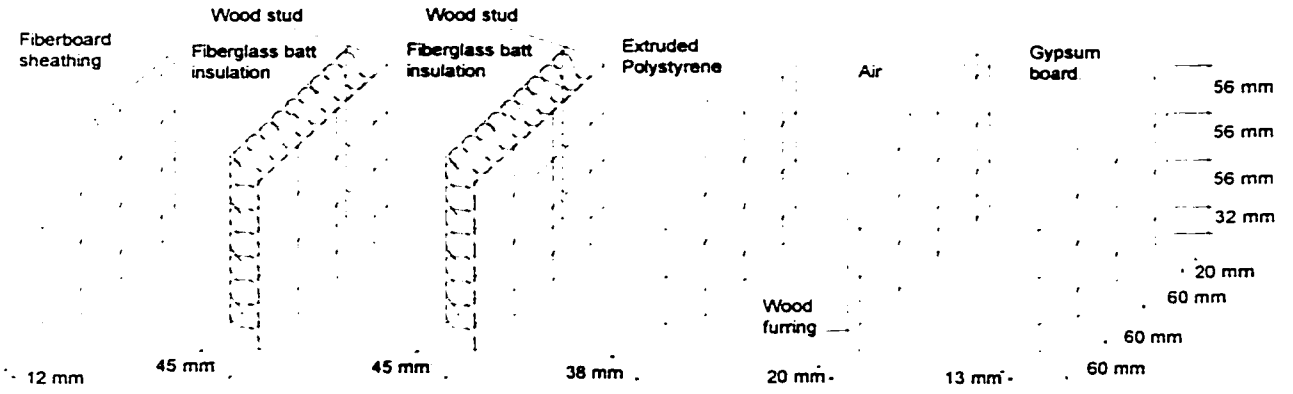

Figure 5.21. Control volumes - insulation added on the warm side.

The temperatures calculated at the cold plane and the warm plane for the assembly with rigid insulation added on its cold side are higher, and those for the assembly with rigid insulation added on its warm side are lower, than those calculated for the base-case assembly. Adding the 38 mm of rigid insulation to the base-case composition also reduces the average temperature gradient across the batt insulation and the wood studs. The average gradient for the base-case assembly is approximately 22°C, while it is only 14°C for the assemblies with rigid insulation added on the cold side or on the warm side.

For the following discussion, the temperatures calculated at the indoor surface of the glass fiber batt insulation will be referred to as *warm plane* temperatures, and those at its outdoor surface as *cold plane* temperatures.

The isotherms generated from the calculated temperatures at the cold and warm planes for the three different compositions examined are shown in Figure 5.22. For all three compositions, the predominant temperature gradient is horizontal, isotherms being mostly parallel to the wood studs. This illustrates the fact that the wood studs are the main thermal bridges in those assemblies. The vertical temperature changes seen in the warm plane isotherms of both the base-case assembly and of the assembly with rigid insulation added on the cold side are due to the horizontal wood strapping. In the base-case assembly (Figure 5.22a), the warm plane of the batt insulation is warmer behind the wood strapping, which acts as a short thermal bridge. For the assembly with rigid insulation added on the cold side (Figure 5.22b), the temperatures are slightly warmer in the space between the studs and the strapping. The impact of the wood strapping is more pronounced for the base-case assembly, where the small oval shapes delimit areas 1°C warmer than the rest of the surface, than for the section with insulation added on the cold

side, where the irregular *donut* shapes delimit areas that are 0.5°C warmer than the rest of the surface. The wood strapping does not have any significant impact on the warm plane temperatures for the assembly with rigid insulation added on the warm side of the batt insulation (Figure 5.22c) or on the cold plane temperatures of any assembly (Figure 5.22d to Figure 5.22f).

The model is also used to calculate the overall R-value for the defined area for the three compositions tested. The R-value for the base-case assembly is 2.45 ($m^2 \cdot °C$)/W. When rigid insulation is added, on either the cold side or the warm side of the batt insulation, the R-value is calculated at 3.81 ($m^2 \cdot °C$)/W, an increase of 55%.

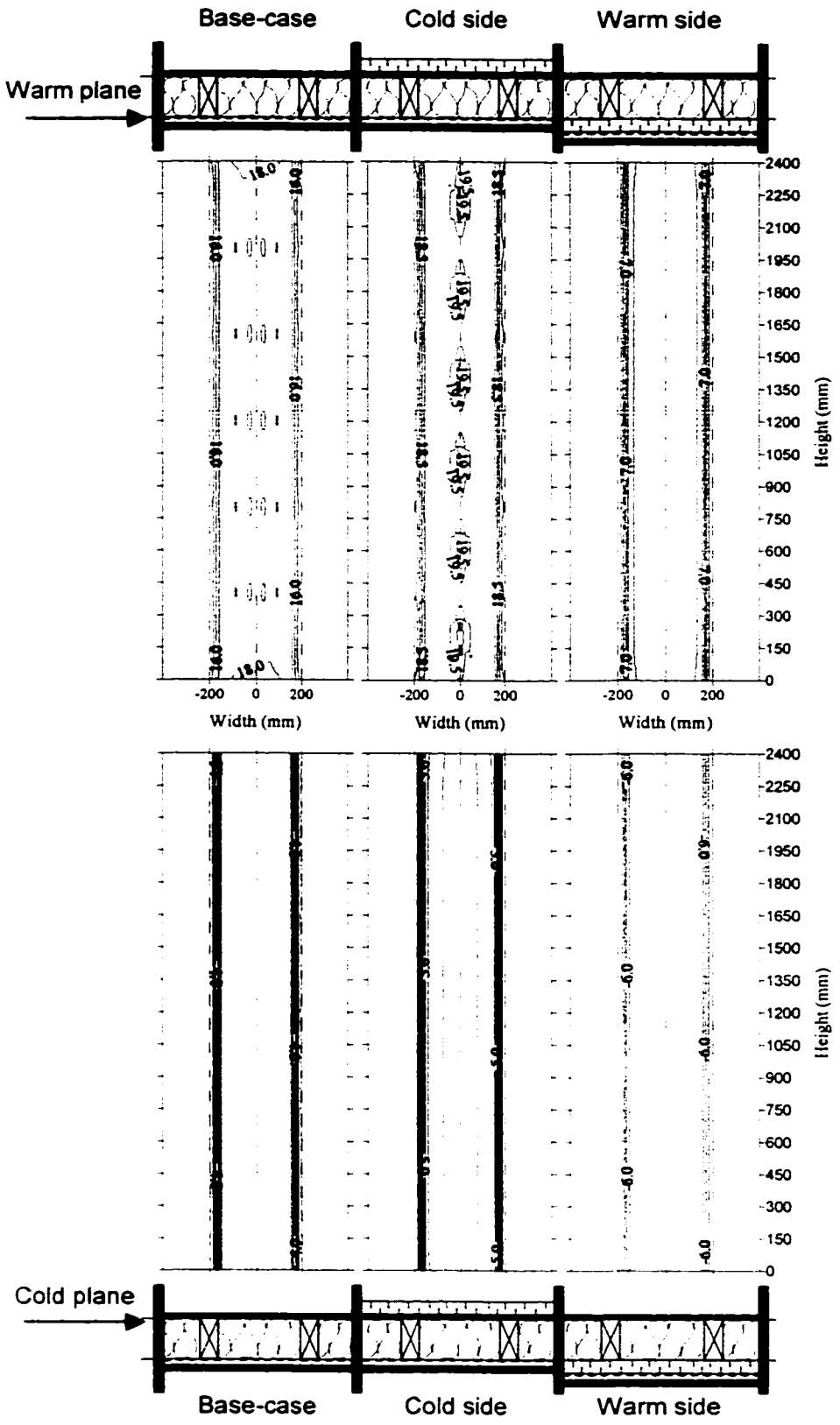

Figure 5.22. Isotherms from the 3-dimensional conductive heat transfer model.

5.2.3 Characterization of thermal effects of air leakage

The plots presented in Figure 5.23 to Figure 5.26 are generated using the difference between the measured warm plane temperatures and their corresponding calculated temperatures, which exclude air leakage, for each monitoring point. The scale used is in colour: from blue for a differential of -5°C to red for a differential of 5°C. Positive numbers mean that measured temperatures are higher than calculated temperatures. In other words, these locations are warmer due to the presence of air leakage. Negative numbers mean that the measured temperature is lower than the calculated temperature, or that the temperatures are cooler at these locations due to the presence of air leakage. As the measured temperatures include the effect of air leakage and the calculated temperatures do not, the generated curves represent graphically the impact of air leakage on the temperatures at the two planes within the assemblies.

It can be seen that the patterns of the curves generated for the warm plane of the assemblies with the long and concentrated air leakage paths (Figure 5.24a, b and c and Figure 5.25a, b and c) are related to their leakage path. This correlation is not as obvious for the cold plane temperatures (Figure 5.24d, e and f and Figure 5.25d, e and f), indicating that the impact of air is less pronounced on the cold side of the batt insulation.

The measured temperatures tend to be lower than the calculated temperatures for the warm plane of the sections with the long, concentrated and distributed leakage paths, and higher than the calculated temperatures for the cold plane of the sections. This would indicate that exfiltrating air cools temperatures at the warm plane and warms temperatures at the cold plane. This also means that air leakage reduces the temperature gradient, especially across the batt insulation.

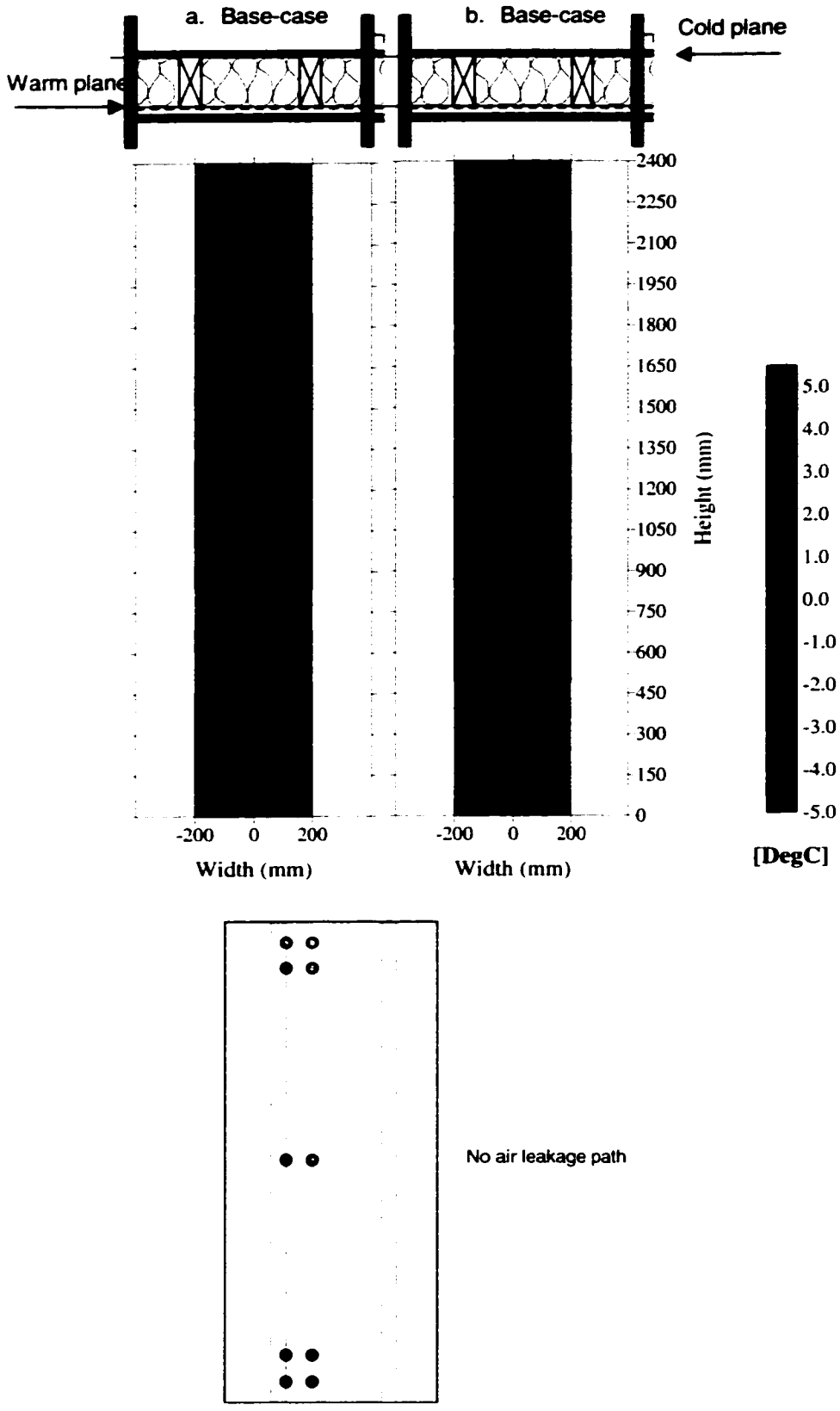

Figure 5.23. Differential isotherms - airtight section.

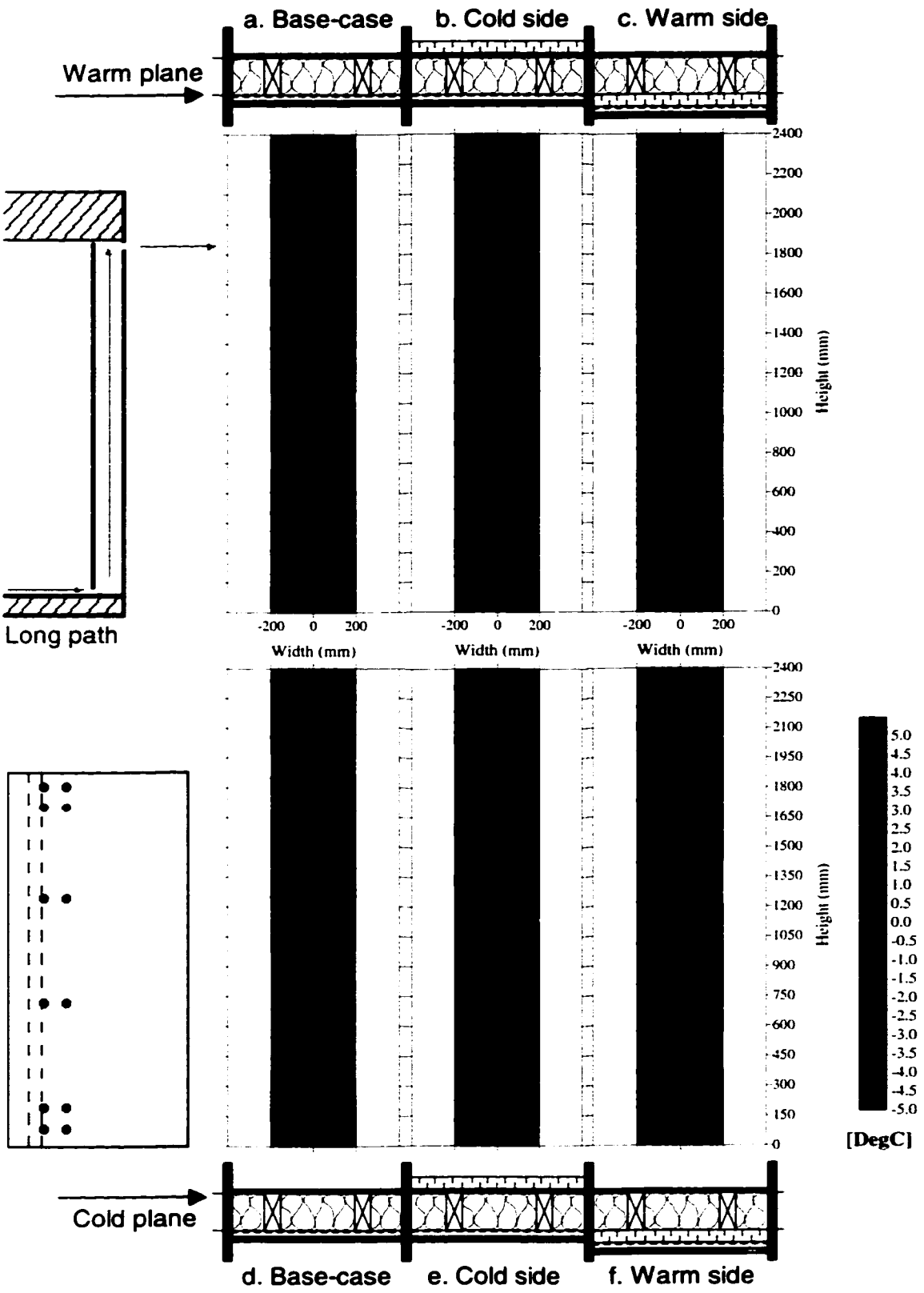

Figure 5.24. Differential isotherms - long leakage path.

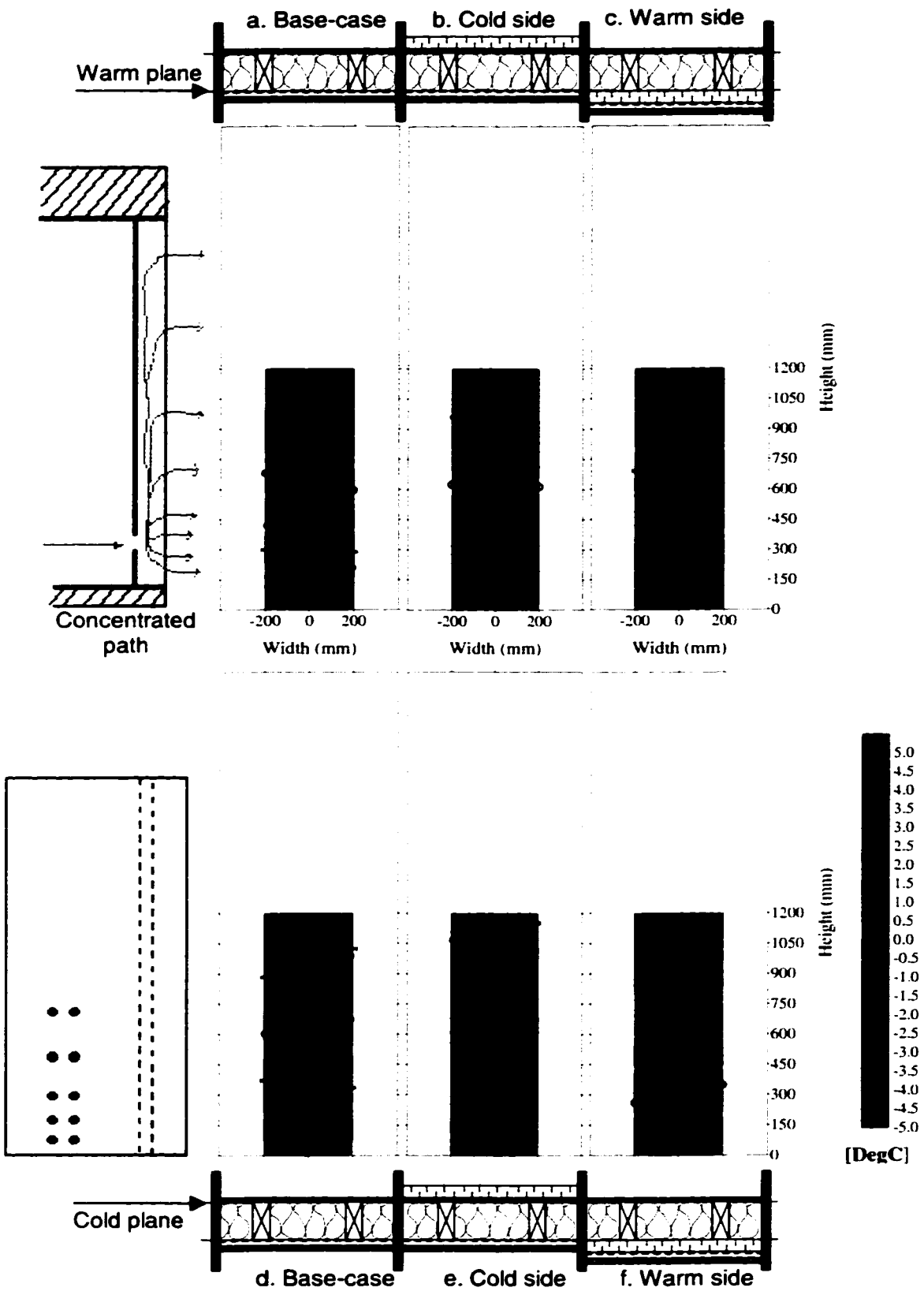

Figure 5.25. Differential isotherms - concentrated leakage path.

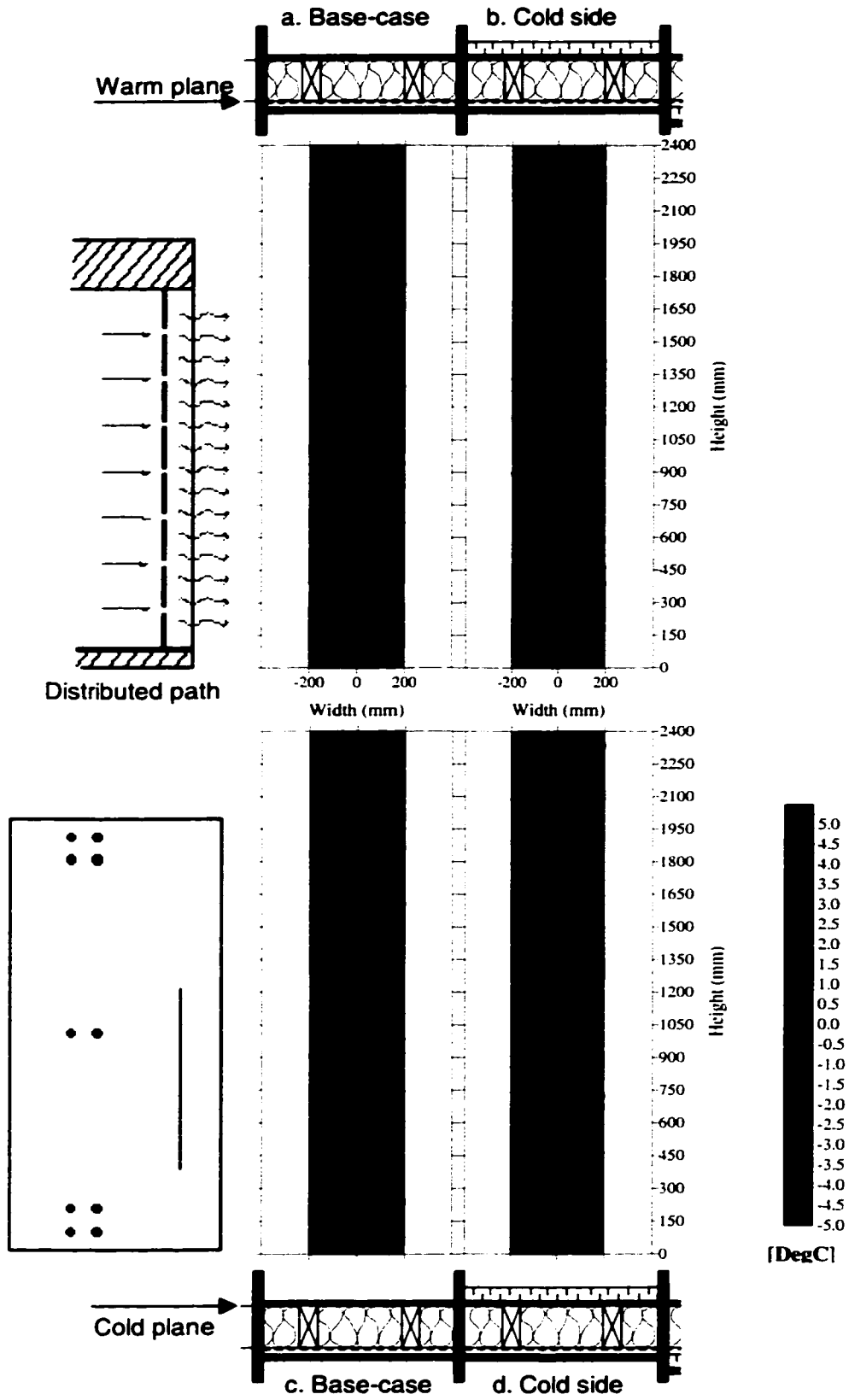

Figure 5.26 Differential isotherms - distributed leakage path.

5.3 Observations on the mapping of air leakage

Of the two methods of mapping presented, the measurement of moisture content by gravimetry tends to produce clearer patterns than the measurement of temperatures. This can be attributed to the fact that the moisture that is measured is actually stored in the material, whereas the temperature measurements are more sensitive to the actual air temperatures and variations in the trajectory of air, which occur even under near-constant conditions. Temperature measurements showed that convection loops must indeed always be present. Moisture content using pins could not be used for the whole range of moisture content levels that occurred in the fiberboard during the test. The results obtained demonstrate that gravimetry moisture content, and to a certain extent temperatures, measured within an assembly according to a grid may allow the mapping of air leakage inside assemblies.

From the maps produced, it was found that it would have been useful to provide the same monitoring grid for all the sections to make comparison between them easier. Furthermore, providing monitoring points covering the whole height of the sections and uniformly distributed along the vertical axis, as well as making the grids tighter, might have provided additional information on the distribution of moisture accumulation and temperature profiles.

The differential isotherms presented in Figure 5.23 to Figure 5.26 highlight graphically the thermal effect of air leakage within envelope assemblies.

The advantages of this monitoring procedure and data representation method are:

- It provides results that highlight areas prone to moisture-related problems;

- The graphics produced can be translated into areas of highest to lowest probability of air leakage;
- Data can be used in computer models to verify them.

However, the implemented protocol also comprises disadvantages:

- The method is labour intensive;
- The reproducibility of the air leakage paths is not ensured;
- There is a multiplicity of possible air leakage paths.

6. CONCLUSION

6.1 Summary and conclusions

A full-scale wood frame test hut with nine wall specimens, typical of low-rise residential construction in the province of Quebec, was built inside an environmental chamber. This test hut was subjected to 66 days of simulated winter and 47 days of late spring climatic conditions to study the modes of moisture dispersion through leaky exterior wall assemblies with and without added insulation and to verify the feasibility of different methods of characterizing air exfiltration. Through a better understanding of the movement of air through the envelope, the risks related to moisture condensation within the envelope when adding insulation to leaky existing exterior wall assemblies can be better ascertained. The air leakage pattern characterization methods implemented were 2-dimensional grid moisture content monitoring and 3-dimensional grid temperature monitoring. In addition, temperatures and thermal resistances without the impact of air leakage are calculated using a 3-dimensional conductive heat transfer model that does not take into account the effect of air leakage.

The temperature and moisture content results are used to assess the impact of adding extruded rigid polystyrene insulation on the hygrothermal behavior of existing leaky exterior wall assemblies. When insulation was added on the warm side, moisture content measurements did not rise above 25%[10], while they increased to 70% when insulation was added on the cold side. On the other hand, the airtight section with no insulation added showed the lowest moisture accumulation. Even though the thermal performance of the base-case airtight section is lower, it performed best in terms of

[10] Except for the wood stud samples in the section with the concentrated air leakage path, where moisture content rose to between 35% to 40% for a few hours after the climatic conditions were changed from wetting to drying.

overall hygrothermal performance. The temperatures measured for both the warm and cold planes for the sections with insulation added on the cold side were higher and the temperatures measured for the sections with insulation added on the warm side were lower than those measured for the base-case assemblies. As calculated using a 3-dimensional heat transfer modeling approach that does not include air leakage or moisture transfer, adding 38 mm of rigid insulation to the cold or warm side of existing assemblies increases the thermal performance by 55%. Experimental results demonstrate that the R-values do not reflect the complete hygrothermal performance of the assemblies with added insulation. The total R-value for the assemblies is the same whether rigid insulation is added on the cold or on the warm side of the base-case assembly insulated with glass fiber batt insulation. However, the performance of these two assemblies in terms of moisture accumulation is very different. From this analysis, it can be concluded that the thermal performance cannot be examined independently from air and moisture transfer, and that air leakage through the envelope should be minimized to avoid moisture problems.

The experimental results of the two air leakage characterization methods show that the 2-D grid moisture content monitoring (by gravimetry) and the 3-D grid temperature monitoring could be used to gain information on the path of air exfiltration through the envelope. Using a graphic mode of presenting the results, it has been demonstrated that there is a correlation between the moisture distribution pattern and the air leakage path, and between the temperature profiles and the air leakage path. Moisture contents measured by gravimetry and with moisture content sensors according to a 2-dimensional grid are used to generate isohygrons. This form of presenting the data permits identifying

local moisture related problem areas and confirms that moisture tends to accumulate at entry points of indoor air into the assembly. Moisture content accumulation patterns are related to the air leakage pattern. Moisture contents measured by both methods generally agree for the airtight section, the base-case sections and the sections with rigid insulation added on the warm side. For the sections with insulation added on the cold side, the moisture contents measured with the moisture sensors were significantly lower than those measured using gravimetry. Cold and warm plane temperature maps generated from experimental measurement show that monitored temperature profiles tend to follow the air leakage path of the section. Cold and warm plane isotherms generated from calculated temperatures highlight the effect of thermal bridging caused by the wood studs. By mapping the difference between the monitored temperature profiles and the calculated temperature profiles, a first attempt toward the graphic representation of the impact of air leakage on temperatures within the wall is obtained. This type of moisture content and temperature data analysis and the information it provides can only be achieved through the extensive monitoring conducted and with the graphic representation of the results.

Some conclusions concerning the execution of the type of retrofit work studied arise from the analysis of the data. The first one is that increasing the airtightness of the building envelope should be considered before adding insulation to existing exterior wall assemblies. This would help in reducing convective heat losses and in lowering the risk for moisture accumulation related problems. Using air leakage as a ventilation strategy is not recommended. Relying on uncontrolled air leaks through the envelope greatly increases the probability for moisture related problems. When adding insulation, it has

been found that adding 38 mm of rigid extruded polystyrene on the cold side of the assembly increases the risk of moisture accumulation related problems because of its low vapour and water permeability and of the temperature conditions at its indoor surface, and that adding insulation on the warm side of the existing building envelope reduces these risks, partly because it helps in improving the airtightness. These recommendations apply for the assemblies tested in this project, under the climatic conditions provided. Though they provide some direction toward the execution of such retrofit work, they cannot be generalized to all existing exterior wall assemblies and all insulation materials.

6.2 Contributions

This research project contributed the following:

1. The development and implementation of a test procedure on re-insulated leaky wall specimens. The development includes the design of the test specimens and the test hut, the definition of the testing conditions and the proposal of a monitoring procedure. The resulting moisture content and temperature data allowed to evaluate the impact of re-insulation strategies depending on the air leakage pattern.
2. The development of a method for characterization of air leakage paths through the building envelope using temperature and moisture content mapping, which included the development and implementation of a moisture content (using gravimetry and moisture content pins) and temperature monitoring protocol and required the production of a calibration curve for the measurement of moisture content in asphalt impregnated fiberboard sheathing with moisture content pins;

3. The production of graphical temperature and moisture content maps of different wall assemblies. The resulting temperature maps were compared with calculated temperature profiles to demonstrate how the method provides data on the impact of air leakage on the temperatures inside assemblies.

6.3 Recommendations for future work

It is recommended that future research should direct its efforts on the following issues:

1. Further the graphic air leakage characterization attempt by refining the method and expanding it to the moisture contents. For this, a 3-d model predicting moisture migration without air leakage would need to be developed and used;
2. Apply this method to other geometries and assemblies with different materials using a more extensive and tighter monitoring grid. For example, wall/window, wall/roof and wall/floor junctions could be evaluated with the type of monitoring procedure developed to identify the path of air leakage within these junctions. In addition, the performance of junctions and wall assemblies with different insulating materials than those included in the present study could be tested.
3. Integrate air leakage patterns into heat, air and moisture transfer modeling and compare simulation results with experimental results.
4. Expand the graphic representation method to be three-dimensional.

7. REFERENCES

ANSI/ASHRAE. 1992. ANSI/ASHRAE 55-1992 "Thermal Environmental Conditions for Human Occupancy" American Society of Heating, Refrigerating and Air-Conditioning Engineers, 20 p.

ASHRAE. 1993. "ASHRAE Handbook of Fundamentals" (SI edition). American Society of Heating, Refrigerating and Air-Conditioning Engineers, Inc. Atlanta, GA., Chapters 20, 21, and 23.

ASTM. 1989. ASTM C 236-89 "Standard Test Method for Steady-state Thermal Performance of Building Assemblies by Means of a Guarded Hot Box" American Society for Testing and Materials, Annual Book of Standards, Vol. 4.06, pp. 52-62.

ASTM. 1992. ASTM D 4442-92 "Standard Test Method for Direct Measurement of Wood and Wood-Based Materials" American Society for Testing and Materials, Annual book of Standards, Vol. 04.10, pp. 493-497.

ASTM. 1991. ASTM E 283-91 "Standard Test Method for Determining the Rate of Air Leakage Through Exterior Windows, Curtain Walls, and Doors Under Specified Pressure Differences Across the Specimen" American Society for Testing and Materials, Annual book of Standards, Vol. 04.07, pp. 486-489.

ASTM. 1999. ASTM E 779-99 "Standard Test method for Determining Air Leakage Rate by Fan Pressurization" American Society for Testing and Materials.

ASTM. 1991. ASTM E 783-91 "Standard Test Method for Field Measurement of Air Leakage Through Installed Exterior Windows and Doors" American Society for Testing and Materials.

ASTM. 1996. ASTM E 1827-96 "Standard Test Methods for Determining Airtightness of Buildings Using an Orifice Blower Door" American Society for Testing and Materials.

Athienitis, A. 1994. "An Electronic Mathcad Book", Center for Building Studies, Concordia University, Montreal, Canada, 189 p.

Bomberg, M.; Brown, W. 1993. "Building Envelope: Heat, Air and Moisture Interactions", Journal of Thermal Insulation and Building Envelope, Volume 16, April 1993, pp. 306-311.

Burch, D.M.; Treado, S. 1978. "A technique for protecting retrofitted wood-frame walls from condensation damage", ASHRAE TRANSACTIONS, Vol. 84, Part 1, pp. 197-206.

CAN/CGSB 149.10 M86. 1986. "Determination of the airtightness of building envelopes by the fan pressurization method", Canadian General Standards Board, Ottawa.

Canadian Mortgage and Housing Corporation. 1999. "Wood-Frame Envelopes in the Coastal Climate of British Columbia", Best Practice Guide Series, Ottawa, Canada.

Colliver, D.G.; Murphy, W.E.; Sun, W. 1994. "Development of a building component air leakage data base", ASHRAE TRANSACTIONS: RESEARCH, Vol. 100, Part 1, pp. 292-305.

Derome, D.; Fazio, P. 2000. "Large-scale Testing of Two Flat Roof Assemblies Insulated with Cellulose", Journal of Architectural Engineering, American Society of Civil Engineers, Vol. 6, No. 1, pp. 12-23.

Derome, D., Fazio, P., Fortin, Y. 1999. "Détermination des coefficients de transfert de masse et de chaleur pour le transfert d'humidité sous un platelage de toit en bois", IVe Colloque Inter-universitaire Franco-Québécois - Thermique des systèmes à température modérée. May 25-27, Montreal, Quebec, pp. 301-308.

Fazio, P.; Athienitis, A.; Marsh, C.; Rao, J. 1997. "An environmental chamber for investigation of building envelope performance", Journal of Architectural Engineering, American Society of Civil Engineers, Vol. 3, No. 2, pp. 97-102.

Fazio, P., Derome; Derome, D.; Gerbasi, D.; Athienitis, A.; Depani, S. 1998, "Testing of flat roofs insulated with cellulose fiber", Thermal Envelopes VII, ASHRAE, Clearwater, Florida, pp. 3-13.

Forest, T.W. 1989. "Moisture transfer through walls", Thermal Envelopes IV, ASHRAE, Clearwater, Florida, pp. 532-542.

Garden, G.K. 1965. "Control of air leakage is important", Canadian Building Digest, CBD-72, National Research Council of Canada.

Hamlin, T.; Gusdorf, J. 1997. "Airtightness and energy efficiency of new conventional and R-2000 housing in Canada, 1997", CANMET (Canada Centre for Mineral and Energy Technology), Ottawa, Canada, 72 p.

Handegord, G.O., 1982, "Air leakage, ventilation, and moisture control in buildings", Moisture Migration in Buildings, ASTM STP 779, M. Lieff and H.R. Trechsel, Ed., American Society for Testing and Materials, pp. 223-233.

Hansen, A.T. 1984. "Moisture problems in walls", Canadian Building Digest, CBD-231, National Research Council of Canada.

Hens, H. 1996. "Final Report - Task 1: Modelling", International Energy Agency - Annex 24 Heat, Air and Moisture Transfer Through New and Retrofitted Insulated Envelope Parts (Hamtie), Vol. 1, 90 p.

Hutcheon, N.B. 1963. "Requirements for exterior walls", Canadian Building Digest, CBD-48, National Research Council of Canada.

Hutcheon, N.B.; Handegord, G.O. 1989. "Building science for a cold climate", (SI edition) Construction Technology Center Atlantic Inc., Fredericton, New Brunswick, Ch. 11.

Jones, D. C. 1995. "Impact of airflow on the thermal performance of various residential wall systems utilizing a calibrated hot box", Thermal Envelopes VI, ASHRAE, Clearwater, Florida, pp. 247-260.

Kumaran, M.K. 1996. "Taking guess work out of placing air/vapour barriers", Canadian Consulting Engineer, Vol. March/April, pp. 32-33.

Latta, J.K.; Beach, R.K. 1964. "Vapour diffusion and condensation", Canadian Building Digests, CBD-57, National Research Council of Canada.

Latta, J.K.; Beach, R.K. 1964. "Vapour barriers : What are they? Are they effective?" Canadian Building Digests, CBD-175, National Research Council of Canada.

National Building Code of Canada. 1995. National Research Council of Canada, Ottawa.

NRCC - IRC. 1997. "Systèmes d'étanchéité à l'air pour murs de bâtiments de faible hauteur : Performance et évaluation", Conseil national de recherches du Canada - Institut de recherche en construction, Ottawa, Canada, 45 p.

Ojanen, T.; Kohonen, R.O. 1995. "Hygrothermal performance analysis of wind barrier structures", ASHRAE TRANSACTIONS: SYMPOSIA, Vol. 101, pp. 595-606.

Ojanen, T.; Simonson, C. 1995. "Convective moisture accumulation in structures with additional inside insulation", Thermal Envelopes VI, ASHRAE, Clearwater, Florida, Vol. 2, pp. 745-752.

Quirouette, R.L. 1985. "The difference between a vapour barrier and an air barrier", Building Practice Note No. 54, National Research Council Canada, Division of Building Research, 13 p.

Rousseau, J. 1989. "Creating effective air barrier: Materials and techniques", Thermal Envelopes V, ASHRAE, Clearwater, Florida, pp. 646-651.

Sherman, M. 1995. "The Use of Blower-Door Data.", Indoor Air 1995, Denmark, pp. 215-224.

Simpson, A.; D.E. O'Connor. 1994. "Timber frame wall: Hygrothermal properties and vapour barrier damage", Building Services Engineering Research and Technology, Vol. 15, No. 3. pp. 179-184.

Straube, J.; Burnett, E. 1995. "Moisture movement in building enclosure wall systems", Thermal Envelopes VI, ASHRAE, Clearwater, Florida, Vol. 1, pp. 177-188.

TenWolde, A. 1989. "Moisture transfer through materials and systems in buildings", Water Vapour Transmission Through Building Materials and Systems: Mechanisms and Measurement, ASTM STP 1039, H.R. Trechsel, M. Bomberg editors, ASTM, Philadelphia, pp. 11-18.

Trechsel, H.R.; Achenbach, P.R.; Ebbets, J.R. 1985. "Effect of an exterior air-infiltration barrier on moisture accumulation within insulated frame wall cavities", ASHRAE Technical Data Bulletin Infiltration, ASHRAE, Atlanta, Vol. 1, No. 2, pp. 23-37.

Trechsel, H.R.; Achenbach, P.R.; Knight, H.J.; Lou, G.W. 1986. "Evaluation of wind effect on moisture content of frame walls with and without an air-infiltration barrier", Thermal Envelopes III, ASHRAE, Vol. 2, pp. 648-662.

Verschoor, J.D. 1986. "Measurement of water migration and storage in composite building construction", ASHRAE Technical Data Bulletin, Vol. 2, No. 5, pp. 140-153.

Wilson, A.G. 1961. "Air leakage in buildings", Canadian Building Digest, CBD-23. National Research Council of Canada.

Zarr, R.R.; Burch, D.M.; Fanney, A.H. 1995. "Heat and Moisture Transfer in Wood-Based Wall Construction: Measured Versus Predicted", NIST Building Science Series 173, Building and Fire Research Laboratory, National Institute of Standards and Technology, Gaithersburg, MD, 72 p.

Appendix A - Stack effect calculations

From "Building for a Cold Climate" (Hutcheon and Handegord, 1989), the pressure due to the stack effect can be calculated from equation A.1.

It is assumed that there is not a lot of resistance to airflow within the building, i.e. that it is not compartmented. Also, that openings are uniformly distributed on both floors, so that the neutral pressure plane is at mid-height. This equation provides the maximum stack effect.

$$p_s = g * h p_t / R_a (1/T_o - 1/T_i)$$ Equation A.1

where:
p_s = pressure due to stack effect (Pa);
g = acceleration due to gravity (9.81 m/s^2)
h = height from neutral plane (m);
p_t = barometric pressure (101000 Pa);
R_a = gas constant (287.1 J/kg*K for air);
T_o = outside temperature (264.5K for winter, 289K for spring);
T_i = inside temperature (295K for winter, 296K for spring).

For winter conditions:
p_s = 9.81 * (2.8 * 101000 / 287.1) (1/264.5 - 1/295)
p_s = 9.81 * 985 * (0.0038 - 0.0034)
p_s = 3.87 Pa or **4 Pa**

For spring conditions:
p_s = 9.81 * (2.8 * 101000 / 287.1) (1/289 - 1/296)
p_s = 9.81 * 985 * (0.0035 - 0.0034)
p_s = 0.97 Pa or **1 Pa**

Appendix B - Temperature monitoring

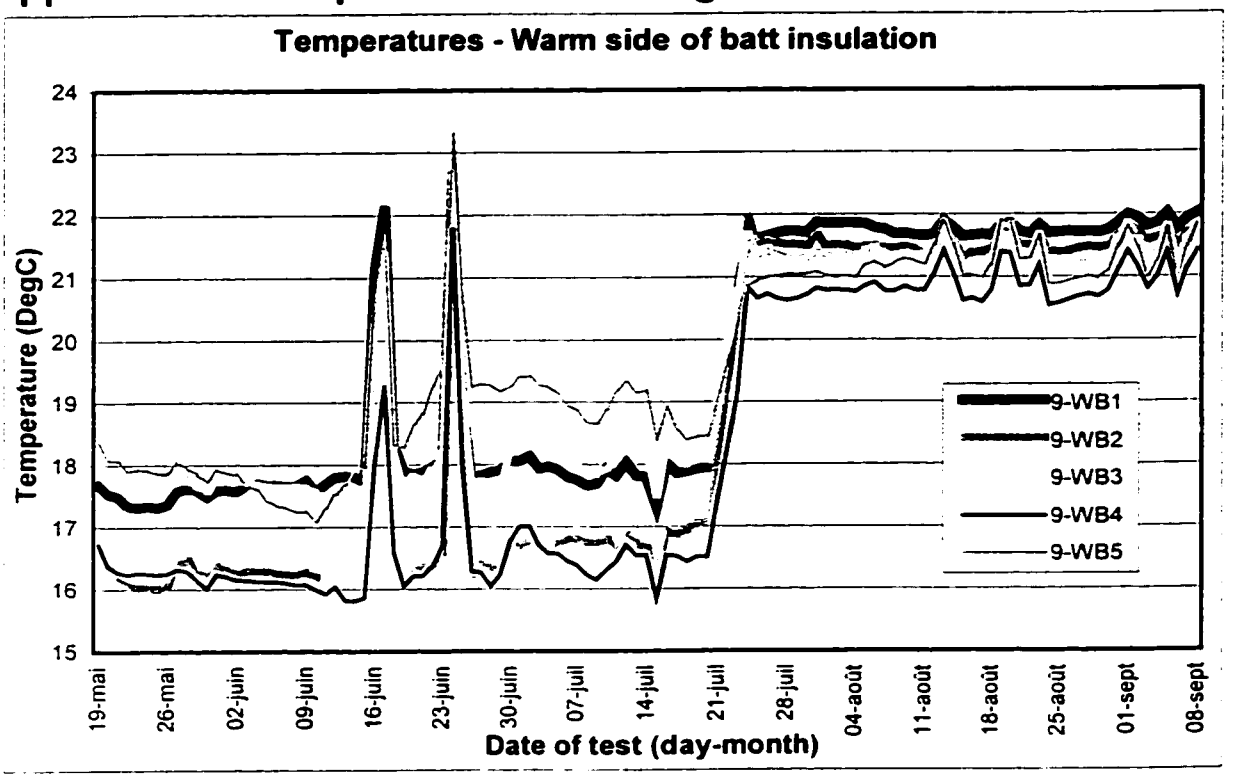

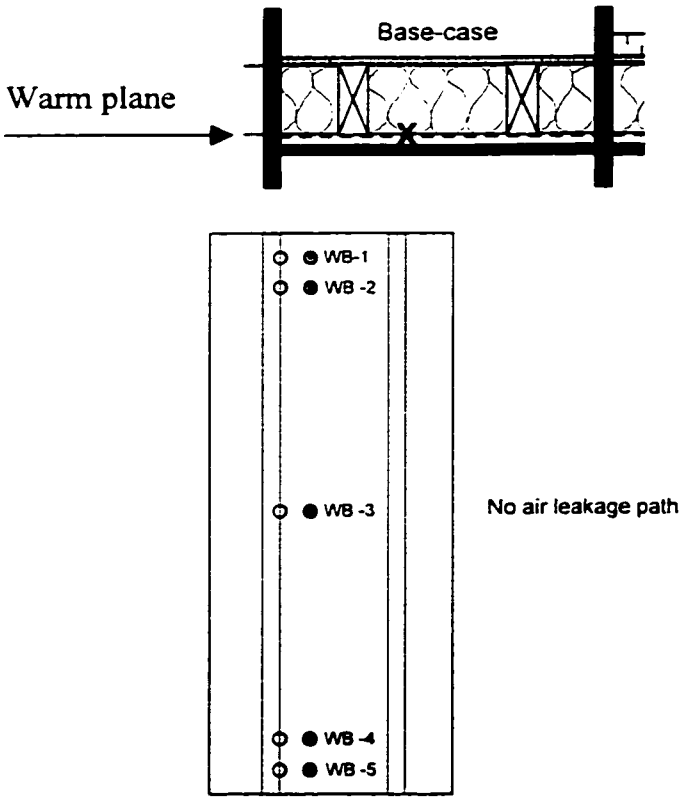

Base-case assembly, airtight.

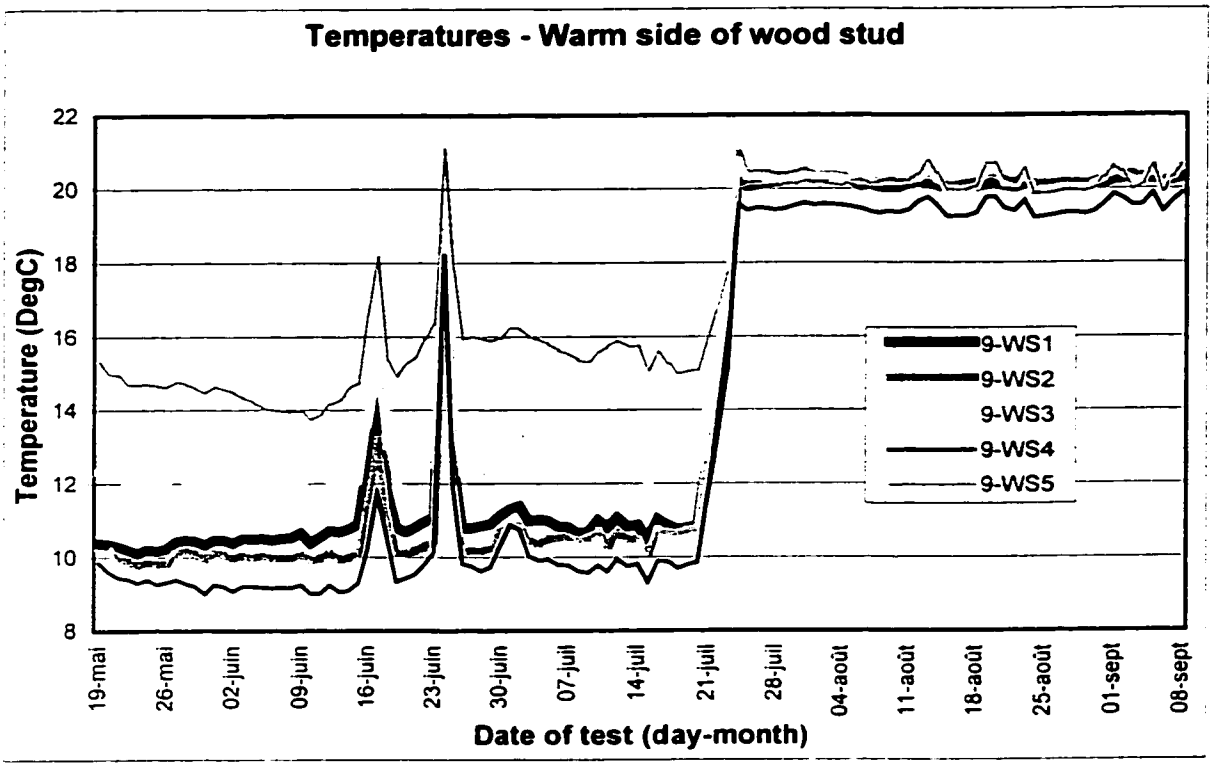

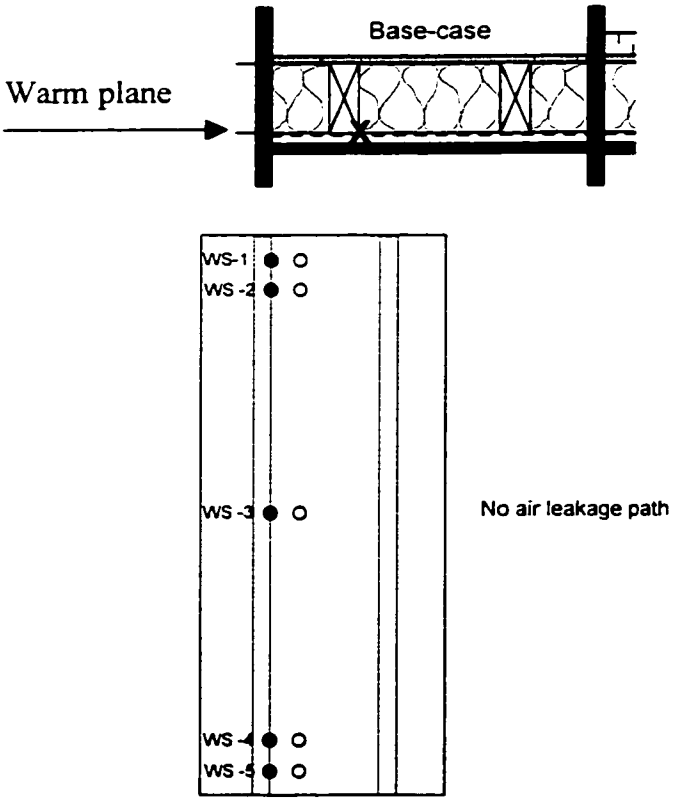

Base-case assembly, airtight.

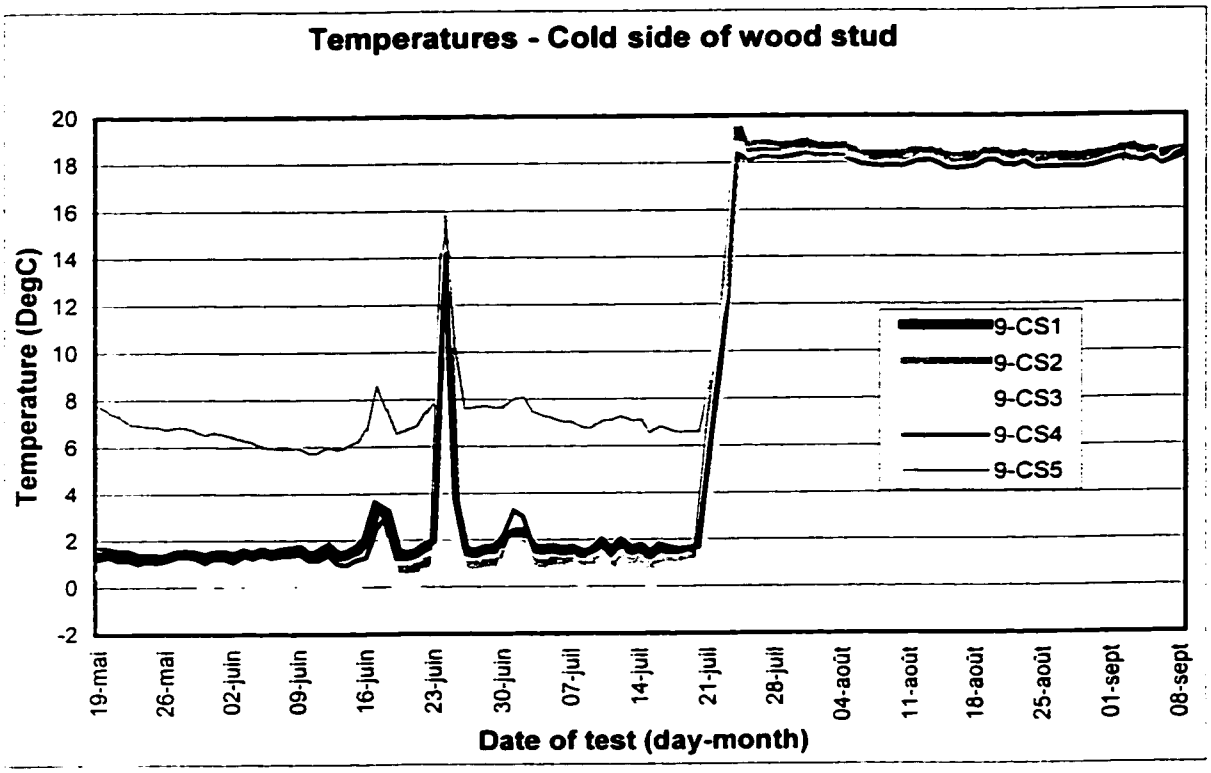

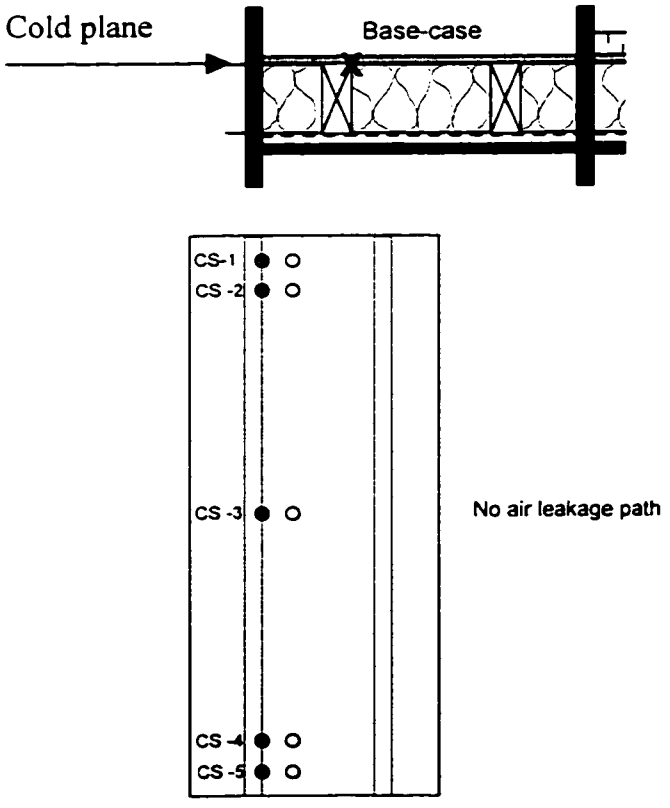

Base-case assembly, airtight.

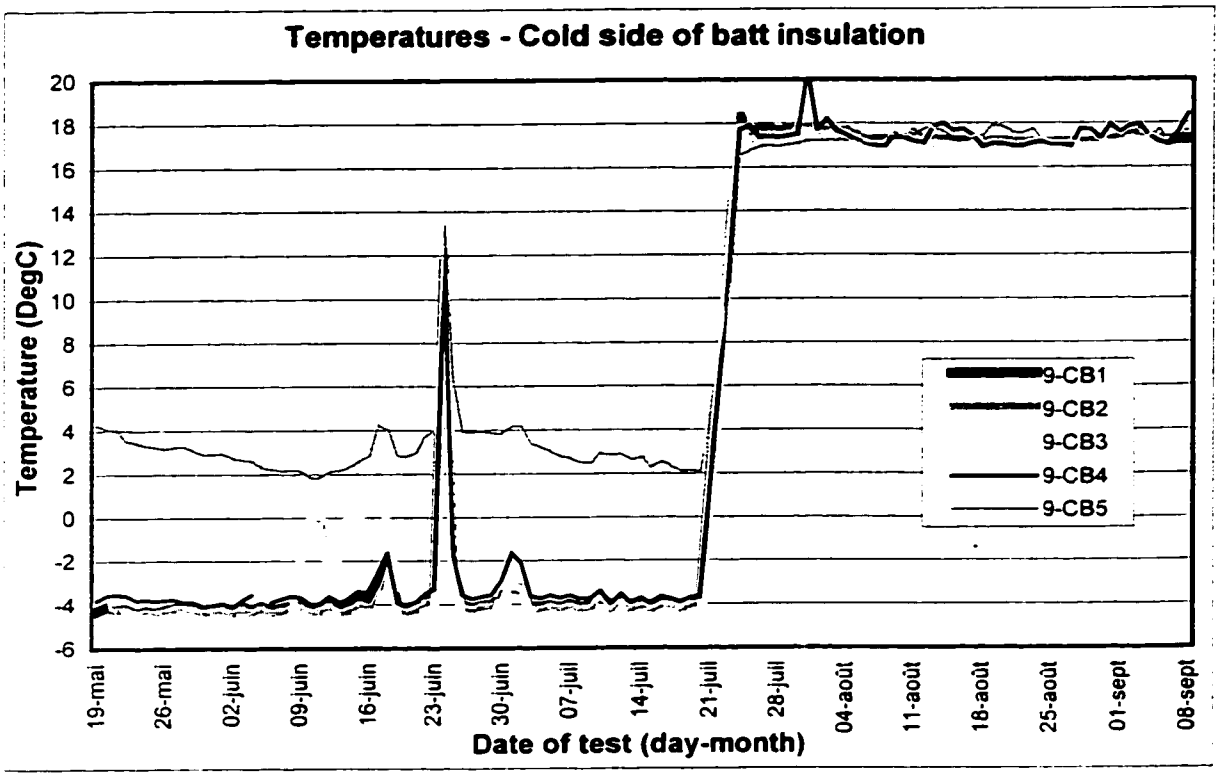

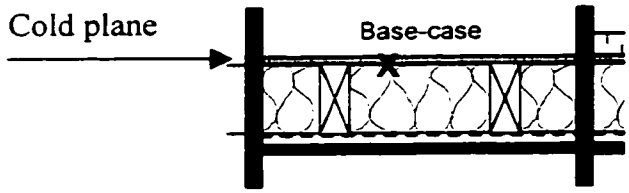

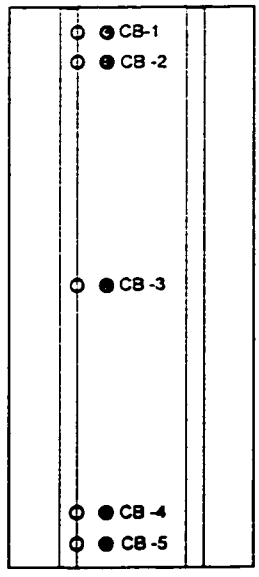

No air leakage path

Base-case assembly, airtight.

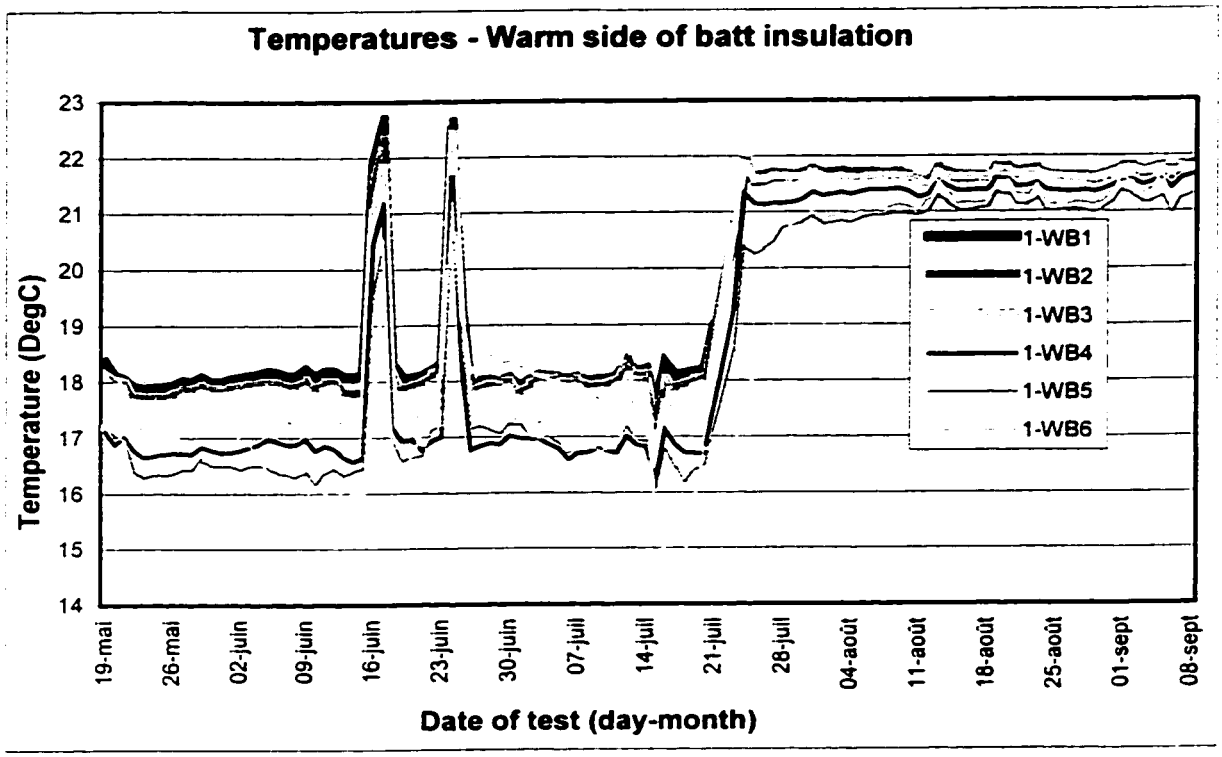

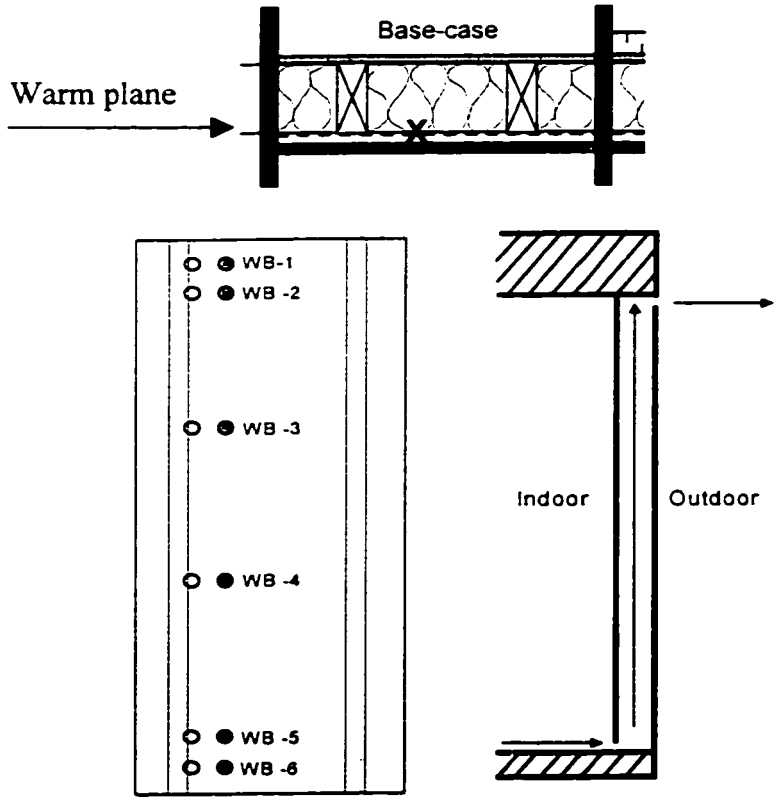

Base-case assembly, long air exfiltration path.

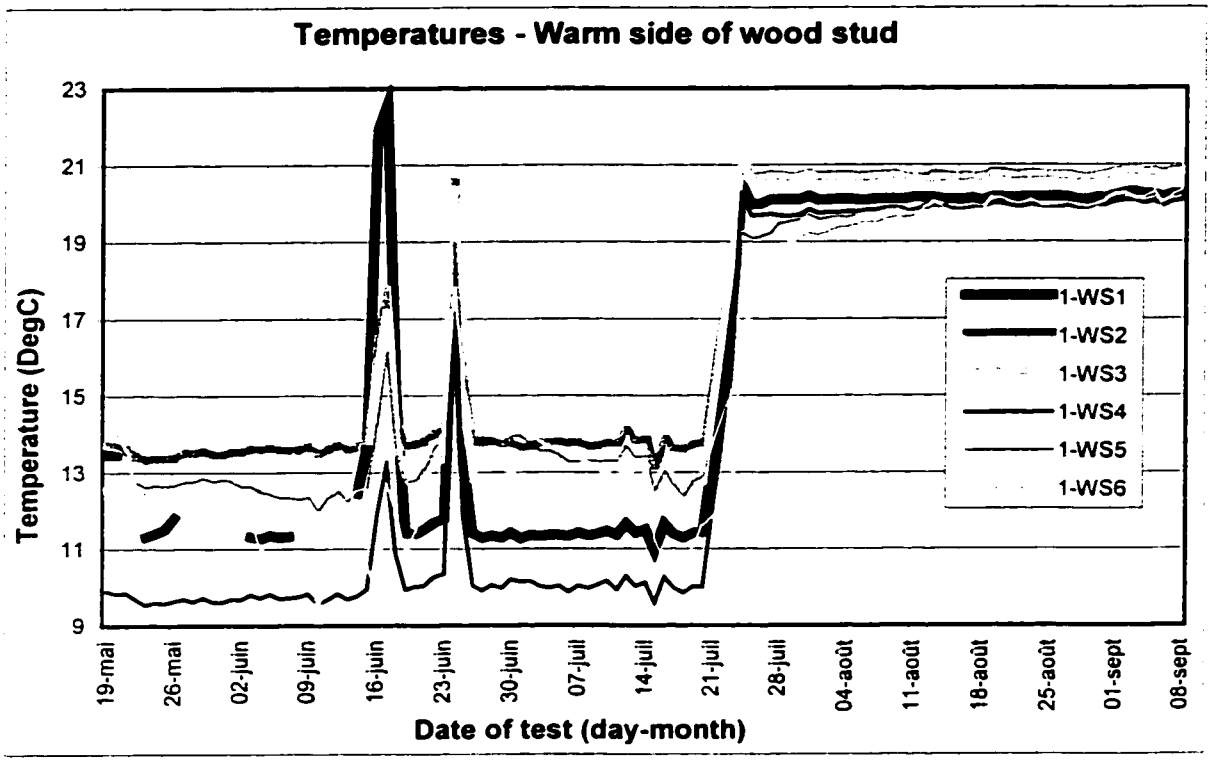

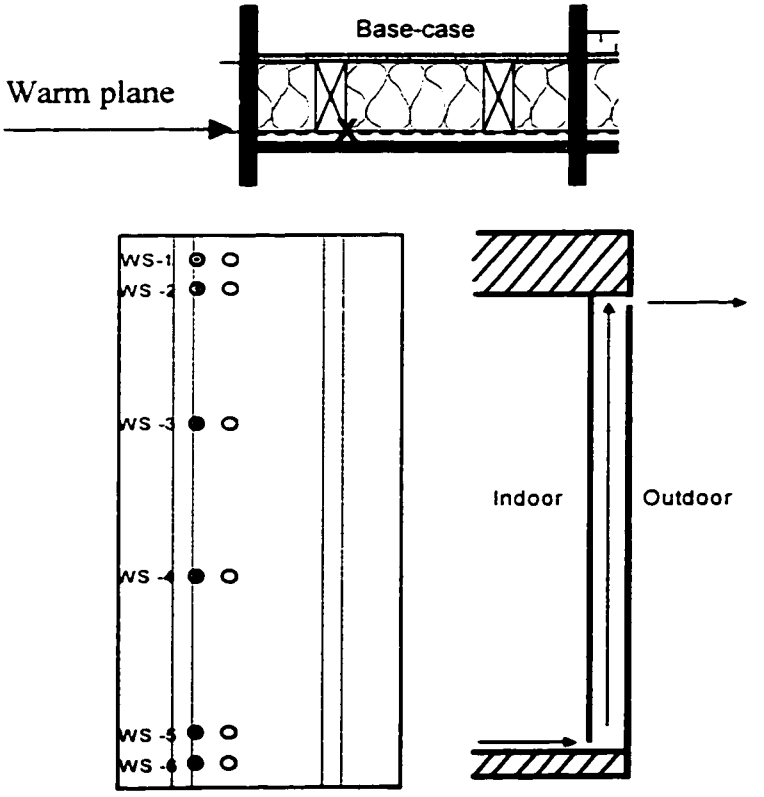

Base-case assembly, long air exfiltration path.

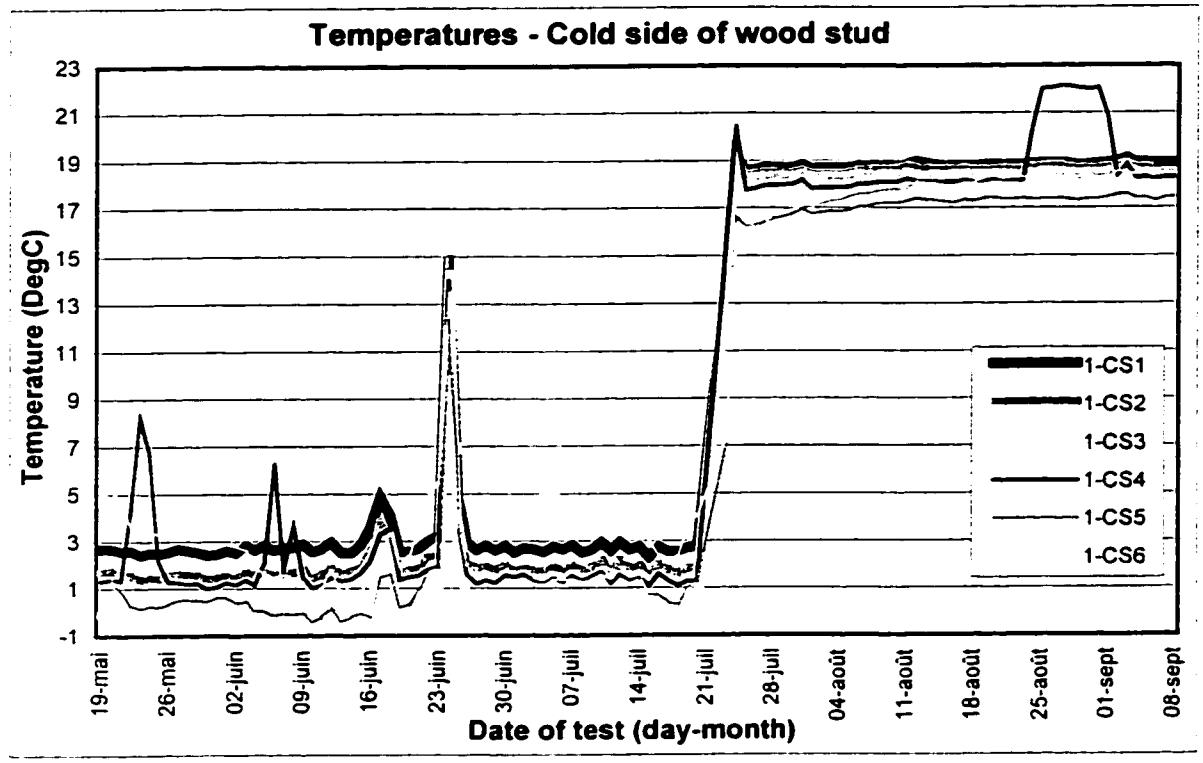

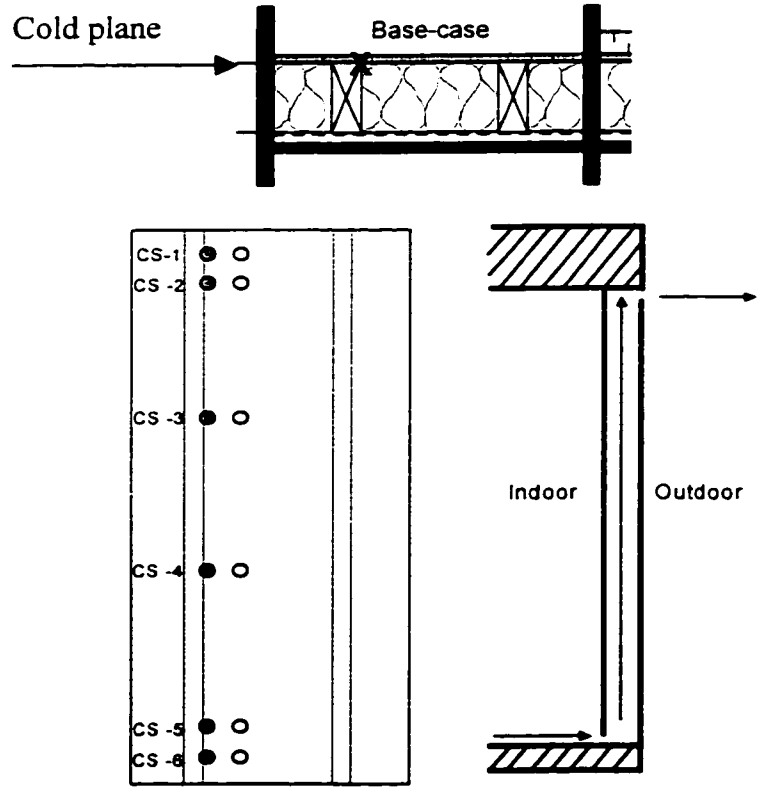

Base-case assembly, long air exfiltration path.

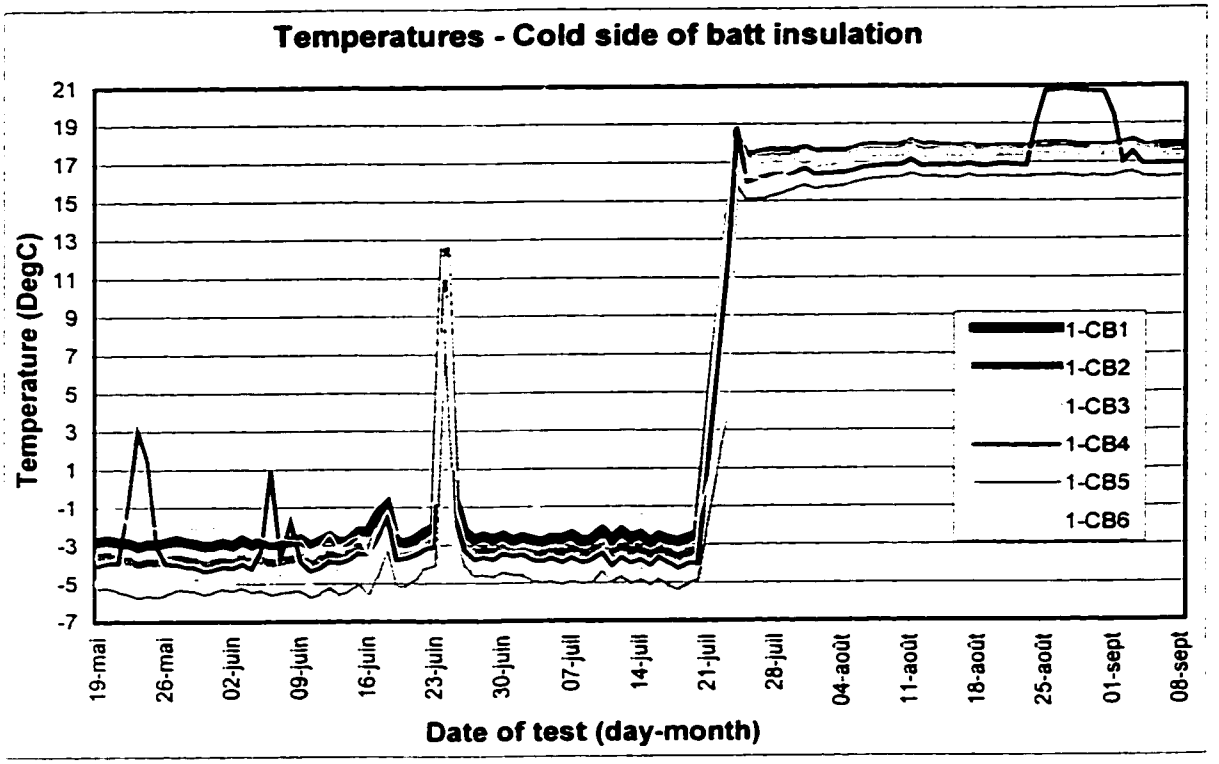

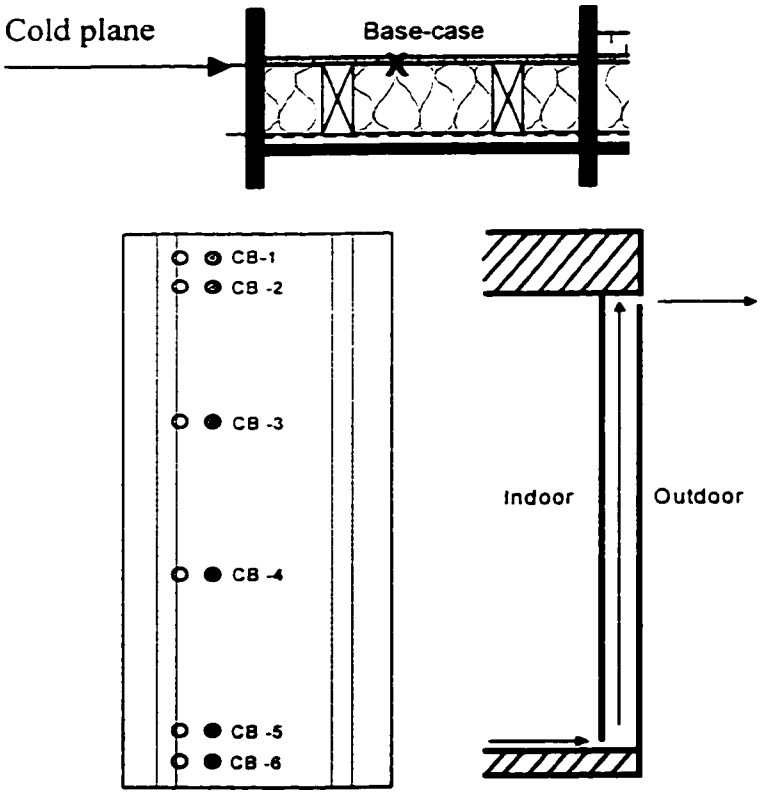

Base-case assembly, long air exfiltration path.

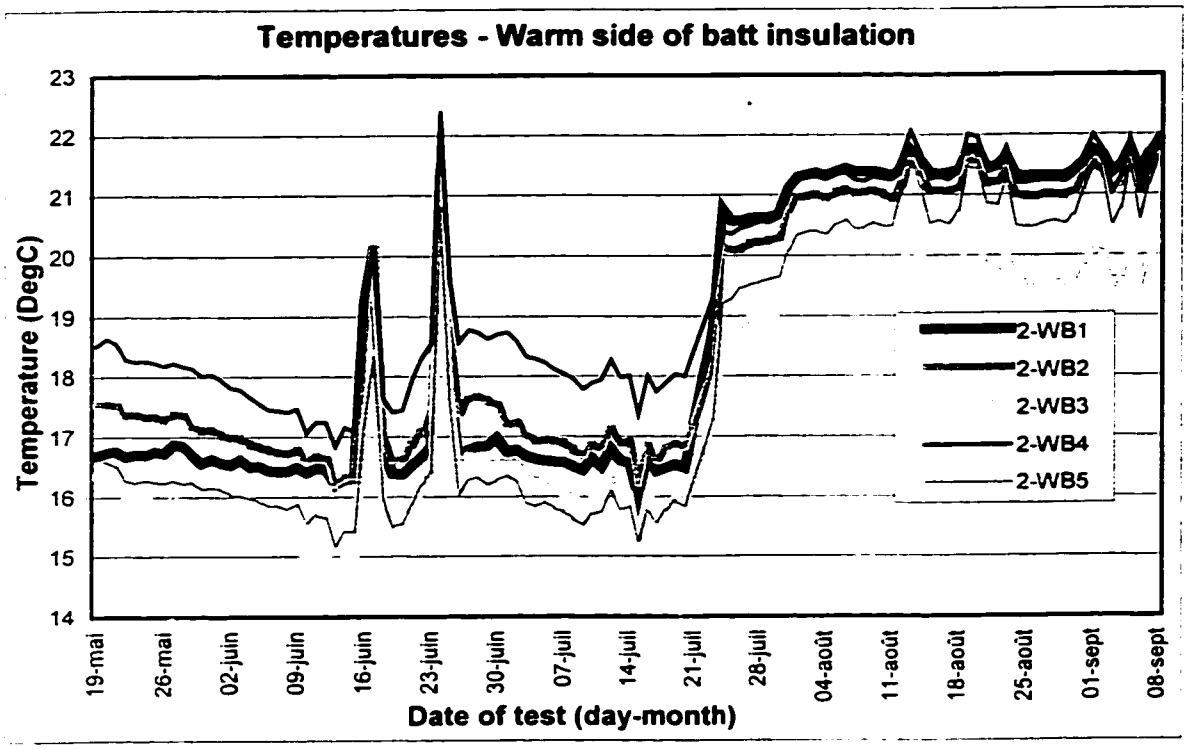

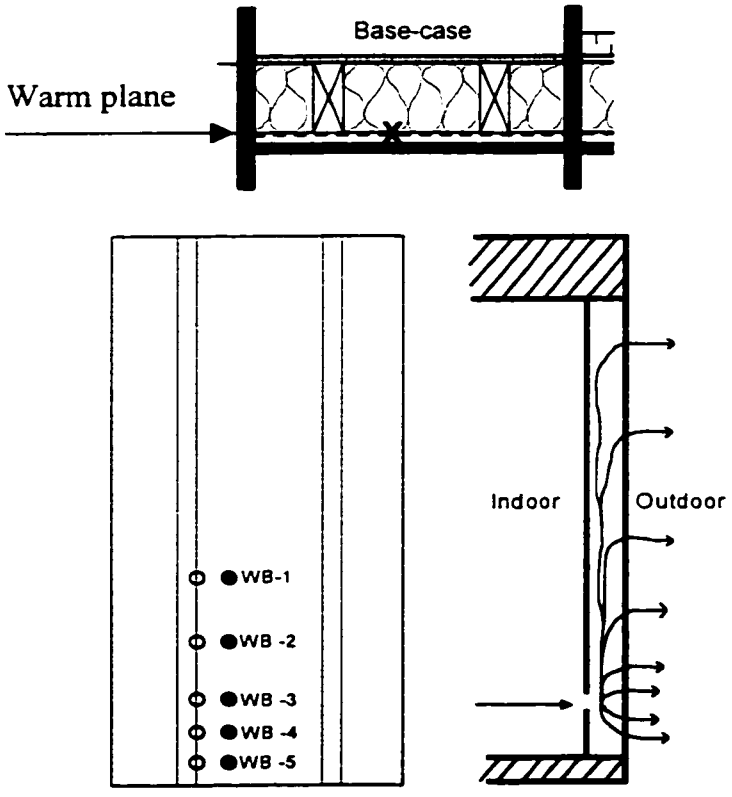

Base-case assembly, concentrated air leakage path.

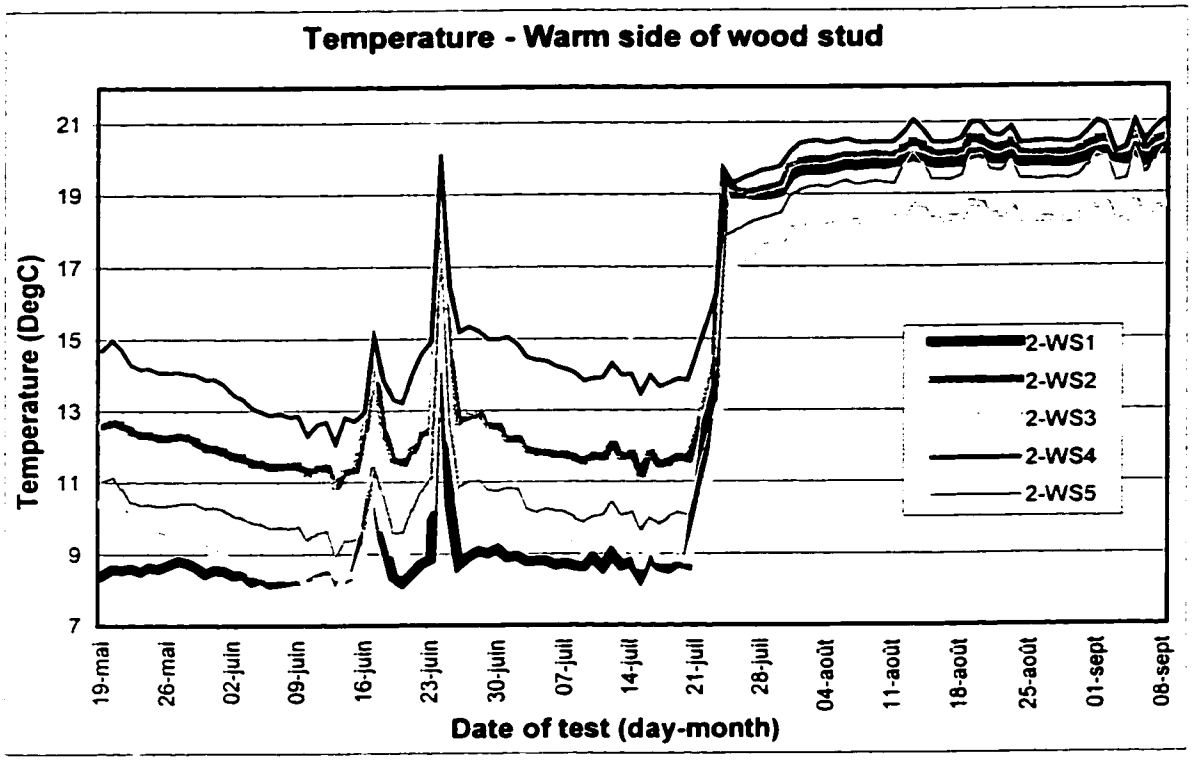

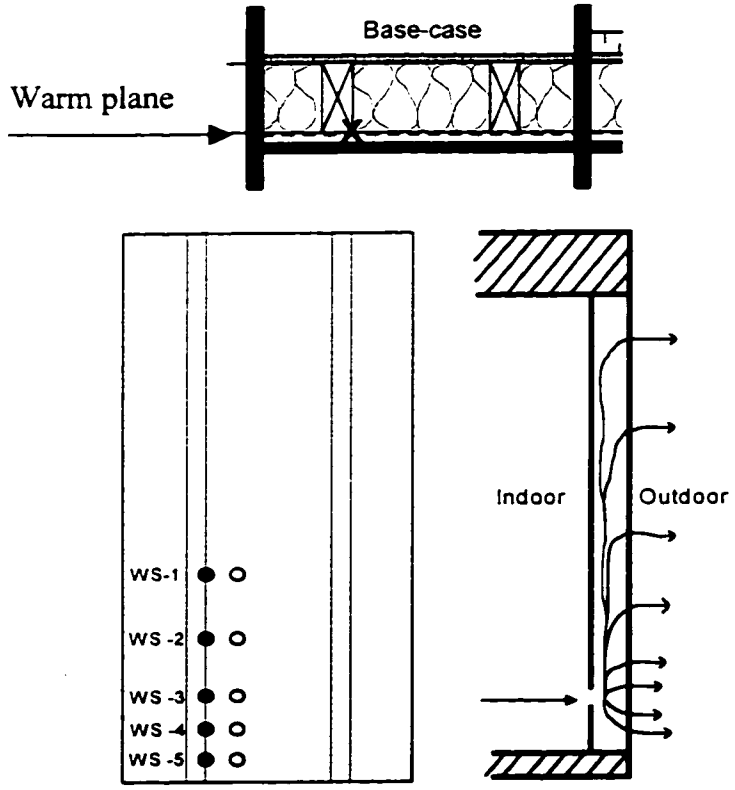

Base-case assembly, concentrated air leakage path.

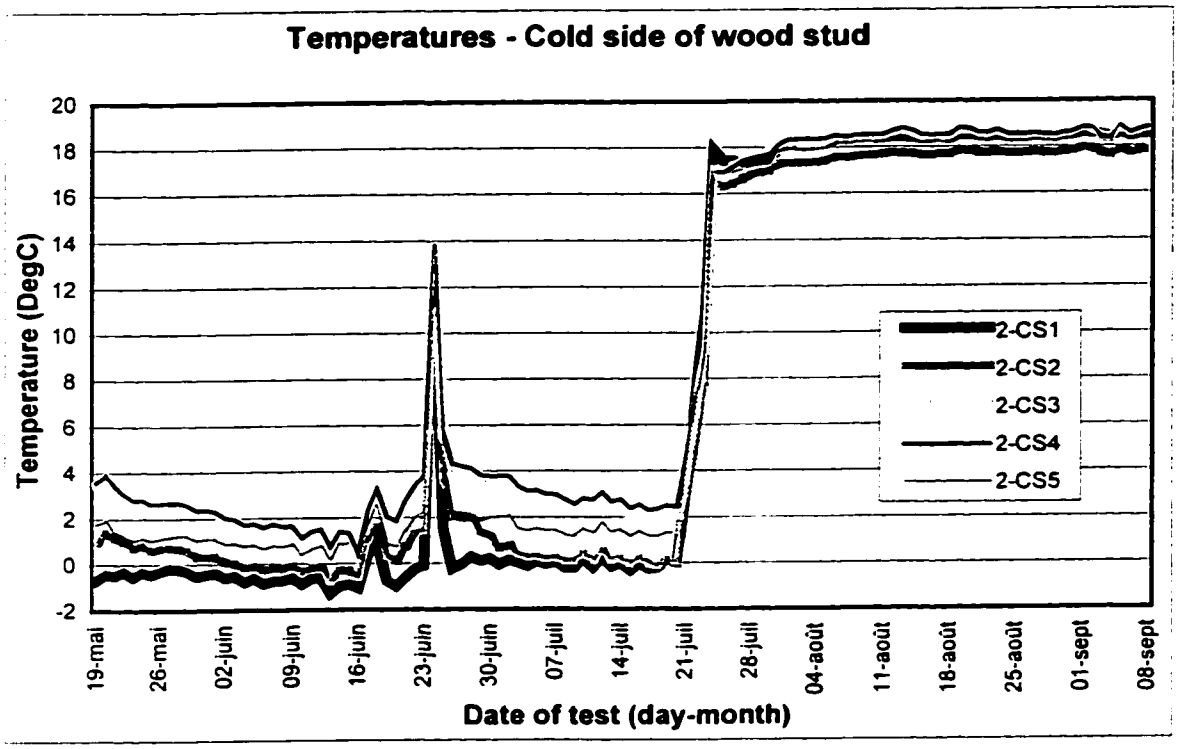

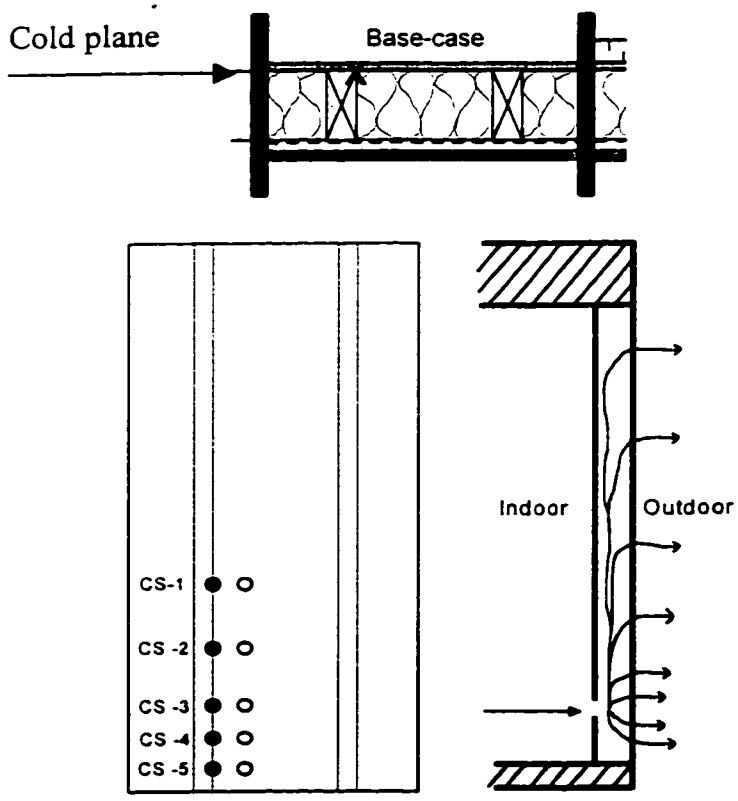

Base-case assembly, concentrated air leakage path.

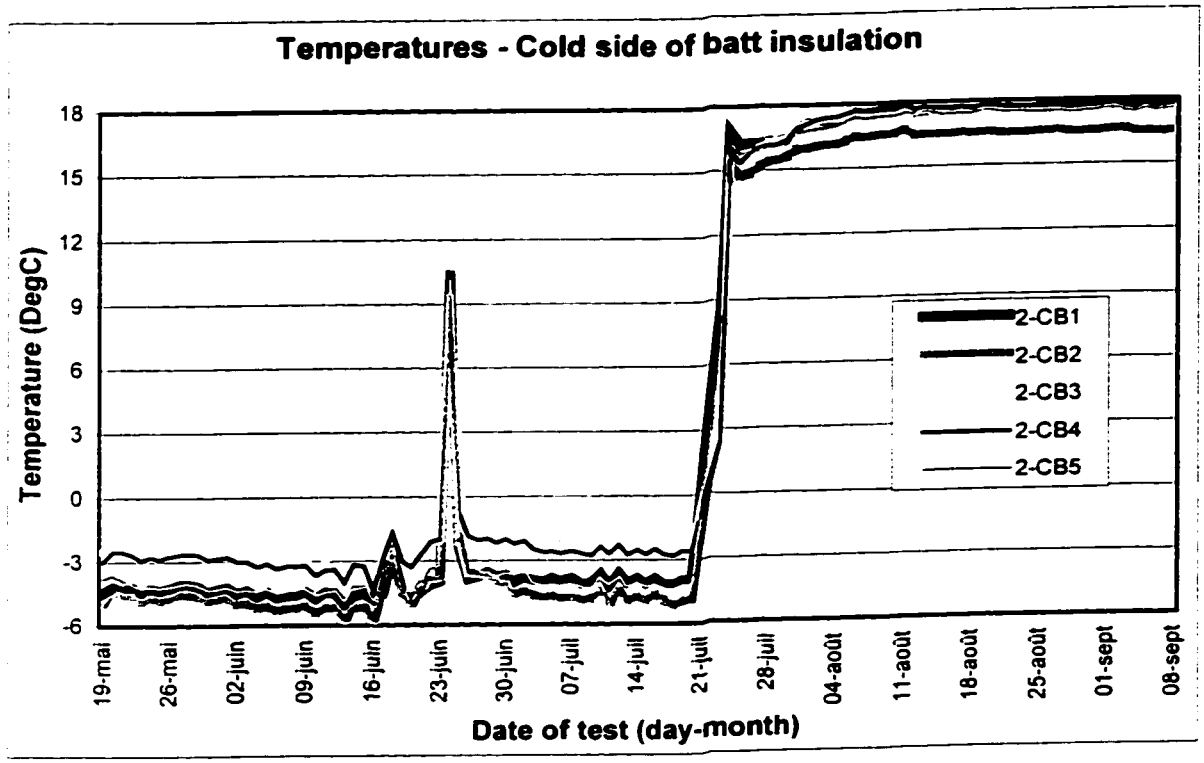

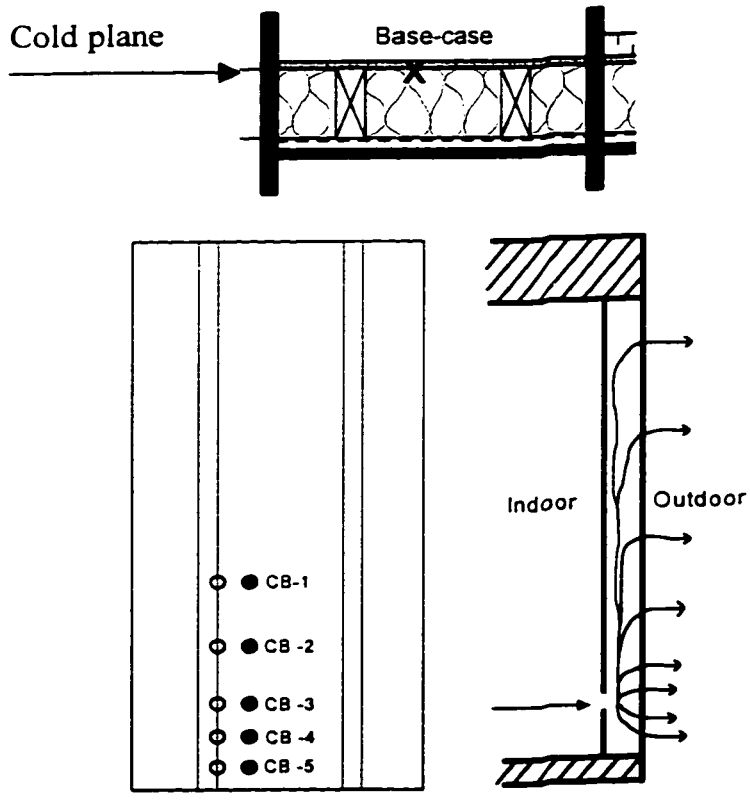

Base-case assembly, concentrated air leakage path.

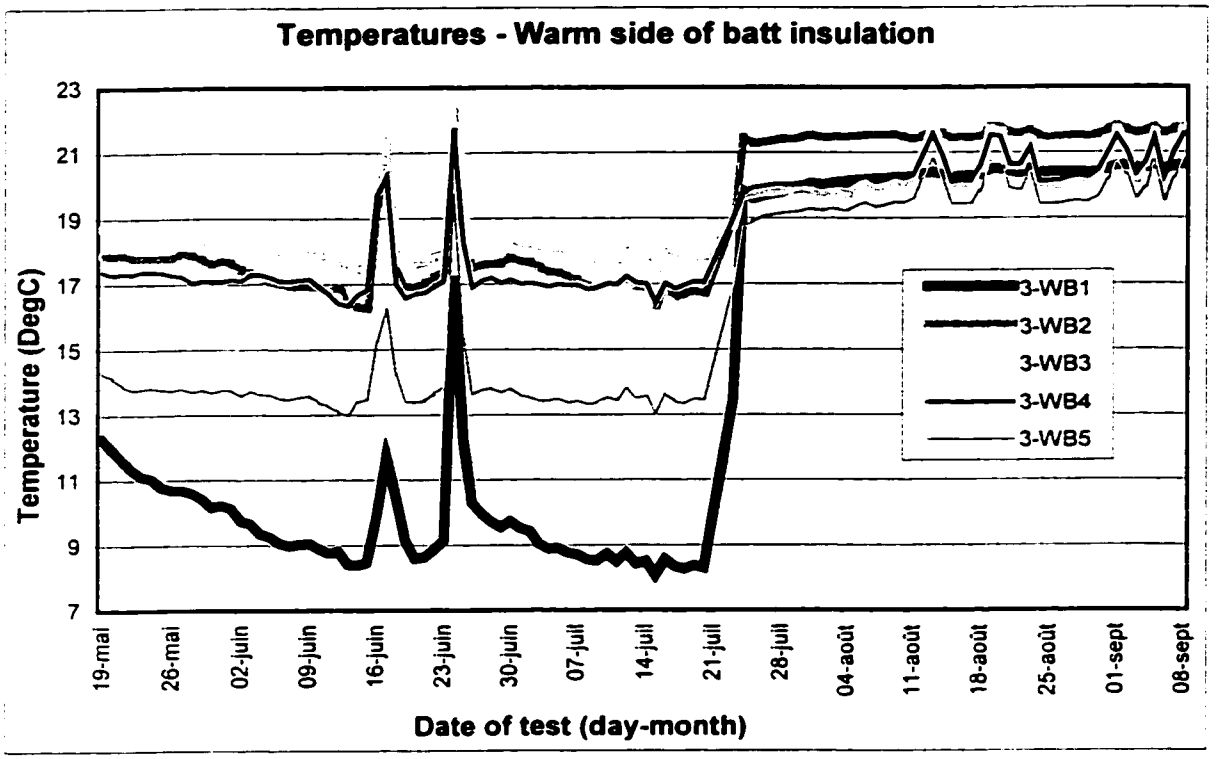

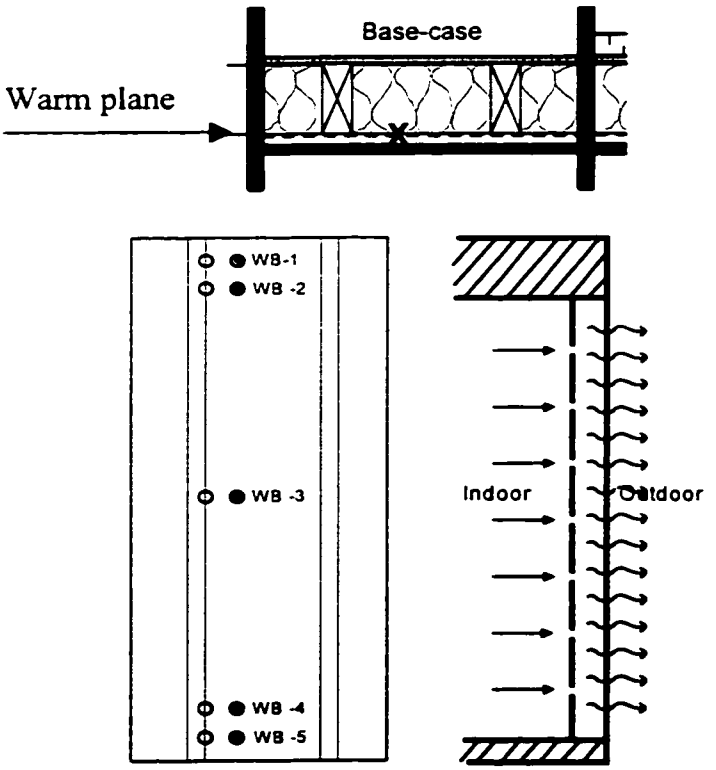

Base-case assembly, distributed air leakage path.

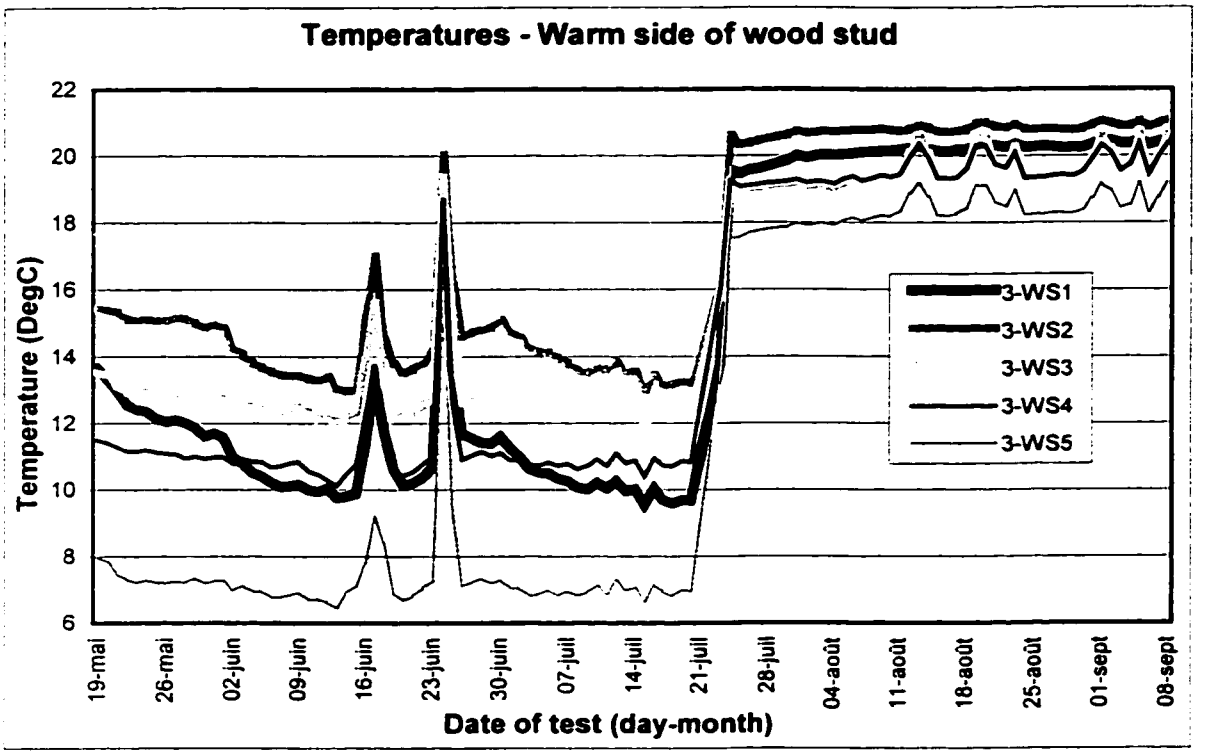

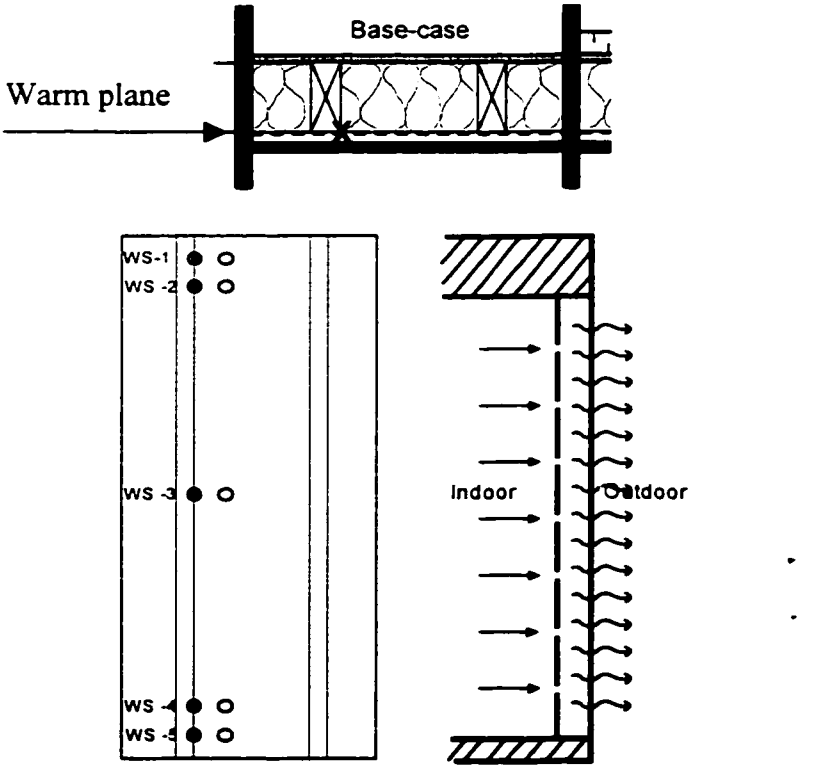

Base-case assembly, distributed air leakage path.

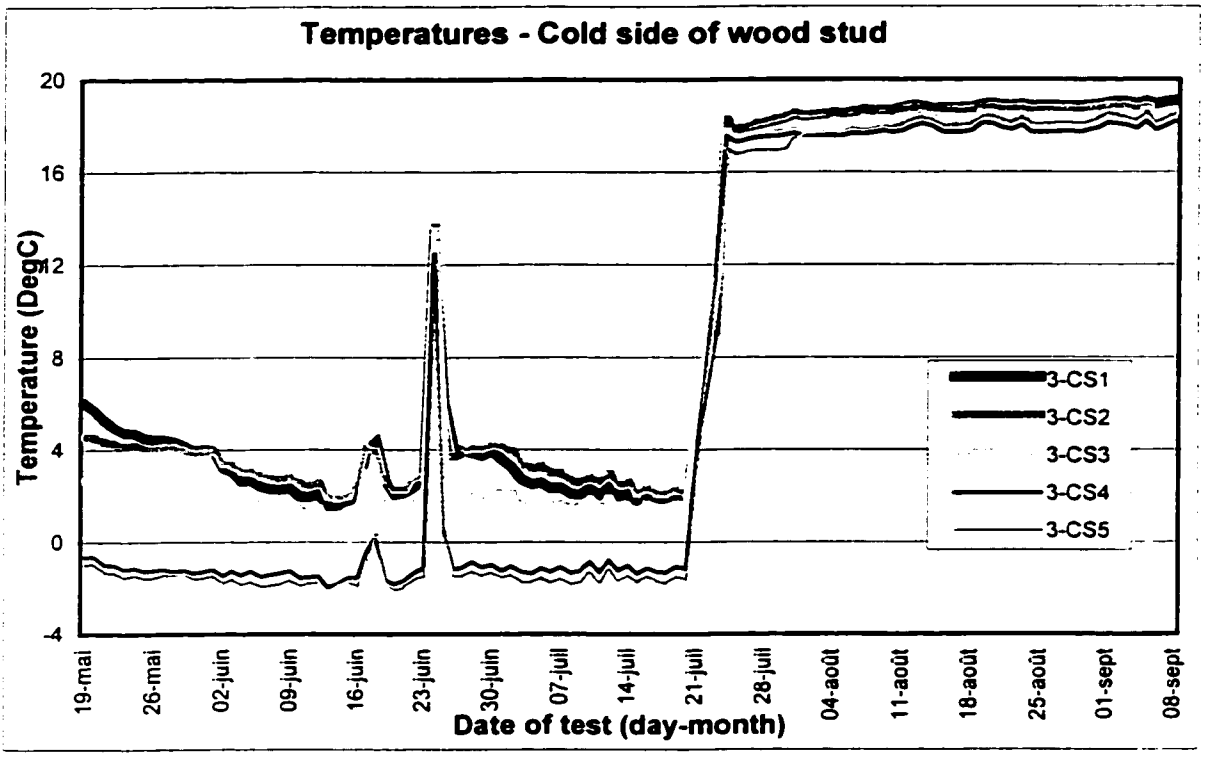

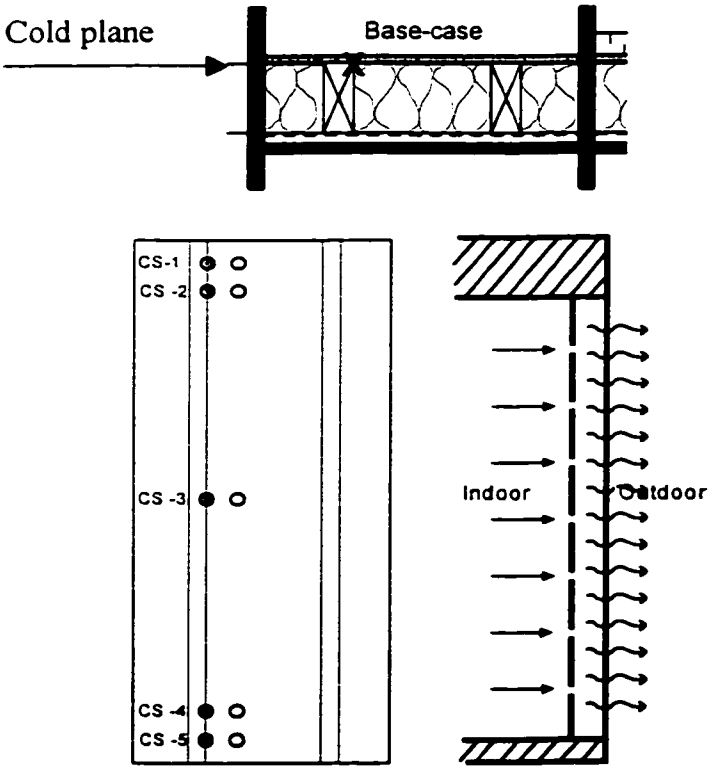

Base-case assembly, distributed air leakage path.

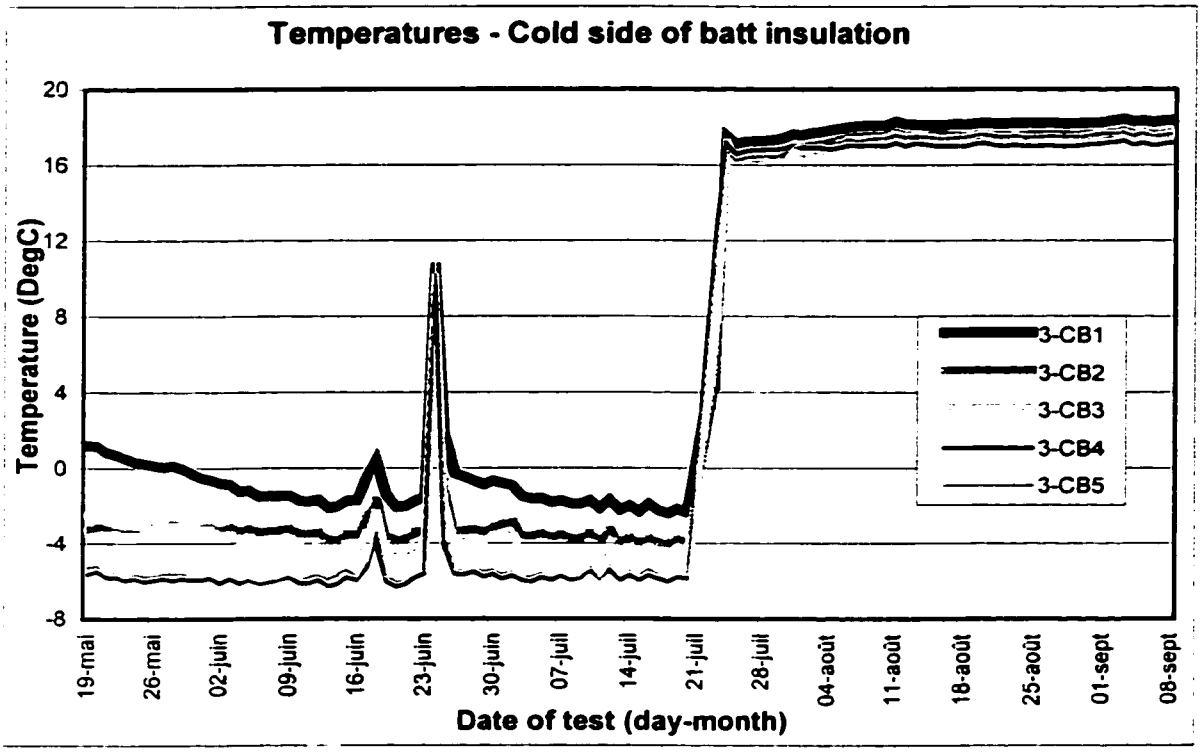

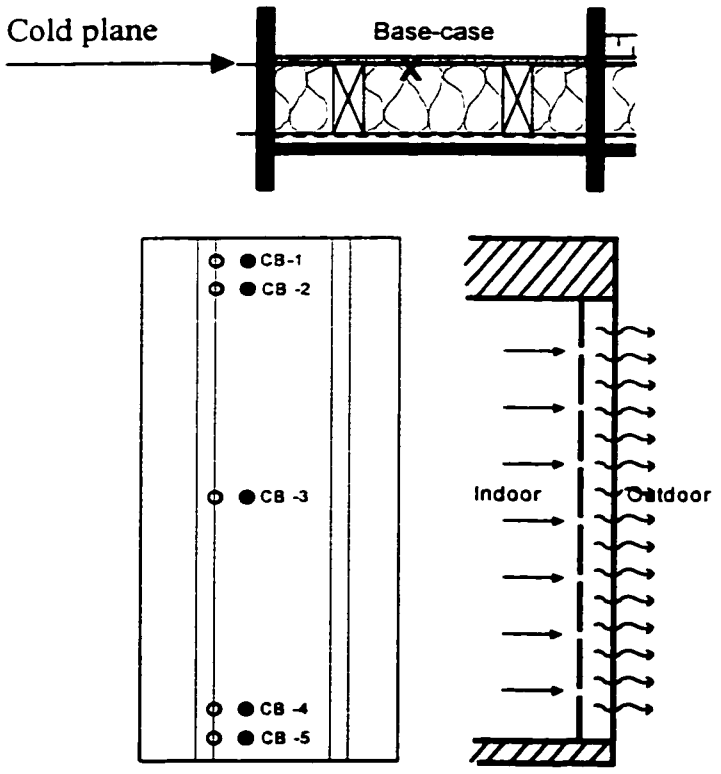

Base-case assembly, distributed air leakage path.

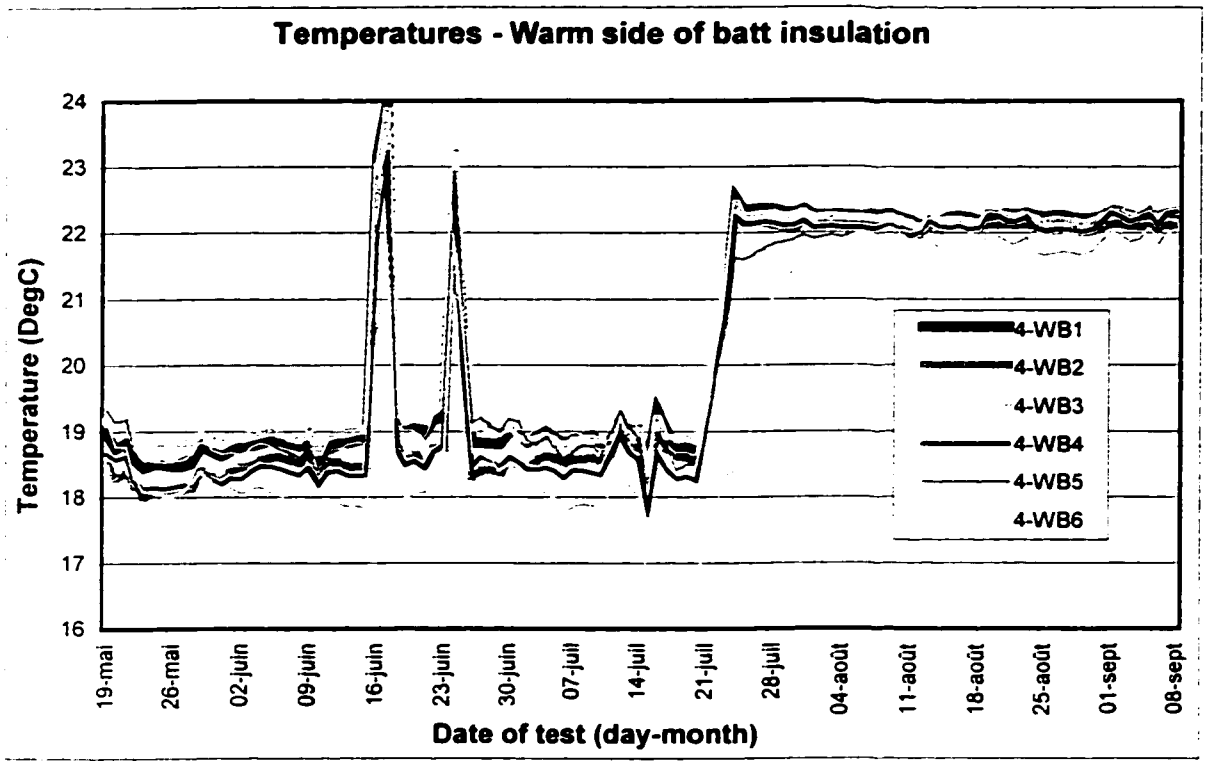

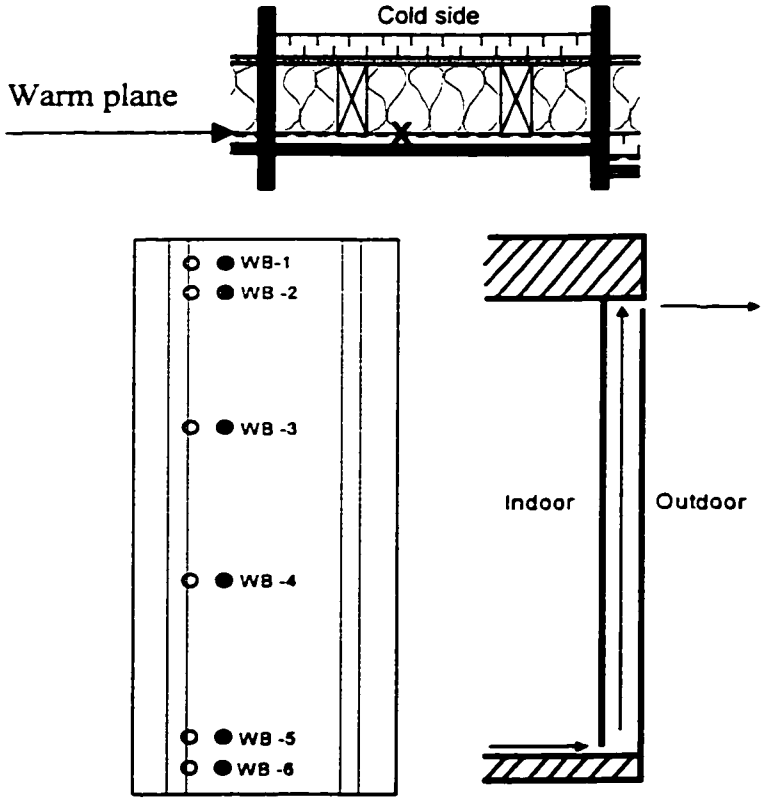

Insulation added on the cold side, long air leakage path.

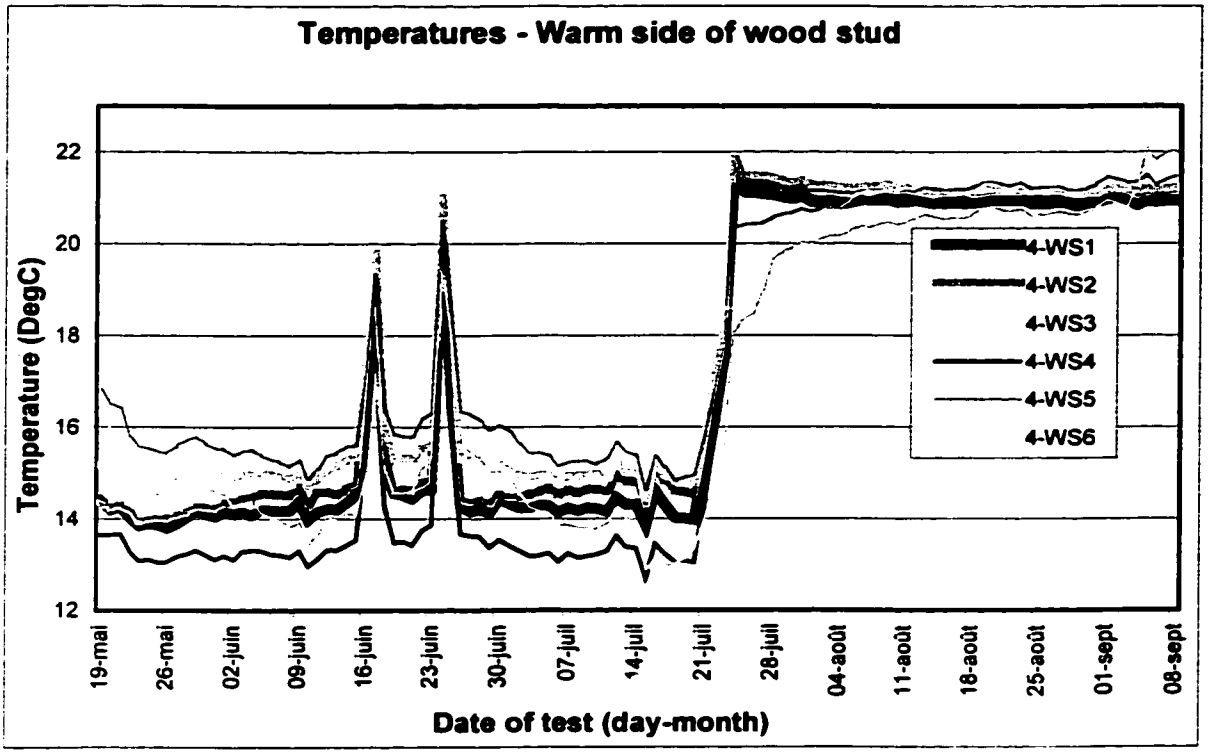

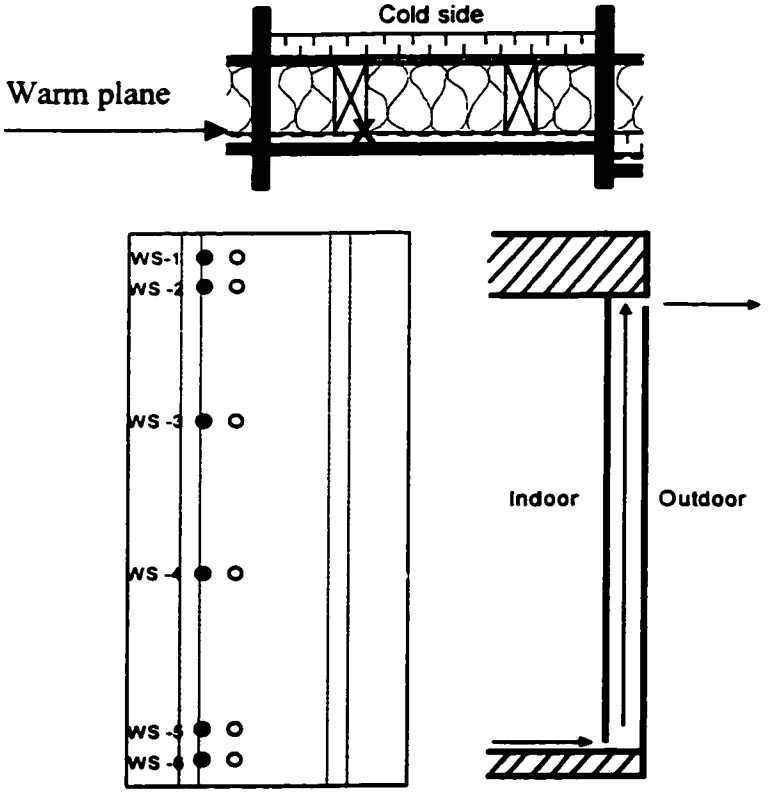

Insulation added on the cold side, long air leakage path.

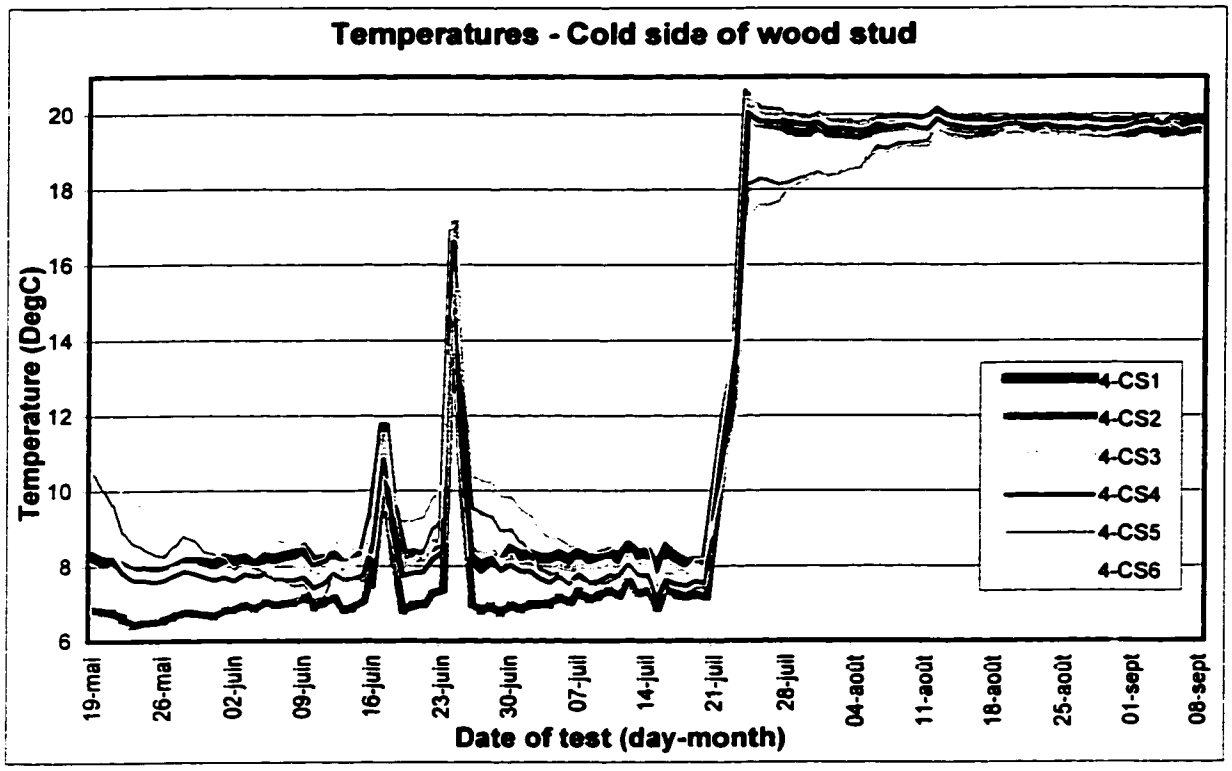

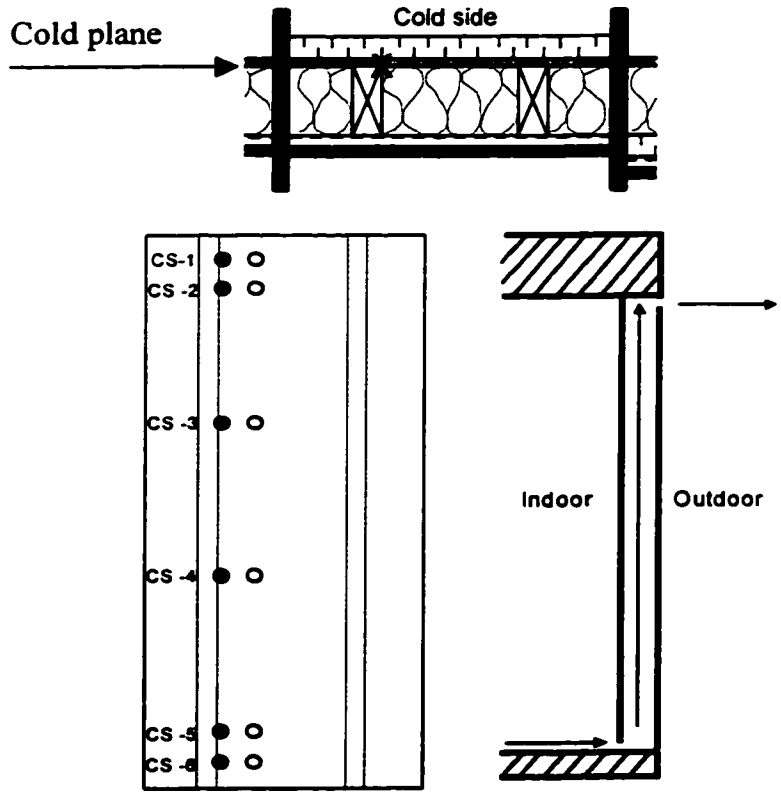

Insulation added on the cold side, long air leakage path.

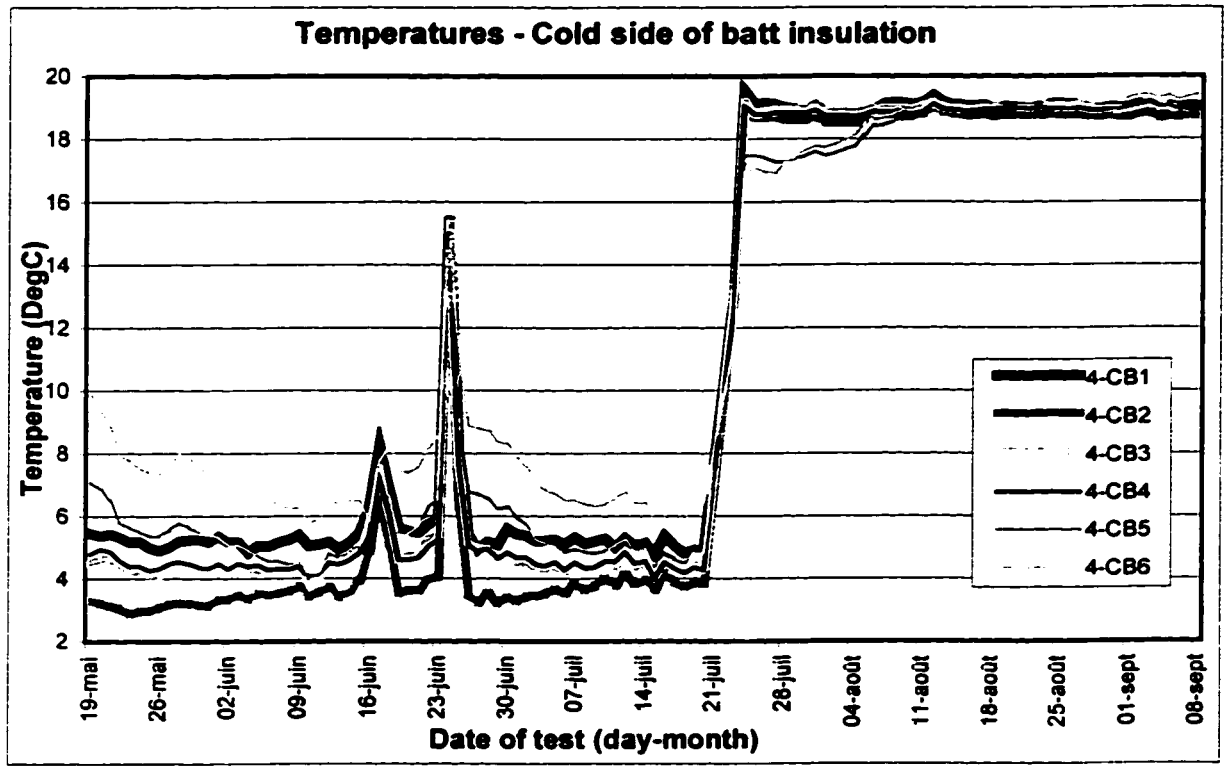

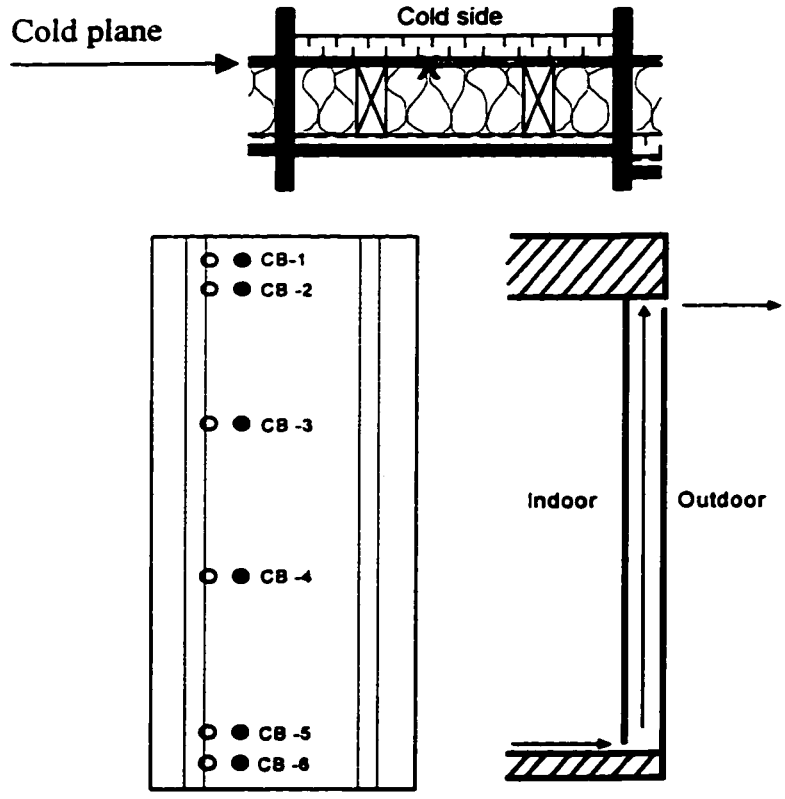

Insulation added on the cold side, long air leakage path.

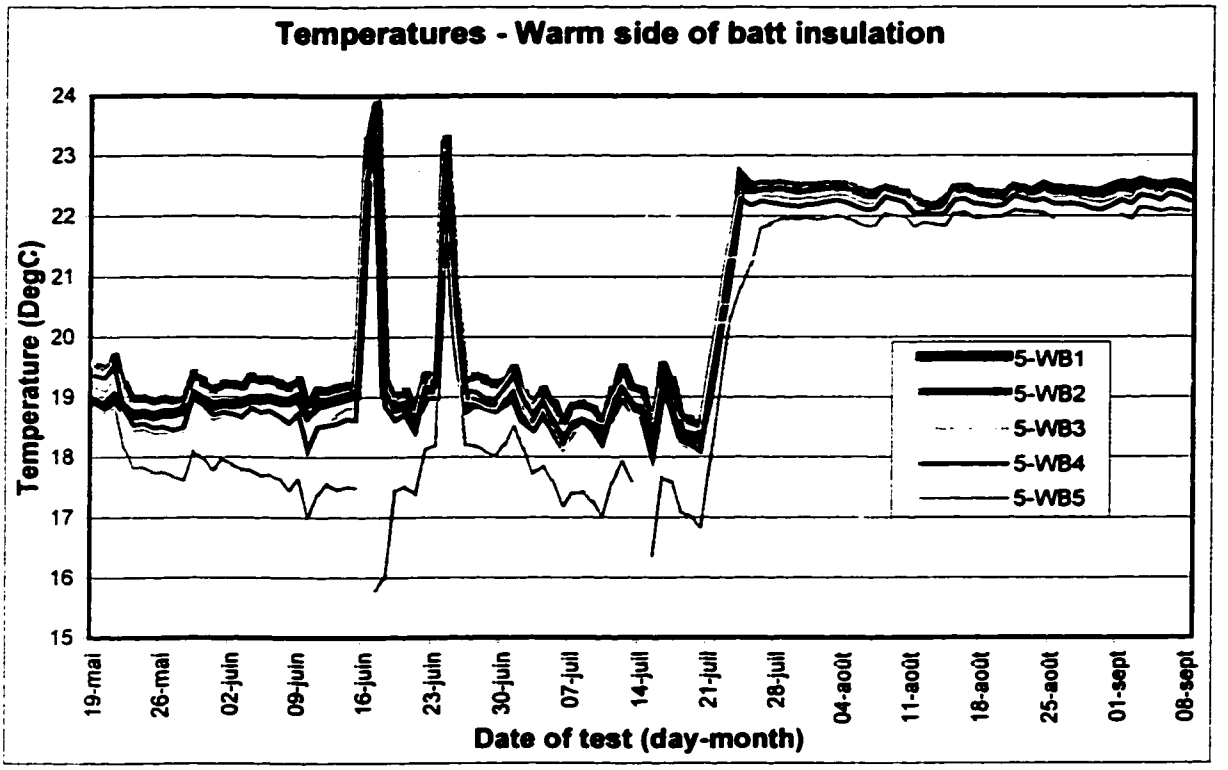

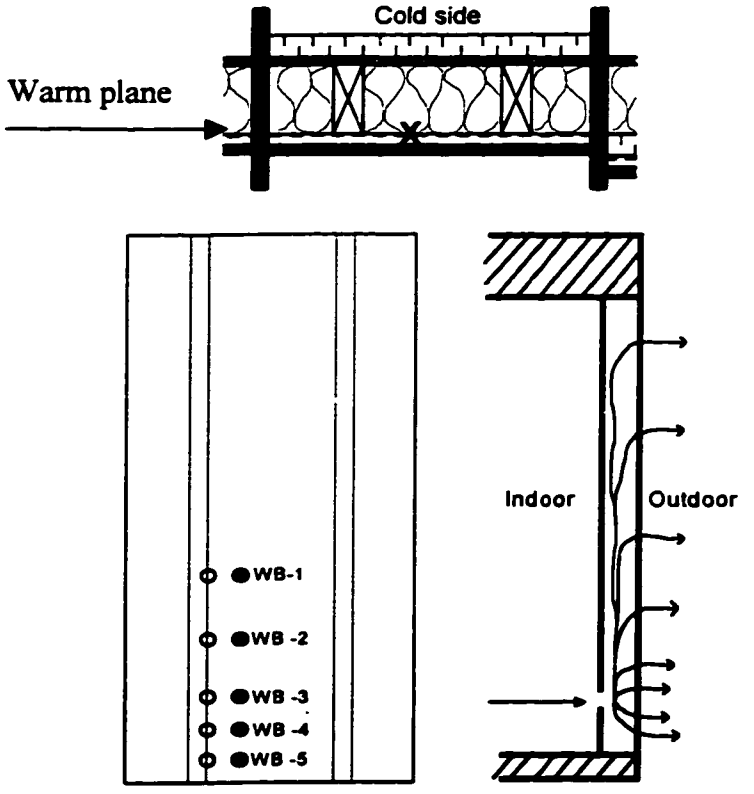

Insulation added on the cold side, concentrated air leakage path.

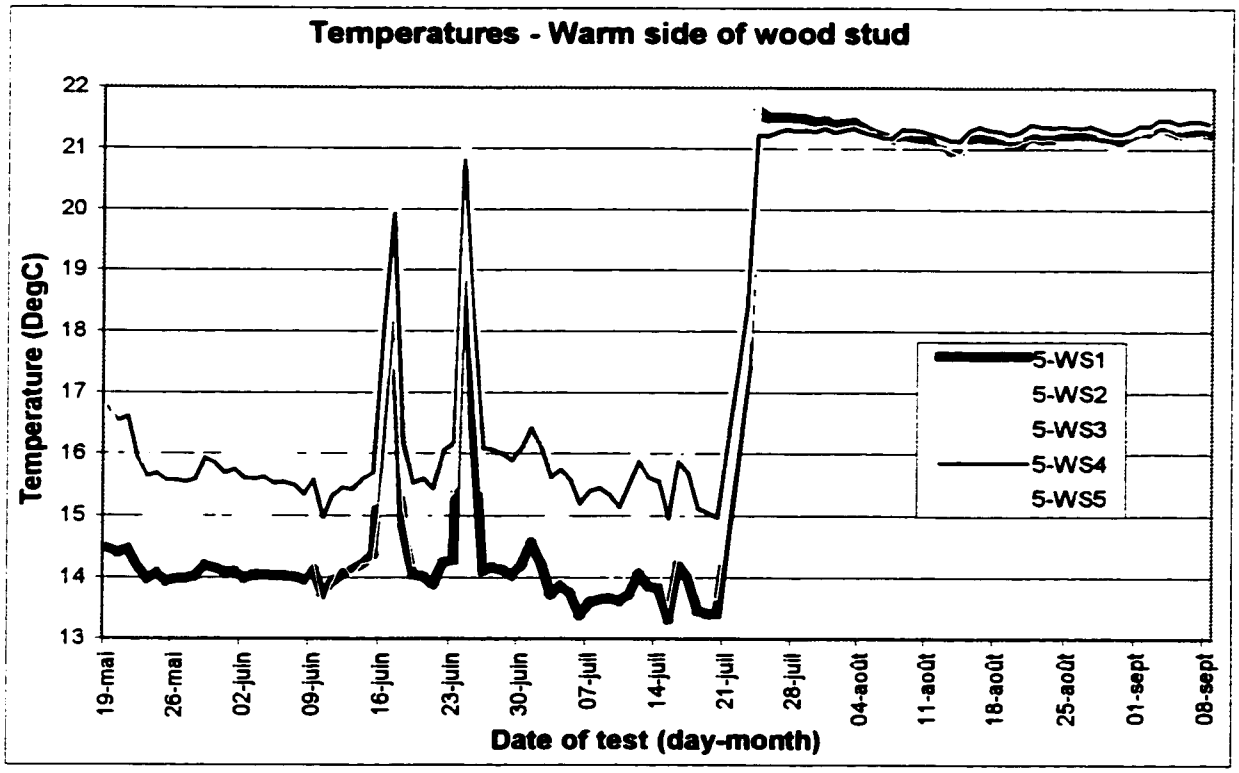

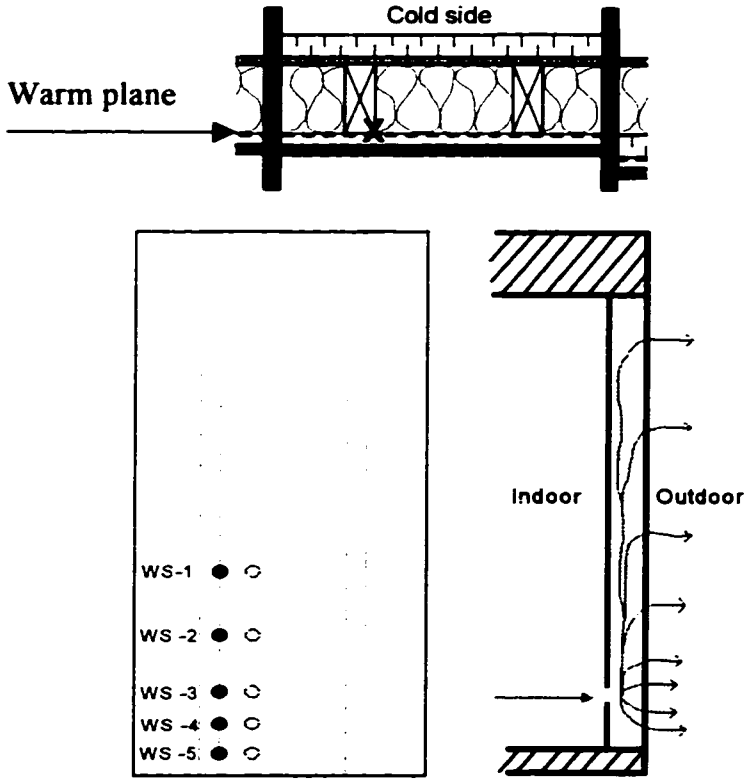

Insulation added on the cold side, concentrated air leakage path.

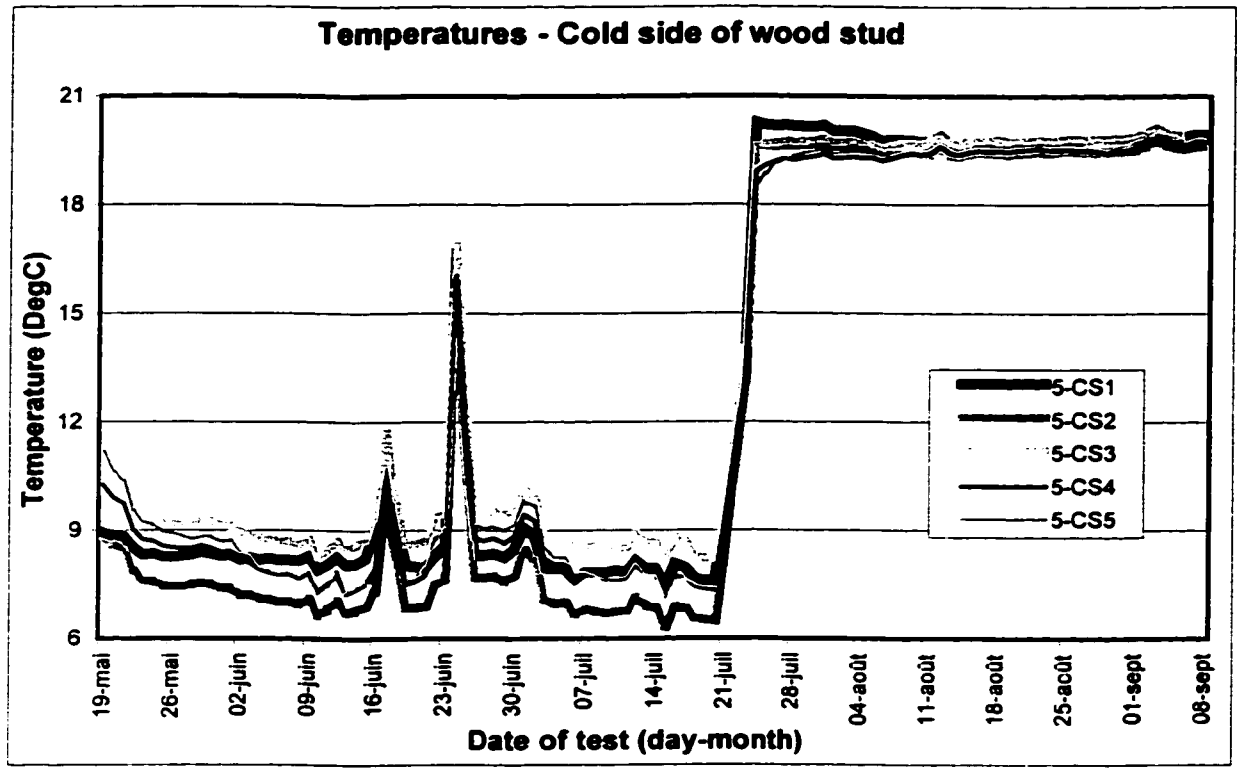

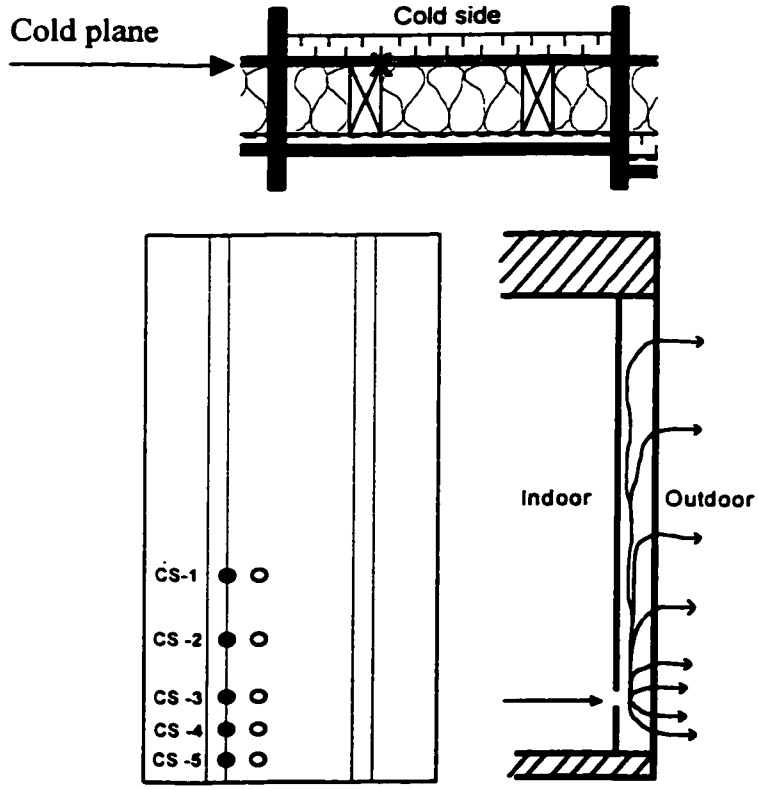

Insulation added on the cold side, concentrated air leakage path.

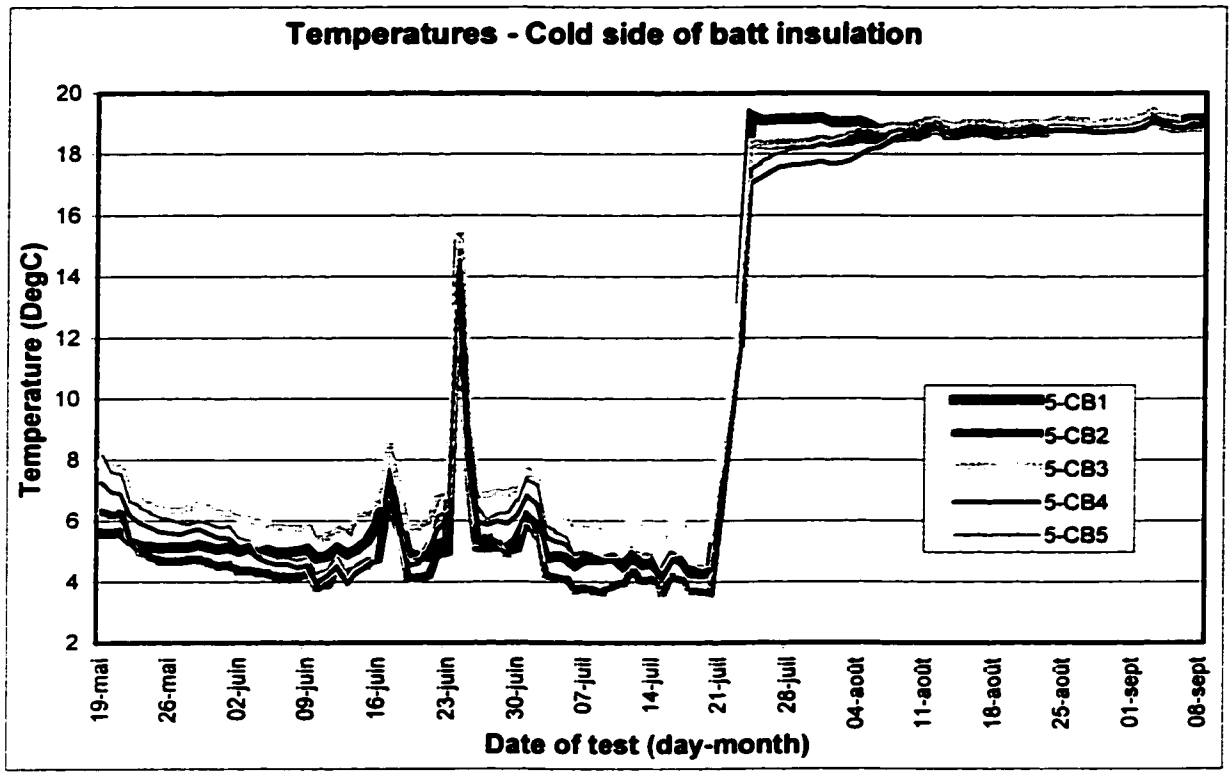

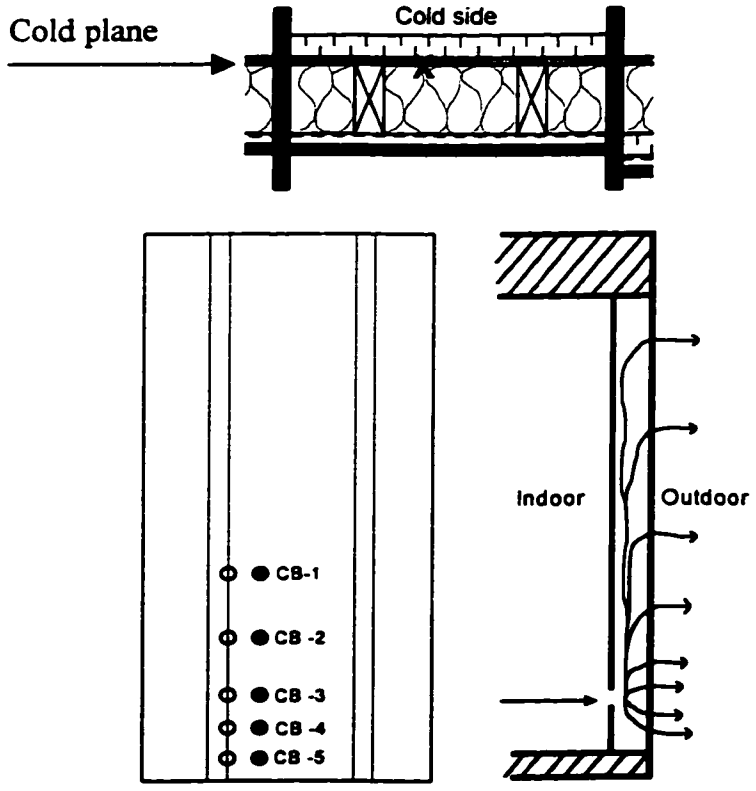

Insulation added on the cold side, concentrated air leakage path.

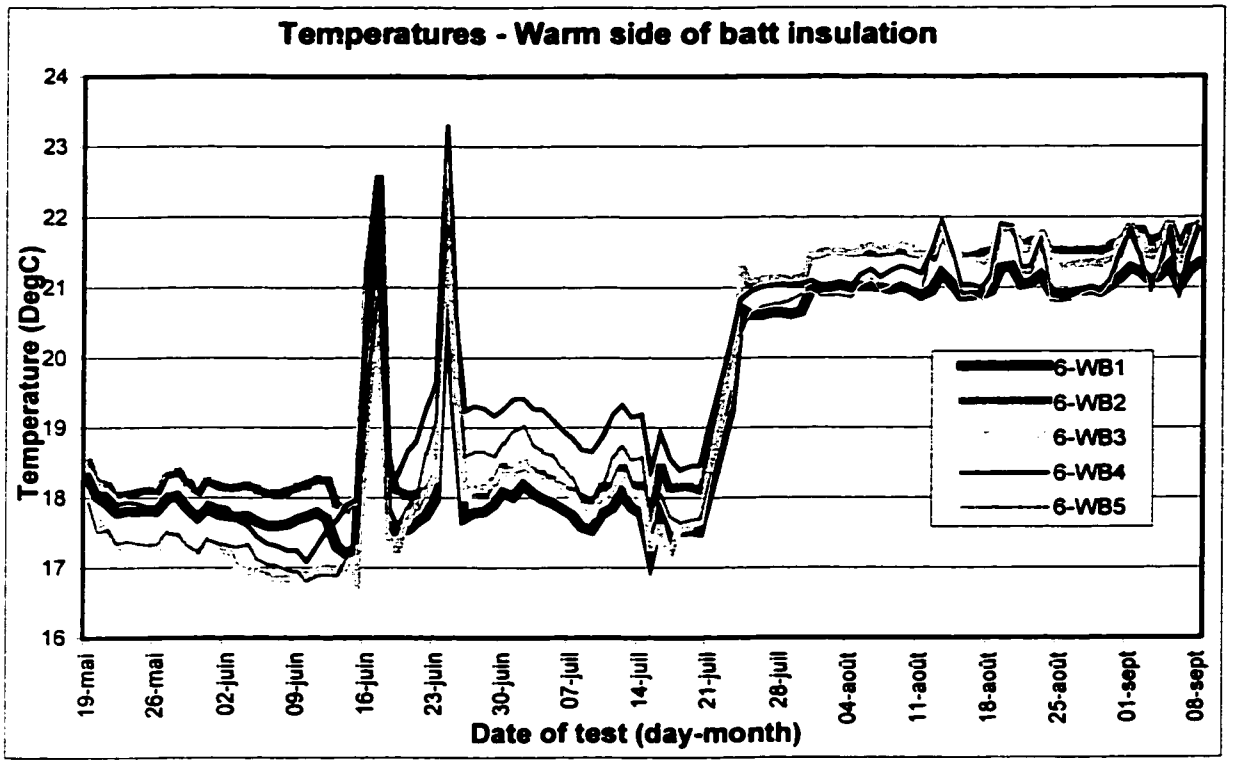

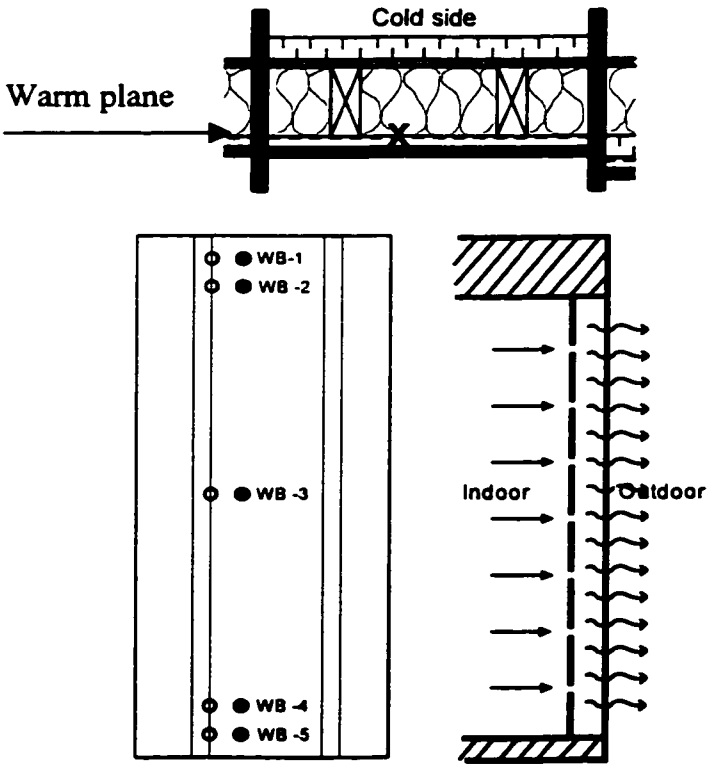

Insulation added on the cold side, distributed air leakage path.

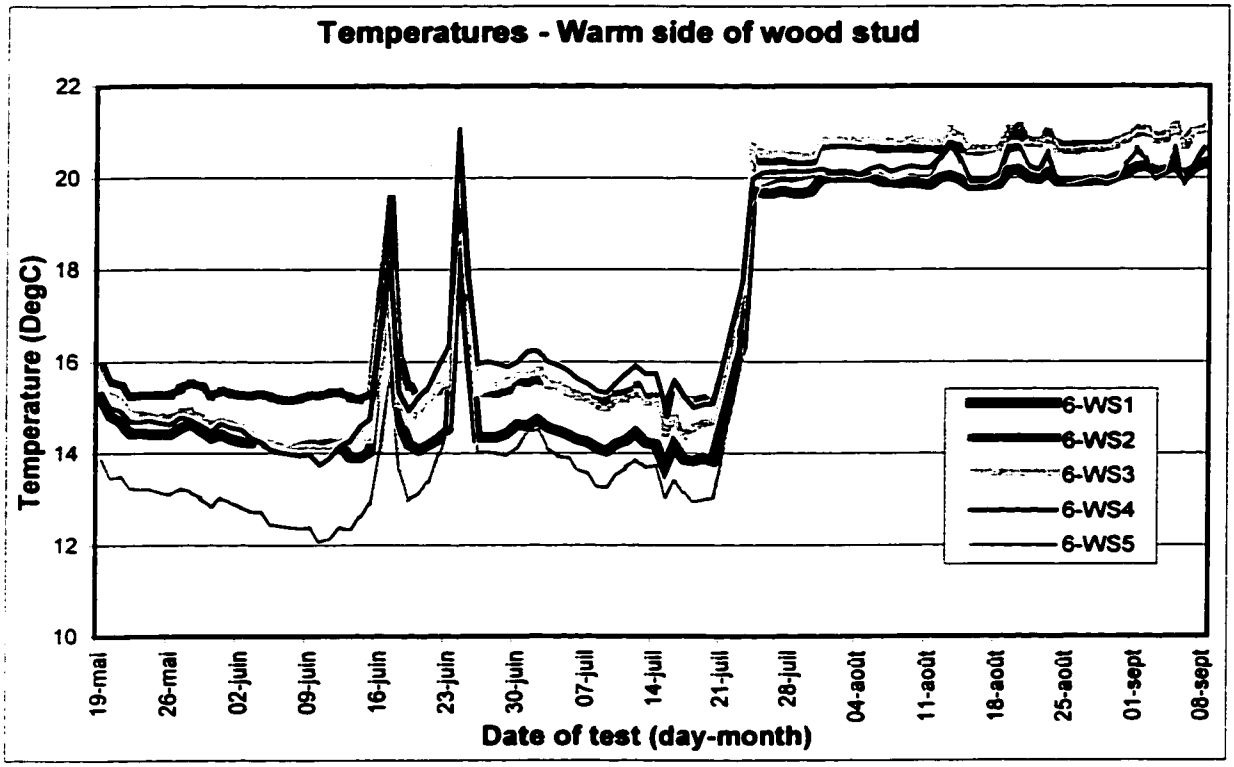

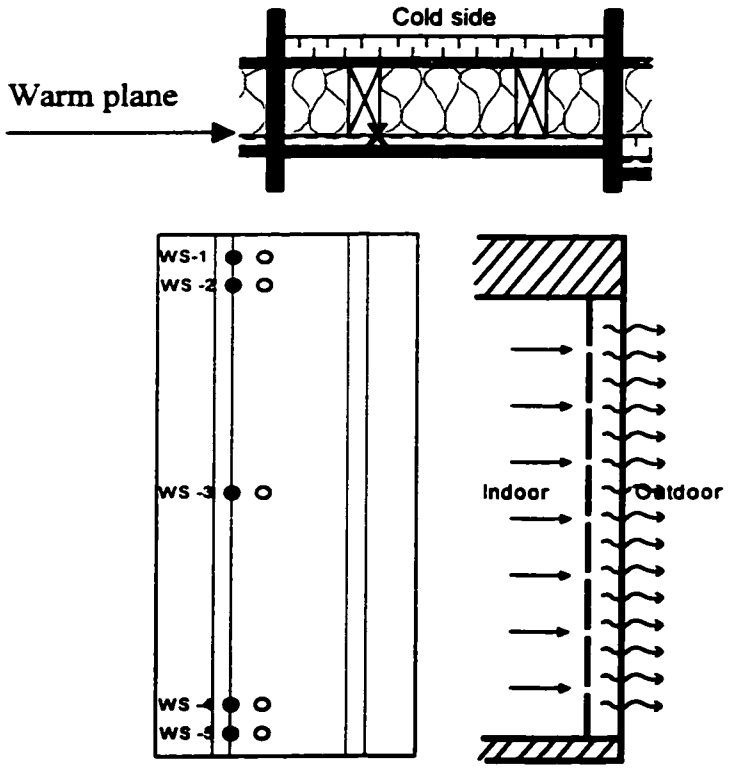

Insulation added on the cold side, distributed air leakage path.

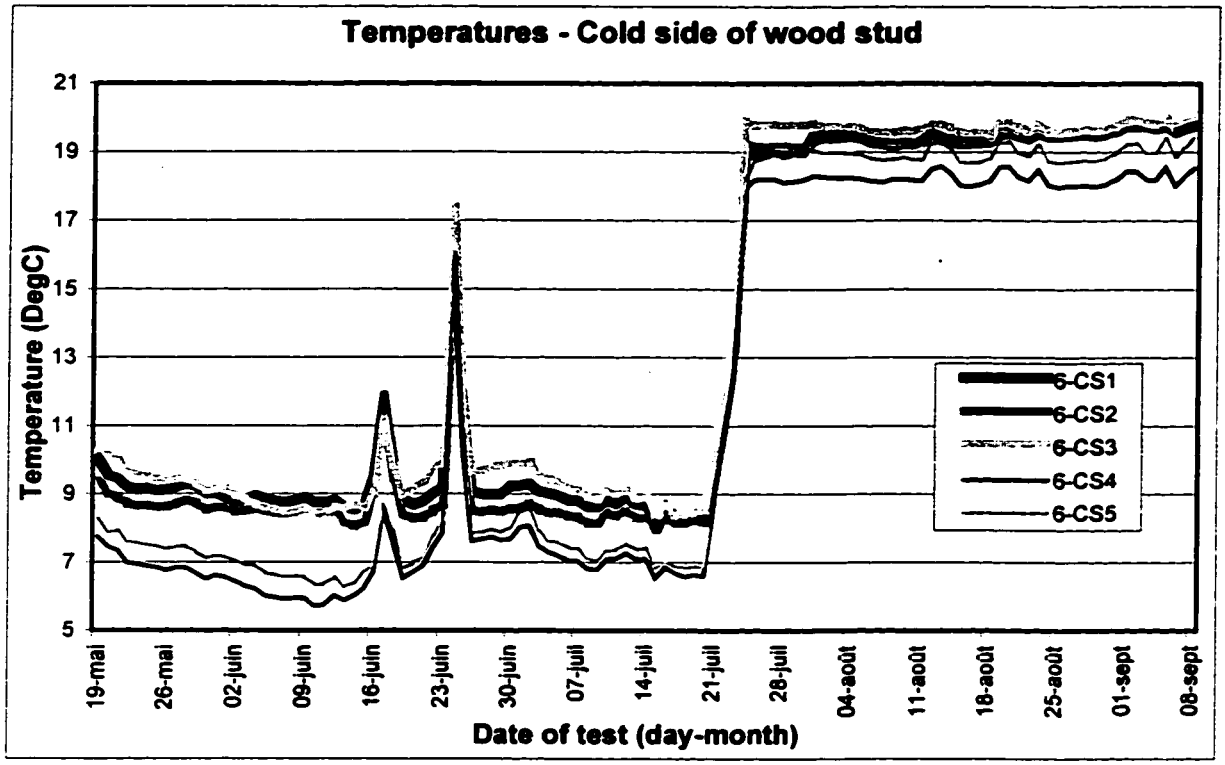

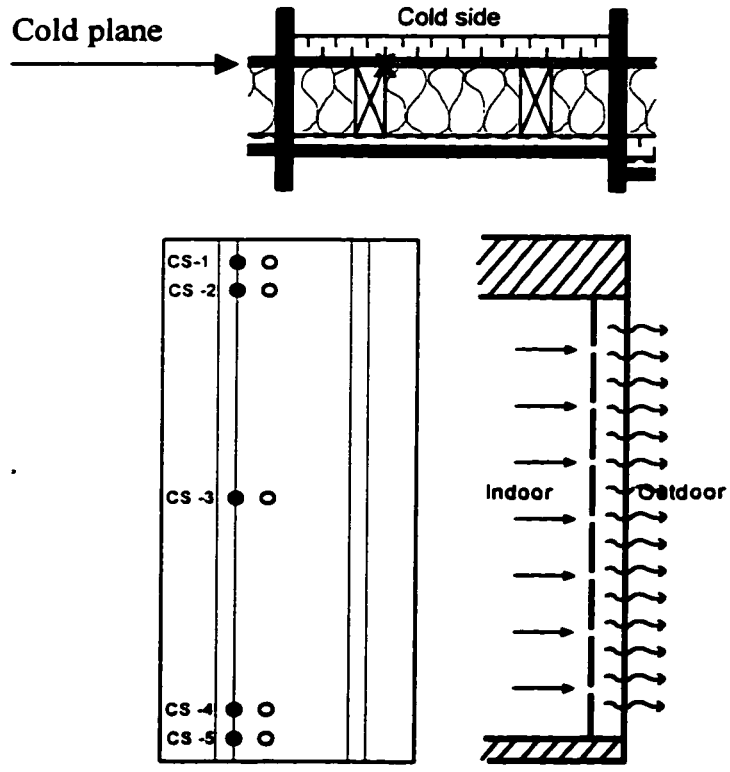

Insulation added on the cold side, distributed air leakage path.

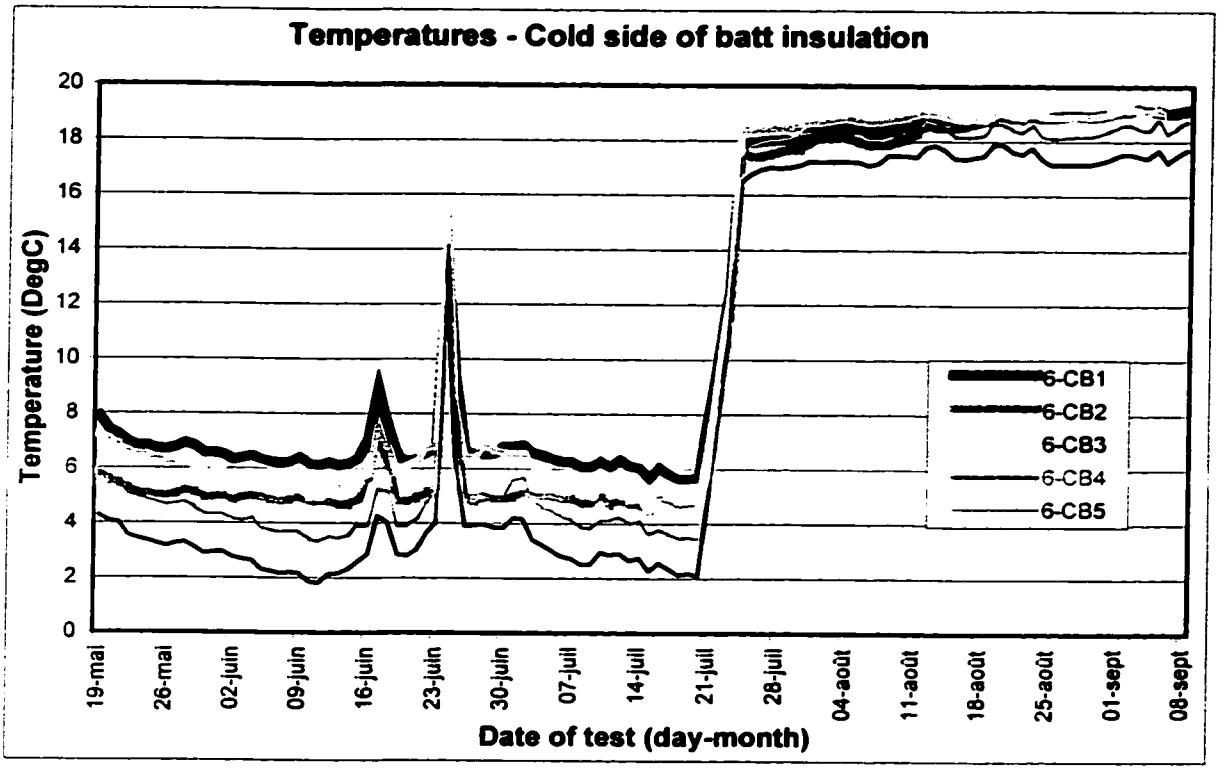

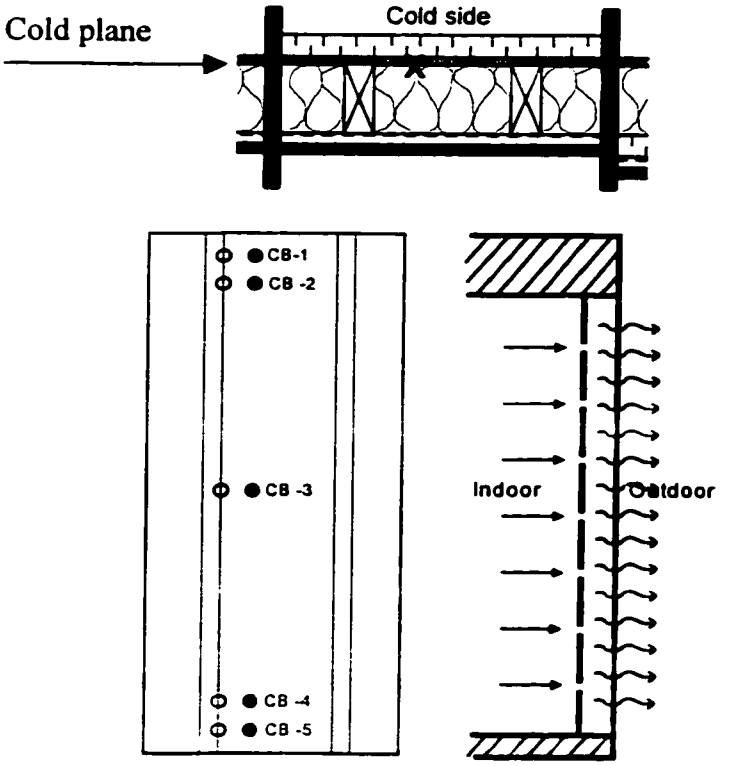

Insulation added on the cold side, distributed air leakage path.

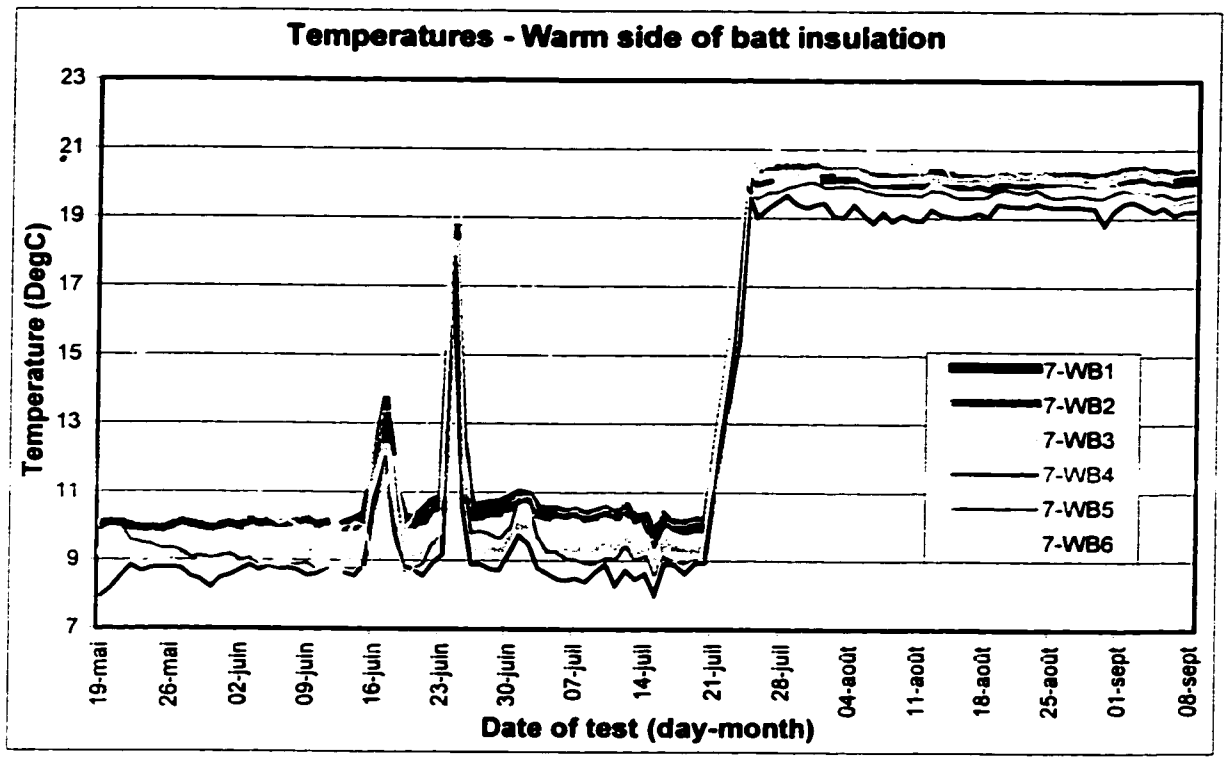

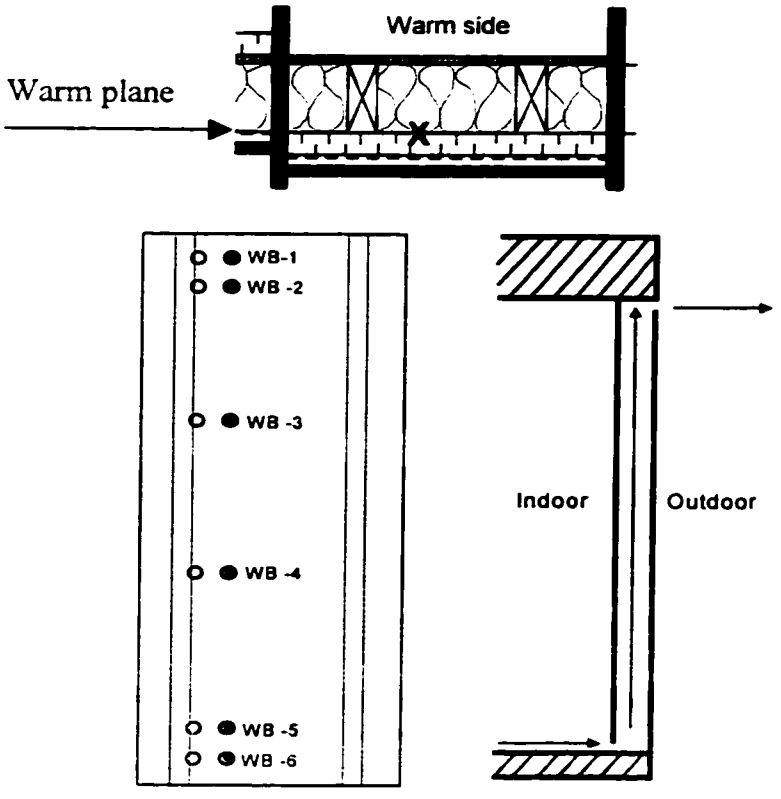

Insulation added on the warm side, long air leakage path.

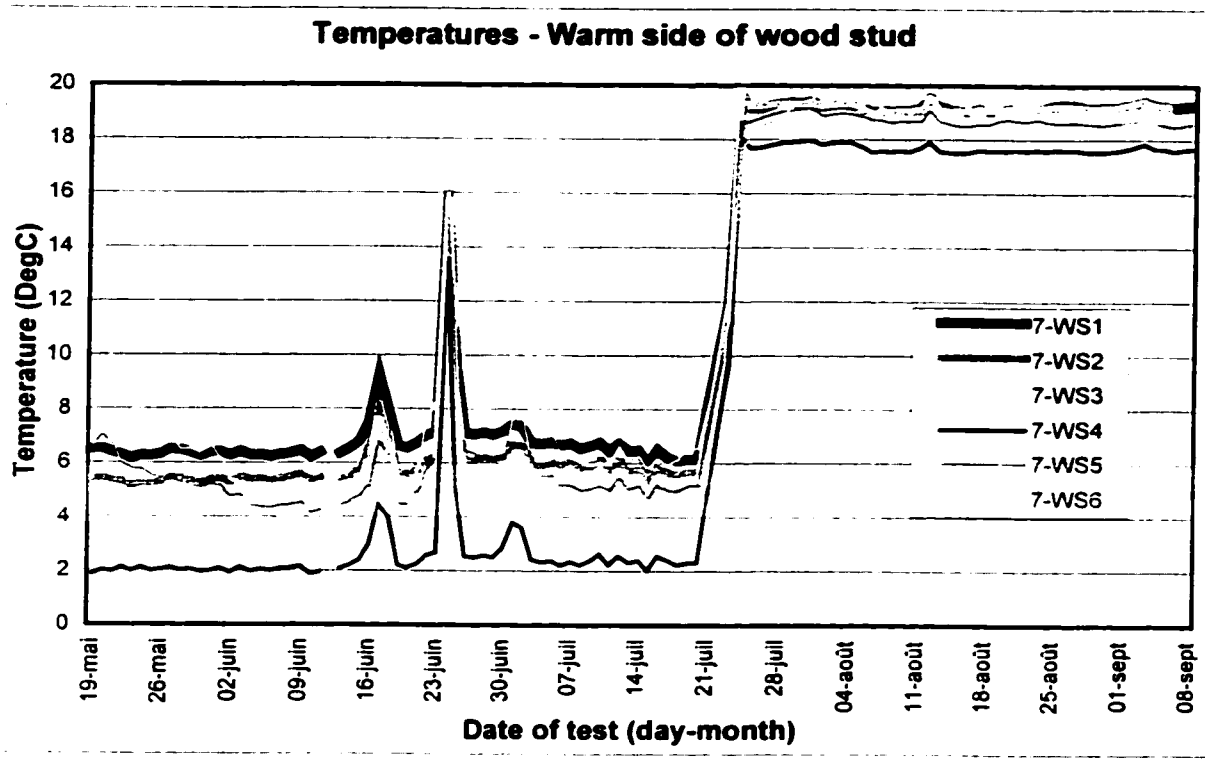

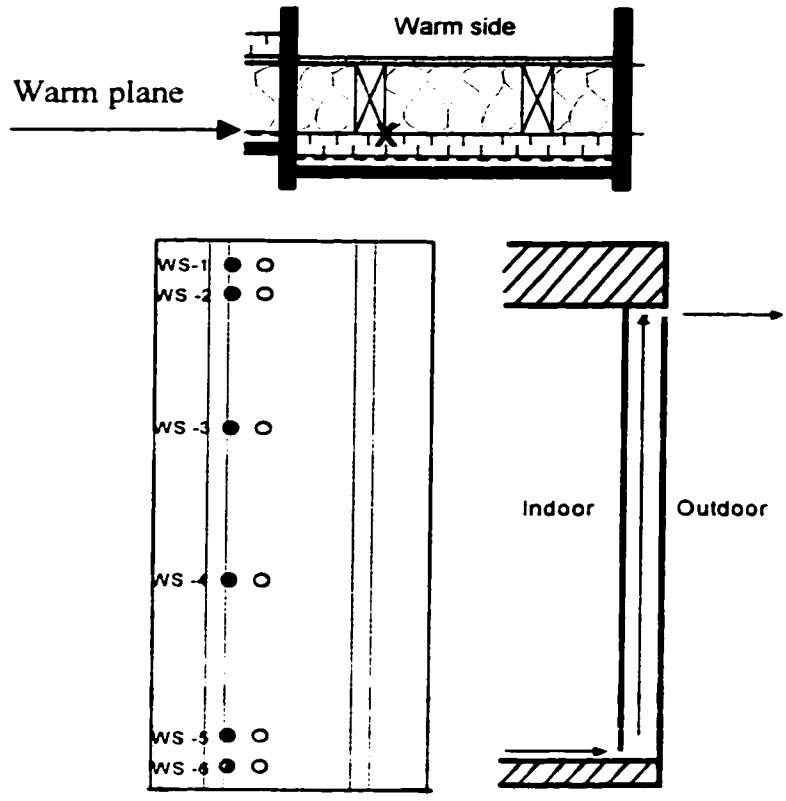

Insulation added on the warm side, long air leakage path.

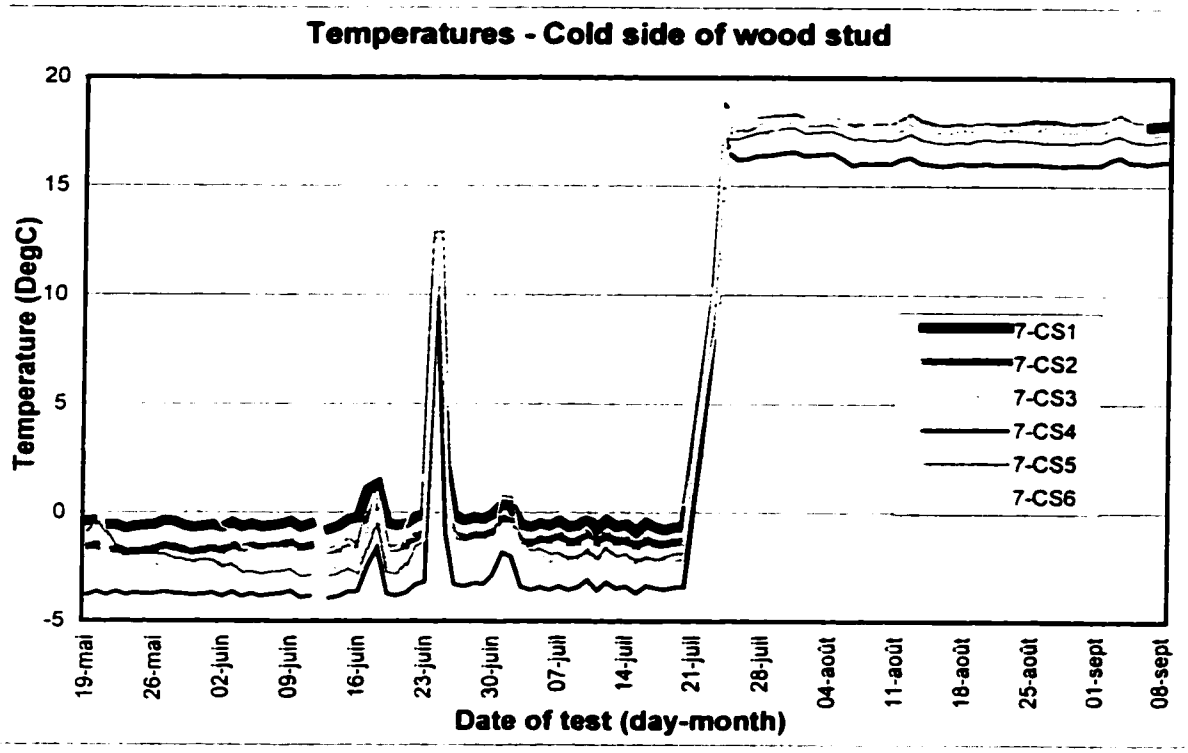

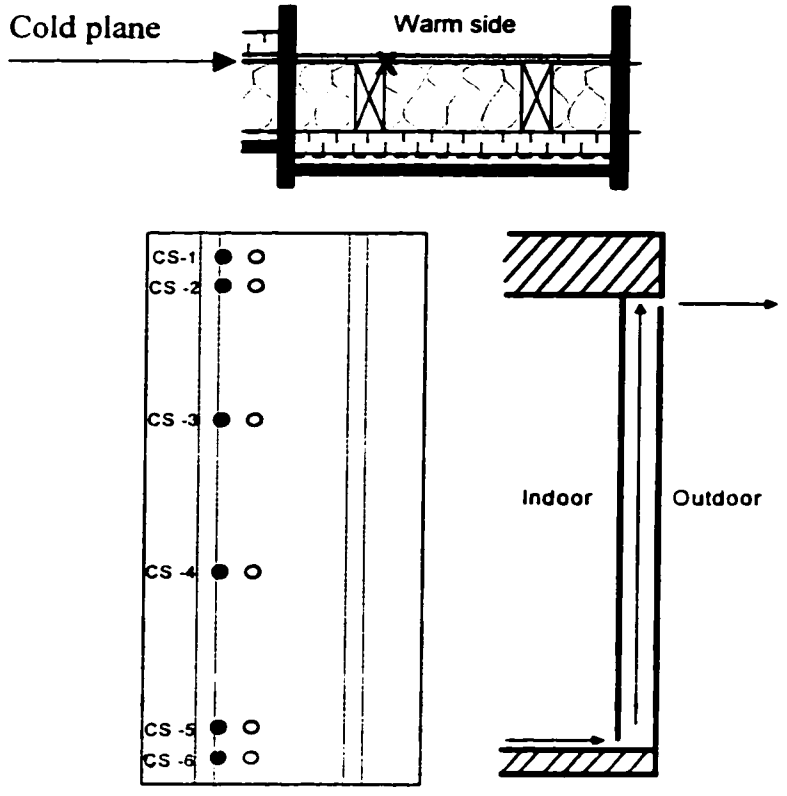

Insulation added on the warm side, long air leakage path.

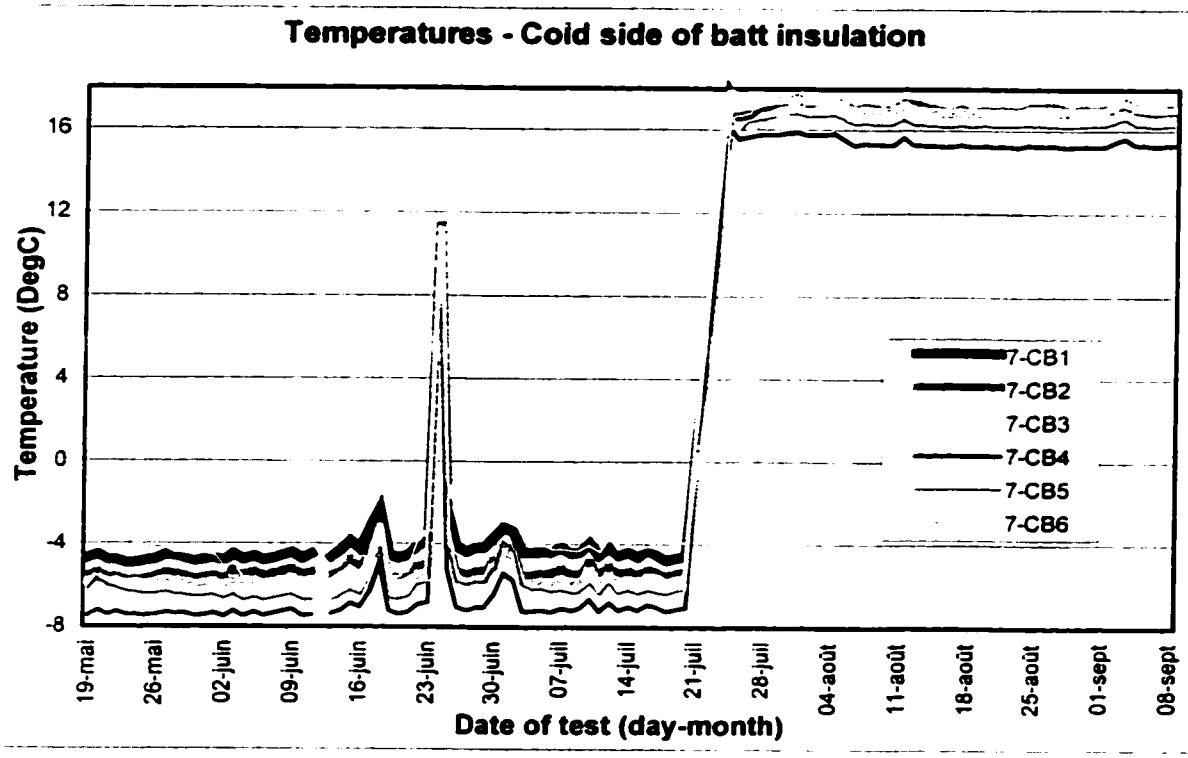

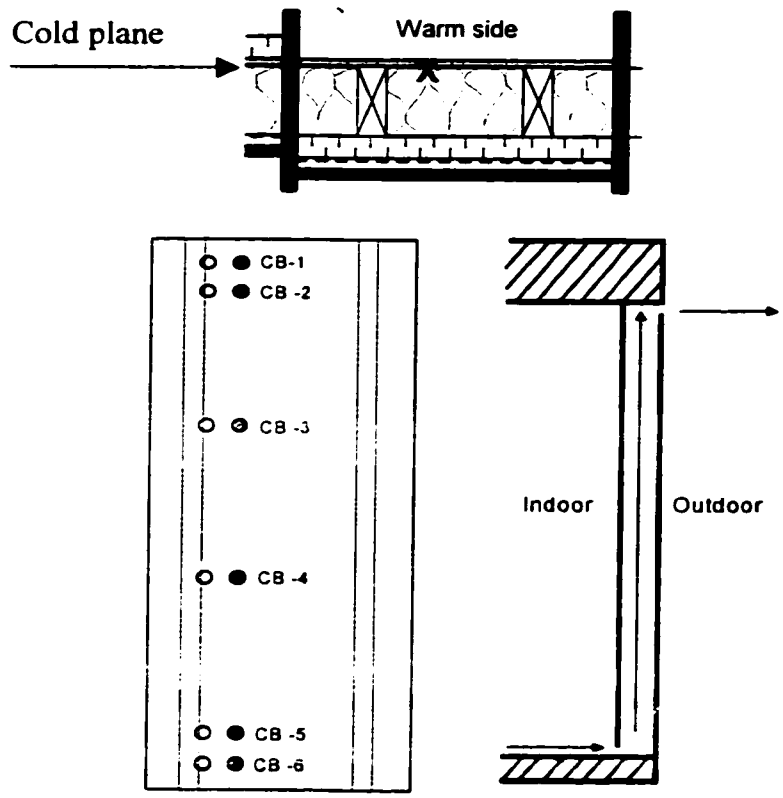

Insulation added on the warm side, long air leakage path.

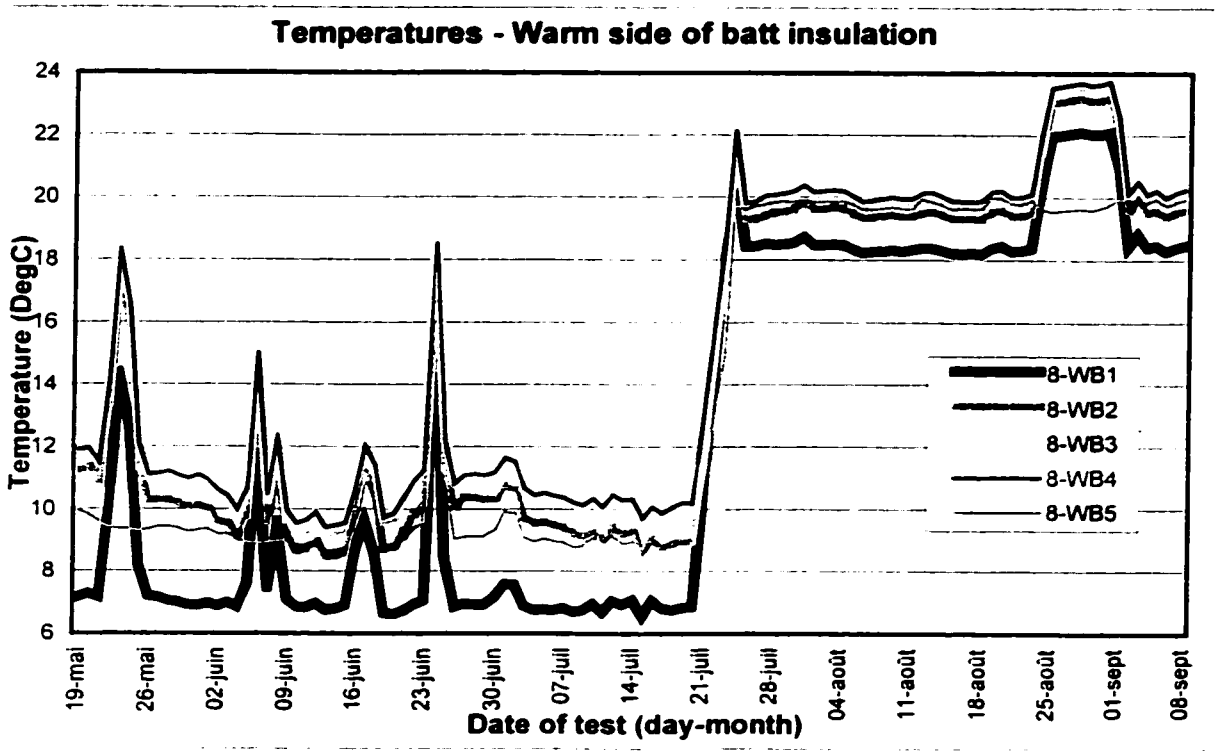

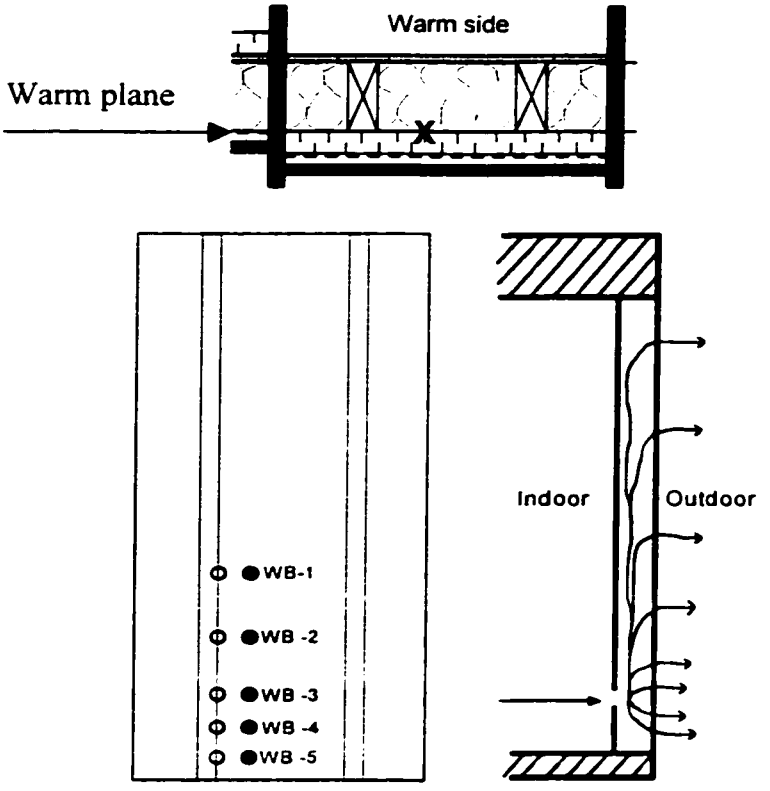

Insulation added on the warm side, concentrated air leakage path.

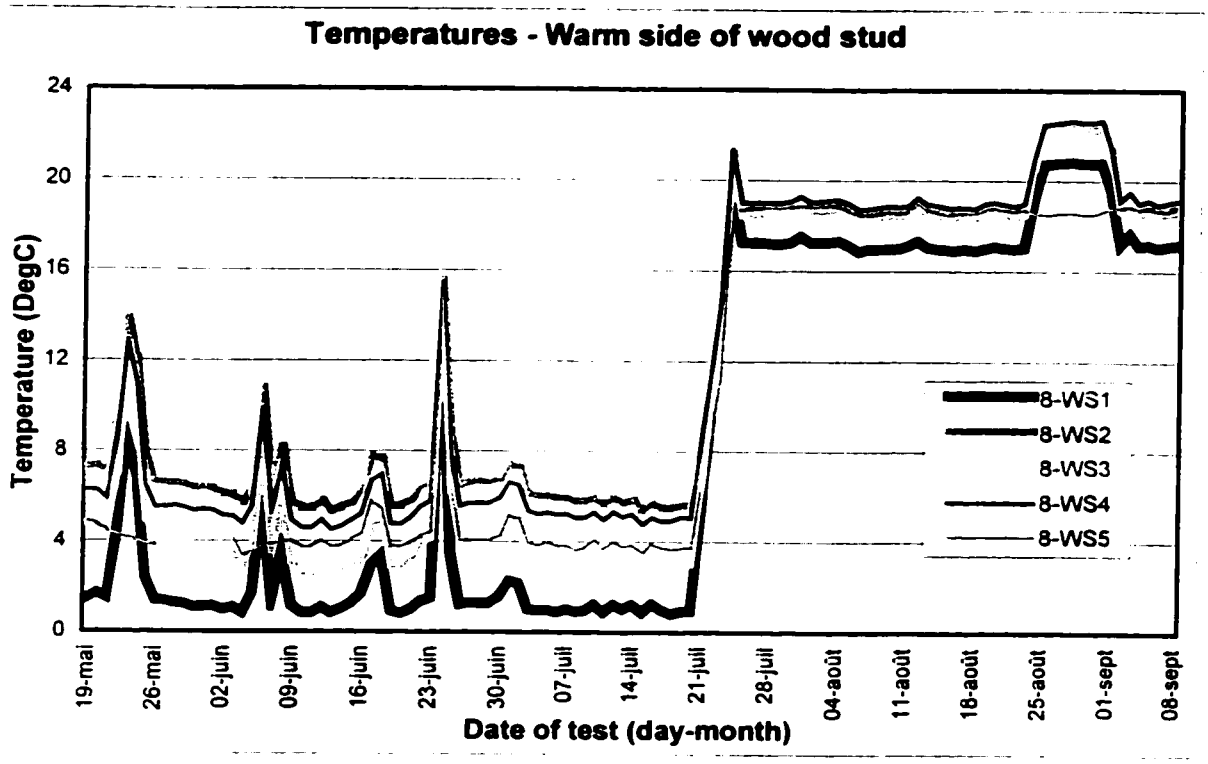

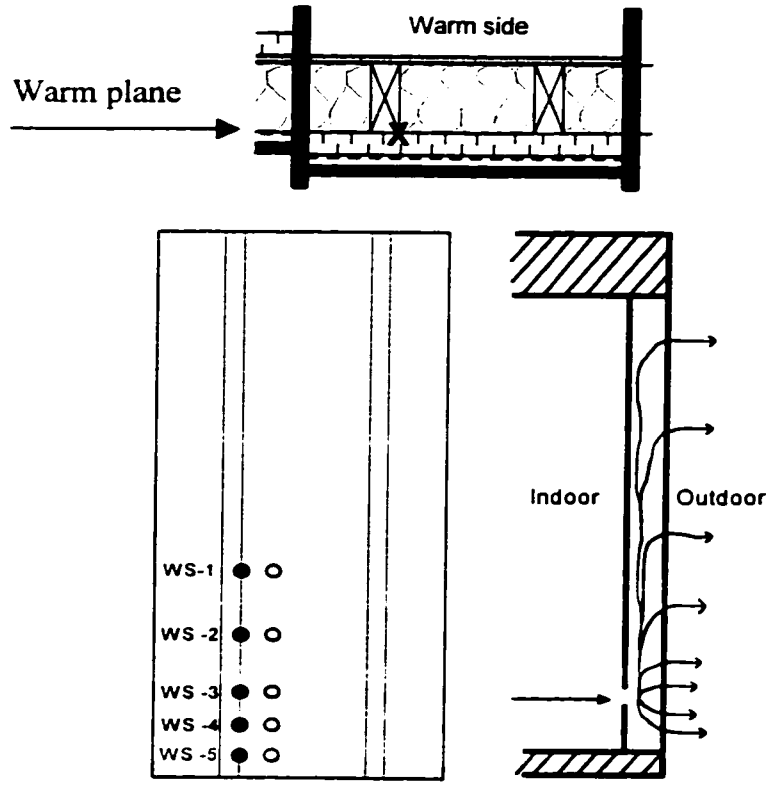

Insulation added on the warm side, concentrated air leakage path.

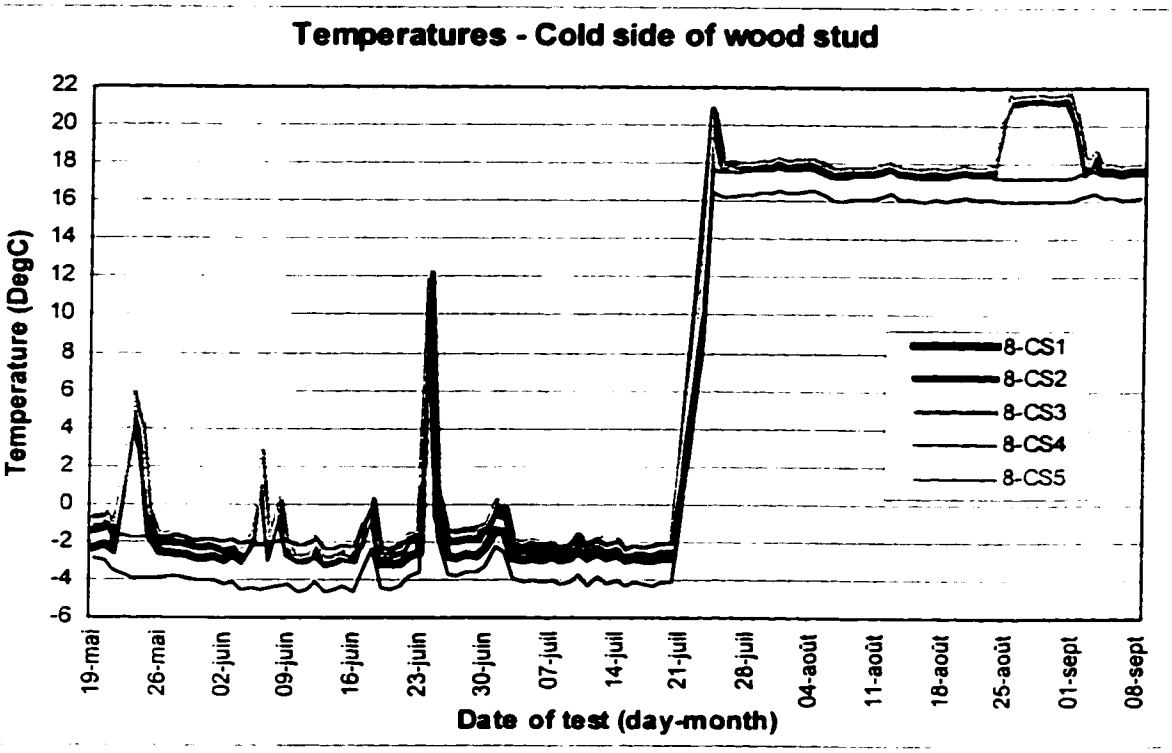

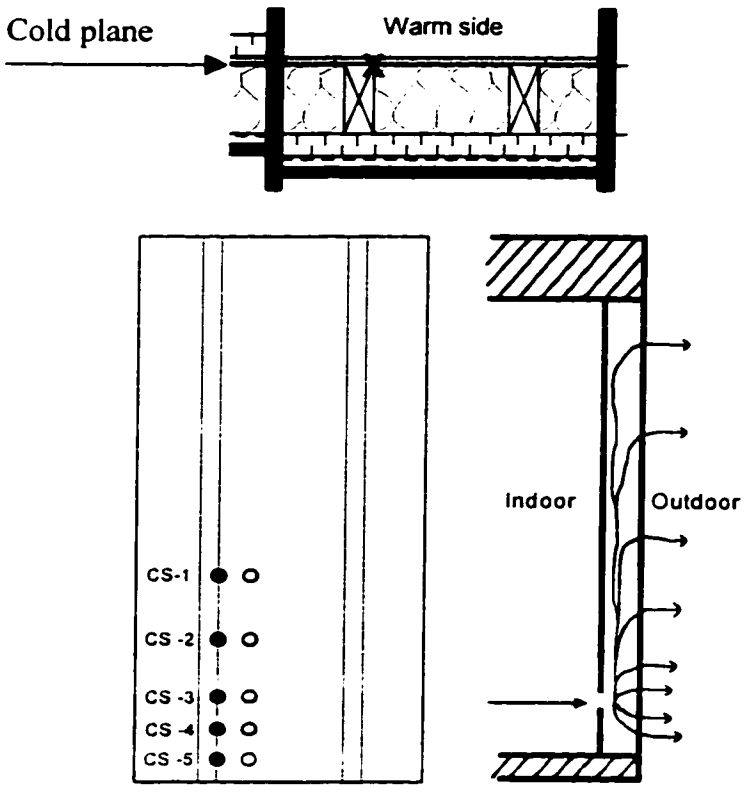

Insulation added on the warm side, concentrated air leakage path.

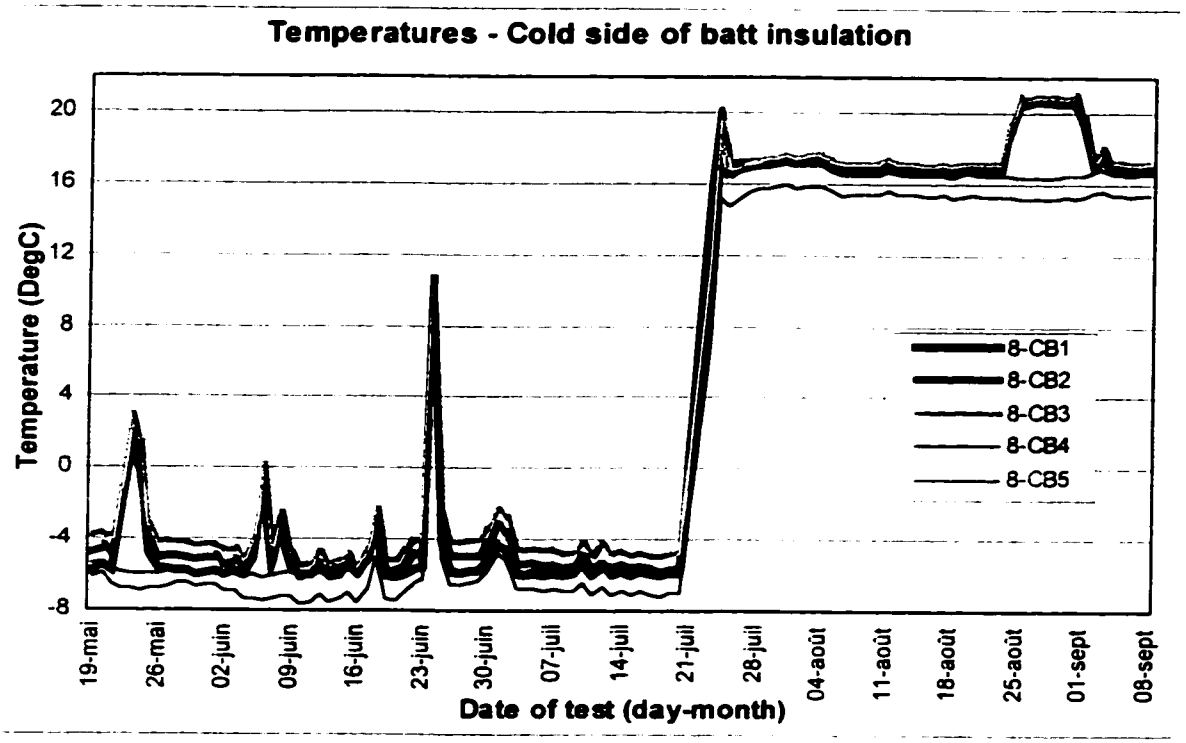

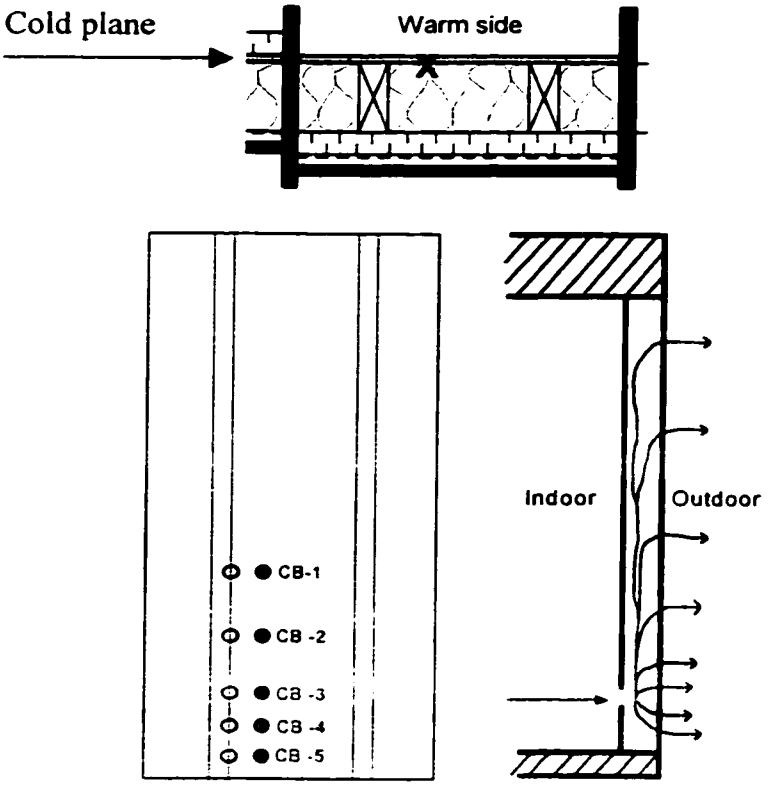

Insulation added on the warm side, concentrated air leakage path